Impact of Barrages on Extreme Water Levels in the Bristol Channel

Qian MA

St Anne's College

Department of Engineering Science

University of Oxford

A thesis submitted for the degree of

Doctor of Philosophy

Trinity 2020

Abstract

The Bristol Channel/Severn Estuary has some of the largest tides in the world with a mean spring tidal range of 12.2 m. On rare occasions, a significant storm surge will coincide with a spring tide and this has potential for very major coastal flooding given the large amount of low-lying land surrounding the estuary and the high population. Due to the high tidal range, numerous proposals have been made to exploit the Severn Estuary for energy extraction. Developing tidal power as a renewable energy resource is currently under consideration in order to meet increased worldwide energy demands and to reduce carbon emissions. The Severn Barrage and the Swansea Bay Lagoon are two options proposed for the Bristol Channel, which have been evaluated in this thesis. A key concern with this technology is that such structures may cause other environmental problems. However, tidal barrages may also have beneficial environmental effects in some areas, such as mitigating coastal flooding from storm surges. In light of this, this study aims to evaluate how the introduction of a tidal barrage would change the susceptibility of storm surge-induced flooding in the Bristol Channel.

In this thesis, the astronomical tides and storm surges are modelled using the open-source hydrodynamic model (ADCIRC DG-SWEM) which solves the two-dimensional shallow water equations. A one-dimensional model is also considered. Both of these models are calibrated and validated with field observations. The models are then modified using an internal barrier boundary to represent the effect on flow of implementing a barrage. During a storm surge event, it is found that to the east of the barrage, the peak water level is significantly reduced by the Severn Barrage. To the west of the barrage, on the ocean side, the presence of the barrage leads to a small increase in the water levels during a surge event. Different operational strategies for the barrage during a storm event are examined, which make a small but perhaps significant difference. The

impact of storm surges on power generation is also investigated and is found to be minor. Overall a barrage can help to mitigate the impact of storm surges on coastal flooding. With respect to the Swansea Lagoon, the flooding protection benefits are found to be limited and localised since it is a relatively small project. The resonant response of the Bristol Channel hydrodynamic system is also examined in this thesis. The Severn Barrage is found to cause little change to the resonant response close to the dominant semi-diurnal frequencies and the changes are localised to the device.

The application of a one-dimensional hydrodynamic model can be computationally cheaper and only key hydrodynamic features are captured. Compared with the two-dimensional DG-SWEM, it is found in this study that the tidal characteristics and barrage behaviour can be accurately simulated by a one-dimensional model while discrepancies occur when modelling storm surges. A one-dimensional model is suitable for a preliminary investigation or a qualitative analysis.

Acknowledgements

First of all, I would like to sincerely thank my supervisor Prof. Thomas A. A. Adcock for his guidance, advice and encouragement throughout this project. Tom has always been patient and supportive, especially over the difficult periods in my research. This thesis would not have been possible without his continuing help and trust. I am also grateful for his support in my scholarship applications. I also wish to show my appreciation for the input from my colleague, Tulio Marcondes Moreira. Although Tulio has transferred to Brazil in 2018, he has always been trying to provide great help throughout this project. Thanks to his quick responses to my questions, most technical problems encountered in the barrage model have been solved. For this project, I want to thank Dr Sena Serhadlıoğlu who did important preliminary work for this study.

I own many thanks to colleagues and friends within the Tidal Energy Research Group for their kindness and support. Special thanks to Tuo Wang, Andrea Schnabl, Bowen Cao and Lei Chen for all the technical help they have provided throughout this project. I would like to thank Dylan Wood of the Ohio State University for his assistance of utilising the DG-SWEM code. I also appreciate the help from Stephen Grey and Nigel Tozer (HR Wallingford) for the meteorological data. In carrying out this project, I would like to express my appreciation to all the staff in the Engineering Science Department. This project would not have been feasible without the service of the Advanced Research Computing (ARC) of the University of Oxford.

I would like to acknowledge the Chinese Scholarship Council (CSC), which has been the funding body of the work presented in this thesis.

Finally, I would like to thank my family, my parents and Xiaodong Shi, who are always there for me. Thank you for all the support and encouragement that you provide, and the patience and trust you have for me. Without your unconditional love, I would never find my ability and

courage to follow my dreams. Particular thanks go to my close friends, Yin Liang and Tianning Tang, for your valuable help and you have always been important parts of my wonderful life in Oxford.

Contents

List of Figures

Nomenclature

η	Turbine efficiency	%
Ω	Angular speed of the Earth	rad/day
ω	Angular speed (frequency)	rad/s
Ω_g	Gravitational potential of a body	m^2/s^2
ω_n	Angular speed (frequency) of a tidal constituent	rad/s
ω_{M_2}	Angular speed (frequency) of M_2 tide	rad/s
Φ	Latitude of the location of interest	$^\circ$
ϕ_n	Phase of a tidal constituent	$^\circ$
ρ	Fluid density	kg/m^3
ρ_a	Air density	kg/m^3
τ_W	Wind shear stress	N/m^2
τ_{Bx}	Bottom friction stress in the positive x-direction	N/m^2
τ_{By}	Bottom friction stress in the positive y-direction	N/m^2
τ_{Wx}	Wind shear stress in the positive x-direction	N/m^2
τ_{Wy}	Wind shear stress in the positive y-direction	N/m^2
ξ	Free surface elevation above a certain datum	m
ξ_{Tn}	Water surface elevation of a tidal constituent specified at the model open boundaries	m
A	Channel cross-sectional area	m^2

a	Amplitude	m
A_b	Surface area of the basin	m^2
a_n	Amplitude of a tidal constituent	m
A_s	Area of the seabed	m^2
A_t	Flow area though the barrage opening	m^2
A_{wet}	Wetted surface area of the tidal range structure	m^2
B	Channel width	m
C	Courant number in the CFL condition	$-$
c	Wave celerity ($c = \sqrt{gD}$)	m/s
C_A	Speed of the travelling atmospheric disturbance	m/s
C_D	Discharge coefficient in orifice equation	$-$
C_d	Drag coefficient between the wind and the water surface	$-$
C_f	Bottom bed friction coefficient	$-$
D	Total water depth	m
d	Channel depth in the 1D model	m
D_t	Turbine diameter	m
E	Extracted energy from a tidal barrage	J
e	Ratio between the extracted energy and the maximum available energy	$-$
E_{MAX}	Maximum theoretically available energy extracted by emptying the basin	J
F	Total stress in the positive x-direction	N/m^2
f	Coriolis parameter	rad/day
F_b	Bottom stress of an element of water	N/m^2
F_s	Surface stress of an element of water	N/m^2
f_g	Grid frequency	Hz

G	Total stress in the positive y-direction	N/m^2
g	Gravitational acceleration	m/s^2
G_p	Number of generating poles	$-$
H	Absolute value of the water head difference over a barrage	m
L	Wavelength	m
l	Channel length in the 1D model	m
n_{11}	Turbine unit speed	rpm
P	Pressure	Pa
P_t	Turbine power	W
P_{atm}	Atmospheric pressure	Pa
Q	Flow rate through the turbines during power generation	m^3/s
Q_{11}	Turbine unit discharge	m^3/s
S_p	Turbine rotation	rpm
t	Time	s
U	Cross-sectionally averaged velocity of the flow	m/s
u	Depth-averaged horizontal velocities in the x-direction	m/s
v	Depth-averaged horizontal velocities in the y-direction	m/s
W	Wind speed	m/s
W_{10}	10-m, 10-minute-averaged wind speed	m/s
Z	Water level	m

Chapter 1

Introduction and Literature Review

A storm surge is an increase of the ocean water level generated as a result of atmospheric depressions and strong winds during a storm. During a storm surge, water levels exceed the normal astronomical tides and can cause coastal flooding as well as reduced river discharge, potentially exacerbating river flooding. A prominent example of a storm surge-induced flooding that occurred within the last decade is the event on the 13th January of 2017 at the east coast of Britain. During this event, a combination of forcing winds along with a high tide resulted in a storm surge of approximately 2.7 m and waves of over 7 m, which led to a warning of danger to life across the entire region [44, 163]. In Great Britain, the Bristol Channel, located in its southwest region, is particularly sensitive to storm surges when depressions move slowly down St George's Channel and the Irish Sea, in addition to having winds that are mainly southwesterly [43]. The tides also play a role in the effect of storm surges on the coast, as the channel is prone to flooding especially when one of these surges occurs at high tide. This particular region is interesting as the Bristol Channel has a local funnel shape and shallow bathymetry, with an approximate quarter wavelength resonance phenomenon, which results in large tidal ranges [67]. There is nearly $80,000$ ha of low-lying land around the channel that is vulnerable to flooding [43], along with significant centres of population, which could lead to coastal flooding having a severe impact.

In recent years, there has been rising public concern around the issues of climate change, the rapid reduction of fossil fuel reserves, and increasing global needs for energy. In 2005, only about 1.3% of electricity came from renewable resources in the UK, although this was expected to increase to 15% in 2020 [128]. This requirement has resulted in a growing enthusiasm for alternative and renewable energy generation. Among options for renewable sources such as wave, tidal, wind or solar energy, a key advantage to tidal energy is that it is highly predictable relative to the other resources

[3, 61]. As such, tidal power could be a prominent consideration of renewable energy source in the UK. However, since tidal power will only be feasible in areas where there is a concentration of tidal energy, the Bristol Channel, which has the second largest tidal range in the world, can be considered as a potential candidate installation site for both tidal stream turbines [149] as well as tidal barrages [23, 88]. This latter technology is the focus of this work.

Identifying any impacts of the implementation of tidal devices on the channel before their installation is essential. In particular, the impacts on the tidal hydrodynamics will need to be understood. A key part of this will be how barrages interact with storm surges and alter the risk of coastal flooding. Barrages could have both positive or negative effects on storm surges. However, through careful design and introduction of appropriate device operation strategies, the barrage can be used for the protection, or even prevention, of surge-induced flooding in the Bristol Channel. The aim of this project is to investigate how surge-induced flooding interacts with a tidal barrage and how barrages can be designed to improve positive impacts and mitigate negative ones, when it comes to flood defence.

1.1 Tides

1.1.1 Basic Physics

The occurrence of tides can be explained by Newton's Law of gravitation [138]. Tides occur due to the response of the ocean to the gravitational force applied by the Moon and the Sun, along with some minor contribution of other celestial bodies. Pugh [138] explained the 'equilibrium theory' of the tides that assumes Earth to be a perfect sphere covered with deep water (so wave speed is not limited by depth) and is not affected by any natural gravitational rotation (i.e. the Coriolis acceleration). Compared with the actual ocean tides, the amplitude of the equilibrium tides is much smaller as the presence of the Coriolis force, the continents, the ocean bathymetry and bed friction also play a role in the ocean response. This gives rise to the so-called 'dynamic theory' of tides.

Tides can be defined as the rise and fall of the water level driven by astronomical movements [36], which also drive the frequencies of tides. Since these are predictable, so are tides. Doodson [54] analysed at what frequencies tides would be expected to occur. In practice, tides are usually dominated by only a few frequencies. Diurnal tides occur once a day with periods of around 24 hours, caused by the relative declination of the Earth with respect to the Moon and the Sun, and the tidal range

variation is determined by the declination [138]. Semi-diurnal tides occur twice a day with periods of around 12 hours, and generally with considerably greater amplitudes than the diurnal tides. The largest semi-diurnal tidal constituent is the M_2, which is the principal lunar tidal constituent. Due to the changes of alignment of the Sun and the Moon with respect to the Earth, the amplitudes of the semi-diurnal tidal constituents can vary, giving rise to the spring-neap cycle with a period of 14.8 days. At the time when the tide-generating forces from the Sun and the Moon are in phase, a spring tide occurs that magnifies the tidal amplitude, and a neap tide occurs when the two forces are in quadrature, resulting in low tidal ranges [138].

Harmonic analysis is the standard method used for tidal prediction from observed sea level and current data [138]. It can be applied to represent the tidal characteristics of a certain region. Tidal harmonic analysis is represented by a Fourier decomposition of observed tidal data into a finite number of tidal harmonic constituents over a time period. Tidal harmonic analysis fits sinusoids at frequencies based on the known astronomical movements which force the tides [54, 137]. The amplitude and phases of those components are related to various astronomical parameters, and each harmonic constituent n is described by:

$$a_n \cos(\omega_n t - \phi_n), \tag{1.1}$$

where a_n is the amplitude, ω_n is the angular speed (frequency), ϕ_n is the phase of each tidal component, and t is time. Similar expressions exist for tidal currents.

1.1.2 Tidal Hydrodynamics of the Bristol Channel

One of the largest tides in the world is observed in the Bristol Channel at Avonmouth (near the head of the channel) with a mean tidal range of 12.2 m at spring tide and 6.0 m at neap tide [87, 121, 143]. Two main mechanisms contribute to the large tidal ranges according to literature: the quarter-wavelength resonance of the channel with the occurrence of the North Atlantic tidal wave [62, 67, 138, 143], and the funnelling effect in the upper regions due to the wedge-shape of the channel [143, 158].

Systems with large-amplitude responses that are driven by oscillations close to their natural period are referred to as resonant systems [138]. Tidal resonance occurs when the basin length is about a quarter of the wavelength of the driving tidal constituent. In recent years, various authors have examined the nature of the tidal resonance in the Bristol Channel. Fong and Heaps [67] have presented a summary of

Table 1.1: Estimates of the fundamental resonance period of the Bristol Channel derived form various theoretical models. ω is the tidal forcing frequency applied at the seaward boundary of the model and ω_{M_2} is the frequency of M_2 tide. ω/ω_{M_2} is the ratio between the two.

Model	Simulation	Area Included	Fundamental period (hrs)	ω/ω_{M_2}
Heath (1981) [87]	A linear resonance model	Celtic Sea Bristol Channel Irish Sea	7.3-9.0	1.12-1.15
Liang *et al.* (2014) [109]	1D numerical model	Severn Estuary Bristol Channel	8.0-9.0	1.38-1.55
Serhadlıoğlu (2014) [149]	2D unstructured-mesh model	Celtic Sea Bristol Channel Irish Sea English Channel	10.3-11.3	1.10-1.20
Gao and Adcock (2017) [70]	2D unstructured-mesh model	Bristol Channel	8.6-10.0	1.20-1.40

significant studies that consider different domain sizes to estimate the resonance period of the Bristol Channel. Their table is extended in Table 1.1 to include some later studies. Fong and Heaps first consider the amplification of the main tidal constituents from the Atlantic continental shelf to the Celtic Sea into the channel and found that the possible resonance is dependent on both the length of the channel and the resonance period. The one-dimensional model results predict that the resonance period of the Celtic Sea is between $12.2-12.6$ hours and it is in the proximity of the M_2 period. Heath [87] presents a fitted linear model to the semi-diurnal tidal constituents and the resulting Celtic Sea resonance period is estimated to be between $10.8-11.1$ hours, while the Bristol Channel's resonance period is estimated to be $7.3-9.0$ hours. A two-dimensional model has been developed by [109] covering only the Bristol Channel and downstream regions of the River Severn. The study was carried out by varying the tidal period at the seaward boundary to drive the model. It was found that the resonance period in the channel is around 8.0 hours. The present study of resonance builds on research into resonance in the Bristol Channel by [149] (domain covers the Irish Sea, the Celtic Sea, the English Channel and the Bristol Channel) and [70] (only the Bristol Channel included). In both these studies, the models are excited with the dominant tidal component and with the varying frequency.

All of the simulation results show that the dominant semi-diurnal frequency is smaller than the natural frequency of the Bristol Channel and indicates that the basin length of the channel is shorter than the quarter wavelength needed to be perfectly

resonant. The wavelength of a shallow-water wave is given by:

$$L = \frac{2\pi\sqrt{gD}}{\omega}, \tag{1.2}$$

where g is the gravitational acceleration, D is the total water depth, and ω is the angular frequency of the tidal constituent [77]. A very simplistic analysis can be made by considering the depth and length of the system. For the Bristol Channel with an approximate water depth of 40 m and the dominant constituent of M_2 [70], the calculated wavelength should be 221 km, which is larger than the channel length of around 160 km.

1.2 Storm Surge

1.2.1 Background

Since ancient times, natural catastrophes resulting from weather conditions have taken or threatened millions of lives and caused damage to infrastructure [175, 90, 98]. Some of the most extreme weather-driven events experienced in the UK are coastal flooding events caused by low atmospheric pressure and high winds during storms. These can cause widespread flooding, destroying valuable natural habitats and causing massive economic upheaval, which can affect regions for a prolonged period. For example the most deadly natural disaster in the UK in the 20th century was the 1953 North Sea flood [98]. Currently, there are estimated to be 40 million people and $3,000$ billion dollars of property at risk globally due to coastal flooding; and these figures are expected to rise to 150 million people and $35,000$ billion dollars by 2070 [122].

It is not known accurately what effects climate change could possibly have on coastal flooding. Sea levels are likely to rise, with obvious consequences to the risk of flooding. There is some evidence, captured by flooding data in 2014, that increased storm frequency or intensity may exacerbate this phenomenon [146].

There have been significant technological advances in terms of flood prediction and mitigation, in order to reduce the risk of inundation. Two approaches may be considered: short-term warnings to mitigate and long-term construction of big structures, of which barriers are an example, to prevent disasters. Through the relevant meteorological surveys about severe storms and hurricanes, specific storm surge early warning systems exist, such as the Flooding Information Service in the UK [80]. An

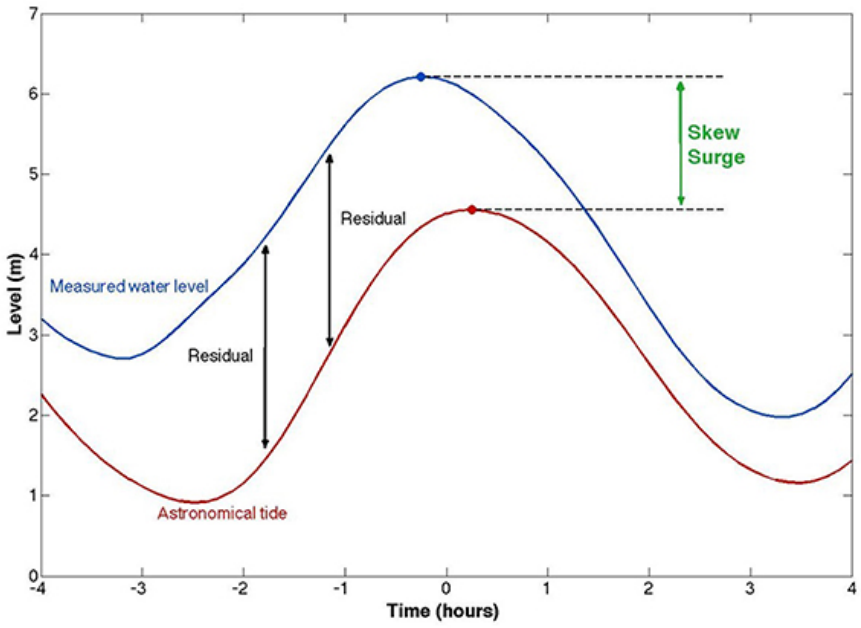

Figure 1.1: Surge residual and skew surge taken from [117].

example of a preventative measure is the construction of dams or storm surge barriers, for instance the Thames Barrier protecting London from the North Sea [90]. They are closed when the populated area is threatened by a storm surge so that the area behind the barrier can be protected. However, they require regular monitoring and possibly raising of the barrier's height to maintain flood protection [43], and the impacts on the outside ocean regions should be considered.

In the study of storm surges, the measurements of the sea level can be broken into a combination of a tidal component and a non-tidal part. The non-tidal component is called the residual, which is one representation of the storm surge. The residual is the remainder from the subtraction of the tidal prediction from total sea level observations. However, during storm surge events, a phase shift in the tidal signal may be induced due to meteorological forcing. The skew surge, another representation of the storm surge, is defined due to this phase shift, and is the absolute difference between the maximum sea level observation and the predicted tidal high water regardless of their timing within a tidal cycle, as illustrated in Figure 1.1. For analysis of storm surge return periods, Williams *et al.* [172] have argued that the skew surge is the more adequate property to describe coastal flooding, following a statistical investigation of flooding around the UK.

1.2.2 Leading-order Physics

Storm surges are generated as a result of meteorological effects on the ocean hydrodynamics, which can be divided into three components: the barometric or pressure variation effects, the wind shear stress and the wave set-up [137]. The relative importance of these varies considerably around the world. The width of the continental shelf is a simplistic driver for the relative importance. A large continental shelf will tend to increase the importance of wind shear stress as this is strongly dependent on depth (see Section 1.2.2.2).

1.2.2.1 Pressure variations

Water level is increased due to lower atmospheric pressure. A simple static analysis suggests that one can expect 1 cm of water rise from each millibar of pressure drop [13]. This inverted barometer effect is useful when considering water level predictions.

The relationship between water level and atmospheric pressure can be analysed theoretically. Under equilibrium assumptions with no current in response to an atmospheric pressure application, the pressure P in the x-direction (one dimensional for clarity) can be expressed as,

$$\frac{\partial P}{\partial x} = 0. \tag{1.3}$$

Assuming the sea water is incompressible and inviscid, the total pressure at depth z is represented by the sea level terms and the atmospheric pressure in the hydrostatic equation,

$$P_z = P_{atm} - \rho g(z - \xi), \tag{1.4}$$

where ξ is the free surface elevation above a certain datum and z is a constant variable with respect to x. The equation can be substituted into Equation 1.3, the following can be achieved:

$$\frac{\partial P_{atm}}{\partial x} + \rho g \frac{\partial \xi}{\partial x} = 0. \tag{1.5}$$

This can be integrated over x to give:

$$P_{atm} + \rho g \xi = constant. \tag{1.6}$$

For local pressure variation over the ocean, the changes of the water level can be found:

$$\Delta\xi = -\frac{\Delta P_{atm}}{\rho g}. \tag{1.7}$$

Over a typical year, atmospheric pressure varies from 980 mb to 1,030 mb. Using the Standard Atmospheric pressure of 1,013 mb, the range of changing sea level predicted is +0.33 m and −0.17 m.

However, there is also a dynamic response of the shallow water to the movement of the atmospheric pressure. When the speed of the travelling atmospheric disturbance is close to the typical water wave velocity, the Proudman resonance exists [20]. Following the simplified analysis in Pugh [138], the response can be written as:

$$Dynamic\,sea\,level\,response = \frac{static\,sea\,level\,response}{(1 - {C_A}^2/gD)}, \tag{1.8}$$

where C_A is the disturbance speed and D is the water depth. The response is amplified as the disturbance speed increases and becomes infinite when the speed of disturbance and shallow-water celerity are equal. Extra care should be taken when considering the shallow-water regions and high-speed pressure tracks. However, in real situations, this resonance can be damped by friction and typically storms move significantly slower than the wave speed $\sqrt{gD}$.

1.2.2.2 Wind shear

The major factor contributing to storm surge events is the wind effects on a variety of scales. Generally, the water level will rise in the direction in which the wind is blowing, as the water level is increased by the shear force of the wind on the water. There exists a drag force or stress on the sea surface due to the wind, which depends on the wind speed W and air density ρ_a. Using a dimensionless drag coefficient C_d between the wind and the water surface, the stress can be expressed as:

$$\tau_W = C_d \rho_a W^2. \tag{1.9}$$

This equation can be used to model storm surge in a depth-averaged model. The value of C_d is usually taken to depend on the 10-m, 10-minute-averaged wind speed (W_{10}). Increases of wind speed and the resulting coefficient account for the increased surface roughness, with response of the rising water level. The drag coefficient is calculated using an empirical correlation and using different coefficients can make a notable difference to model predictions. Details can be seen in [34]. There are

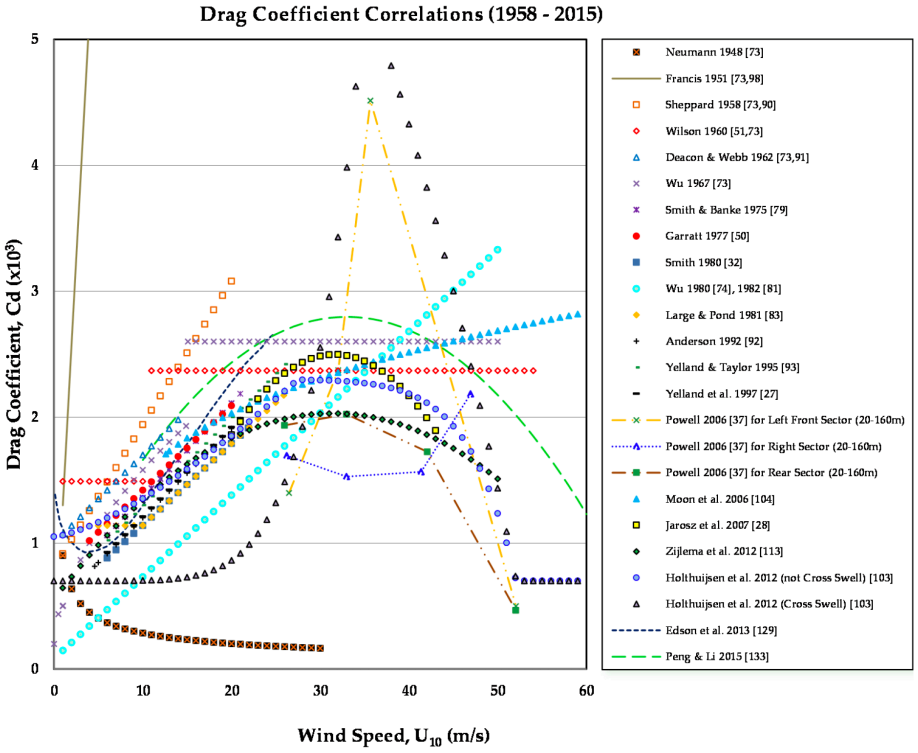

Figure 1.2: Drag coefficient correlations (1958-2015) taken from [34]. The variable U_{10} in the x-axis label is represented by W_{10} in this thesis.

various drag coefficient correlations with respect to varying wind speed as shown in Figure 1.2 [34]. The commonly accepted value for C_d is given by Garratt as: $C_d \times 10^3 = 0.75 + 0.067 \times W_{10}$. This correlation was derived from the data from 1967 to 1975 and has been widely applied in many models, including the ADCIRC simulations [160]. However, the most suitable drag coefficient may differ depending on the project.

A simplistic understanding of wind shear can be deduced from the simple model given in Pugh [138]. The steady-state effect of the wind stress on the water surface for a constant depth is found as an equivalence between the pressure P and total stress F:

$$\frac{\partial P}{\partial x} = \frac{\partial F}{\partial z}. \tag{1.10}$$

The depth-integrated wind stress can then be derived by integrating between the water surface and the sea bed:

$$\frac{1}{D}\int_{-D}^{0} \frac{\partial F}{\partial z} dz = \frac{1}{D}\left(F_s - F_b\right) \tag{1.11}$$

where F_s and F_b are respectively the surface and bottom stress, and D is total water level. By considering the Hydrostatic Equation, see Equation 1.4, the relationship of stress and water height is:

$$\frac{\partial \xi}{\partial x} = \frac{F_s - F_b}{g\rho D}. \tag{1.12}$$

Neglecting the bottom friction as there is no velocity at steady state, the effects of winds on the changes of surface elevation can be expressed as:

$$\frac{\partial \xi}{\partial x} = \frac{C_d \rho_a W^2}{g\rho D}. \tag{1.13}$$

From the non-linear relationship between the risen water height and the wind speed, the effect of wind stress on water levels increases inversely with the water depth and is a function of the square of wind speed. This shows that areas with long shallow shelves are likely to be particularly susceptible to storm surges.

1.2.2.3 Wave set-up

The water level can also be increased due to the phenomenon of wave breaking, which occurs because of the existence of excess flow of momentum in onshore waves when approaching the shore [138]. The horizontal changes of the (wave-induced) radiation stress leads the incoming waves to exceed the retreating waves, which results in the corresponding water accumulation [110]. The wave set-up is dependent on the bathymetric profile in the path of the storm and is an active participant in generating hurricane storm surge [165]. For instance, the study on the storm surge in Tosa Bay during Typhoon Anita (1970) demonstrated that the radiation stress contributed up to 40% of the maximum sea level rise during the event [100].

However, in the UK, effects of wave set-up are relatively small, as shown in the work of Wolf [175], who analysed the amount of wave set-up during UK storms. The current study will consider the major possible contributions to surge-induced flooding in the Bristol Channel. Typically wave set-up contributes to the water level increment near coastlines, thus its consequence for barrage structures remains unclear and would increase the complexity of the problem. Including such effects in this study would be trivial and would require additional assumptions. As such, the wave set-up will not be explicitly modelled in this thesis. This is consistent with other recent work such as [164].

1.2.3 Storm Surge in the Bristol Channel

The Bristol Channel is an area easily susceptible to storm surge events. It is in a location where the prevailing wind is towards the head of the channel in a region where winds can be strong. The funnel shape of the channel will tend to increase water levels near the head of the channel and the shallow water will, as described in Section 1.2.2.2, give large surges. Furthermore, the region is surrounded by some low-lying land, notably the Somerset levels. Based solely on this, it would be expected that the region would be exceptionally prone to severe surge events.

However, the likelihood of serious flooding events is complicated by the nature of extreme tidal ranges. In an area like the Bristol Channel where tidal ranges can be extreme, the occurrence of a storm surge coinciding with lower tides will not cause severe flooding as the total water level in such a situation would be lower than that of the extreme tides. For the port of Avonmouth, water levels are only within 1.5 m of the HAT (the highest astronomical tide) for 2.1% of the year (calculated from the field-measurements). From these data it can be deduced that flooding is unlikely to occur for 97.9% of the time as its occurrence is dependent on the coincidence of a severe storm with extreme (spring) tides. In addition, [70] found that the most severe meteorological conditions occurred in winter seasons whereas the highest tides occur at the equinoxes in spring and autumn. Thus, it is even rarer for an event to take place which actually causes flooding. However, if spring tides and meteorological events do coincide then there is the possibility of considerable flooding.

1.2.3.1 Past events

Substantial damage has been caused due to surge-induced flooding. Possibly the most devastating natural disaster in recorded UK history was the flooding of the Bristol Channel in 1607. It is estimated that this event resulted in the death of more than $2,000$ people, and the floods covered 200 mi^2 sweeping away entire villages. The economic damage has been estimated to be the equivalent of between 7 and 13 billion Pounds in modern money [91, 142]. The event occurred at spring tide. Accounts from the time mostly suggest a low-pressure system along with extreme winds, which would have caused a storm surge at this location [71]. Another UK record of a devastating storm surge, though not at the Bristol Channel, occurred in the winter of 1953. This particular storm caused the tidal surge to locally exceed 5.6 m and claimed over 300 deaths in southeast England [123, 176]. Specifically at Avonmouth, where water levels have been scientifically measured for 102 years, the worst recorded

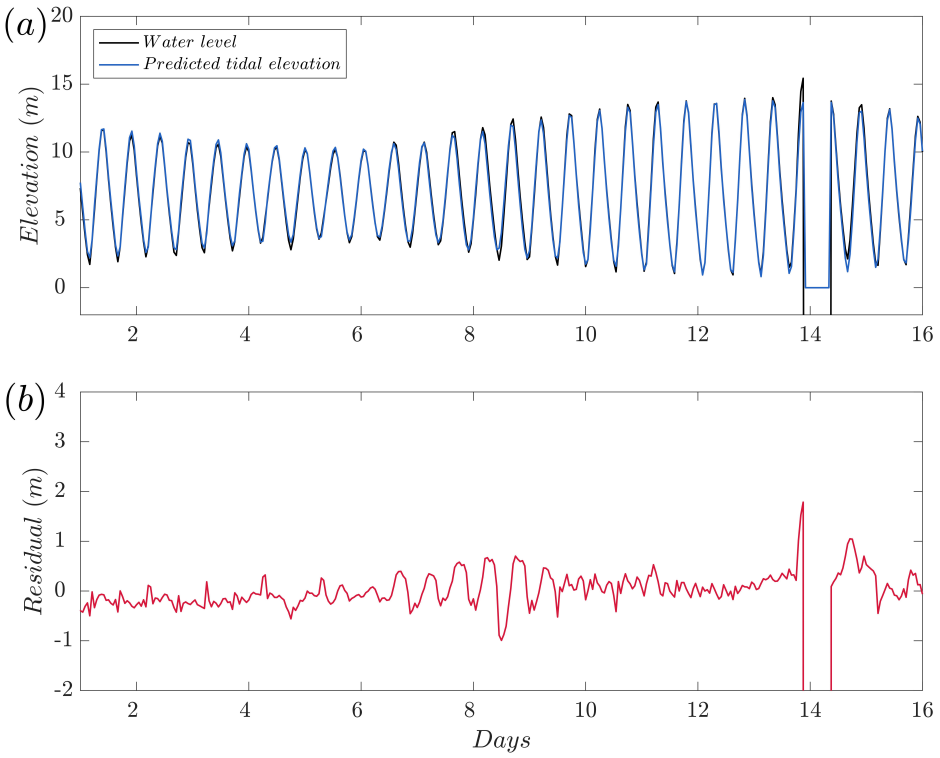

Figure 1.3: Water level at Avonmouth during the 1981 events, field measurement is obtained from BODC.

event occurred on 13 December 1981. Figure 1.3 shows the measured water levels at the time at Avonmouth, along with the predicted tidal elevation (i.e. what the water level would have been without atmospheric forcing). Prior to the sensor failure, the surge can be observed to be at least 1.8 m high. The event resulted in severe flooding along the south side of the channel [83, 173].

Gao [70] used historical data to analyse the storm surge residual based on its return period (T, in years) at various stations along the Bristol Channel. Her extreme value analysis predicted lower residual levels further from the head of the channel. For example, at Avonmouth, the residual for $T = 10$ and $T = 50$ were 2.47 m and 2.97 m respectively. Whereas, at Ilfracombe, the $T = 10$ and $T = 50$ values of the residual were 1.38 m and 1.70 m.

1.2.3.2 Weather pattern in historical storm surge events in the Bristol Channel

The characteristics of storm surge events can be examined from water level measurements and meteorological hindcasts from the ERA5 dataset [50]. The five most extreme storm surge events are summarised in Table 1.2. All have surge heights

Table 1.2: Five most severe storm surge events in the Bristol Channel: surge measurements obtained from field measurements and meteorological input from the ERA5 dataset (the events with a surge over 1 m).

Date and Duration	Surge Measurement		Meteorological Condition			
	Locations Affected	Max Surge (m)	Time	Wind Speed (m/s)	Wind Direction	Surface Pressure (kPa)
25/01/90	Avonmouth	2.91	0600	17.82	SW	98.03
0900-1600	Ilfracombe	1.51	1200	21.58	W	96.90
7 hrs	/	/	1800	14.98	W	98.84
19/01/95	Avonmouth	2.58	0600	9.81	SSW	99.60
1315-1745	Newport	2.54	1200	15.62	W	97.90
4.5 hrs	Hinkley Point	1.83	1800	9.79	WSW	98.72
04/01/98	Avonmouth	2.91	0600	14.40	S	98.92
1000-1815	Newport	2.45	1200	20.99	WSW	97.55
8.25 hrs	Hinkley Point	2.21	1800	16.55	W	99.03
13/12/00	Avonmouth	2.53	0000	22.17	WSW	99.46
0000-0345	Newport	2.31	0600	14.34	WSW	100.29
3.75 hrs	Hinkley Point	1.99	1200	16.60	WSW	100.35
12/02/14	Newport	2.29	0600	12.56	SSW	99.43
1115-1715	Hinkley Point	1.90	1200	21.06	SE	97.88
6 hrs	Ilfracombe	1.46	1800	16.57	WSW	98.42

larger than 1 m. From the Table, it can be concluded that extreme storm surge events in the Bristol Channel last around $4 - 8$ hours, and their surge heights are site-dependent with worse surges experienced at the channel head (e.g. Avonmouth) than mid-channel region. Except for the event that occurred in the year 1995, for the remaining four storm surge events, the maximum wind speeds, larger than 20 m/s, coincide with annual or seasonally maximum wind speed during the year. These surges tend to happen when high winds come from the southwestern and western directions. Considering the atmospheric pressure, each extreme surge event is associated with low atmospheric pressure relative to the mean sea level pressure of 101.33 kPa.

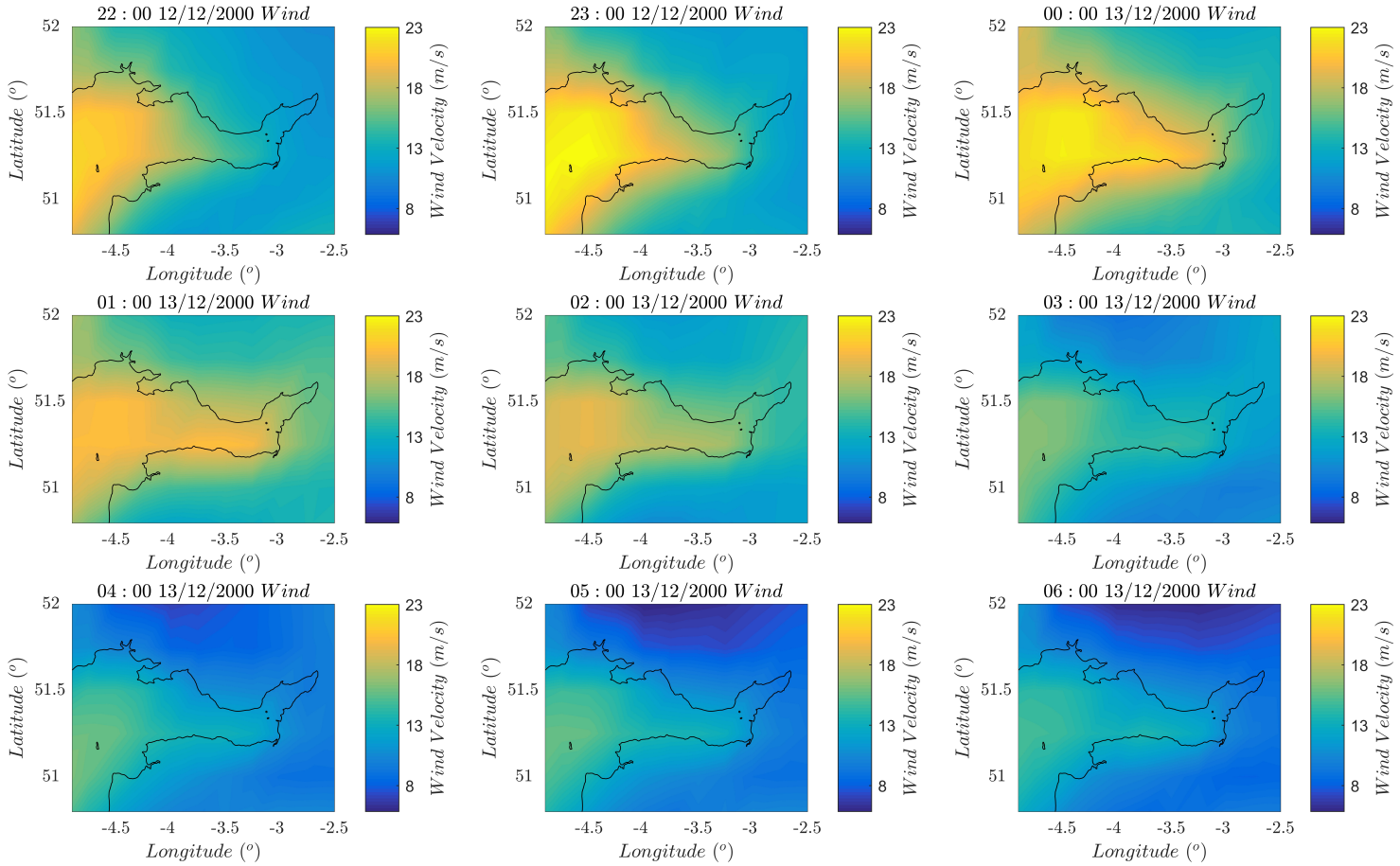

Figure 1.4: Wind conditions (wind velocity in m/s) in Bristol Channel for the storm surge event on 13 December 2000 from ERA5 dataset.

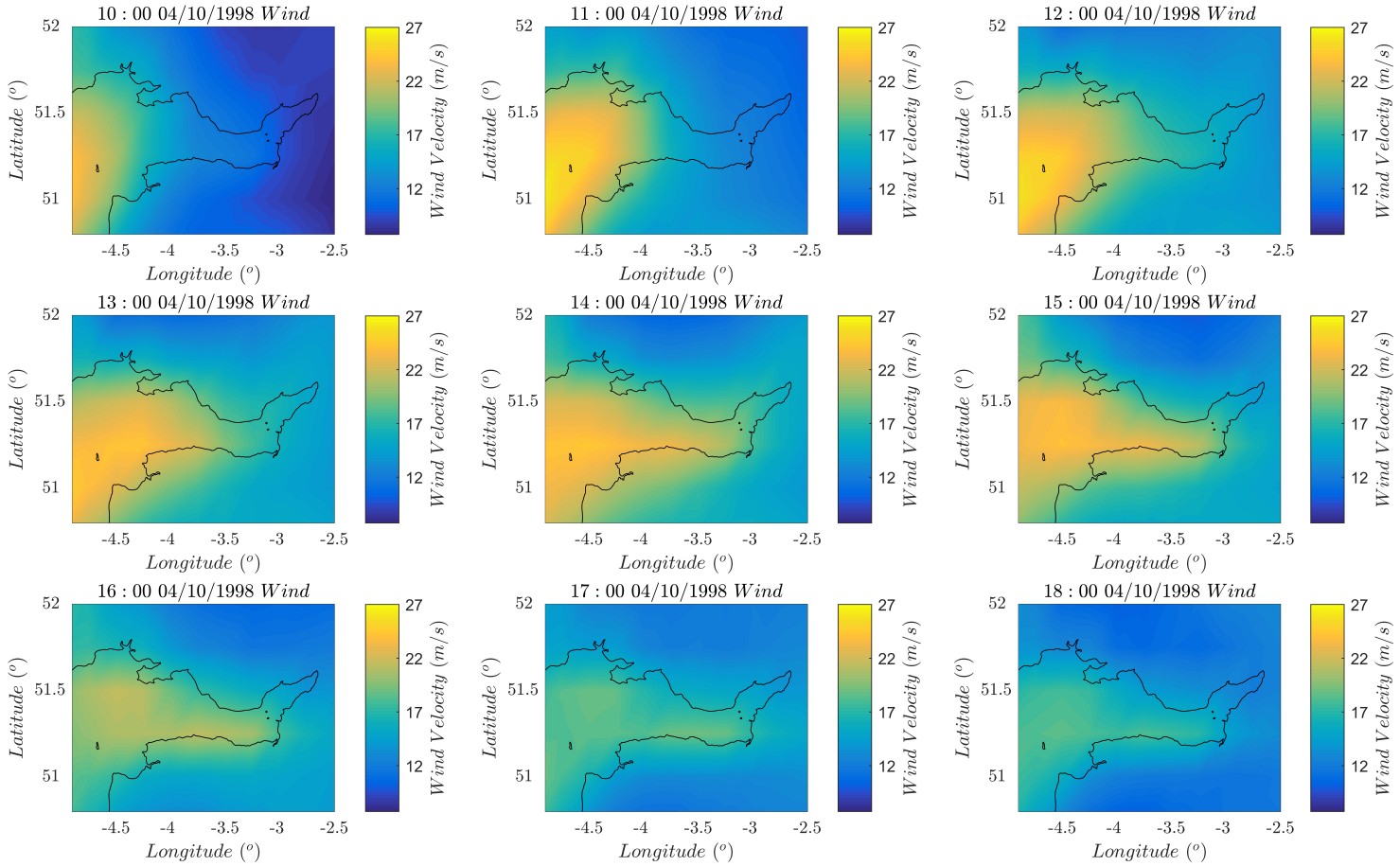

Figure 1.5: Wind conditions (wind velocity in m/s) in Bristol Channel for the storm surge event on 4 October 1998 from ERA5 dataset.

1.2.3.3 Relationship between meteorological inputs and surge height in the Bristol Channel

To understand the leading-order characteristics of storm surges in the Bristol Channel, analysis is carried out on two extreme storm surge events in the year 2000 and 1998. The objective is to identify what weather systems lead to storm surges in the Bristol Channel region.

The wind speed is calculated from its components in the x- and y-directions from ERA5. The detailed wind speed pattern of the events, including that prior, during and after the surge peak time, is shown in Figure 1.4 and 1.5 for the two events. The wind details for the remaining three extreme events, as shown in Table 1.2, are given in Appendix B.

For the storm in the year 2000, as shown in Table 1.2, the surge event happened between 00:00 and 03:45 on 13 December. From Figure 1.4, the pattern with wind speed higher than 20 m/s can be observed from 22:00 on 12 December to 02:00 on 13 December. The magnitude and spatial extent of the high wind speed builds up until the peak of the surge and returns to normal afterwards with the speed of $10 - 15$m/s. The maximum wind speed of around 23 m/s occurred at 00:00 at the entrance region of the channel, and the largest averaged wind speed over the channel also happened at peak surge time. The large wind stress at the location of approximately 51.3°N 4.5°W, which would be generated by the high wind speed around the channel entrance, would lead to the accumulated high water level approaching the head of the channel due to its funnel effect. Similar conclusions can be drawn from the storm surge event in 1998. Larger wind speeds can be observed during this event compared to those in the year 2000. The pattern of the wind speed larger than 20 m/s can be observed over all times shown in Figure 1.5. The largest wind speed of about 27 m/s happened at 12:00 on 4 October at the location of approximately 51°N 5°W. Along with the consideration of the wind pattern of other storm surge events (see Appendix B), this suggests that, for a significant storm surge to occur, wind speeds should exceed 20 m/s with the highest wind speeds in the storm near the channel entrance.

Detailed wind direction patterns in the Bristol Channel will be investigated here by first looking at the wind direction at the event peak throughout the channel region. Figures 1.6 and 1.7 show the wind velocity information at the peak of the surge events in the year 2000 and 1998, respectively. Generally, both events show the dominant wind direction of southwest over the whole channel during the event.

In order to get a preliminary understanding of the impact of the wind conditions on surge residual levels in the region, simulations are run using the two-dimensional

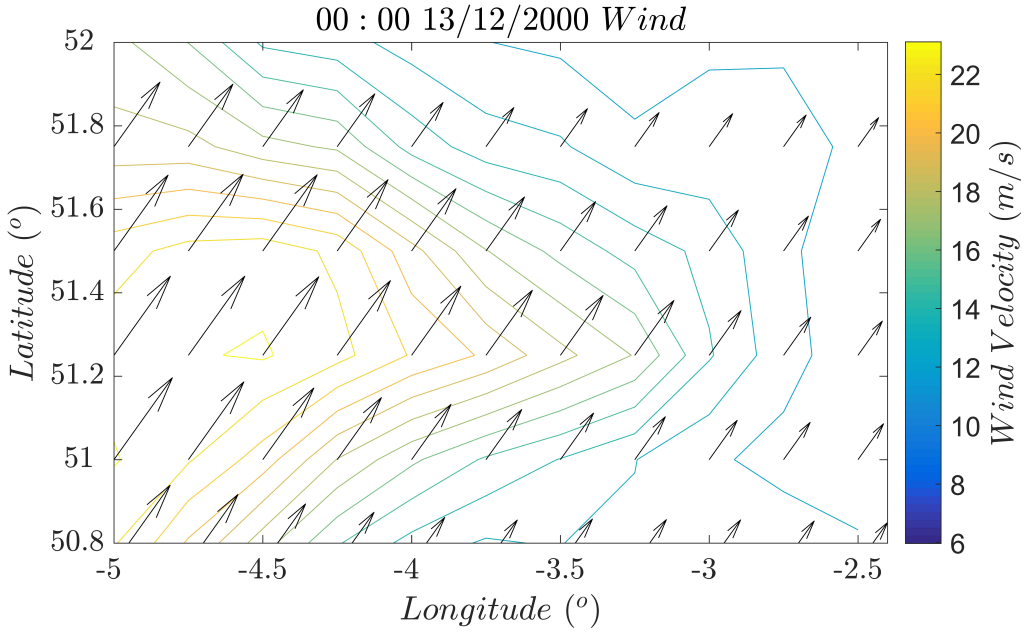

Figure 1.6: Wind direction and velocity (m/s) in Bristol Channel at the time of storm surge event on 13 December 2000 from ERA5 dataset. The contour shows the wind speed through the channel.

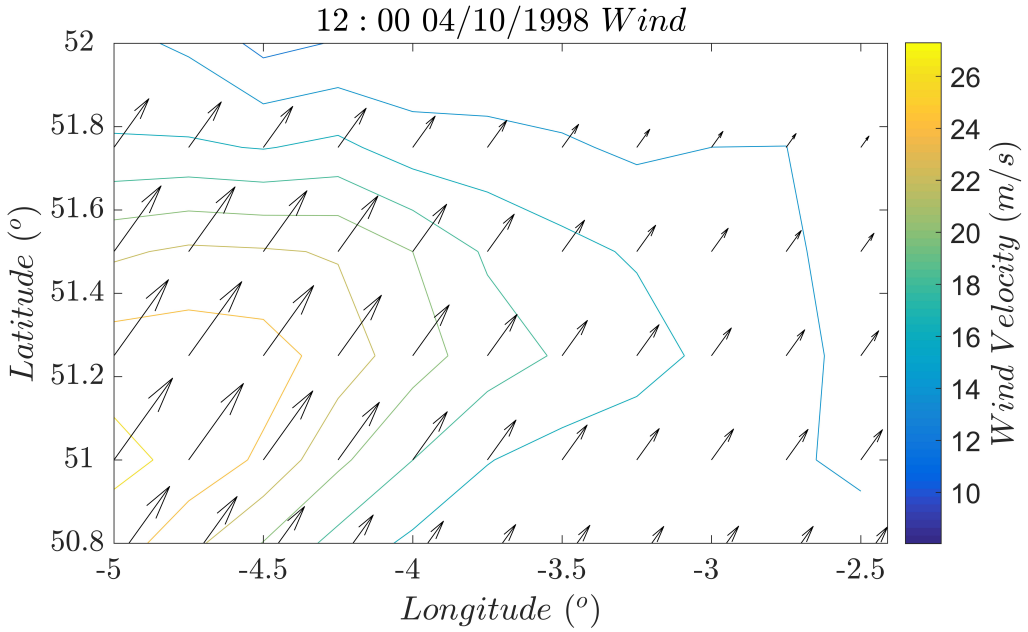

Figure 1.7: Wind direction and velocity (m/s) in Bristol Channel at the time of storm surge event on 4 October 1998 from ERA5 dataset. The contour shows the wind speed through the channel.

model developed in Chapter 2, where more details will be introduced. Only simplified scenarios are simulated here in order to investigate wind conditions at a high level. Simulations are run with a constant wind speed of 30 m/s from five different directions: north, northwest, south, southwest and west. Other wind directions are unlikely to cause positive surges in the Bristol Channel region. No astronomical tides are included in the simulations. The simulation are run for a total seven days period and the wind is increased linearly from 0 m/s to 30 m/s from 00:00 to 12:00 on day 3, kept constant afterwards for 24 hours until 12:00 of day 4, and then linearly decreased to 0 m/s. Only surge residuals are investigated in this artificial surge event and the results are shown at different measurement stations: Avonmouth (51°31'N 2°44'W), Flat Holm (51°23'N 3°05'W), Hinkley Point (51°12'N 3°8'W) and Ilfracombe (51°12'N 4°7'W). It is seen in Figure 1.8 that for all stations, when the wind comes from northerly and northwesterly directions, negative storm surges occur. When southerly, southwesterly and westerly winds occur, significant positive storm surge events result. It takes around one day for the water level to become zero at the end of day 4. For all three stations at the head of the channel (i.e. Avonmouth, Flat Holm and Hinkley Point), Avonmouth experiences the largest residual level and the peak reaches to 2.46 m when there is a westerly wind. Southerly and southwesterly winds lead to slightly lower residual levels and the southerly wind causes some lag of the residual peak. For the Ilfracombe station near the middle of the channel, the residual level is the lowest among the four stations during the artificial event, with a peak of around 1.21 m when winds come from the southern direction. The southwesterly and westerly winds give lower residual levels at that station.

The most severe wind direction is slightly different in the mid-channel region compared to the head of the channel. In the mid-channel region, a southerly wind produces the worst surge; for the head of the channel, the most severe surge is due to winds from the south and southwest. This is presumably due to the mid-channel residual levels being primarily driven by the wind from the Celtic Sea. However, local forcing within the channel has more of an influence further up the channel.

The depressions that are associated with severe winds can lead to more severe surge events. The atmospheric pressure condition during the storm surge event in the year 2000 is shown in Figure 1.9. From the Figure, it can be seen that generally the pressure over the channel decreases when approaching the storm surge event (around 00:00 13 December), then returning to normal levels afterwards. The lowest atmospheric pressure can be observed at the head of the channel during the storm

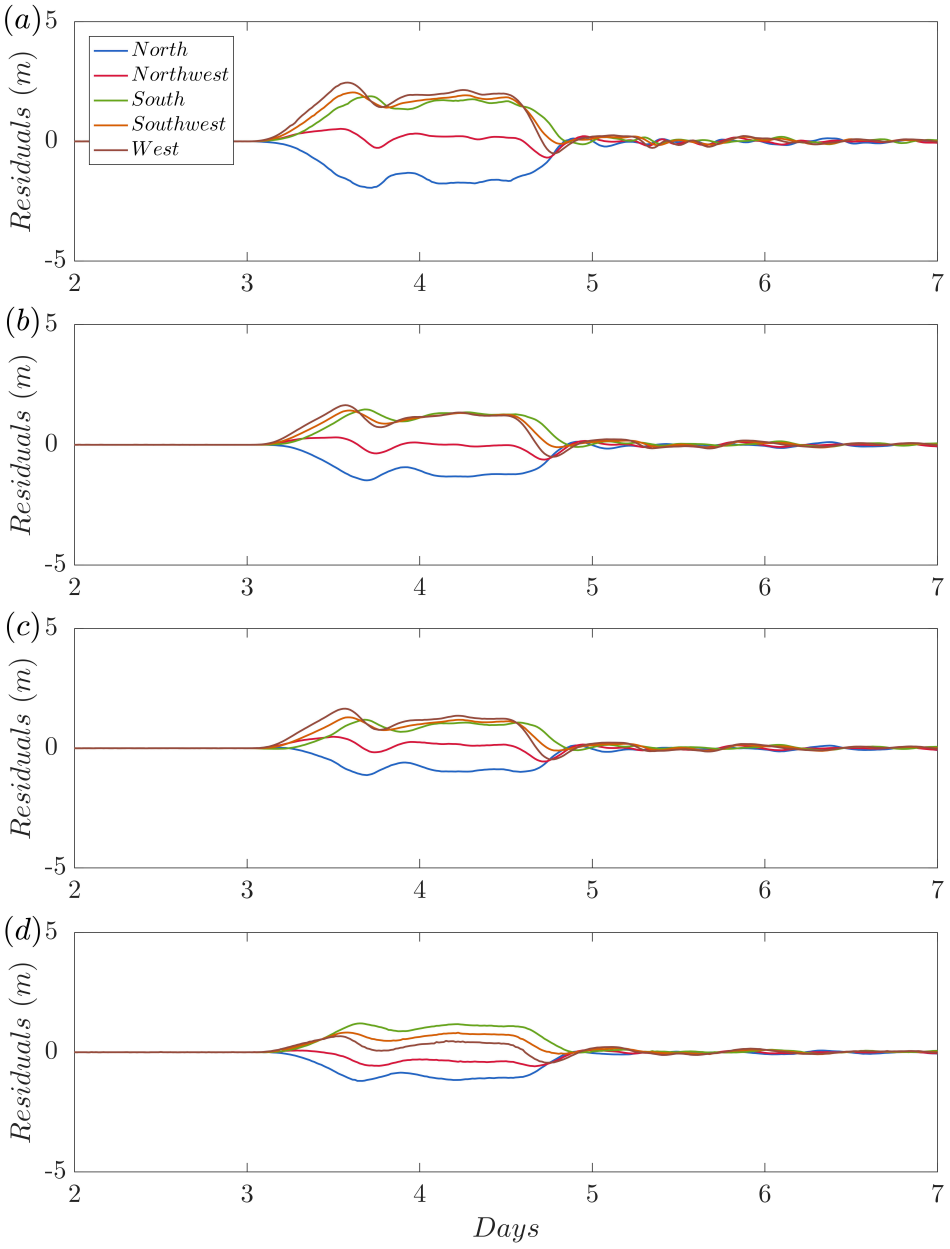

Figure 1.8: Simulated residual results of the artificial storm surge event with different wind directions at several measurement stations: a) Avonmouth; b) Flat Holm; c) Hinkley Point; d) Ilfracombe.

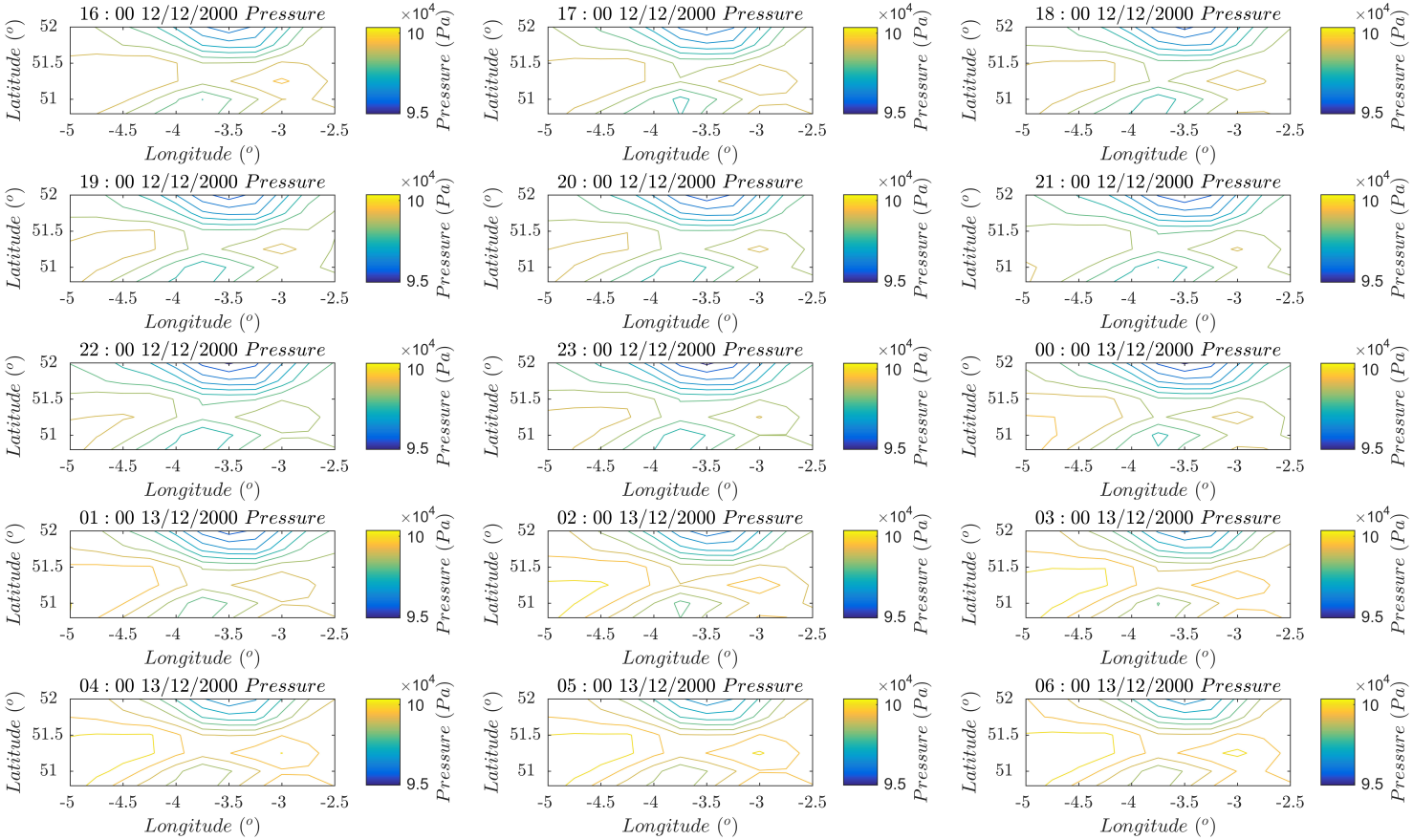

Figure 1.9: Atmospheric pressure conditions (Pa) in Bristol Channel for the storm surge event on 13/12/2000 from ERA5 dataset.

surge event of about 98 kPa. However, pressure appears to be a secondary factor in inducing surges compared to wind stress for the Bristol Channel.

1.3 Numerical Modelling of Tides and Storm Surges

1.3.1 Shallow Water Equations

In unstratified estuarine and coastal waters, the shallow water equations can be time-marched to model the hydrodynamic processes of the longitudinal variations of the free surface and velocity of water. Based on the assumption of a large ratio between the wavelength and water depth, as well as a negligible vertical velocity, the three-dimensional reality can be simplified by depth-integration into a two-dimensional problem [48]. It is assumed that the water is incompressible and pressures are hydrostatic and, neglecting diffusion of momentum due to turbulence. The depth-integrated equations of mass and momentum conservation (including terms necessary to model ocean-scale processes) are shown as follows [138]:

$$\begin{aligned}
&\frac{\partial \xi}{\partial t} + \frac{\partial (Du)}{\partial x} + \frac{\partial (Dv)}{\partial y} = 0, \\
&\frac{\partial u}{\partial t} + v\frac{\partial u}{\partial y} + u\frac{\partial u}{\partial x} - fv = -\frac{\partial \Omega_g}{\partial x} - \frac{1}{\rho}\left(\frac{\partial P}{\partial x} - \frac{\partial F}{\partial z}\right), \\
&\frac{\partial v}{\partial t} + u\frac{\partial v}{\partial x} + v\frac{\partial v}{\partial y} + fu = -\frac{\partial \Omega_g}{\partial y} - \frac{1}{\rho}\left(\frac{\partial P}{\partial y} - \frac{\partial G}{\partial z}\right),
\end{aligned} \tag{1.14}$$

where ξ represents the free surface elevation above a certain datum, D is the total water depth of the water column, which is equivalent to the sum of the free water elevation ξ and the bathymetric depth, u and v are depth-averaged horizontal velocities in the x- and y-directions, $f = 2\Omega \sin \Phi$ is the Coriolis parameter, $\Omega = 2\pi$ rad/day is the angular speed of the Earth and Φ is the latitude of the location of interest, $-\frac{\partial \Omega_g}{\partial x}$ and $-\frac{\partial \Omega_g}{\partial y}$ represent the tidal gravitational potential in the x- and y-directions, P is the atmospheric pressure, F is the total stress in the positive x-direction and G is in the y-direction. The direct effects of the tide-generating forces, barometric forcing as well as the stress forcing are considered and included in the right-hand side of the momentum equation. Stress can be applied as the combination of the surface wind stresses τ_{Wx} and τ_{Wy}, and the bottom friction stresses τ_{Bx} and τ_{By}. In terms of a conventional quadratic law, the friction (e.g. x-direction) can be parameterized as [57]:

$$\tau_{Bx} = C_f \rho u (u^2 + v^2)^{1/2}, \tag{1.15}$$

where C_f is the bottom friction coefficient. Together with the hydrostatic equation and the surface wind stress expression as introduced in Section 1.2.2, the mass and momentum equations have been widely used to describe the ocean's physical response to the tides and the meteorological forces (i.e. storm surge).

The solutions to these governing equations are forced by the boundary conditions. Tidal forcing is specified at the open boundaries, which is the sum of the major tidal constituents (such as M_2 and S_2). Each tidal constituent, ξ_{Tn}, at the boundary can be expressed as a time series,

$$\xi_{Tn} = a_n \cos(\omega_n t - \phi_n). \tag{1.16}$$

Here, a_n and ϕ_n are the amplitude and phase of the corresponding tidal constituents [97, 156].

The two-dimensional scenario can be integrated across the width of the channel to produce the one-dimensional shallow water equations or Saint-Venant Equations. These assume uniform velocity across any singular cross-section of the channel [48]. For a rectangular channel, the one-dimensional sectionally averaged and linearized continuity and momentum equations are given by:

$$\begin{aligned} \frac{\partial \xi}{\partial t} &= -\frac{1}{B}\frac{\partial AU}{\partial x}, \\ \frac{\partial U}{\partial t} &= -g\frac{\partial \xi}{\partial x} - \frac{C_f U|U|}{(D+\xi)} - U\frac{\partial U}{\partial x}, \end{aligned} \tag{1.17}$$

where U is the cross-sectionally averaged velocity of the flow, measured positively towards the head of the channel, ξ is the free surface elevation above mean sea level, B is the channel width, A is the cross-sectional area of the channel, g is the gravitational acceleration, C_f is the drag coefficient of the channel bottom, and x is the distance from the open sea boundary [121]. The friction and advective acceleration are included in the equation of motion, while the small value of surface elevation is ignored in the area calculation in the equation of continuity in this analysis.

The one-dimensional model is computationally cheaper than a two-dimensional model and also saves cost in terms of data collection. It is only applicable in cases where simple predictions of the main hydrodynamic features are required [16, 143]. As suggested by Adcock *et al.* [3], the one-dimensional model is an appropriate option for the investigation of estuary-type sites. A detailed comparison of the one-dimensional and two-dimensional numerical models of the Bristol Channel will be presented in this thesis in Chapter 5.

There are a variety of approaches to solving the shallow water equations, such as the finite difference method [151], the finite volume method [107], and the discontinuous Galerkin (DG) method [148]. Whilst each of the different methods have their own advantages and disadvantages, the key difficulty is not usually solving the equations but handling the boundary conditions (for instance, dealing with wetting and drying).

In this project, the two-dimensional DG shallow water equation model (DG-SWEM), that utilises the DG finite element method, is applied to solve the fully nonlinear form of the shallow water equations numerically through the use of generalised wave continuity equation (GWCE) formulation [103]. The code is based on the advanced circulation (ADCIRC) model, which has been used extensively to model ocean hydrodynamics [39, 167]. The DG-SWEM itself has been applied for simulations of tides and storm surges [119]. The choice of DG-SWEM for the present work is due to its excellent scaling properties when run in parallel [104]. The model has been thoroughly verified by Serhadlıoğlu [149]. The basic mesh and setup have been taken from models previously developed by Serhadlıoğlu (discussed further in Chapter 2), although it has not been previously used for the study of storm surges.

1.3.2 Meteorological Datasets for Numerical Modelling of Storm Surges

The numerical model can be forced using meteorological data, wind velocity and pressure variation from hindcasts as inputs for the storm surge simulations. As discussed in Section 1.2.2.3, the forcing from radiation stress from the waves is neglected as this is expected to be relatively small in the Bristol Channel region. Three meteorological datasets are considered: ERA-Interim and ERA5 reanalysis data from the European Centre for Medium-Range Weather Forcasts (ECWMF), and Met Éireann Re-Analysis (MÉRA) data for climate analysis. Parameters of wind speed at 10 m height (W_x and W_y) and surface pressure are taken from datasets as the storm surge inputs for the model. The three datasets show the results of a global climate reanalysis and cover different periods of time. Generally, ERA5 has much higher spatial and temporal resolution than ERA-Interim (other detailed information about the datasets can be found in [58]). ERA5 is expected to have much better results but both are included here to help understand the sensitivity of the model to the resolution of the meteorological data. MÉRA is the newest dataset of the three and has higher resolution (for Ireland) in comparison with the reanalysis data of ECWMF, particularly

Table 1.3: Differences between ERA-Interim dataset, ERA5 dataset and MÉRA dataset [58].

	ERA-Interim dataset	ERA5 dataset	MÉRA dataset
Period covered	1979 - present	1950 - present	1983 - present
Spatial resolution	79 km globally	31 km globally	2.5 km Ireland
Temporal resolution	6-hourly field	Hourly field	3-hourly field

for surface wind data [59]. Table 1.3 highlights major differences between the ERA-Interim, ERA5 and MÉRA datasets that are of interest to this project. Comparisons of the simulation performance of these three datasets will be made in Chapter 2.

1.3.3 Coastal Flooding Modelling

Coastal flooding or inundation is a globally significant hazard that can have huge environmental, economic and social impacts on coastal regions. Evaluation of coastal flooding risk is an essential requirement in hazard management [144, 18]. In recent years, there has been considerable progress in the development of coastal flood modelling, along with the risk assessment of coastal inundation [159, 18]. There are two main categories of coastal flooding modelling methods: deterministic and probabilistic modelling.

Deterministic models assume that the flooding is a result of a direct relationship between the geophysical hazard process and the terrain, without consideration of any uncertainties or randomness [84]. This makes deterministic models useful when predicting coastal flooding given certain inputs [51, 68, 159]. The outputs of the models can then be utilised along with geographic information systems (GIS) to create hazard layers that depict flooding exposure, such as the process of flood inundation mapping. Socioeconomic data can be applied to assess the flooding exposure in a populated area and the sensitivity to specific flooding hazards can then be evaluated [68, 42, 177]. Deterministic models are therefore useful for flooding identification and exposure, as well as the development of flooding mitigation methods, but they are limited in application as only certain scenarios are considered which may lead to important phenomena being missed [84]. Further, no flooding risk can be calculated.

To calculate risk, probabilistic models are required, as they provide a probabilistic distribution of flooding events and give more information about the range of risk. Such models can examine the uncertainty of the input data through the evaluation

of many thousands of model simulations [18] and account for extreme statistics and event dependence [69]. As such, probabilistic models can be applied to target flooding mitigation in areas of higher risk rather than all exposed areas susceptible to flooding [38, 102, 159]. However, probabilistic coastal flooding models are computationally expensive and only individual coastal flooding impacts are simulated at one time [159, 76]. Another drawback is that a long history of flood records is a requirement as input to the model [118] or to provide crucial validation. Recently, several studies have been carried out to combine the two types of flooding modelling methods to produce a more complete method of flooding modelling and the associated risk assessments [51, 94].

This project applies deterministic models to simulate coastal flooding that are induced by storm surges, by which the impact of flooding can be evaluated. The metric of flooding risk will not be calculated in this project. The mechanisms of storm surge-induced flooding in the Bristol Channel have been examined in Section 1.2.3. Severe storm surge events in the Bristol Channel will be simulated.

Several deterministic models have been used in the literature to predict storm surge events. It is standard practice to use numerical models that solve the shallow water equations (see [149]) to evaluate sea surface elevations due to tides and storm surges. The first recorded storm surge model, SPLASH, was developed by Jelesnianski [96] for surge amplitude evaluation. Following this, SLOSH was a finite difference model established for the simulation of coastal flooding and storm surge [76]. After these early models, many others have been established including the ADCIRC model which utilises an unstructured finite element mesh within the domain for simulation of tides and surges [167]. In recent years, due to the more severe surge-induced flooding along with sea level rise and global warming, there is increased interest in storm surge research, and a wide range of storm surge numerical models are currently under development in the UK [73]. The most relevant ones with respect to the Bristol Channel are discussed in detail here, summarised in Table 1.4.

In 1962, Brewer [31] used a physical model for investigating the interactions between tides and storm surges. Then in 1963, the meteorological patterns contributing to major storm surges on the west coastline of the British Isles were identified by [154], and the Lennon's criterion for meteorological patterns of wind directions contributing to storm surges was applied for further research in the Bristol Channel [65, 162]. Based on numerical finite difference models, a new storm surge prediction model was developed in 1976 used by the UK Meteorological Office [62]. As shown in the Table, both the Continental Shelf Sea Model (CSM) and West Coast Sea Model

Table 1.4: Past numerical models of storm surges for the Bristol Channel.

References	**Surge Simulation Model**	**Comments**
Flather (1979) [63]	Numerical sea model: Continental Shelf Sea Model (CSM)	Less accuracy on the western coastline of the UK
Flather (1981) [64]	Higher resolution sea model: West Coast Sea Model (WCM)	Improved simulation results compared to CSM
Proctor and Flather (1989) [136]	Higher resolution numerical atmospheric model by the Meteorological Office	Improvement of storm surge forecast; Less accuracy in prediction of the secondary depression
Flather *et al.* (1998) [66]	2-D tidal-surge model for the northwest European continental shelf	Good representation of surges on shelf and applicable for UK flood warning; Less accuracy in the regions with coarse model resolution
Williams and Horsburgh (2013) [171]	Operational Surge model at POL (CS3X), BCM and SRM models are applied for prediction of the five largest storm surges in Bristol Channel from 2008-2012	Systematic comparisons of different models and BCM has the best performance overall
O'Neil *et al.* (2016) [124]	2-D depth-averaged tidal NEMO-surge configuration by the Met Office and the National Oceanographic Centre	Good harmonic tidal constituents' analysis in UK Class A tidal gauges

(WCM) were then developed for the prediction of the 1981 Bristol Channel floods, but no obvious flooding can be observed from the simulation. Flather *et al.* [65] concluded that the accuracy of the meteorological data input or their interpolation over the simulation period, as well as the reliability of the gauge measurements, led to the model inaccuracies and needed to be considered for efficient surge evaluation. Then in 2012, Williams *et al.* [173] examined and reanalysed the 1981 storm surge event in the Bristol Channel using the Bristol Channel Model (BCM) and Severn River Model (SRM) with reliable meteorological forcing inputs that include the surface pressure and the 10 m wind speed in both x- and y-directions within the domain, from ERA-Interim hindcast.

Coastal flooding events derive from the combination of extreme tides, storm surge and waves [26]. This project mainly considers surge-induced coastal flooding and evaluates the metrics that depict the impact of storm surge events in the Bristol Channel. Regions are considered flooded when the water level is higher than the highest tidal elevation. Generally, in storm surge modelling systems, the level of flooding is evaluated by the predicted extreme water levels and surge residual levels that result from process drivers like tidal conditions and meteorological conditions during certain storm surge events at flooded locations [18, 21, 47, 140]. This methodology has been applied in the literature. For example, the studies carried out by [76, 157] utilised the SLOSH model, and [144] applied the LISFLOOD-FP model, to calculate residual heights to assess the impact due to certain storm surge events. In addition, in this project, flooding metrics are evaluated at selected locations to represent the level of flooding of the surrounding regions in the ocean. This is the same approach as in the study of the 1981 storm surge event by [136] and by [91] in their study of the 1607 flood — justification is given for this methodology in these papers.

The calculated extreme water levels and surge residual heights can then be used to interpolate the extent of storm surge-induced inland inundation [159] and flood inundation maps [144], which can be used for the planning and management of coastal floodplains. The investigations carried out by [69] and by [18] used the LISFLOOD-FP model for simulation of coastal floodplain inundation. However, accurate complex topographic data landward of the coastline and socioeconomic data such as population density would be required for inundation investigations [18, 21], which is not within the scope of the present study. Another metric used for assessing the extent of coastal flooding in terms of extreme water levels is the run-up, which is the water height shoreward above still water level [53]. According to Anselme *et al.*, in inland

inundation studies, without consideration of the run-up component, under-prediction occurs when only considering the observed storm tide level. The effect of run-up would be significant in such studies [86, 52] but will not be considered in this project as the main interest is in the ocean regions and not on the shoreline regions. Only a simple investigation considering the inundation during a storm surge event will be conducted in this project, using a modified numerical model by extending the original model domain to the areas subject to inundation (low-lying regions surrounding the Bristol Channel). Topographic data can be obtained from the GEBCO gridded bathymetry dataset as suggested by [141]. The methodology has been introduced in [32, 69] to create flood mapping.

1.4 Tidal Barrages

Extracting energy from the tide goes back many centuries. Currently, there are two main methods for energy extraction: tidal barrages and tidal stream turbines, both of which are of interest to engineers. The most famous and successful example is the 240 MW La Rance barrage in France, which has been successfully operational since 1966 [3]. A detailed introduction for various tidal barrage schemes is given in Section 1.4.2.

1.4.1 Basic Principles

1.4.1.1 Theoretical principles

Tidal barrages utilise the hydraulic head difference at the barrage site to generate electricity. According to [16], a tidal barrage has four key components: turbines, sluice gates, locks and caissons. Through the turbines and sluice gates, sea water is allowed to flow into an artificial impoundment during the high tide period until the minimum operation head is achieved between the ocean and basin. Then, power is generated by allowing water to pass though the turbines driven by the artificial head differences. In this process, potential energy is eventually converted into electricity [10, 134]. Two main operation methods are possible for tidal barrages. Firstly there is the one-way ebb generation method, which allows water to flow into the enclosed basin during the rising tides and generates power on the falling tide when the impoundment empties. Secondly there is the two-way power generation method, which generates power on both the rising and falling tide, as can be shown schematically in Figure 1.10. In the Figure, the dashed line indicates the ocean water level and the impounded basin is shown as the black line, which is controlled by the minimum water head

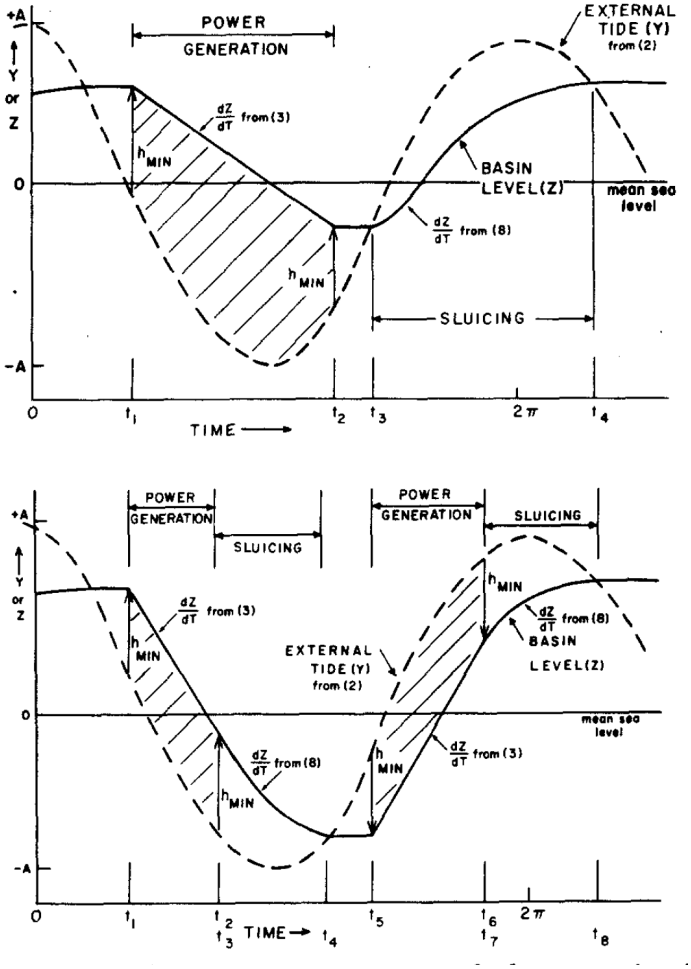

Figure 1.10: Schematic representation of the operational mode of one- and two-way power generation taken from [134]. The x-axis is the water level and the y-axis is the time. The variable A here is represented by a in this thesis to indicate the tidal amplitude, and the variable h is represented by H in this thesis to indicate the water head difference over a barrage.

difference. Detailed discussion of the modelling of tidal barrages is presented in Section 1.4.3. However, useful insight can be drawn from the approximate model developed in Prandle [134]. In this model, the energy extracted can be calculated as:

$$E = -\rho\, g \left[A_b \int_{Z_1}^{Z_2} Z\, dZ - Q\, a \int_{t_1}^{t_2} \cos \omega t\, dt \right], \tag{1.18}$$

where a and ω are the amplitude and frequency of an assumed sinusoidal external tide, Q is the flow rate through the turbines, ρ is the water density, g is the gravitational density, A_b is a constant basin area, and Z_1 and Z_2 are the basin water levels at times t_1 and t_2 respectively.

Theoretically, the energy extraction from emptying the basin can be found by assuming that the enclosed body of water empties instantaneously; the same is true for the energy extraction from filling the basin. The maximum energy should equal to the change of the potential energy by both filling and emptying the basin. The maximum theoretically available energy is calculated by:

$$E_{MAX} = 2\rho g\,(volume \times average\,head) = 2\rho g\ \times \left(2aA_b \times \frac{2a}{2}\right) = 4\rho g a^2 A_b, \quad (1.19)$$

where the factor 2 is introduced to account for the energy extraction in both emptying and filling the basin. By rewriting the above equations, the amount of energy extracted can be expressed as a fraction of the maximum available energy: $e = \frac{E}{E_{MAX}}$. Prandle [135] showed that not all of the available energy can be practically used. According to Prandle, the energy produced, e, can be 0.37 for the two-way scheme, compared to a value of 0.27 for the one-way ebb generation. This is essentially due to the finite time required to fill and empty the basin. This emptying and filling time effect significantly reduces the average head across the turbines.

During power generation, pumping can be applied when the sluice gates are closed at high tide to further raise the water level in the basin. Some turbines are capable of working in reverse as pumps, and this action is stopped when the ocean has ebbed sufficiently. In this case, the generation of power will start earlier than the case for simple ebb generation [16]. Pumping can enhance the ability of water capture (pumped storage), increase the water head difference across the turbines and, consequently, result in a potential net gain in energy [116, 181]. The benefit of pumping may be more significant when pumping occurs during periods of low electricity demand (such as the period before the morning rise) as the cost of electricity used for pumping is low [16, 125]. In addition, pumping can also mitigate the inefficiency of the process due to existing energy losses and tidal range difference between spring and neap tide, by providing constant operational water head differences for turbine energy generation. The detailed trade-offs and issues for pumping application along with the power generating process have been further discussed by Baker [16] and MacKay [116].

There are three main types of turbines that are available to be used in a tidal barrage [99]. According to Baker [16], the tubular turbine, as proposed for the Severn Barrage, is designed with the generator mounted at a 45-degree angle from the top of the turbine and placed into a dry enclosure. The blades of this turbine are connected by a long shaft at an angle through the water-passing plane. A gearbox between the

generator and therefore the runner helps to increase the speed of the generator and results in a significant reduction of cost. As well, the adjustable blade allows the turbine to work efficiently to match the electricity demand. Alternatively, a rim turbine is designed such that its runner is mounted horizontally, and the generator rotor is applied on the tips of the turbine blades. This arrangement helps ameliorate issues of operational stability, but has the disadvantages of being unsuitable for pumping and has difficulties in regulating the performance. When the third turbine type, the bulb turbine, is used, the generator is located inside of the turbine runner. This means its efficiency, due to the space and size, is high. However, bulb turbines have to be maintained by stopping the flow of water, which is quite time-consuming and involves a loss of power generation. Cavitation is another consideration in the design of hydraulic turbines, which is defined as the formation of numbers of small vapour bubbles when the static pressure of the flow falls below its evaporation pressure due to the increased flow speed. Cavitation is most likely to occur near the runner blades of turbines and results in damages to the turbine surface due to the erosion and high local stresses induced by the bubbles collapsing [105].

1.4.1.2 Practical issues

As discussed by O'Rourke *et al.* [125], the current issues restricting tidal barrage development are the high construction costs, the social concerns and the environmental impacts. Economic viability is one of the greatest practical constraints for tidal energy extraction. Generally, there are high capital costs, including costs for construction materials, turbines and sluice gates. There are also considerations for accumulated costs and long payback periods, which make such projects unattractive to many investors [16]. Figure 1.11 illustrates the extremely high cost of marine energy compared to other forms of renewable energies [40]. In terms of the social consequences regarding barrage development, its implementation may necessitate long construction times, which will impact surrounding communities in terms of traffic and noise.

The biggest disadvantages for barrage construction, besides the cost, are possibly associated with the environmental or ecological impacts on local regions. These impacts are generally due to the changes in the flow of tidal currents caused by barrage construction. The overall water quality may be affected, such as the occurrence of sediment and nutrient transportation [3, 125], which can result in changes to the water turbidity (see detailed criteria concerning water quality by Baker [16]). These variations will have large impacts on the animal life that lives in the ecosphere and

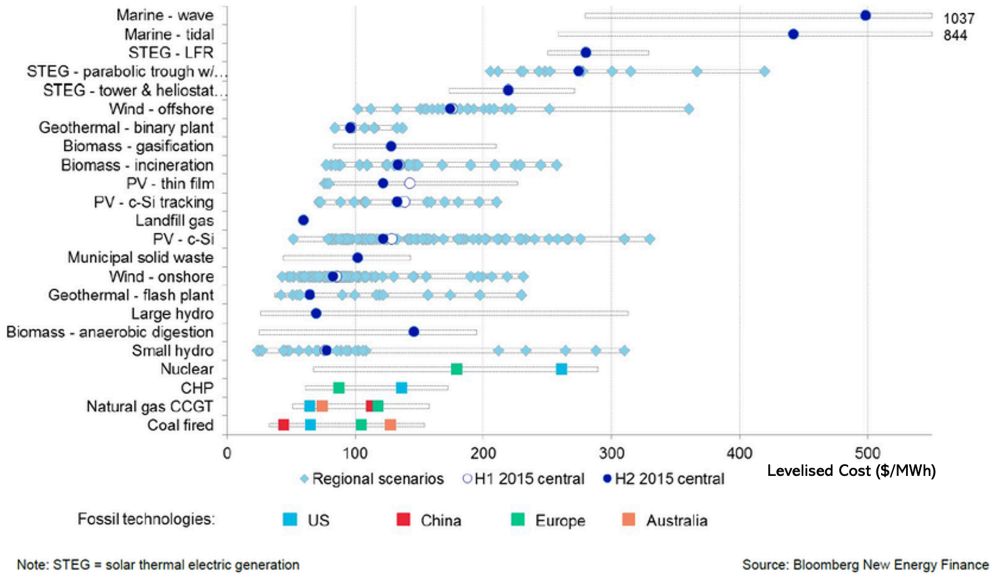

Figure 1.11: Levelised cost of electricity with respect to various renewable energy sources for 2015 taken from [40].

depends on the water environment. Such animals, like fish and birds, may also be affected by the disruptive water movement, food web dynamics and availability, as well as the loss of inter-tidal habitat areas.

However, a potential advantage of a tidal barrage in terms of the environmental impact is that it may offer coastal flooding protection. Falconer *et al.* [61] and Xia *et al.* [179] suggest that the construction of a barrage would lead to the reduction of the maximum water level and tidal current, and an approximately 50% drop in discharge compared with the case of having no barrage. Under basic operation mode, the existence of a barrage is beneficial by acting as a physical barrier to help control the degree of flooding into the basin. The barrage can also keep tides out of the impoundment, allowing the empty basin to be filled with river water during high rainfall weather conditions. The Thames Barrage is used in this way. As a result, upstream river flooding, as well as possible coastal flooding caused by the river discharge, can be reduced [3].

1.4.2 Existing and Proposed Schemes

Numerous sites worldwide are considered as appropriate for tidal development. The first large-scale commercial tidal range structure, the 240 MW La Rance barrage located on the river Rance in Brittany, France, has been operational since 1966. The facility has been in operation for over 40 years without mechanical breakdown

Table 1.5: Other current existing tidal barrages worldwide.

Name	**Location**	**Power Capacity**	**Comments**
Annapolis Royal tidal generation (1984)	Canada	20 MW	Single turbine; producing 30 GW h per year
Kislaya Guba power facility (1968)	Russia	1.7 MW	The smallest tidal power facility; suitable for feasibility studies
Jangxia tidal power station (1980)	China	3.2 MW	Ebb and flood tide operation
Lake Sihwa tidal power station (2011)	South Korea	254 MW	Single biggest tidal energy installation

and supplies 0.12% of the power demand of France annually [125]. The La Rance Tidal Power Plant is one of the facilities that demonstrates the success of tidal power generation and indicates that tidal power is safe, reliable and predictable. There has however been a severe impact on the environment of the La Rance estuary, especially for local water quality and ecosystems [101]. Other existing tidal barrages are given in Table 1.5 [125, 150].

Currently, there are numerous potential tidal barrage sites around the world; one of the larger sites that is currently undergoing feasibility studies is the Severn Estuary in the UK. The detailed options are still being considered by the government and include the possibility of stream turbines, a tidal barrage (e.g. the Severn Barrage) or a lagoon (e.g. the Swansea Bay Lagoon) [8, 88]. Of these, the Severn Barrage is considered to be the most controversial (given its size) but is the most widely published proposal. One of the locations considered is given in Figure 1.12. The barrage is designed to be 16 km long and is to include 166 sluice gates and 216 turbines, each with a diameter of 9 m. Approximately 500 km^2 of water would be impounded and transferred between a large height difference over the barrage to produce energy. The total power generated is estimated to be 17 TWh/year (approximately 5% of the national electricity need of the UK). A comparatively smaller project, the Swansea Bay Lagoon, has also been considered for the Severn Estuary with an application of 16 turbines and 320 MW installed capacity. The location of the proposed lagoon can been seen in Figure 1.12. Detailed information of the Severn Barrage and the Swansea Lagoon will be introduced in Section 2.4.2.

There have been many proposals and numerical simulations considering a Severn Barrage implementation in the Severn Estuary to extract energy from the large tidal range [24, 88]. However, its effects on tidal hydrodynamics would have to be evaluated

Figure 1.12: Location of the proposed Severn Barrage shown as a red line across the estuary and the Swansea Lagoon shown as a blue line.

at the early stages of the decision-making process. This is important both in assessing the power output and in determining the environmental change caused by such a structure. Various studies have examined the impact of a barrage on the tidal water levels in the surrounding area within the channel. According to [179], different barrage operating modes would lead to varying amount of maximum water level decrease in the region upstream of the barrage. For the operating mode of ebb generation, the maximum water levels within the basin were predicted to decrease by $1.0 - 2.0$m. Similar findings have been concluded by [126] for the two-way generation method, for which the maximum water level may be reduced by 2.5 m at Avonmouth on the basin side of the barrage and therefore suggests a method of flood protection. The model results also predict the rise of the maximum water level by 0.4 m to the opposite non-basin side of the barrage. Studies by [27] and [28] have also predicted reduced tidal range within the basin. For the water increments on the non-basin side, concerns are raised from the Severn Barrage proposal [24, 88] about the Somerset Levels region as it is not protected by the proposed barrage.

1.4.3 Hydrodynamic Modelling of Tidal Barrage

The implementation of a tidal barrage is a multi-scale problem. The smallest scale is that of the turbine and sluices and their components. There will also be an intermediate scale looking at the flow local to the barrage as the flow accelerates through the turbine and then mixes out downstream (e.g. [95]). This thesis focuses on the largest scale, specifically the large-scale hydrodynamic flows. The smaller scales are simplified and parameterised in the modelling at this largest scale. Note that all

modelling at this scale has to be done numerically. Physical experimentation at the basin scale are not feasible because of the large difference between the vertical and horizontal scale lengths.

1.4.3.1 Representation of a barrage within the model

A very crude model of a barrage in a basin-scale tidal model was given by Robinson [143]. He assumed the barrage would be effectively impermeable. The additional inner boundary condition therefore assumes a velocity of zero at the barrage site. The solid barrage model has been used to investigate the resonant response to different barrage locations [67].

There are several more realistic ways of simulating the detailed tidal barrage performance within the domain, which can be split into outer and inner sub-domains linked by the discharge or velocity through the barrage [11, 61, 120]. For a turbine or sluice gate, the simplest relationship between the absolute value of the water head difference, H, and the flow rate, Q, is based on the orifice equation, as suggested by Baker [16]:

$$Q = C_D A_t (2gH)^{\frac{1}{2}}, \tag{1.20}$$

where C_D is the discharge coefficient, which depends upon the types of hydraulic structure, and A_t is the flow area though the opening (assumed constant during the fall and rise of tides for simple cases). This is an acceptable empirical approach for discharge calculation [9, 30]. It is possible for the sign of Q to be negative depending on the flow direction. For better representation of the turbine performance in relation to the discharge and water head calculations, a Hill chart can be applied to evaluate the proposed turbine behaviour as was used in [78].

The simplest model to represent the tidal barrage is the zero-dimensional (flat-estuary) model. This assumes a flat water level in the basin [3]. According to Prandle's classical analysis [134], ocean tidal forcing at the domain boundary to drive the differential head through the barrage can be simply represented as a single sine wave. The water level (Z) inside the basin can be found by:

$$\frac{dZ}{dt} = \frac{Q}{A_{wet}}, \tag{1.21}$$

where A_{wet} is the wetted surface area of the tidal range structure facing basin side, assuming a constant water level in the basin. Equation 1.20, coupled with Equation 1.21, can be time-marched for calculation of H and in turn Q can be determined as

well. Compared with the other models, the key advantage of the zero-dimensional model is the computational time, which makes it useful for the optimisation of the barrage design (e.g. [6]).

The zero-dimensional model assumes that the water level outside the barrage remains unchanged. The next level of complexity is to use the one-dimensional shallow water equations as introduced in Section 1.3.1. Such a model has been applied for the assessment of the location and impact of a barrage in the Bristol Channel [67].

To model the complexities of flow at a regional scale, multidimensional models should be applied. Such models have been developed to include the sub-grid scale model of flow within the barrage sites into the basic numerical model, which is then applied to solve the two-dimensional shallow water equations as introduced in Section 1.3.1 [3, 8, 23]. There have been a number of authors who have investigated tidal barrages with two-dimensional models, such as the analysis on the effects of the implementation of the Severn Barrage by Evans *et al.* [60]. A two-dimensional model is excellent at modelling large-scale hydrodynamics, but flow through a barrage is three-dimensional. So, ideally, at a local scale, the flow should be simulated in the three-dimensional model numerically or physically. A three-dimensional numerical model for the Bristol Channel has been created by Owen [127] but fewer models of this type have been developed to simulate barrage effects at this time.

1.5 Interaction between Storm Surge and Barrage

1.5.1 General Discussion of the Problem

As introduced above, implementation of a tidal barrage will have significant hydrodynamic impacts on the channel and generally will lead to a reduction of maximum water level. The different barrage operation modes and the combinations of sluice gates and turbines will affect the water level in several ways in both upstream and downstream regions of the barrage site. As a result, this may lead to either an increment or decrement of the water level during storm surge events. How the barrage is operated may also influence the flow of any excess water that could lead to flooding. This project aims to extend existing knowledge of the impacts of the Severn Barrage and Swansea Lagoon on storm surges in the region.

1.5.2 Past Modelling Work

Whilst there has been much work on understanding and modelling tidal barrages and storm surges separately, only a few studies have considered these together. To the author's knowledge, nobody has yet investigated how different barrage operations lead to different flooding outcomes. As such, this work is the first to do so and hence it is the central contribution of this thesis.

Of the few studies investigating the potential impact of storm surges on tidal hydrodynamic devices, Lewis *et al.* [108] suggested that storm surges will have effects on annual resource estimations, which may result in significant changes to tidal power generation. The investigation utilised zero-dimensional modelling to represent the performance of the tidal barrage. The tidal forcing from the model was obtained both from the tide gauge records of storm tide (including the storm surge effects) and the astronomical tide (tide-only) scenarios. The zero-dimensional model applied is similar to the approach introduced in Section 1.4.3, with a backward difference numerical method and the relevant Hill chart. The conclusion drawn from this investigation showed that surges do alter the available resource for tidal power generation in both the timing and magnitude, even though the effects are small, on an annual scale when compared with other uncertainties.

An investigation by Lyddon *et al.* [112] was carried out in 2015 on the viability of tidal lagoons to mitigate future flood risks. The effects of extreme flooding events following the construction of a lagoon with different seawall heights under several climate change conditions were simulated using a two-dimensional hydrodynamic model, LISFLOOD. Simplified solutions of the two-dimensional shallow water equations were applied. The future climate conditions, regarding different scenarios with different sea level rise values, were considered in the model and the detailed domain with implementation of the lagoon wall was created in Arc GIS. The author concluded that there is a potential benefit of tidal lagoons for flood risk reduction in coastal areas, which depends on their shape, size, location and local bathymetries.

In addition, using the barrage as an impermeable wall during storm surge events could be considered as one tidal barrage operation strategy. This makes it similar to a storm surge barrier. According to the investigation carried out by Bowman *et al.* [29] for New York City, the barriers would be closed during storm surge events to stop the storm water or closed during high tides for a few days. Hydrodynamic models such as ADCIRC have been used in this research. The detailed location of the barrier, numbers and combinations of closed barrier gates, and sequence of the opening and closing of the barrier gates were also analysed. Such measures have already been

placed into effect for the protection of the city of London. The Thames Barrier was completed in 1982 and provides protection against flooding. Research was carried out by Prandle [133] on the potential effect of the implementation of a barrier to storm surges in the southern North Sea and River Thames with consideration of the 1953 surge event. The numerical models applied the one-dimensional and two-dimensional shallow water equations, with addition of wind and pressure data, and barrier effects were represented by appropriate boundary conditions [133].

1.6 Aims of this Thesis

The aim of this work is to assess the benefits of a tidal barrage to minimise the risk of surge-induced coastal flooding in the Bristol Channel in the UK. The research has the following objectives;

- To develop a validated two-dimensional ADCIRC DG-SWEM for the southwest coastal region of the UK that simulates major tidal constituents and storm surge phenomena,
- To modify the ADCIRC DG-SWEM code in order to represent the Severn Tidal Barrage and the Swansea Lagoon under storm surge events, and investigate the hydrodynamic effects of implementation of a barrage and the impact of barrage operating strategies on the storm surge in the Bristol Channel region,
- To examine how power prediction would change with consideration of storm surges, and evaluate the impact of barrage operating strategies on the power generation during a storm surge event in the Bristol Channel region,
- To create a verified one-dimensional hydrodynamic model that computes the main hydrodynamic features of the Bristol Channel,
- To carry out a study comparing the one- and two-dimensional models,
- To reproduce the 1607 storm surge event and investigate the barrage impact and,
- To study tidal resonances in the Bristol Channel and understand how they are impacted by the construction of a barrage or lagoon.

1.7 Thesis Outline

The objective of this thesis is to consider the impacts of the Severn Barrage and Swansea Lagoon on water levels in the Bristol Channel. In this thesis, water levels are essentially taken as a determinant for the level of flooding, an assumption which is explored in Appendix A. Numerical modelling is used to explore the impact on tides and storm surges when building such structures.

This work mainly uses the open-source hydrodynamic model (ADCIRC DG-SWEM) to solve the two-dimensional shallow water equations. The model is developed in Chapter 2. This Chapter calibrates and validates the models against field measurements and develops the composite storm surge event used as a representative storm later in the thesis. Chapter 3 describes the assessments of the impact of a barrage or a lagoon on the hydrodynamics of the Bristol Channel and their flooding protection provided during storm surge events. A combined project of both barrage and lagoon implementation is also considered. Different barrage operation strategies are investigated during the surge event, and approaches for optimal flooding protection that can be provided by a barrage or a lagoon are suggested. This Chapter is drawn from the journal paper [115] which looked at the Severn Barrage and the conference paper [114] which looked at the Swansea Lagoon. These were coauthored with Tulio Marcondes Moreira who implemented the barrage model in the code. In Chapter 4, the interaction between storm surge and power output from the tidal devices is explored, as well as the impacts of barrage strategies on power generation during storm surge events. A one-dimensional model is also considered in this project. The model is developed and verified in Chapter 5. The Chapter also presents comparisons between the one- and two-dimensional models and their simulation results of the hydrodynamic predictions. Different barrage operation strategies of flooding mitigation during storm surge events are considered. Chapter 6 describes the reconstruction of a devastating coastal flooding caused by a storm surge in 1607 in the Bristol Channel. The established two-dimensional model in the barrage-absent scenario is also utilised to evaluate its flooding prevention function during this extreme surge event. Finally, to gain a deeper fundamental understanding of the hydrodynamics of the Bristol Channel, and how these are changed when a barrage is included, its resonant properties are explored in Chapter 7. This has been published as a journal paper [113]. Chapter 8 presents the main conclusions of this thesis and proposes areas for future work.

Appendix A introduces a modified model including the surrounding low-lying areas approaching the channel head in order to fully investigate the impact of barrage implementation with consideration of the flooding area. Additional barrage visualisation results are presented when different barrage operation strategies are employed. Appendix B provides supplementary information of wind patterns found in the severe storm surge events in the year 1990, 1995 and 2014, which can be considered along with other typical events to obtain the wind-surge relationship in the Bristol Channel.

Chapter 2

2D Model Details and Validation

This chapter presents details of the two-dimensional shallow water model of the Bristol Channel and surrounding regions. The model is validated against measurements and other models. The chapter also presents details and verification of the tidal barrage implementation within the model.

Section 2.1 provides information about the model domain and other details of the DG-SWEM. The model is calibrated using various bed friction coefficients, wind surface drag coefficients and other relevant model features in Section 2.2. The calibrated model is then validated against available measurements of tidal elevation amplitudes (using harmonic analysis of field measurements) and current magnitudes and directions. A series of historical storm surge events are simulated and compared with measurements, as explained in Section 2.3. Section 2.4 describes the approach of barrage implementation into the model. Section 2.5 discusses the accuracy of the two-dimensional ADCIRC model with respect to the surge events selected, and how these real events have been adapted for the purpose of this study. Section 2.6 presents brief conclusions from this chapter.

2.1 2D Model

2.1.1 Domain and Mesh

This section describes the two-dimensional shallow water model of the Celtic and Irish Seas and the English Channel. This area includes the Bristol Channel. The model uses an extensively validated numerical solver DG-SWEM. This uses the DG method to solve the shallow water equations with unstructured triangular mesh [46, 168]. DG-SWEM was developed within the ADCIRC framework and has similar

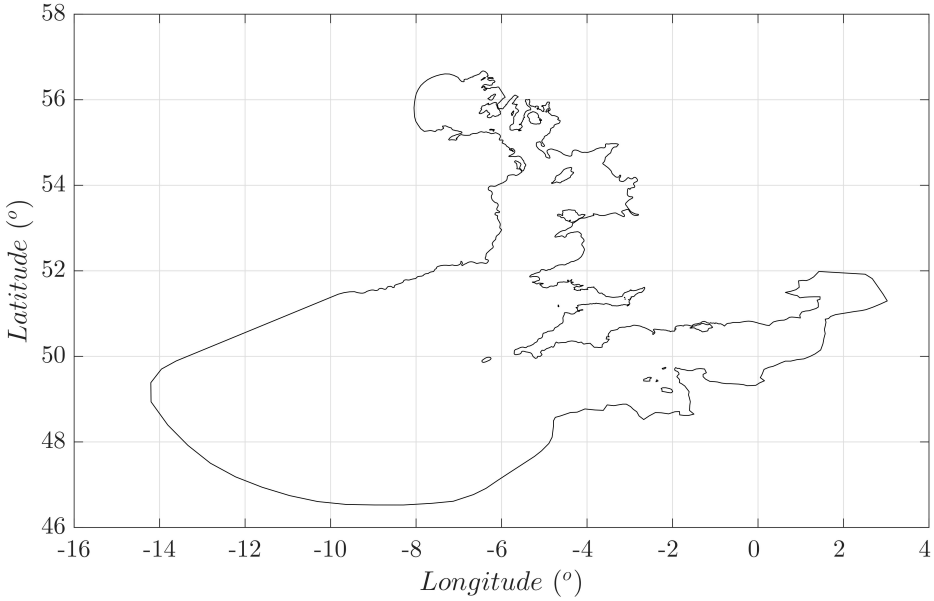

Figure 2.1: 2D model domain.

input and output files [104]. The choice of code is governed by the code's excellent scaling properties and the additions to the code already developed in Oxford.

Figure 2.1 depicts the domain of the two-dimensional numerical model, which consists of the Irish Sea, Celtic Sea and Bristol Channel from Serhadlıoğlu's model [149], and the English Channel from Adcock and Draper [2]. Two sets of bathymetries are used in this study. Both are from SeaZone. In the Bristol Channel itself, high-quality survey data are used. Across the rest of the domain, lower quality data are employed based on Admiralty Charts. Bathymetry is 'corrected' for mean water levels where the raw data has a different datum.

The model has three open boundaries on which tidal forcing is specified. The western boundary is located on the edge of the Celtic Sea, just beyond the continental shelf to reduce the impact of reflected waves off the boundary, which in reality would propagate out into the ocean beyond [1]. The eastern boundary is in the English Channel and the northern boundary extends to the Scottish Isles of Coll and Tiree. On these boundaries, it is not practical to extend the model to the continental shelf but they are sufficiently far from the Bristol Channel that they are not expected to cause significant error at the location of interest. The domain is chosen to give good resolution within the area of interest but to be large enough that any changes to the tidal regime due to the introduction of a barrage can be captured. For example, it

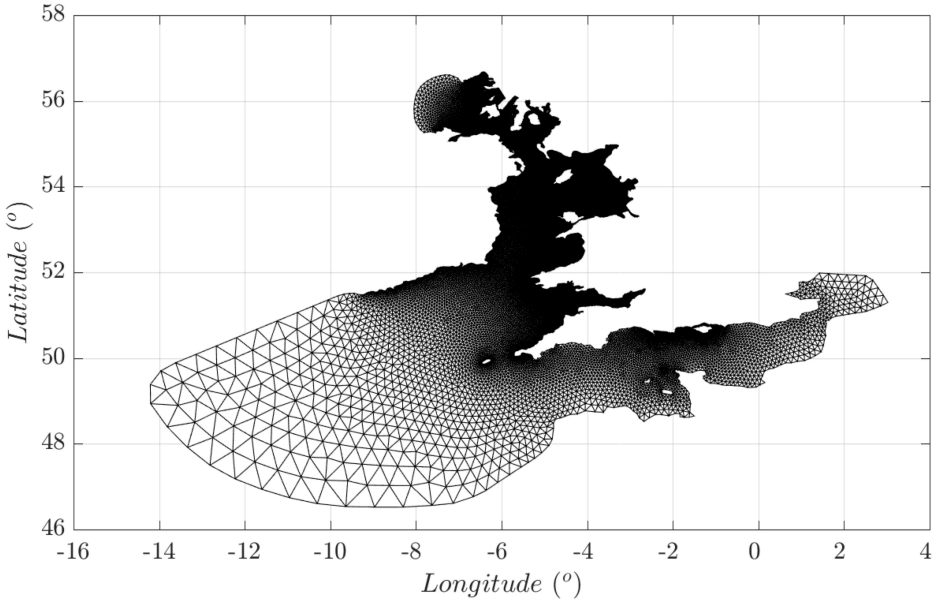

Figure 2.2: 2D model mesh including the Irish Sea, Celtic Sea, English Channel and Bristol Channel.

is not thought necessary to model the North Sea as the change in hydrodynamics there would be negligible by altering the Bristol Channel. At the open boundaries the water level is specified *a priori* whilst the current at the boundary is not specified and the model solves for this.

The model domain is divided into $98,278$ elements with $51,458$ nodes and uses unstructured triangular cells, as shown in Figure 2.2. Serhadlıoğlu [149] carried out a thorough mesh independence analysis and so this is not repeated in this thesis. When barrages are included, the mesh has to be modified to allow this. Changes to the mesh are only made in the specific areas where barrages are to be installed, ensuring that the majority of the domain remains unmodified. At the barrage locations, mesh resolution has been increased, but not overly so by simulating a number of turbines or sluices per node pair. Such care has been taken so that this operation has not introduced significant grid dependency.

2.1.2 Simulation Parallelization

Numerical simulations for this project are run on the supercomputer. Domain decomposition is used to parallelize the numerical simulations with the spatial model typically split into 32 domains (see [104] for general results on the parallelization of

this code). A parallelization test of simulations with a Personal Computer (PC) and the Advanced Research Computing (ARC) supercomputer is carried out for the cases with and without barrage implementation. The barrage addition to DG-SWEM has been recently implemented by [147]. As such a parallelization test with barrage implementation is essential. Other basic parallelization performance has been evaluated by Serhadlıoğlu [149]. The comparison results of water elevation can be seen in Figures 2.3 and 2.4.

Both Figures show simulations at two points of interest: a location near the channel entrance and the measurement station at Hinkley Point in the Bristol Channel near the barrage site. In the case where no barrage is implemented and the simulations consider only the channel hydrodynamics (Figure 2.3), nearly perfect agreement can be observed between the PC and ARC models. Even though they both tend to slightly underestimate the water elevation at Hinkley Point in comparison to field measurements, the discrepancy is minor and more importantly the two simulated curves still are in close agreement (with average difference of 0.05 m). Similarly for the case where a barrage is added (Figure 2.4, which lacks field measurement comparisons because no barrage exists in reality), the agreement between the the two simulation models is close to perfect. The only aspect to note is that, for the results at Hinkley Point, irregular high-frequency oscillations can be observed in the curve produced by the ARC supercomputer, which also exist for the no barrage case. It is hypothesised that these oscillations are due to inherent modelling complexities, and they will be further explored in Section 2.4.3.

In order to thoroughly test the parallelization, a comparison of the cases with barrage implementation during a storm surge event with and without parallelization has also been conducted. The simulation results are the surge residual levels and can be seen in Figure 2.5. Similar to the findings above, the results with parallelization at the entrance of the channel are in agreement, while those at the measurement station are agreeable but with high-frequency oscillations observed at certain points in time.

2.1.3 Tidal Forcing

Artificial open boundaries are applied to separate the region of interest from the wider ocean. These are 'forced' by certain tidal constituents with specified amplitude and phase. The forcing parameters can be obtained from various tidal databases. This model is forced with the Le Provost tidal database [106].

The Le Provost database includes 13 principal tidal constituents: $2N_2$, K_1, K_2, L_2, M_2, MU_2, N_2, NU_2, O_1, P_1, Q_1, S_2 and T_2. The dominant constituent in the

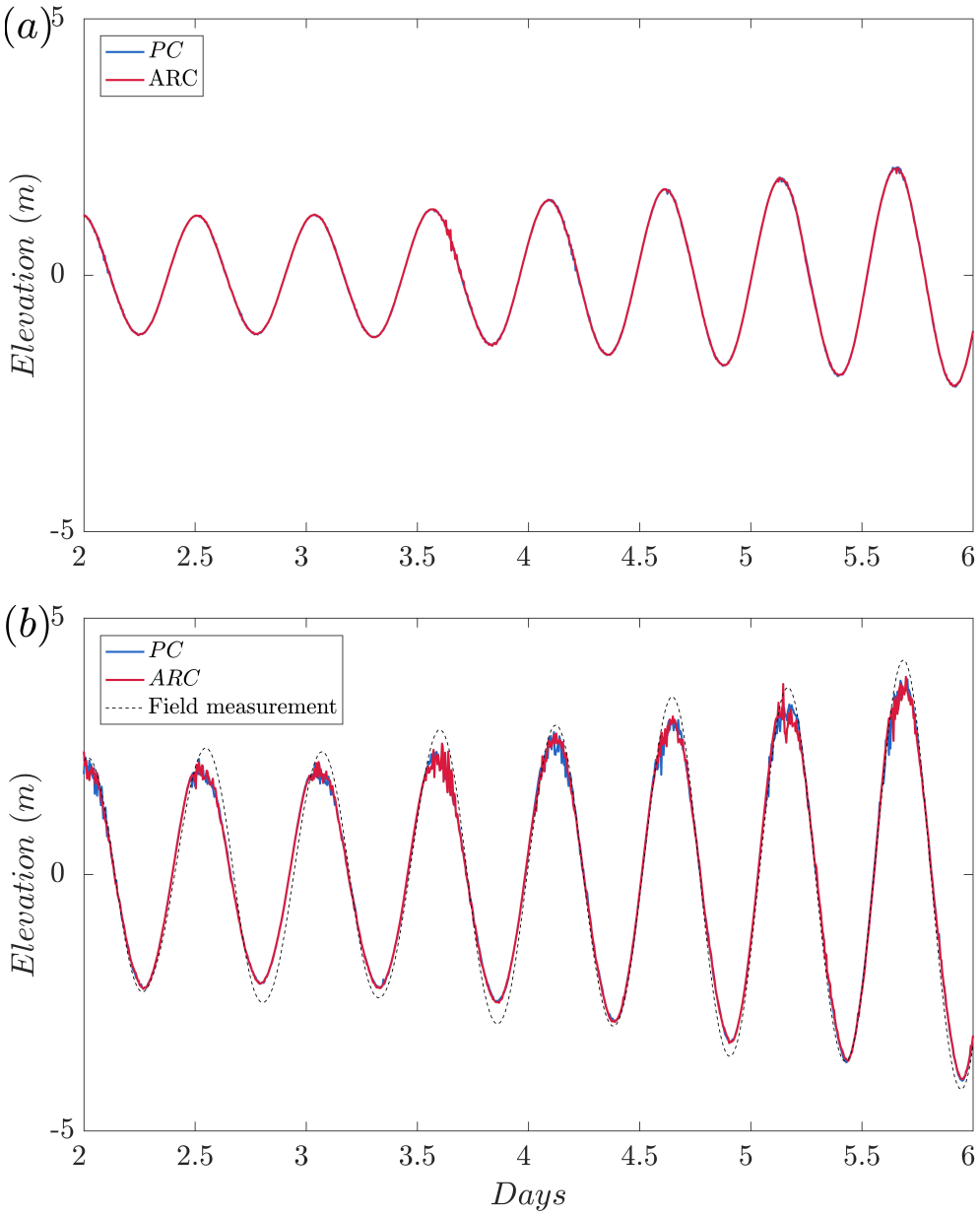

Figure 2.3: Model parallelization test for no barrage case: a) water elevation at the channel entrance (51°9.72'N 5°11.28'W) (top); b) water elevation at station Hinkley Point (51°16.76'N 3°8.16'W) (bottom). PC simulation indicates no parallelization applied while ARC indicates with parallelization, field measurement is obtained from BODC.

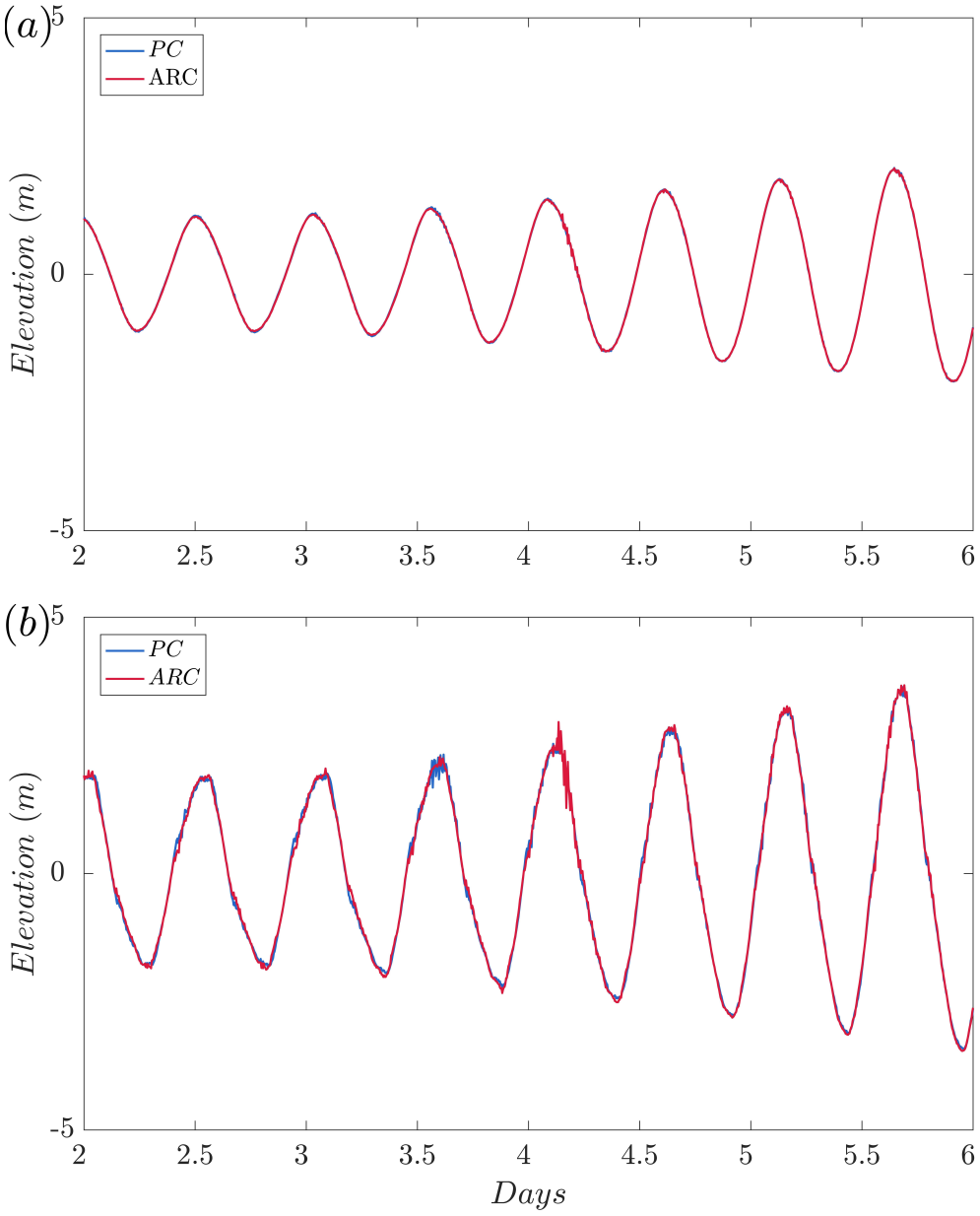

Figure 2.4: Model parallelization test with barrage case: a) water elevation at the channel entrance (51°9.72'N 5°11.28'W) (top); b) water elevation at station Hinkley Point (51°16.76'N 3°8.16'W) (bottom). PC simulation indicates no parallelization applied while ARC indicates with parallelization.

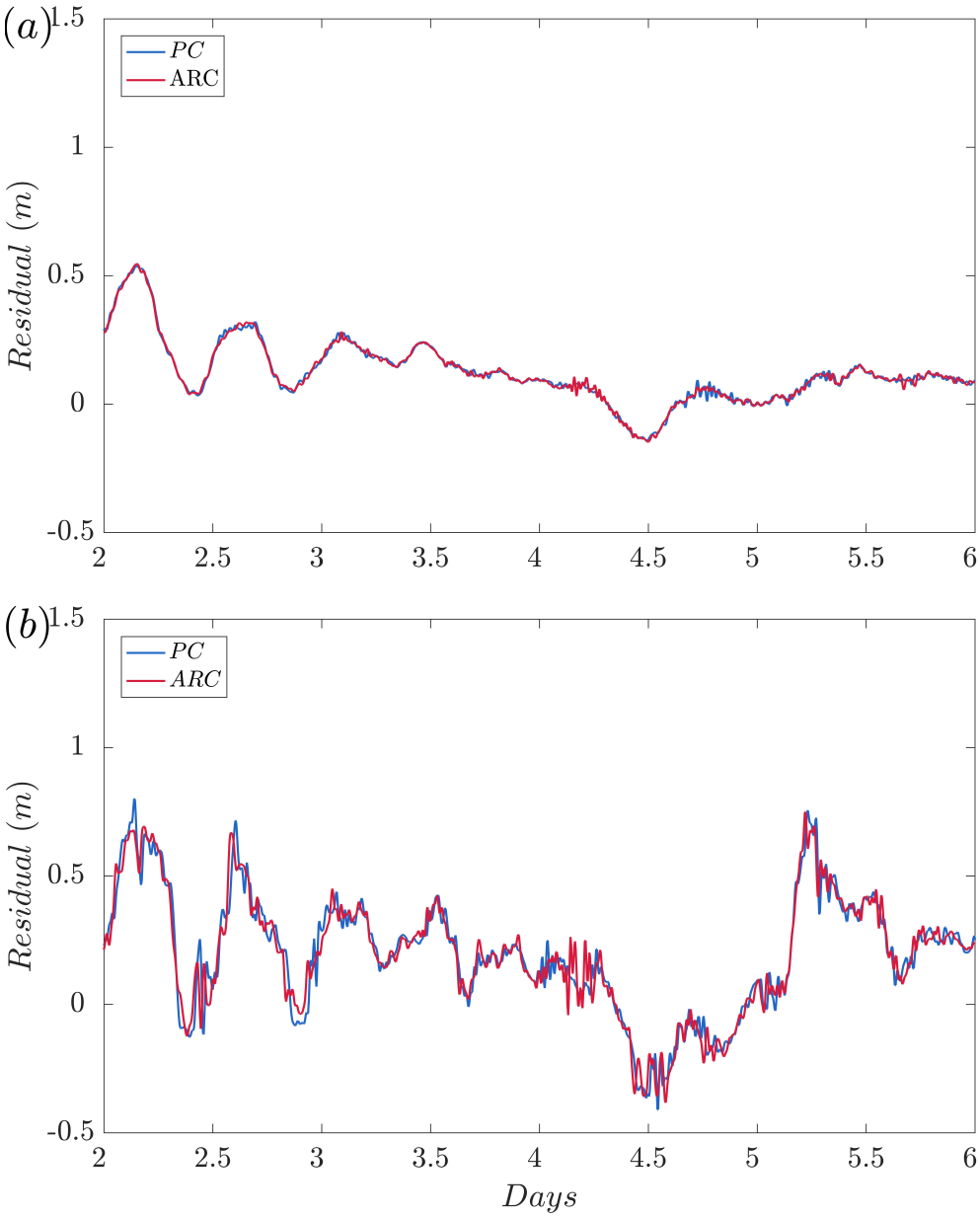

Figure 2.5: Model parallelization test with barrage case during a storm surge event in Bristol Channel: a) surge residual level at the channel entrance (51°9.72'N 5°11.28'W) (top); b) surge residual level at station Hinkley Point (51°16.76'N 3°8.16'W) (bottom). PC simulation indicates no parallelization applied while ARC indicates with parallelization.

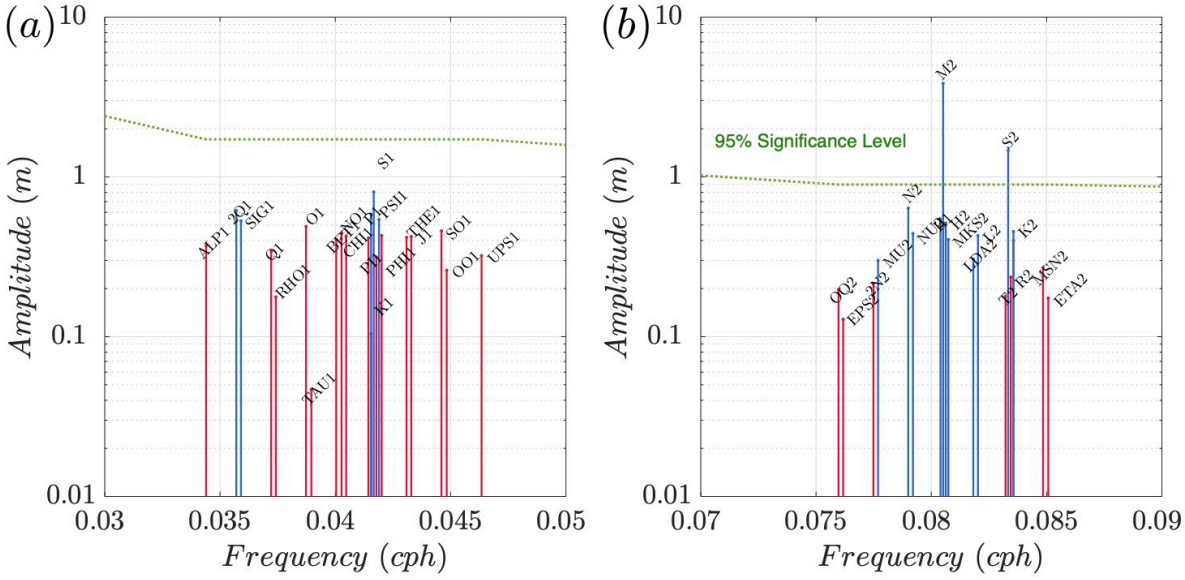

Figure 2.6: Amplitude of analysed components with 95% significance level by T_Tide: a) the diurnal tidal components (left); b) the semi diurnal tidal components (right). The blue line indicates the significant constituents and the red line shows the insignificant ones. The green line shows the significance level.

Bristol Channel is the M_2 tide, followed by the S_2, N_2 and MU_2 tides [85]. This is confirmed by analysing the one-year, field-measured data at Avonmouth from the British Oceanographic Data Centre (BODC) using harmonic analysis as implemented in the T-Tide software [129]. Figure 2.6 shows the analysis results and indicates that the major tidal constituents in the Bristol Channel are indeed the M_2 and S_2 tides. The line of 95% significance level indicates that these two constituents, which are above the line, can be combined to represent over 95% of the water level in the Bristol Channel; the N_2 tide is additionally considered in this study for further accuracy. These three main semi-diurnal tidal components can be applied as the tidal forcing specified at the ocean boundary conditions. They are interpolated from the Le Provost tidal database [106]. Interpolation from this database in the SMS software used is known to have issues, and obvious errors have been corrected by hand. It is possible to use additional constituents, despite being somewhat time-consuming because of the requirement to hand-correct errors in interpolation. However, using just three constituents gives an excellent approximation to the tidal variations for the whole model domain and crucially greatly simplifies the analysis (and ease of understanding) compared to using all available constituents. Validation of the tidal constituents within the model is given in Section 2.3.

2.2 Model Calibration

Calibration of the model has been carried out with respect to the different bed friction coefficients, wind surface drag coefficients from different meteorological datasets and comparisons of different datasets for storm surge meteorological input. Initially, the simulation is run for a 30-day period with tidal forcing but without any meteorological inputs or barrage implementation for calibration of friction coefficients. Following this, the simulations are run for a spring-neap cycle period of 14 days with the meteorological inputs and without the barrage implemented, in order to calibrate the wind coefficients and select the most applicable dataset. A hyperbolic tangent ramp function lasting two days is applied to the forcing boundary conditions. Tidal waves are ramped in gradually on the open boundaries during this period in order to reduce the effect of initial transients. As a result, the characteristics of the modelled waves are not representative during the ramp-up period. Thus the predictions during the spin-up period are omitted from the data analysis. The elevation results are recorded every 20 minutes for each grid node. The meteorological inputs (the wind stresses and pressure variations) are applied to each grid node and change every half hour.

2.2.1 Friction Coefficient

The calibration of the friction coefficient is carried out using Admiralty Tide Tables data [81] for M_2 and S_2 tidal elevation amplitudes and phases at selected stations. This is done in the absence of meteorological forcing as this in itself has significant uncertainty whereas the tidal conditions are well known. As shown in Section 2.1.3, the M_2 and S_2 constituents are the dominant semi-diurnal tidal components and comprise 95% of the total amplitude in the Bristol Channel, and will thus be most sensitive to variations in bed friction. The calibration is done by adjusting the bottom friction coefficient C_f until the model-predicted results and observed tidal amplitudes and phases are in closest agreement. Here the drag force of the fluid is modelled using $\vec{F} = C_f \rho A_s \vec{v} \, |\vec{v}|$, where A_s is the area of the seabed and $\vec{v}$ is the velocity vector. According to the ADCIRC approach (DG-SWEM is developed within the ADCIRC framework), different types of bottom friction can be defined by the choice of the friction coefficients [22].

As stated in the recent work of Warder [164], uncertainty in bottom friction can lead to up to 20 cm inaccuracy in the surge height computations. The numerical modelling of the Bristol Channel requires careful consideration of types and values

of bed friction coefficients, particularly for the shallow areas [70]. In reality, the bed friction coefficient will vary with the channel bathymetry, but generally a constant value is used over the whole domain due to simulation complexities and computational costs. However, to replicate realistic situations more closely, it is possible to consider a hybrid nonlinear bottom friction where the coefficient is constant with a quadratic friction law in the deep water, while it increases as the depth decreases in the shallow water. Comparison results between using the hybrid bed friction and constant bed friction for the simulation of M_2 and S_2 amplitudes and phases can be seen in Table 2.1 and Table 2.2. The observed data is extracted from tide tables, while the predicted values are obtained by another numerical model presented by Davis & Jones [45], which are approximated readings from their co-tidal charts. The calibration results indicate the application of a hybrid nonlinear bottom friction law does not give significant improvements compared with a constant one (consistent with the findings of Gao [70]). For simplicity, the constant quadratic bed friction coefficients will thus be used.

Tables 2.3 and 2.4 present the predicted M_2 and S_2 tidal elevation amplitudes and phases for four different constant bed friction coefficients ($C_f(1) = 0.002$, $C_f(2) = 0.0025$, $C_f(3) = 0.003$ and $C_f(4) = 0.004$).

The root-mean-square error (RMSE), mean error (E), and error standard deviation values are computed for all stations using different C_f values to be used as statistical indicators between predicted and observed results. Mathematical expressions of these statistical measures are shown in the following equations. Here, x is the series data and N represents the number of data points. The subscripts 'pred' and 'obs' denote the model predicted results and field observations, respectively.

$$RMSE = \left\{ \frac{1}{N} \sum_{i=1}^{N} \left(x_{pred_i} - x_{obs_i} \right)^2 \right\}^{\frac{1}{2}}, \tag{2.1}$$

$$E = \frac{1}{N} \sum_{i=1}^{N} \left(x_{pred_i} - x_{obs_i} \right), \tag{2.2}$$

$$Error\ Standard\ Deviation = \left\{ \frac{1}{N} \sum_{i=1}^{N} \left(\left(x_{pred_i} - x_{obs_i} \right) - E \right)^2 \right\}^{\frac{1}{2}}. \tag{2.3}$$

The error analysis of different C_f values can be seen in Table 2.5 and Table 2.6. Both the method of RMSE and the mean error are indications of how closely the predictions align with observations, inferring better performance when the values are

Table 2.1: M_2 tidal elevation amplitudes and phases at different stations using different types of bed friction coefficients.

Station	M_2 Amplitude (m)				
	Location	Obs.	Hybrid C_f	Const. C_f	Prediction
Stackpole Quay	4.85W 51.63N	2.51	2.31	2.31	2.70
Mumbles	4.00W 51.57N	3.18	2.71	2.72	3.25
Barry	3.28W 51.40N	3.82	3.22	3.22	3.33
Flat Holm	3.12W 51.37N	3.90	3.27	3.27	4.00
Hinkley Point	3.13W 51.20N	3.80	3.25	3.25	3.90
Ilfracombe	4.12W 51.20N	3.04	2.67	2.67	3.20
Lundy	4.65W 51.17N	2.67	2.32	2.32	2.90
Station	M_2 Phase (°)				
	Location	Obs.	Hybrid C_f	Const. C_f	Prediction
Stackpole Quay	4.85W 51.63N	168	179	179	162
Mumbles	4.00W 51.57N	171	182	182	168
Barry	3.28W 51.40N	185	194	194	205
Flat Holm	3.12W 51.37N	190	199	199	200
Hinkley Point	3.13W 51.20N	185	195	195	190
Ilfracombe	4.12W 51.20N	162	174	174	160
Lundy	4.65W 51.17N	160	170	170	160

Table 2.2: S_2 tidal elevation amplitudes and phases at different stations using different types of bed friction coefficients.

Station	S_2 Amplitude (m)				
	Location	Obs.	Hybird C_f	Const. C_f	Prediction
Stackpole Quay	4.85W 51.63N	0.90	0.81	0.81	0.85
Mumbles	4.00W 51.57N	1.12	0.95	0.96	1.00
Barry	3.28W 51.40N	1.37	1.17	1.17	1.06
Flat Holm	3.12W 51.37N	1.37	1.20	1.20	N/A
Hinkley Point	3.13W 51.20N	1.42	1.19	1.19	1.00
Ilfracombe	4.12W 51.20N	1.10	0.95	0.95	1.00
Lundy	4.65W 51.17N	0.94	0.82	0.82	0.95
Station	S_2 Phase (°)				
	Location	Obs.	Hybird C_f	Const. C_f	Prediction
Stackpole Quay	4.85W 51.63N	214	225	225	210
Mumbles	4.00W 51.57N	221	232	232	220
Barry	3.28W 51.40N	240	251	251	225
Flat Holm	3.12W 51.37N	246	258	258	240
Hinkley Point	3.13W 51.20N	237	254	254	255
Ilfracombe	4.12W 51.20N	209	222	222	210
Lundy	4.65W 51.17N	207	217	217	205

Table 2.3: M_2 tidal elevation amplitudes and phases at different stations using different values of constant bed friction coefficients. $C_f(1)$=0.002; $C_f(2)$=0.0025; $C_f(3)$=0.003 and $C_f(4)$=0.004.

Station	M_2 Amplitude (m)					
	Obs.	C_f (1)	C_f (2)	C_f (3)	C_f (4)	Prediction
Stackpole Quay	2.51	2.61	2.54	2.49	2.39	2.70
Mumbles	3.18	3.17	3.09	3.00	2.85	3.25
Barry	3.82	4.06	3.91	3.77	3.51	3.33
Flat Holm	3.90	4.19	4.02	3.87	3.59	4.00
Hinkley Point	3.80	4.13	3.97	3.82	3.56	3.90
Ilfracombe	3.04	3.09	3.01	2.93	2.80	3.20
Lundy	2.67	2.62	2.56	2.51	2.42	2.90
Station	M_2 Phase (°)					
	Obs.	C_f (1)	C_f (2)	C_f (3)	C_f (4)	Prediction
Stackpole Quay	168	171	174	177	180	162
Mumbles	171	172	176	179	184	168
Barry	185	177	183	188	196	205
Flat Holm	190	181	188	193	201	200
Hinkley Point	185	178	184	189	198	190
Ilfracombe	162	163	167	170	175	160
Lundy	160	162	165	167	171	160

Table 2.4: S_2 tidal elevation amplitudes and phases at different stations using different values of constant bed friction coefficients. $C_f(1)$=0.002; $C_f(2)$=0.0025; $C_f(3)$=0.003 and $C_f(4)$=0.004.

Station	S_2 Amplitude (m)					
	Obs.	C_f (1)	C_f (2)	C_f (3)	C_f (4)	Prediction
Stackpole Quay	0.90	0.94	0.90	0.87	0.82	0.85
Mumbles	1.12	1.14	1.09	1.05	0.97	1.00
Barry	1.37	1.48	1.39	1.31	1.18	1.06
Flat Holm	1.37	1.53	1.43	1.35	1.21	N/A
Hinkley Point	1.42	1.51	1.41	1.33	1.19	1.00
Ilfracombe	1.10	1.12	1.07	1.03	0.96	1.00
Lundy	0.94	0.95	0.91	0.88	0.83	0.95
Station	S_2 Phase (°)					
	Obs.	C_f (1)	C_f (2)	C_f (3)	C_f (4)	Prediction
Stackpole Quay	214	214	217	219	223	210
Mumbles	221	216	220	224	229	220
Barry	240	226	233	238	247	225
Flat Holm	246	231	238	244	254	240
Hinkley Point	237	227	234	240	249	255
Ilfracombe	209	207	211	215	220	210
Lundy	207	205	208	210	214	205

Table 2.5: Statistical errors of M_2 tidal elevation amplitudes and phases between computed and observed data used for calibration of the model.

Station	M_2 Amplitude (m)				
	C_f (1)	C_f (2)	C_f (3)	C_f (4)	Prediction
RMSE	0.19	0.10	0.10	0.27	0.23
Mean Error	0.14	0.03	-0.08	-0.26	0.05
Error Standard Deviation	0.15	0.11	0.08	0.07	0.25
Station	M_2 Phase (°)				
	C_f (1)	C_f (2)	C_f (3)	C_f (4)	Prediction
RMSE	5.46	4.14	6.46	12.04	9.06
Mean Error	-2.43	2.29	6.00	12.00	3.43
Error Standard Deviation	5.29	3.73	2.58	1.00	9.05

Table 2.6: Statistical errors of S_2 tidal elevation amplitudes and phases between computed and observed data used for calibration of the model.

Station	S_2 Amplitude (m)				
	C_f (1)	C_f (2)	C_f (3)	C_f (4)	Prediction
RMSE	0.08	0.03	0.06	0.16	0.21
Mean Error	0.06	0.00	-0.06	-0.15	-0.17
Error Standard Deviation	0.06	0.03	0.02	0.05	0.17
Station	S_2 Phase (°)				
	C_f (1)	C_f (2)	C_f (3)	C_f (4)	Prediction
RMSE	8.90	4.42	3.70	9.04	9.31
Mean Error	-6.86	-1.86	2.29	8.86	-1.29
Error Standard Deviation	6.12	4.34	3.15	1.95	9.96

small. Meanwhile, the standard deviation of errors is an indication of the precision of predicted values between different stations—the larger the standard deviation, the larger the discrepancy between errors between stations. From the Tables, by observing both the RMSE and mean error values, the coefficient value of $C_f(2) = 0.0025$ has the best performance relative to the others. Additionally, the model here evidently matches observed data better than the Davis and Jones prediction model. For example, looking at the M_2 amplitude, the calculated RMSE of the model from literature is 0.23 m compared to a value of 0.10 m using $C_f(2)$ in the prediction model used in this thesis.

Since the entire two-dimensional model is most sensitive to changes in bed friction [164, 70], the error analysis within the bed friction coefficient calibration can be taken as a guideline or criteria for further analysis. A percentage RMSE is calculated by taking the RMSE value using $C_f(2)$ and dividing it by the corresponding mean predicted results across all stations for M_2 and S_2 amplitudes. The percentage RMSE analysis is not applicable to phases. In the same example as above, the M_2 amplitude RMSE of 0.10 m is divided by the averaged amplitude of 3.30 m using $C_f(2)$ to obtain an error percentage of 3.10%. Similarly, the error percentage for the S_2 amplitude is 2.65%. The result comparisons of M_2 and S_2 tides using $C_f(2)$ are shown in Figure 2.7. According to these results and consideration from other literature [8, 61, 179, 178], in the rest of this thesis, any error below 6% will be referred to as acceptable, i.e. an acceptable error percentage; furthermore, any error below 3% will be considered as satisfactory, i.e. a satisfactory error percentage.

2.2.2 Wind Surface Drag Coefficient

The storm surge model of DG-SWEM, with meteorological inputs, is tuned by adjusting the wind surface drag coefficient, C_d. This is done by comparing the model predictions against field measurements. There is a natural cross-over between calibration and validation in this type of modelling. As much as possible, one storm has been used for calibration and another has been used for validation. However, there are very few suitable storms available in the historical record, which makes this difficult. The sea-level measurements can be separated into a combination of a tidal component and a non-tidal component. The residual (the non-tidal component) is used to represent the storm surge in this project. The storm surge event selected for calibration purposes is the flooding at Avonmouth on 13 December of 2000. Five different coefficient correlations that were considered in literature review – separately discovered by Sheppard (1958), Deacon and Webb (1962), Wu (1967), Garratt (1977) and Smith

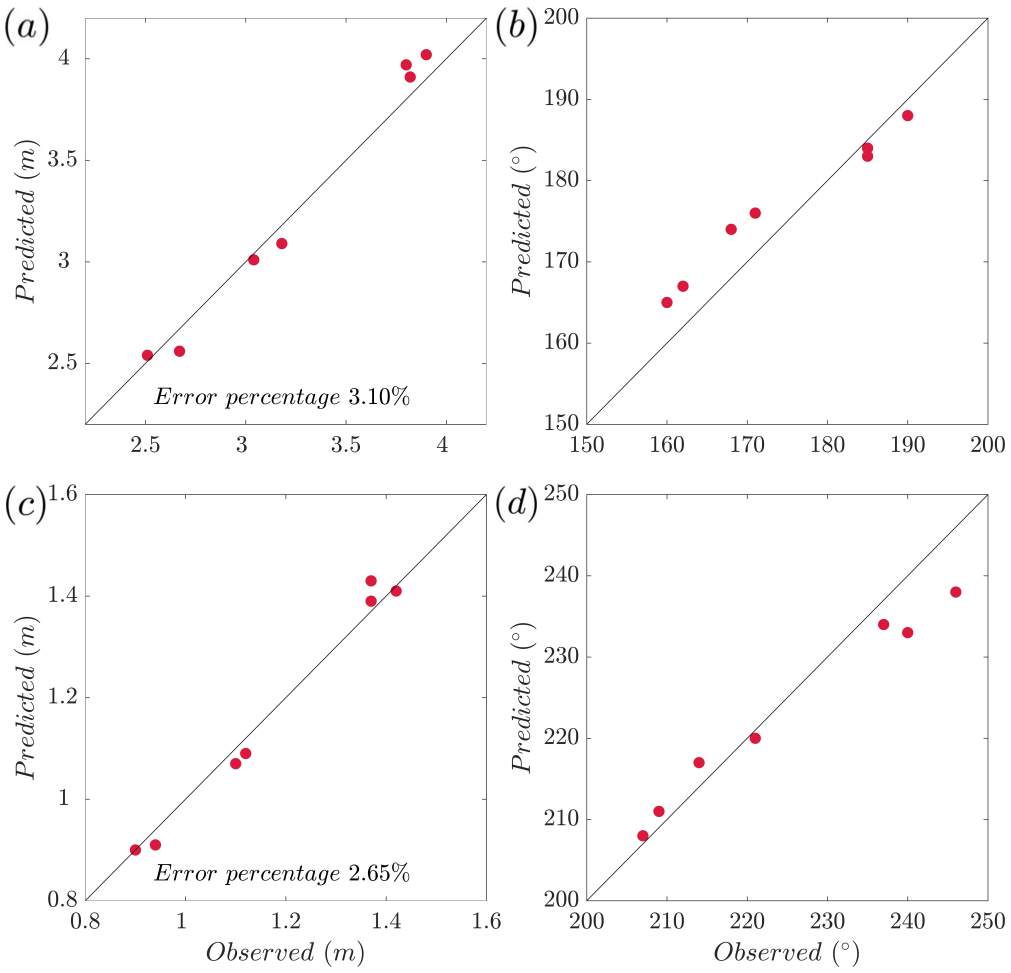

Figure 2.7: Comparison of tidal amplitude and phase of major tidal constituents between model predictions and field observations: a) M_2 amplitude (top-left); b) M_2 phase (top-right); c) S_2 amplitude (bottom-left); d) S_2 phase (bottom-right).

(1980) (see detailed discussions of each in [34]) – are applied in the surge simulations. The simulation residual is calculated by the difference between the simulation with meteorological forcing and tides, and the simulations with tides only.

As introduced in Section 1.3.2, three meteorological datasets can be considered. In this section the best wind drag coefficients for storm surge simulations in the Bristol Channel will be selected with consideration of all three datasets, while in the next section the selection of the best dataset for surge simulations will be examined in further detail.

Figures 2.8, 2.9 and 2.10 show the model simulation results at Avonmouth for the 2000 surge event with different drag coefficient based on the different datasets. The simulation using higher wind drag coefficient (Sheppard's approach) makes an over-prediction when forced with the ERA-Interim dataset. From the Figures, it is seen that there is not a unique value of wind drag coefficient that provides the best agreement with the observations. Table 2.7 shows the RMSE analysis of the entire simulation period of this event between applications of different wind drag coefficients and observed data. However, simply with this analysis, as shown by the results from the Table, it is not possible to select a single drag coefficient that is the best fit for the model, as their RMSE values are within a few percent of each other. As such, a further RMSE analysis has been carried out with only consideration of surge peaks as the extreme residual levels would be a more significant factor during a storm surge event. Table 2.8 indicates the observations and the model residual results with respect to the different wind drag coefficients according to the different datasets for specific surge times, and Table 2.9 shows the statistical error analysis of the peak surge residual. The optimal solutions can be determined by the achievement of the minimum RMSE and mean error over the five options.

From Table 2.9, the best fit overall between the observations and the model results is achieved by using the drag coefficient correlation from Wu (1967), which has the smallest RMSE and mean error considering all three datasets. If Table 2.9 is examined in conjunction with Table 2.7, the discrepancy between the performance of Wu's approach can be explained by the assumption that this particular wind drag coefficient provides a relatively better data fit during surge peak times, which is the more significant consideration in the model. Wu's wind drag coefficient is calculated by the equation:

$$C_d = \begin{cases} 0.5W_{10}^{0.5}, & 1 < W_{10} < 15 \\ 2.6, & W_{10} < 15 \end{cases}, \tag{2.4}$$

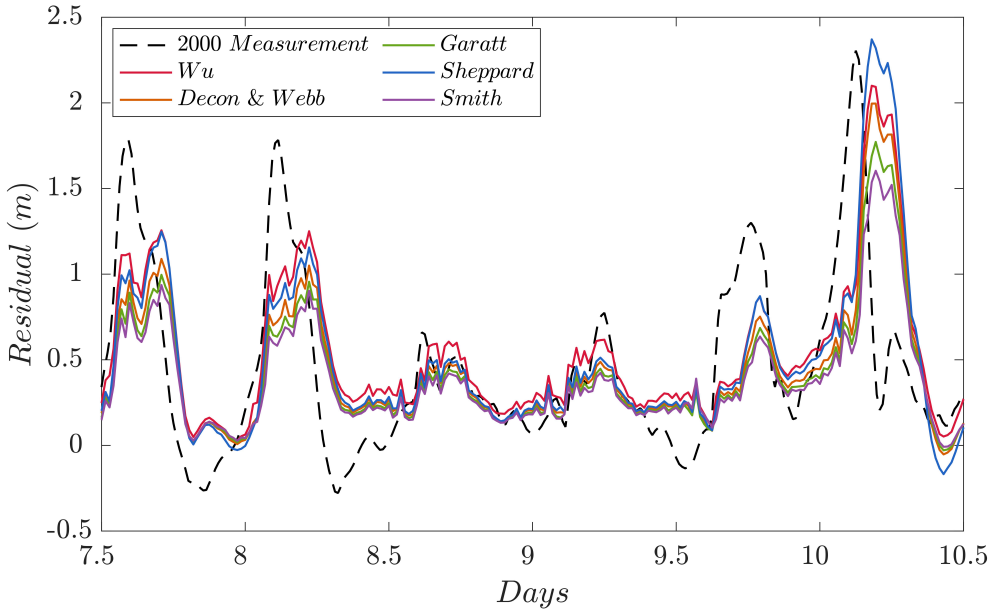

Figure 2.8: Residual results of varying wind surface drag coefficients for 2000 storm surge events at Avonmouth (51°30.53'N 2°43.58'W) based on ERA-Interim dataset.

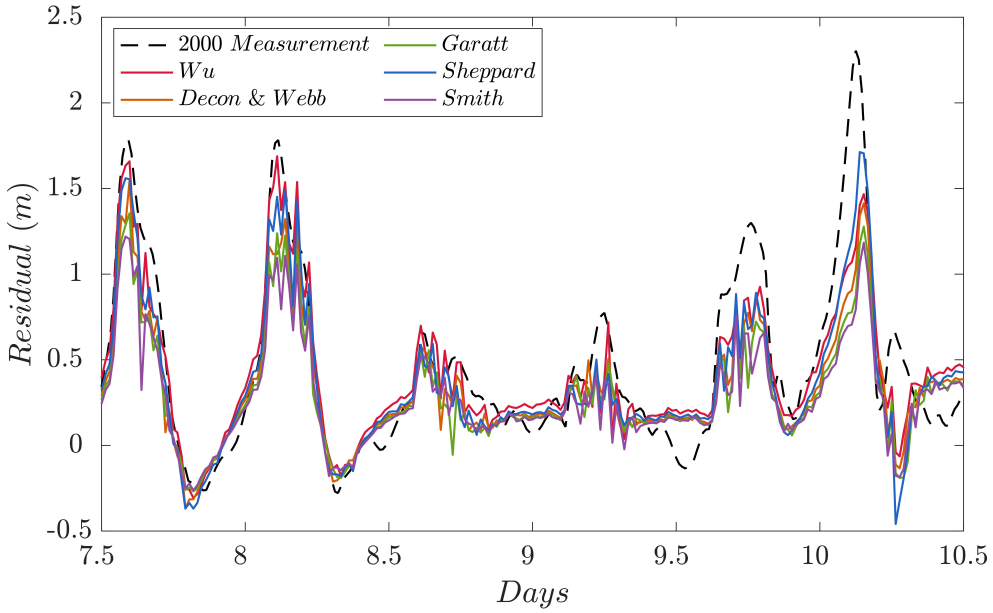

Figure 2.9: Residual results of varying wind surface drag coefficients for 2000 storm surge events at Avonmouth (51°30.53'N 2°43.58'W) based on ERA5 dataset.

where W_{10} is the wind speed at 10 m height in m/s. Surge simulation errors will be analysed in Section 2.3 and the surge peak will be modified in this project (introduced in Section 2.5.2).

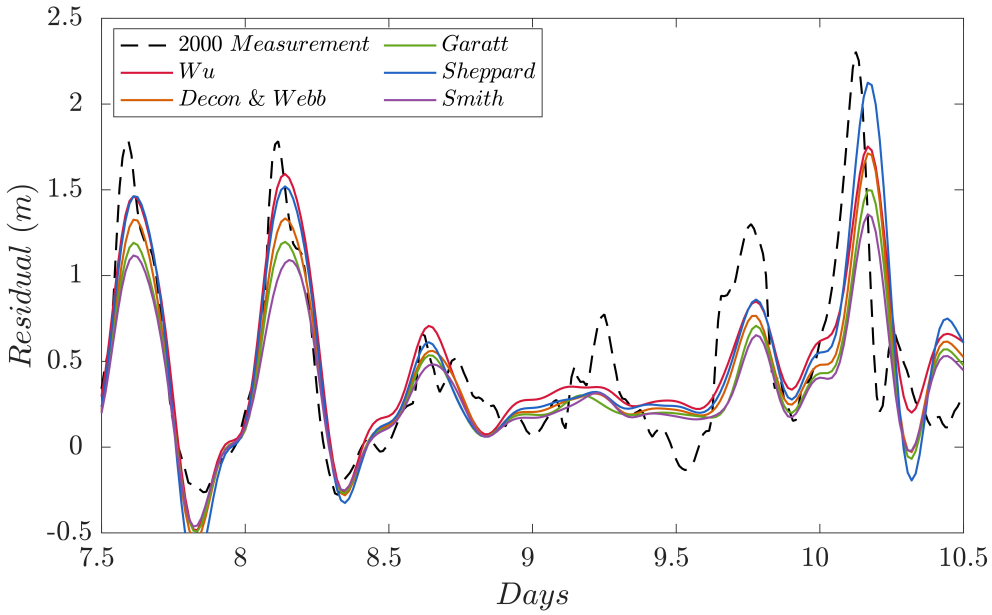

Figure 2.10: Residual results of varying wind surface drag coefficients for 2000 storm surge events at Avonmouth (51°30.53'N 2°43.58'W) based on MÉRA dataset.

Table 2.7: Root-mean-square error of surge residual results (m) between computed and observed data used for calibration of the model.

Method	ERA-Interim dataset				
	Sheppard	Deacon	Wu	Garatt	Smith
ERA-Interim dataset	0.51	0.48	0.50	0.47	0.47
ERA5 dataset	0.49	0.48	0.50	0.48	0.48
MÉRA dataset	0.49	0.47	0.49	0.46	0.46

Table 2.8: Storm surge residual results at different simulation time using different wind drag coefficients for different datasets.

Wind drag coefficients						
Time	Obs. (m)	Predictions (m)				
		Sheppard	Deacon	Wu	Garatt	Smith
10/12/2000 14:15	1.78	1.02	0.96	1.12	0.89	0.83
11/12/2000 02:45	1.78	0.83	0.72	0.93	0.64	0.58
12/12/2000 18:14	1.30	0.72	0.61	0.72	0.54	0.49
13/12/2000 16:04	1.39	1.10	0.82	1.10	0.65	0.59
ERA5 dataset						
Time	Obs. (m)	Predictions (m)				
		Sheppard	Deacon	Wu	Garatt	Smith
10/12/2000 14:15	1.78	1.56	1.54	1.66	1.36	1.22
11/12/2000 02:45	1.78	1.45	1.32	1.69	1.24	1.11
12/12/2000 18:14	1.30	0.89	0.89	0.93	0.73	0.66
13/12/2000 16:04	1.39	1.10	0.99	1.22	0.88	0.79
MÉRA dataset						
Time	Obs. (m)	Predictions (m)				
		Sheppard	Deacon	Wu	Garatt	Smith
10/12/2000 14:15	1.78	1.42	1.28	1.44	1.16	1.09
11/12/2000 02:45	1.78	1.50	1.13	1.58	1.18	1.03
12/12/2000 18:14	1.30	0.80	0.73	0.80	0.64	0.58
13/12/2000 16:04	1.39	1.19	0.97	1.11	0.85	0.77

Table 2.9: Statistical errors of peak surge residual results (m) between computed and observed data used for calibration of the model.

Method	ERA-Interim dataset				
	Sheppard	Deacon	Wu	Garatt	Smith
RMSE	0.69	0.80	0.63	0.90	0.96
Mean Error	-0.65	-0.78	-0.59	-0.88	-0.94
Error Standard Deviation	0.28	0.21	0.24	0.19	0.19
Method	ERA5 dataset				
	Sheppard	Deacon	Wu	Garatt	Smith
RMSE	0.32	0.39	0.22	0.52	0.62
Mean Error	-0.31	-0.38	-0.19	-0.51	-0.62
Error Standard Deviation	0.08	0.10	0.13	0.06	0.05
Method	MÉRA dataset				
	Sheppard	Deacon	Wu	Garatt	Smith
RMSE	0.35	0.54	0.35	0.61	0.70
Mean Error	-0.34	-0.53	-0.33	-0.60	-0.69
Error Standard Deviation	0.13	0.10	0.12	0.05	0.06

2.2.3 Storm Surge Meteorological Input

As introduced in Section 1.3.2, the three datasets are potential model inputs for calibrating the wind drag coefficients. This section will concentrate on the selection of which dataset to use for the storm surge model.

2.2.3.1 Skew surge

As mentioned in the literature review in Chapter 1, both the skew surge and the surge residual can be used in storm surge investigations. Here, the simulation results of a storm surge event are compared with respect to the skew surge and the surge residual, and they are validated with the BODC field measurements. The 2000 surge event is applied for demonstrating the concept. As can be seen in Figure 2.11, the simulation results of the skew surge can represent some features of the surge events (according to the measurements of the 2000 event). However, compared with the results of the surge residual, the skew surge results do not capture most of the surge peak, which is rather significant for storm surge event simulations. This may be due to the short duration of the surge-tide interaction in the Bristol Channel. A similar conclusion has been drawn by Gao [70] through the return level analysis of the tides as the return levels of skew surges are always lower than the residuals in the Bristol Channel. Thus only the surge residual will be used in simulations to represent the storm surge phenomenon in this project, which is calculated by subtracting the tidal prediction from total sea level observations.

2.2.3.2 Datasets

Three datasets are considered in this project with different spatial and temporal resolutions. This section will select the most suitable dataset for the surge simulations in this project. It was found that one of the datasets required pre-processing. The MÉRA dataset has strong and presumably un-physical variations in wind speed (both in space and time). To remove these, a smoothing function is used on the wind speed which is chosen to conserve kinetic energy. This is applied to the data before any modelling application, as seen in Figure 2.12.

One thing to note is that the surface pressure parameter in the MÉRA dataset appears to have rather poor quality compared with the others. Figure 2.13 shows the pressure comparison between the different datasets and MÉRA can only capture the general trends of the pressure within the region of interest, clearly underestimating the pressure variation.

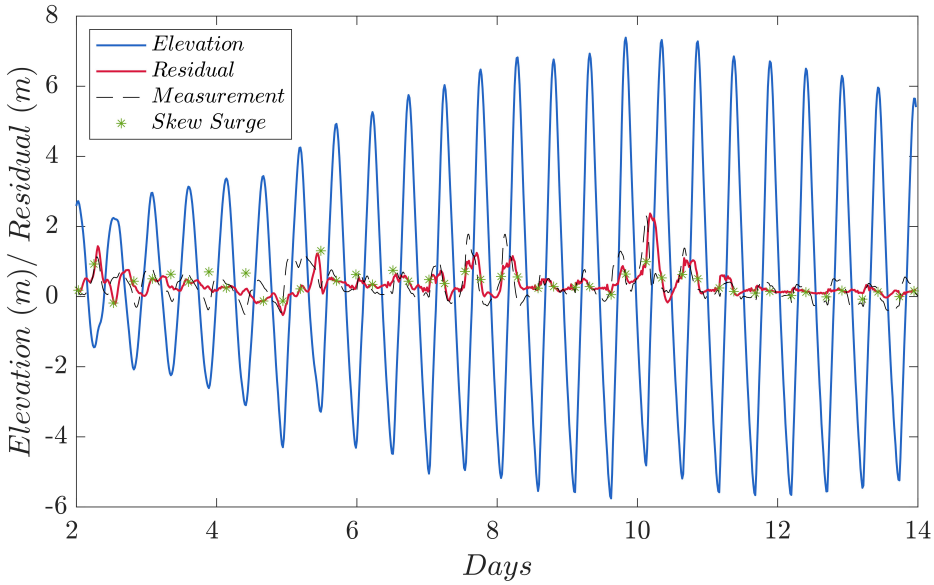

Figure 2.11: Storm surge representation according to skew surge and surge residual for the 2000 event at Avonmouth.

Figure 2.14 and Figure 2.15 show the simulation results for the year 2000 storm surge event and the 2014 event respectively based on the different datasets. The 2000 event is a significant surge event with over 2 m surge levels according to *in-situ* measurements. Generally, all three datasets have minor phase shifts compared with the measurements. Only ERA-Interim captures the event peak on the day of 13 December of 2000 (day 10 of the simulation period). However, this dataset overestimates simulation results for other periods and has the most significant time lag of all the datasets. For the ERA5 and MÉRA datasets, despite not delivering good simulation results on the peak-event day, they are more accurate at capturing other surge events near the peak time. Between these two, the ERA5 dataset has better simulation results by visual inspection. For the 2014 surge event, none of the three datasets can perfectly simulate the correct surge peak level, even though ERA5 and MÉRA have better performance. ERA-Interim again shows the longest time lag for the whole simulation period. As a result, the ERA5 and MÉRA datasets give better predictions for residual elevations for both surge events.

Table 2.10 shows the error analysis in the application of different datasets with these two storm surge events. From the Table, conclusion can be drawn that the application of ERA5 would give the minimum RMSE compared with the observed data and would have the best performance amongst the three.

Considering the dataset input resolutions (see Table 1.3), the ERA-Interim dataset

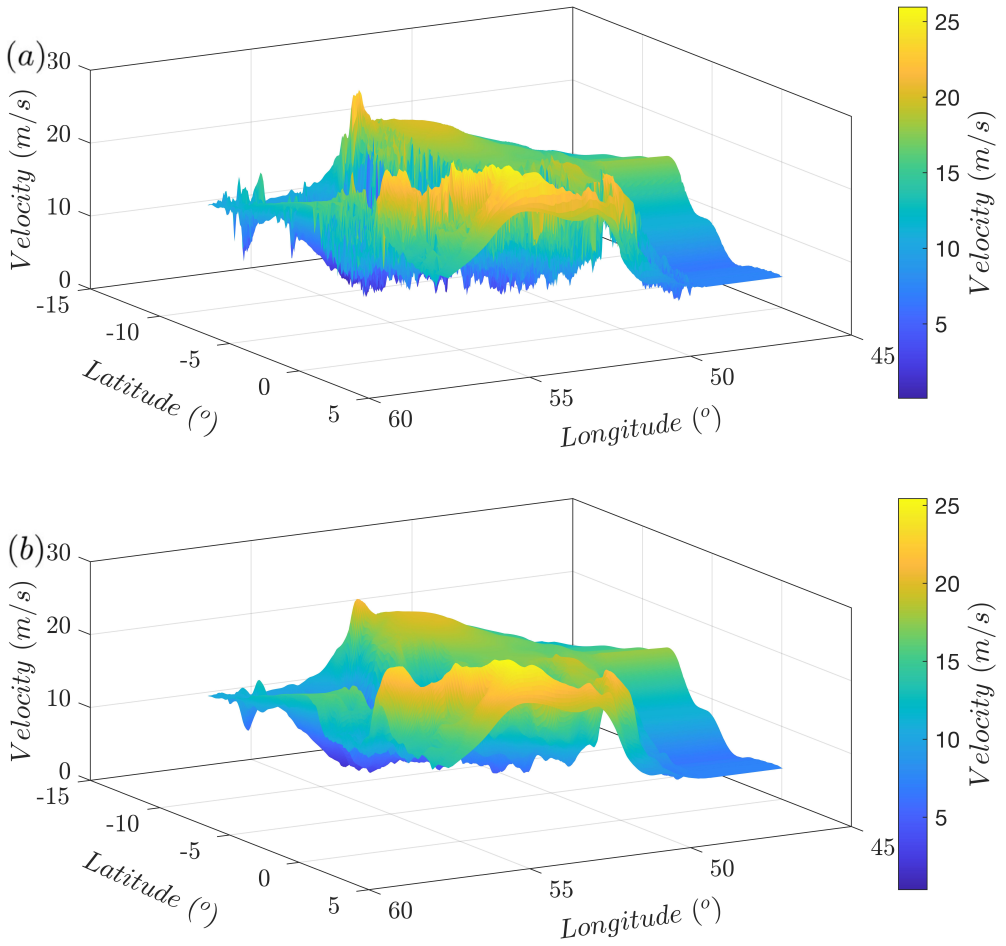

Figure 2.12: Meteorological input, wind speed smoothing for MÉRA dataset for the whole domain at 13/12/2000, speed obtained from U- and V- velocity components of the dataset: a) un-smoothed case (top); b) smoothed case (bottom).

Table 2.10: Root-mean-square error of surge residual results (m) between computed and observed data used for selection of suitable dataset.

Dataset	ERA-Interim dataset	ERA5 dataset	MÉRA dataset
2000 event	0.24	0.19	0.52
2014 event	0.15	0.11	0.46

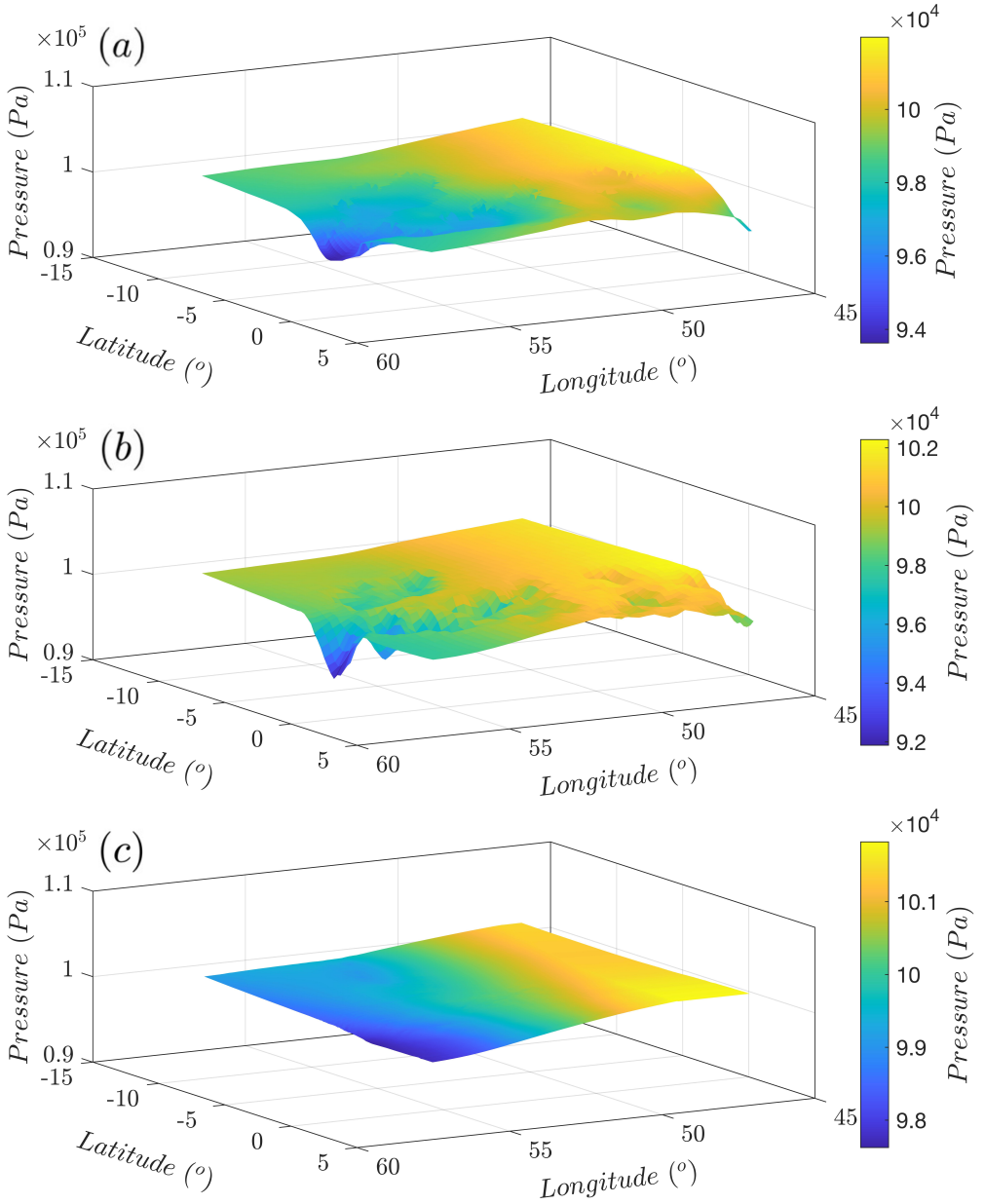

Figure 2.13: Comparison of the meteorological pressure input for ERA-Interim, ERA5 and MÉRA datasets for the whole domain at 13/12/2000: a) pressure for ERA-Interim dataset (top); b) pressure for ERA5 dataset (middle); c) pressure for MÉRA dataset (bottom).

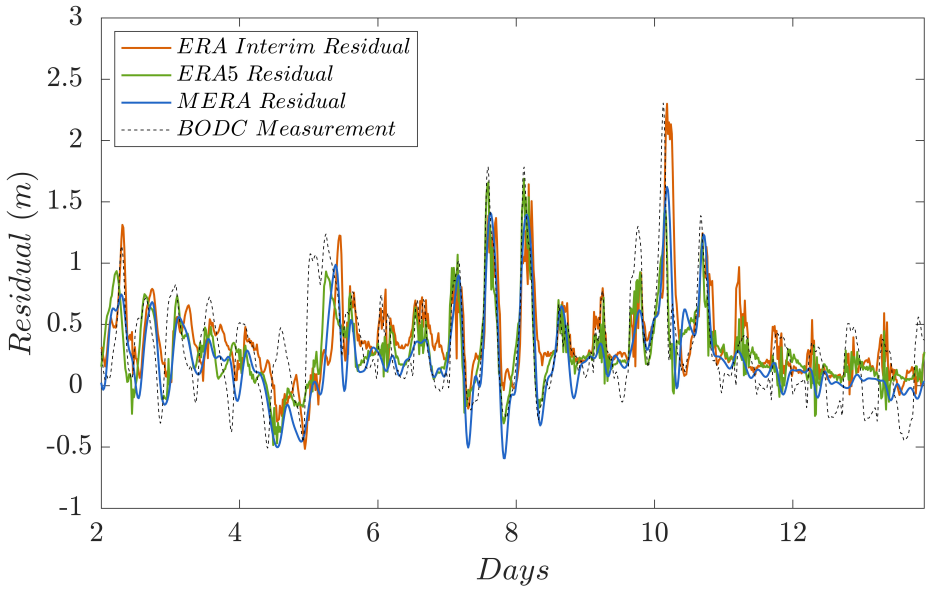

Figure 2.14: Comparison of the simulation results for 2000 storm surge event at Avonmouth between the three sets of data: MÉRA, ERA5 and ERA-Interim predicted by DG-SWEM.

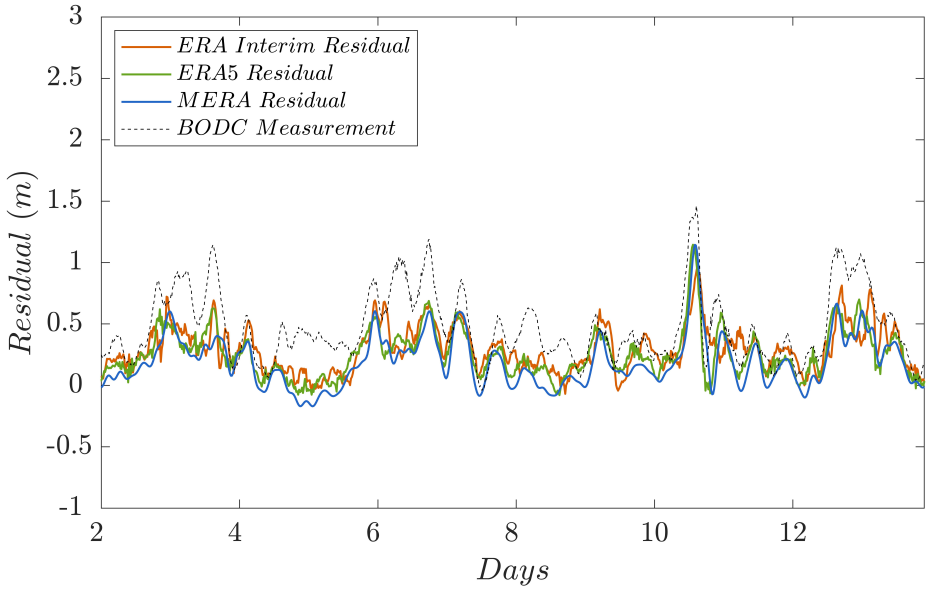

Figure 2.15: Comparison of the simulation results for 2014 storm surge event at Ilfracombe between the three sets of data: MÉRA, ERA5 and ERA-Interim predicted by DG-SWEM.

has the coarsest spatial and temporal resolution of the three. ERA5 has the best temporal resolution with hourly interval input and MÉRA has the best spatial resolution. As presented in [173] in their re-analysis of the 1981 storm surge event, the accuracy of simulation results of the surge events may be affected by the frequency of the forcing data in the re-analysis dataset (i.e. the temporal resolution). The rapidly developing nature of the meteorological situation may not be resolved accurately if the input frequency is too small. Thus the temporal resolution is more significant than the spatial resolution for the meteorological input datasets and, based on this along with the error analysis above, the ERA5 dataset is selected as the meteorological input for the storm surge simulations in this project.

2.3 Model Validation

Model validation is undertaken against harmonic constituent field measurements taken from the TotalTide software, a numerical model by Davis and Jones [45], and the British Oceanographic Data Centre (BODC) measurements during the surge events, at locations in and a little beyond the Bristol Channel region. TotalTide is a tidal prediction program providing the tidal height and current prediction for more than $7,000$ ports worldwide based on the output of harmonic analysis at these locations. The validation study includes the tidal harmonic analysis in Section 2.3.1 for M_2, S_2 and N_2 tidal components for the whole computational domain. Due to the significance of M_2 and S_2 in the Bristol Channel, as stated in Section 2.2.1, only these and not N_2 are considered in detail. Section 2.3.2 describes current velocities in the Bristol Channel region. Section 2.3.3 considers the different storm surge events' validation with application of the calibrated storm surge model and Section 2.3.4 looks at the effect of bed friction (the dominant variable parameter) on the storm surge event.

In the harmonic analysis and current validation studies, the model is run without any meteorological inputs or barrage implementation in order to observe the general flow of tides though the Bristol Channel region. While for the storm surge validation, the corresponding meteorological inputs of the selected surge events are applied to the model. This thesis does not present an analysis of the diurnal constituents as these are relatively small compared to the semi-diurnal constituents that are considered. However, the analysis of K_1 (the largest diurnal constituent) has in fact been done, and though the predictions have been found to agree with measured observations, the inclusion of K_1 as an additional boundary forcing tide also showed no difference in the model results.

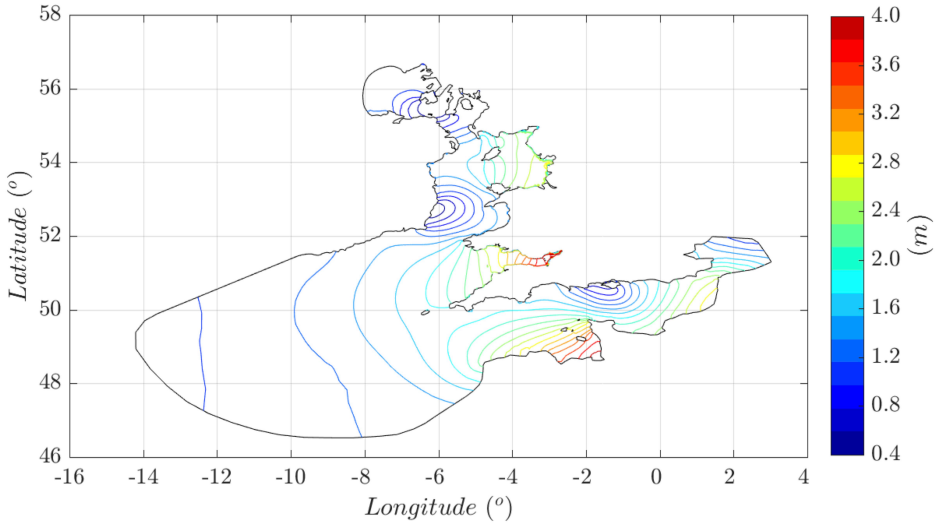

Figure 2.16: M_2 co-tidal amplitude contours (m) predicted using DG-SWEM.

2.3.1 Tidal Water Levels

Tidal harmonic analysis is used here for the tidal water level investigations. The numerical model is forced by semi-diurnal M_2, S_2 and N_2 tidal components on the open boundaries, and the simulation results are compared against co-tidal charts generated by Davis and Jones [45] and the Admiralty Chart (2006) data from several observation stations.

For the purpose of harmonic analysis, the simulation runs for a period of 30 days, over a complete spring-neap cycle, with a spin-up period of two days.

Figure 2.16 shows the computed co-tidal contours of the M_2 amplitude by DG-SWEM and Figure 2.17 presents the predicted phase in degrees. Figure 2.18 and Figure 2.19 show the amplitude and phase of the S_2 tide respectively, and Figure 2.20 and Figure 2.21 present the data for the N_2 tide. The model predictions of the co-tidal charts of these three tidal constituents are in very good visual agreement with the maps presented by Davis and Jones [45] (not shown).

Quantitative comparisons have been carried out for the M_2 and S_2 tidal components. The predicted simulation results are compared against observations from the Admiralty Chart (2006) and the corresponding results obtained by Davis and Jones (approximate results captured from the co-tidal charts). Table 2.11 and Table 2.12 present the results for the M_2 and S_2 tidal components. The observation stations of Pwllheli, Barmouth and Fishguard are beyond the Bristol Channel while the others are inside the channel region. As shown by the Tables, the simulations from the

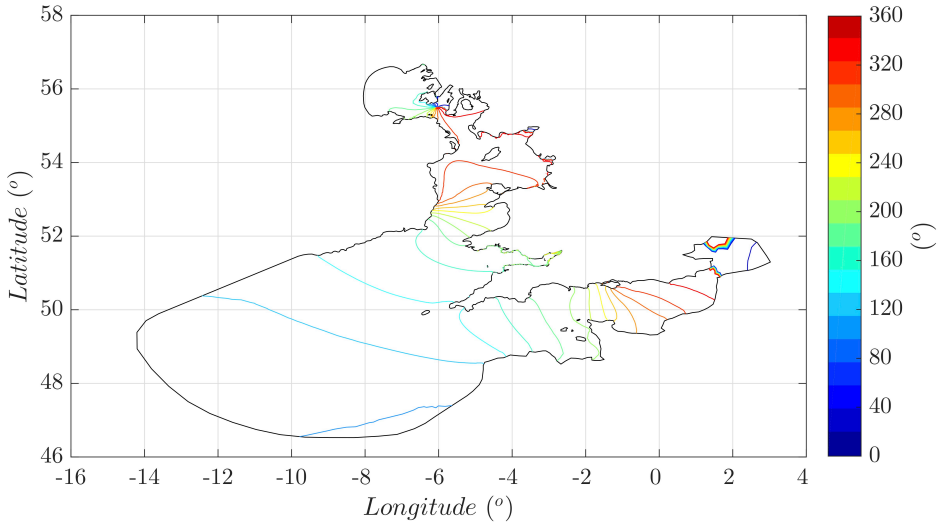

Figure 2.17: M_2 co-tidal phase contours (degrees) predicted using DG-SWEM.

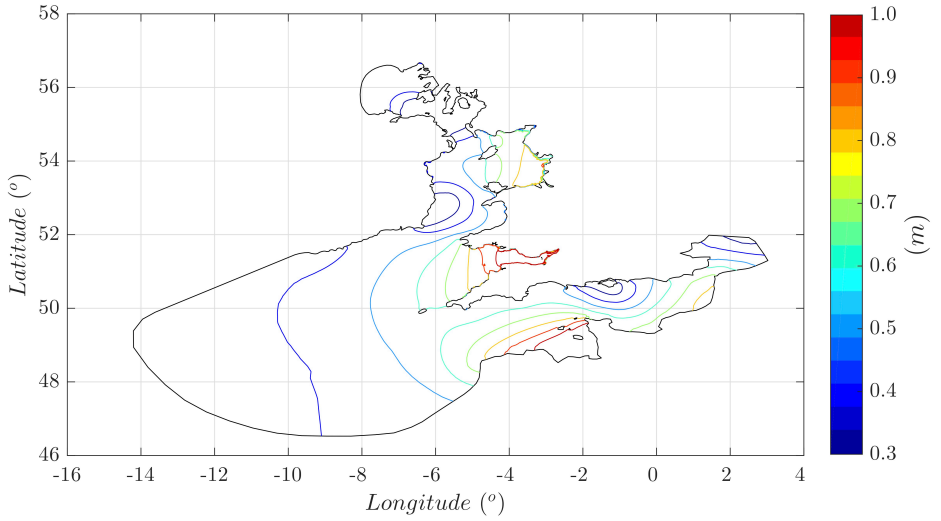

Figure 2.18: S_2 co-tidal amplitude contours (m) predicted using DG-SWEM.

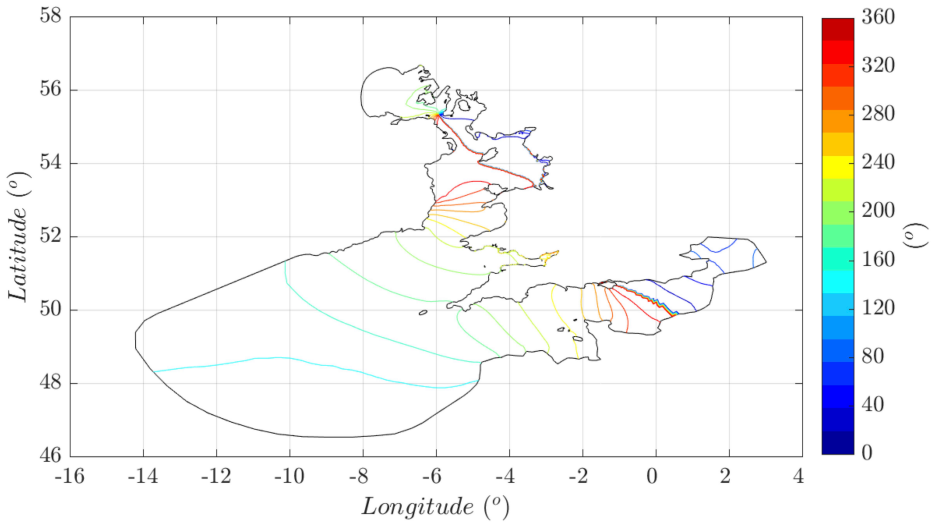

Figure 2.19: S_2 co-tidal phase contours (degrees) predicted using DG-SWEM.

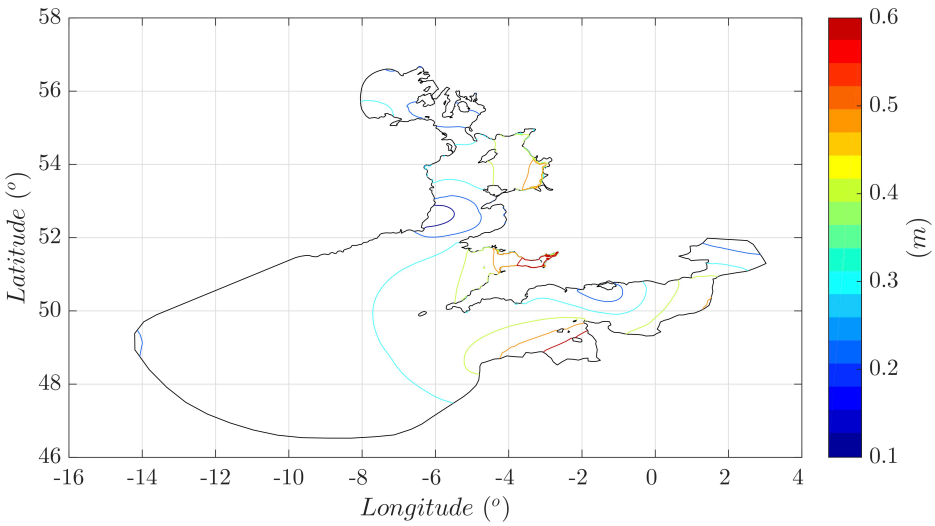

Figure 2.20: N_2 co-tidal amplitude contours (m) predicted using DG-SWEM.

Table 2.11: Harmonic analysis of M_2 tidal elevation amplitudes and phases at different stations within and beyond the Bristol Channel.

Station	M_2 Amplitude (m)		
	Observations	Predictions	Davis & Jones [45]
Pwllheli	1.48	1.51	1.50
Barmouth	1.47	1.52	1.60
Fishguard	1.35	1.42	1.60
Stackpole Quay	2.51	2.54	2.70
Mumbles	3.18	3.09	3.25
Barry	3.82	3.91	3.33
Flat Holm	3.90	4.02	4.00
Hinkley Point	3.80	3.97	3.90
Ilfracombe	3.04	3.01	3.20
Lundy	2.67	2.56	2.90
Station	M_2 Phase (°)		
	Observations	Predictions	Davis & Jones [45]
Pwllheli	239	239	225
Barmouth	244	236	220
Fishguard	207	208	185
Stackpole Quay	168	174	162
Mumbles	171	176	168
Barry	185	183	205
Flat Holm	190	188	200
Hinkley Point	185	184	190
Ilfracombe	162	167	160
Lundy	160	165	160

Table 2.12: Harmonic analysis of S_2 tidal elevation amplitudes and phases at different stations within and beyond the Bristol Channel.

Station	S_2 Amplitude (m)		
	Observations	Predictions	Davis & Jones [45]
Pwllheli	0.58	0.57	0.65
Barmouth	0.53	0.57	0.70
Fishguard	0.53	0.53	0.65
Stackpole Quay	0.90	0.90	0.85
Mumbles	1.12	1.09	1.00
Barry	1.37	1.39	1.06
Flat Holm	1.37	1.43	N/A
Hinkley Point	1.42	1.41	1.00
Ilfracombe	1.10	1.07	1.00
Lundy	0.94	0.91	0.95
Station	S_2 Phase (°)		
	Observations	Predictions	Davis & Jones [45]
Pwllheli	276	277	280
Barmouth	283	274	265
Fishguard	248	248	230
Stackpole Quay	214	217	210
Mumbles	221	220	220
Barry	240	233	225
Flat Holm	246	238	240
Hinkley Point	237	234	255
Ilfracombe	209	211	210
Lundy	207	208	205

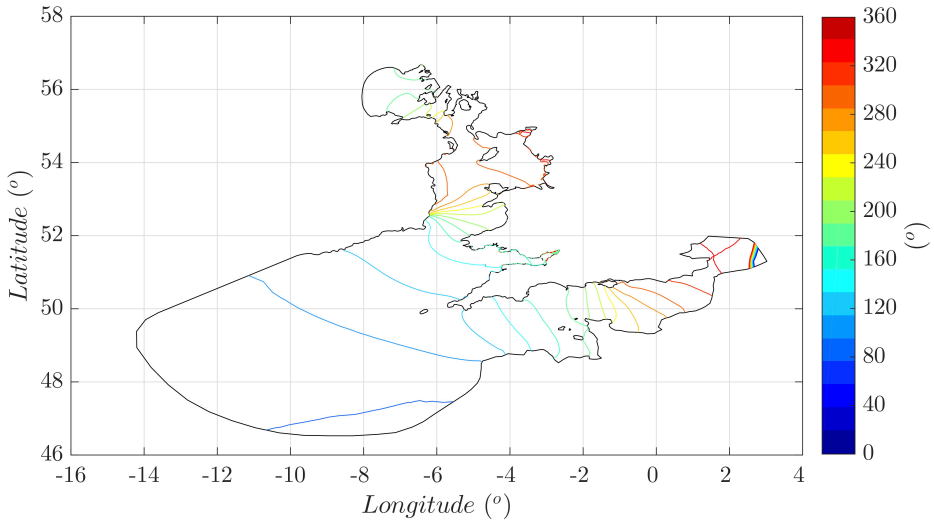

Figure 2.21: N_2 co-tidal phase contours (degrees) predicted using DG-SWEM.

model are found to be mostly in satisfactory agreement with the observations, with the level of agreement defined by the error criteria in Section 2.2.1. It has been calculated that the RMSE values and error percentages between model predictions and observations are 0.09 m and 3.28% respectively for the M_2 amplitude, and 0.03 m and 2.95% respectively for the S_2 amplitude. This model also gives better prediction results than those presented by Davis and Jones (e.g. the RMSE value and error percentage between their predicted values and observations for the M_2 amplitude calculate out to be 0.21 m and 7.66% respectively), which indicates the benefits of the application of the unstructured finite element mesh by DG-SWEM for simulations of complex coastlines as the Bristol Channel region. With respect to the simulated phase results, again, this model has better performance than the Davis and Jones's simulations for both sets of semi-diurnal constituents. The RMSE values are calculated to be 4.30° and 4.68° respectively for the M_2 and M_2 phases. The values can be compared with the ones from Davis and Jones's simulations, which are 13.53° and 11.27°, respectively. The discrepancy between phase and amplitude results may be due to the less realistic, constant bed friction coefficient applied. However, it is very difficult to model a varying bed friction [164], especially as it is also affected by the flow velocity. Although there are slight differences between the simulation and observation values at specific stations, the overall predictions appear to be in a satisfactory agreement with the tidal dynamics in the channel region.

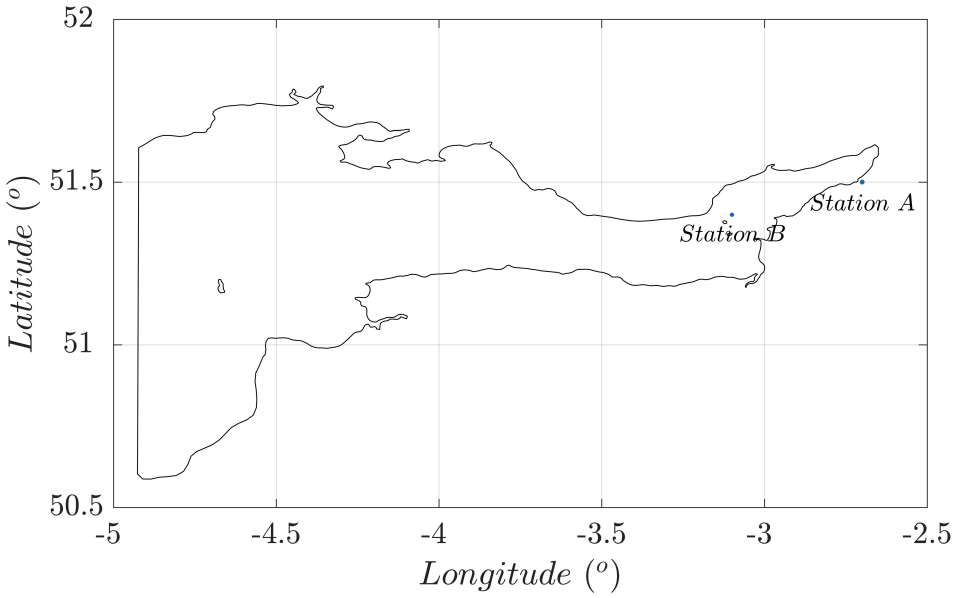

Figure 2.22: Location of current velocity stations (TotalTide) in the Bristol Channel used in the tidal current validation tests.

2.3.2 Tidal Current

Even though this project focuses on water elevation predictions in the Bristol Channel, correctly simulating the naturally occurring flows is important in giving confidence in the numerical modelling. In general, currents are usually harder for simulations to capture accurately compared to water levels.

The model simulation for current validation is carried out for a period of 14 days with the spin-up period of two days. Neither meteorological inputs nor barrage characteristics are included. Predicted water current velocities from DG-SWEM are compared against Admiralty TotalTide data at selected locations: station A near Avonmouth (51°30.53'N 2°43.58'W) and station B near Flat Holm (51°23.23'N 3°05.07'W) (see Figure 2.22).

The analysis of currents is different to the water elevation analysis as the observations are a vector time series of current speed and direction [138]. Figures 2.23 and 2.24 present comparisons between the model predictions of tidal current magnitude (overall and in the north-south and east-west directions) obtained using DG-SWEM and the hourly processed measurements of sea surface current by TotalTide at station A. Figure 2.25 and Figure 2.26 illustrate results at station B for overall magnitude and separate directions, respectively. It is noted that the quality of the current data derived from TotalTide is unknown [92, 93, 37], which would be a source of uncertainty

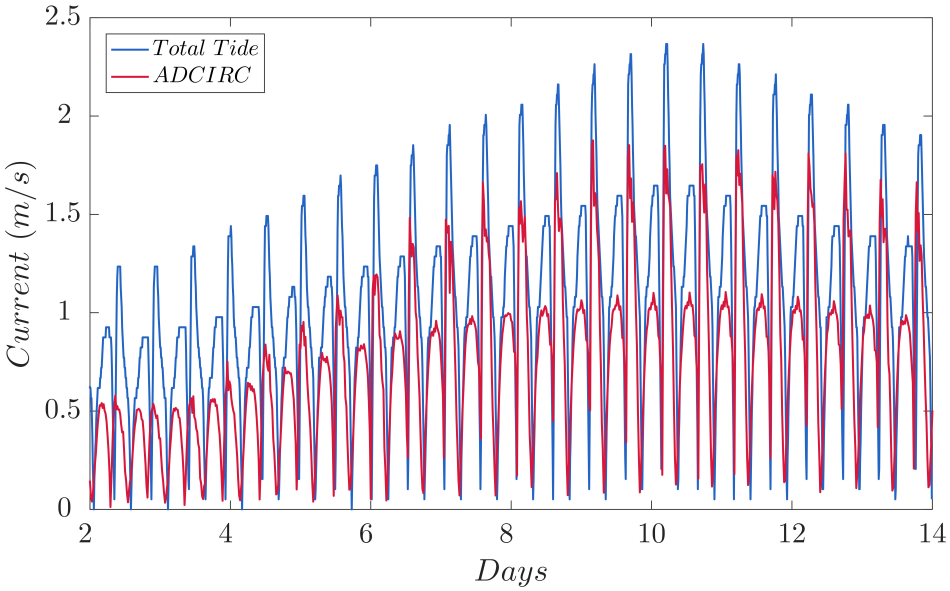

Figure 2.23: Predicted tidal current magnitude time histories at station A, 51°30.53'N 2°43.58'W, using DG-SWEM and TotalTide.

for data comparisons.

The predicted phases from DG-SWEM provide a visually acceptable level of agreement with the TotalTide predictions for both directions of current components at station A. The small amount of phase shifting may be explained by the difference in the number of harmonics included in the analysis by ADCIRC and TotalTide. For the magnitude, however, the predictions are underestimated compared with the TotalTide data. Similar levels of underestimations of the magnitude in both north-south and east-west directions indicate approximately the correct current directions are being simulated. While, at station B, there is better agreement between the two sets of predictions of current phases. The predicted amplitudes of the current are also in better agreement than station A for both directions. Table 2.13 lists the predicted amplitudes of the major semi-diurnal tidal current constitutes by harmonic analysis within the time period of simulation at station B. DG-SWEM predicts a current of lower amplitude of M_2 than that by TotalTide.

It should be noted that perfect agreement is not expected for the tidal current validation. Currents are three-dimensional and vary rapidly over short length scales and are difficult to analyse in a two-dimensional depth-averaged model. Especially for station A, where the station is almost at the head of the channel with rapid changes in water level in a shallower water region, the model simulations may not capture the flow physics correctly. The application of the constant bed friction coefficient

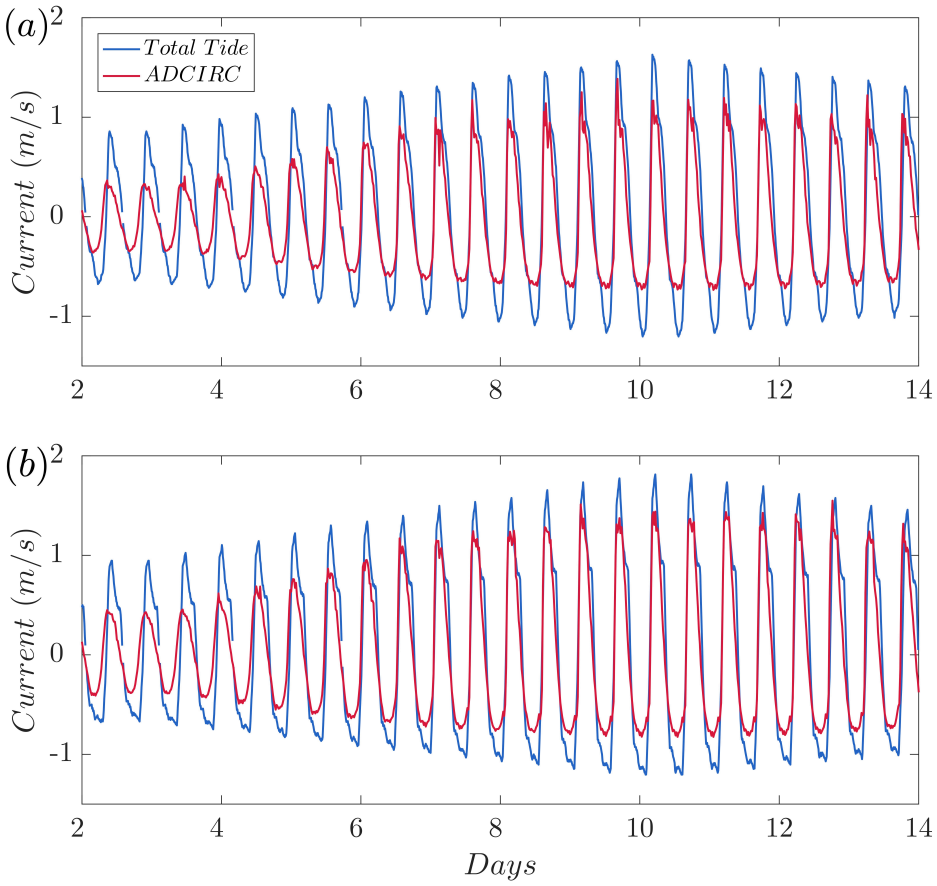

Figure 2.24: Predicted tidal current magnitude time histories at station A, 51°30.53'N 2°43.58'W, using DG-SWEM and TotalTide: a) north/south direction (top); b) east/west direction (bottom).

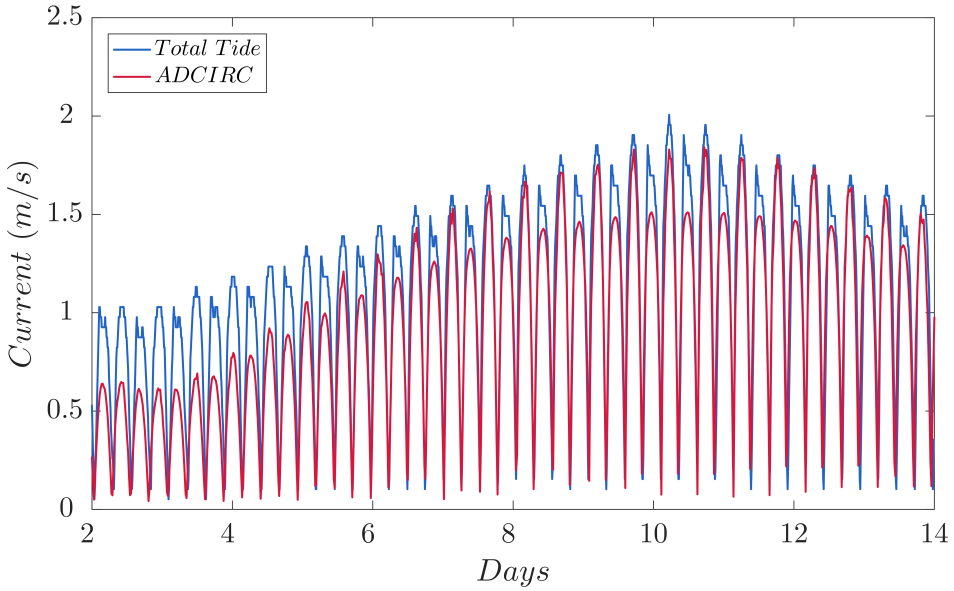

Figure 2.25: Predicted tidal current magnitude time histories at station B, 51°23.23'N 3°05.07'W, using DG-SWEM and TotalTide.

Table 2.13: Comparison between TotalTide observation and DG-SWEM predictions for magnitudes of the tidal current harmonic currents (m/s) at station B.

Station	Observed magnitude		Predicted magnitude	
	M_2	S_2	M_2	S_2
Station B	1.50	0.46	1.30	0.46

may also limit the accurate representation of the flow hydrodynamics in the two-dimensional model. Moreover, it is important to bear in mind that it is not certain whether the model applied gives an under-prediction or if the TotalTide output gives an overestimate of the actual phenomenon. Overall the Figures suggest that the general pattern of the current is well reproduced and dominant tidal hydrodynamics are captured by the model.

2.3.3 Storm Surge Events

There are five severe positive storm surge events with a surge of over 1 m in the Bristol Channel that have been recorded in the available water level measurements from BODC. These are shown in Table 2.14 and the locations of the measurement stations are shown in Figure 2.27. The two most recent events have been selected to validate the DG-SWEM for surge simulations in this project: the surge events on 13

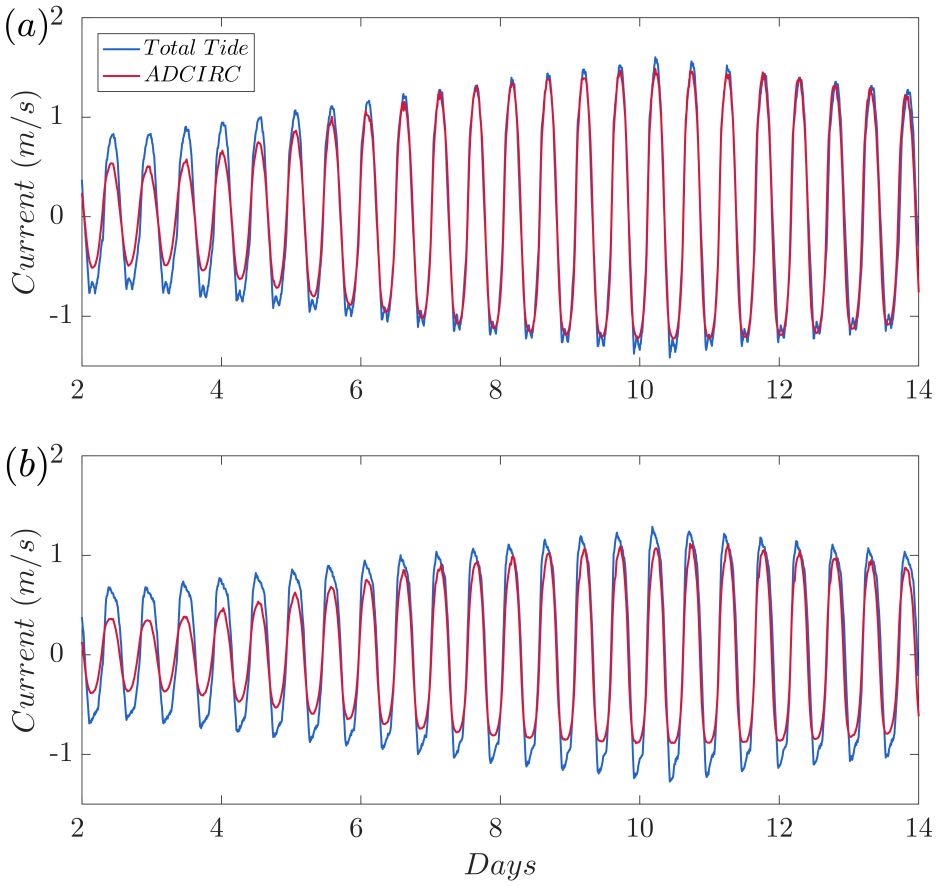

Figure 2.26: Predicted tidal current magnitude time histories at station B, 51°23.23'N 3°05.07'W, using DG-SWEM and TotalTide: a) north/south direction (top); b) east/west direction (bottom).

Table 2.14: Five largest positive storm surge events in the Bristol Channel, derived from BODC.

Date and duration (surge > 1 m)	Locations affected	Max surge (m)
25/01/1990, 0900-1600, 7hrs	Avonmouth	2.91
	Ilfracombe	1.51
04/01/98, 1000-1815, 8hrs15mins	Avonmouth	2.91
	Newport	2.45
	Hinkley Point	2.21
	Mumbles	1.97
19/01/95, 1315-1745, 4hrs30mins	Avonmouth	2.58
	Newport	2.54
	Hinkley Point	1.83
	Ilfracombe	1.13
13/12/00, 0000-0345, 3hrs45mins	Avonmouth	2.35
	Newport	2.31
	Hinkley Point	1.99
	Mumbles	1.59
12/02/14, 1115-1715, 6hrs	Newport	2.29
	Hinkley Point	1.90
	Ilfracombe	1.46

December of 2000 and 12 February of 2014. It should be noted that the simulation results would be meaningless when the corresponding field measurement stations are located at wetting and drying regions of the model (no effective prediction results would be obtained within those regions). Also there are limited station measurements (tide gauge data) available for certain surge events in the record and some gauge errors exist as well. After selecting the date, the following locations have been chosen for analysis: the Avonmouth station for the 2000 surge event and the Ilfracombe station for the 2014 event.

The observed surge level at Avonmouth is 2.35 m during the 2000 surge event. Figure 2.28 shows the simulated surge pattern with clear flooding risks at the head

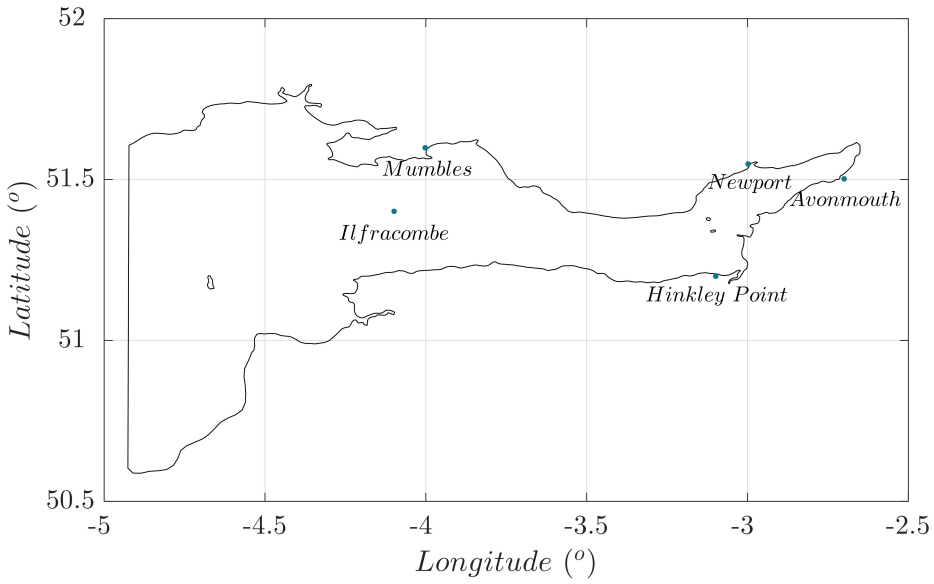

Figure 2.27: Location of measurement stations at the inner Bristol Channel from BODC.

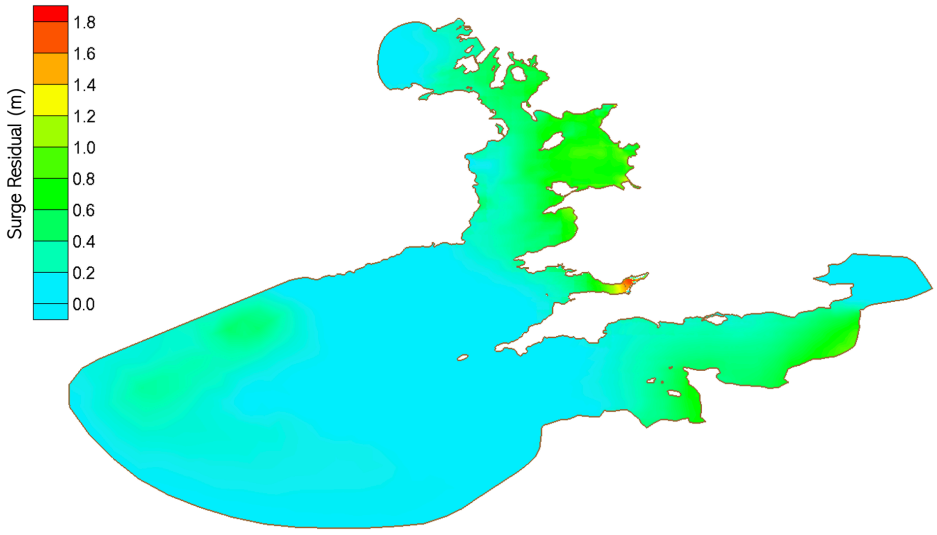

Figure 2.28: Simulated surge residual results (m) of storm surge events of 2000 for whole domain (from BODC) predicted and shown by DG-SWEM with ERA5 data set.

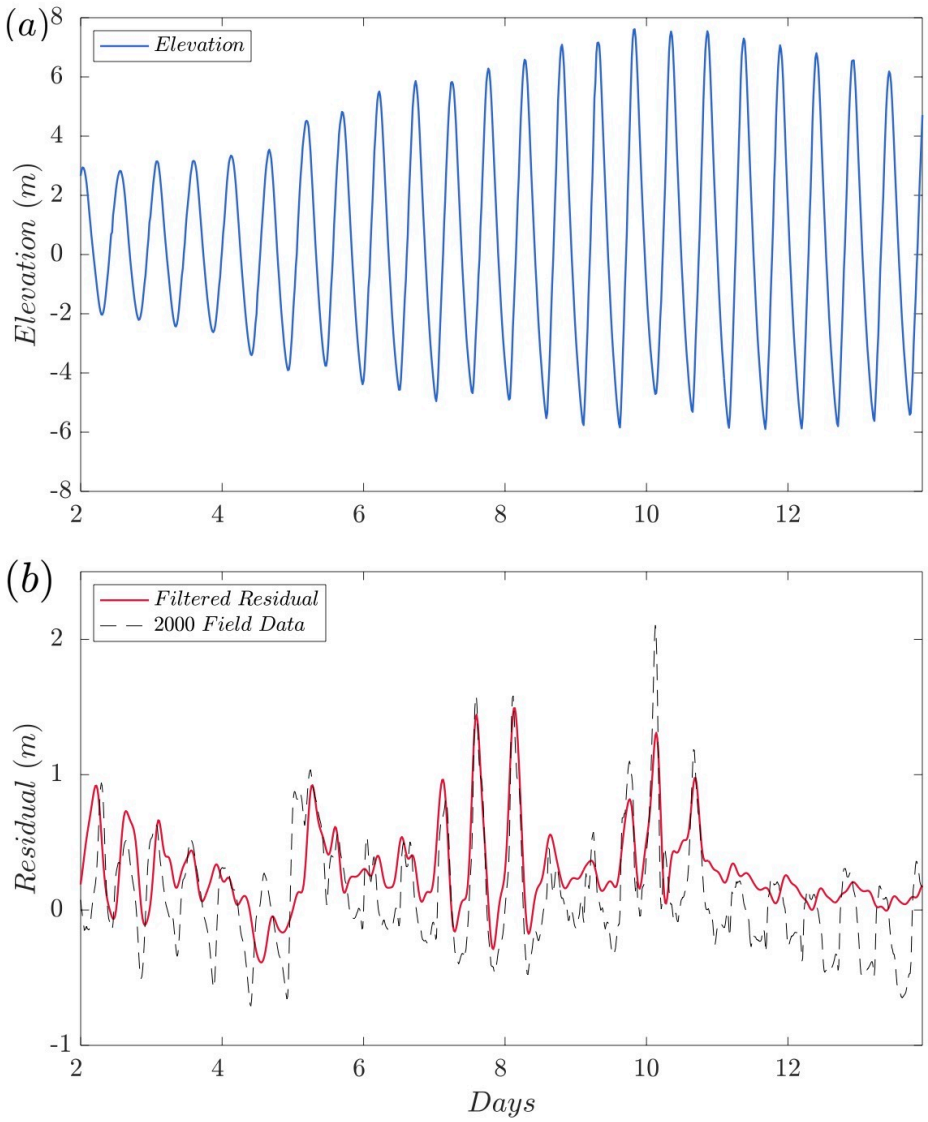

Figure 2.29: Simulation results of storm surge events of 2000 at Avonmouth predicted by DG-SWEM and compared with field measurements: a) water level (top); b) residual level (bottom).

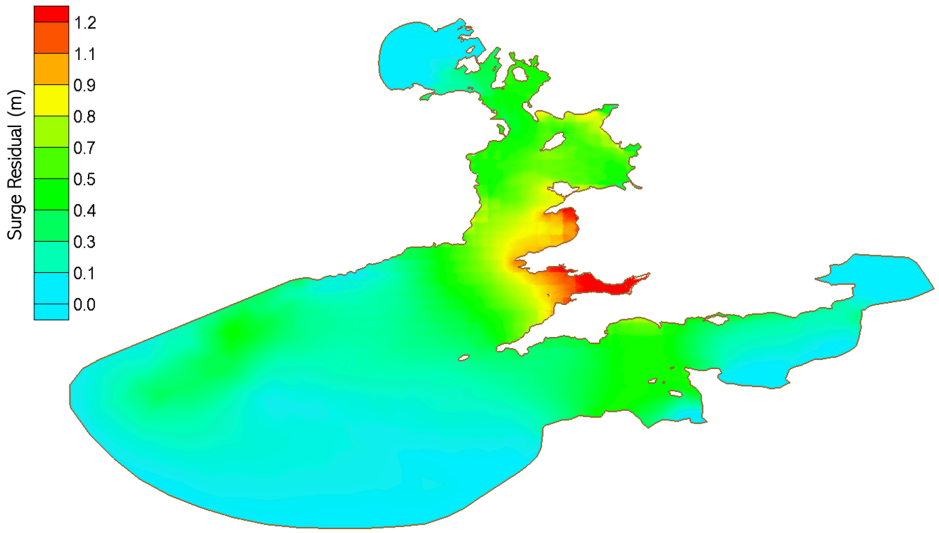

Figure 2.30: Simulated surge residual results (m) of storm surge events of 2014 for whole domain (from BODC) predicted and shown by DG-SWEM with ERA5 data set.

of the channel, illustrated in SMS, and Figure 2.29 displays the model predictions compared with the field measurements. As can be seen in the Figure, there are small phase shifts and reduced surge (residual) peak from the simulation results. The model's prediction of the peak in the surge is delayed compared to the observations and the peak surge value is under-predicted by an amount of 0.84 m at Avonmouth. Other than the global maximum peak of the surge, there are also other relatively large surge events within this period that are local maximums, like the event at 8.1 days of the simulation period. To calculate an error percentage for the level of agreement between prediction and measurements, the three largest local peaks (other than the global maximum) are taken to calculate their RMSE and then error percentage, which results in a value of approximately 7%. While this exceeds the limit set for acceptable data agreement criterion, the specific discrepancies that result in this value are explained below. Meanwhile, in the 2014 storm surge event, large portions of the Bristol Channel region and areas around the St George's Channel may be at risk from flooding (taken to be situations where the surge levels exceed 1 m), as can be seen in Figure 2.30 where the surge pattern is red. Figure 2.31 illustrates the simulation predictions against field measurements in the 2014 event. The phase of the modelled surge peaks is acceptable, being approximately 40 minutes early, and the maximum modelled surge is underestimated by approximately 0.12 m. For other simulation periods, the ADCIRC predictions generally give lower results than the field measurements.

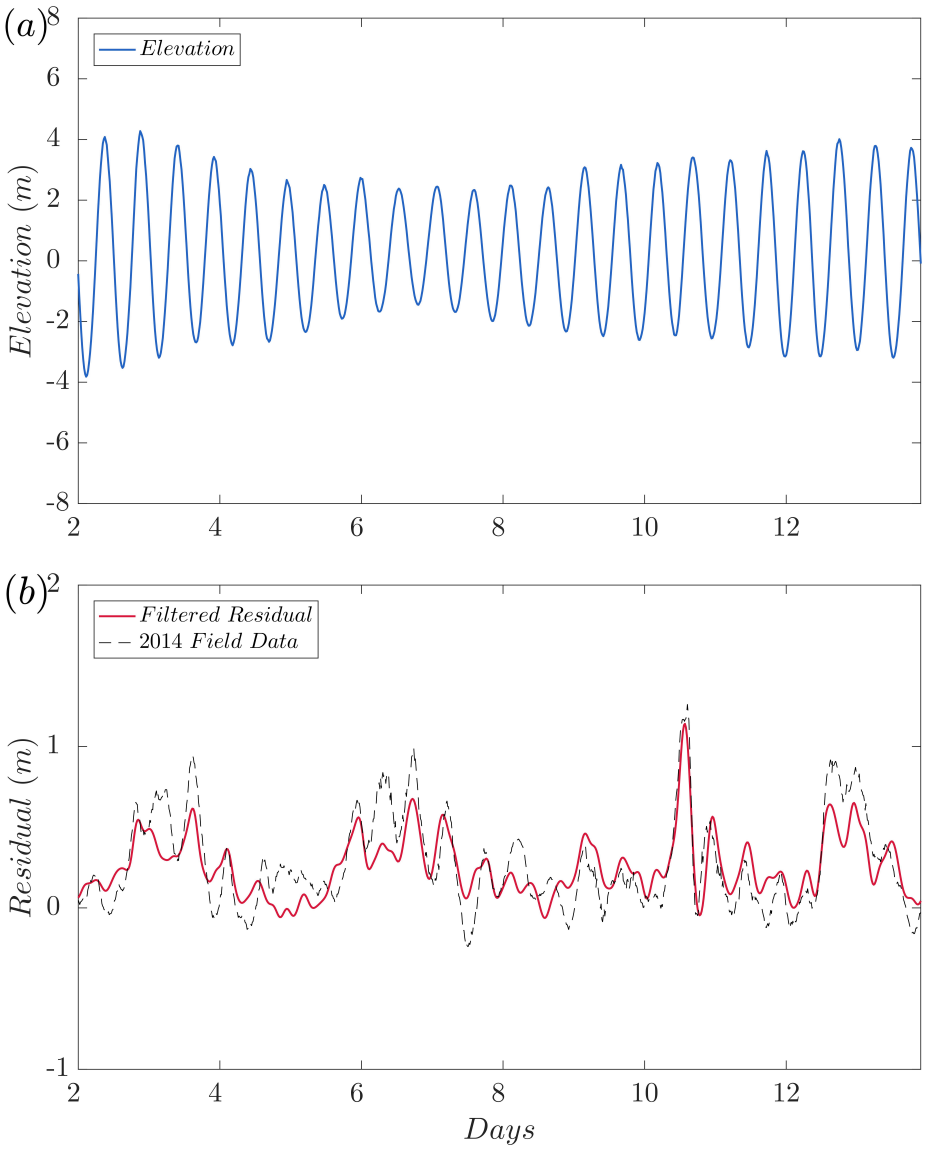

Figure 2.31: Simulation results of storm surge events of 2014 at Ilfracombe predicted by DG-SWEM and compared with field measurements: a) water level (top); b) residual level (bottom).

While there are discrepancies between measurements and model predictions in these two surge events and the error percentages are larger than expected, the results are deemed acceptable for the surge and further barrage interaction studies in this project, for a few reasons. A key reason for the discrepancy, which is considered in detail during this work, is some inaccuracy occurring in the meteorological inputs from the ERA5 dataset, which can be evidenced by the poor estimation of the peak surge in the 2000 event. This is consistent with the work of Williams *et al.* [173] who highlight the problem of inaccurate meteorological data for studies of this kind. Another significant reason is inaccuracies inherent in the field measurements, as these values are also not an exact reflection of surge event elevations. Measuring equipment have their own limitations and manufacturers usually provide an error range expected when using such equipment. Furthermore, there are several possible reasons in the simulation for discrepancies, including neglecting wave set-up and the constant bed friction applied in the present model. An additional phenomenon that would affect storm surge simulation can be the excess discharge from River Severn. However, in this region the discharge is not expected to play a major role in altering water levels. According to simulations, a typical flow rate in the estuary (estimated at the location of the barrage) is approximately $200,000$ $\mathrm{m^3 s^{-1}}$. The maximum discharge ever recorded from River Severn is 533 $\mathrm{m^3 s^{-1}}$ [4], which is negligible and should make limited difference to the water level in the region.

Despite having analysed the storm surge events of 2000 and 2014 in this section, they are in fact the only two events that have both BODC and ERA5 measurement data available for study. Even then, as two of the worst surge events in the Bristol Channel in the recent 50 years, they are not considered extreme storm surges, defined by the coincidence of the surge event with high astronomical tides. Additionally, as shown by this section, there are several sources of errors involved with the datasets of actual field measurements of storm surges. Therefore, in order to examine the impacts of such a severe surge and to reduce the negative impacts of errors from meteorological inputs, an artificial simulation based on the storm surge event of the year 2000 is used, which will be introduced in Section 2.5.2.

2.3.4 Effect of Bed Friction on Storm Surges

As discussed in Section 2.2.1, the model applied here, which has also been calibrated by Serhadlıoğlu [149], is sensitive to variations in bed friction. In Section 2.2.1 it is found that the model calibration with consideration of only tides is achieved by applying $C_f = 0.0025$ with the constant quadratic friction law in the Bristol Channel.

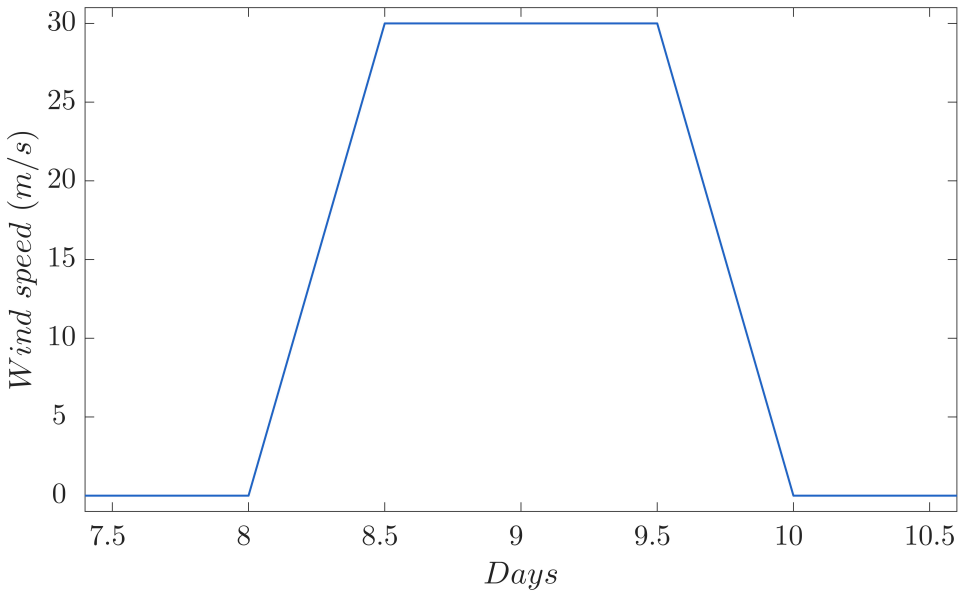

Figure 2.32: Variation of input wind forcing with simulation time.

In this section, the effect of the variations of bed friction coefficients will be further investigated in order to clarify the applicability of the model to surge events.

Due to the lack of extreme surge meteorological data, an artificial extreme surge event is used. According to Gao [70], extreme winds could reach over 20 m/s in the Bristol Channel and winds blowing from the south-westerly directions are more frequent and stronger than that from other directions. The simulations here (14-day period) apply south-westerly winds that are increased from 0 to 30 m/s linearly in time beginning on day 8 (from 00:00 to 12:00), kept constant for 24 hours and then decreased to 0 on day 10 (Figure 2.32). For the rest of the simulation period, the wind is kept at 0 m/s. For the whole simulation, the atmospheric pressure is applied with a constant value of $101,325$ Pa. Different friction coefficients of $C_f(1) = 0.002$, $C_f(2) = 0.0025$, $C_f(3) = 0.003$ and $C_f(4) = 0.004$ are applied for the designed surge cases without any astronomical tides. The resulting peak residual conditions of the cases, in terms of their amplitudes and phases, are presented in Table 2.15. The measurement stations of Avonmouth, Ilfracombe, Hinkley Point and Flat Holm are included.

The simulation cases in the absence of tides consider the potential impact of friction coefficients on the surge residual during a surge event. From Table 2.15, limited difference in residual amplitude can be observed over varying friction coefficients when a surge event is applied. At Avonmouth, the variance results between coefficients cases is the largest with 0.02 m. Considering the timing of the event, the largest variance

Table 2.15: Surge residual magnitude and timing at different stations using different values of constant bed friction coefficients regarding to designed storm surge event. $C_f(1)$=0.002; $C_f(2)$=0.0025; $C_f(3)$=0.003 and $C_f(4)$=0.004. The 'Max. Difference' value at a station is the largest difference between surge residual magnitudes or peak timings across different bed friction coefficients.

Station	Peak Magnitude (m)				
	C_f (1)	C_f (2)	C_f (3)	C_f (4)	Max. Difference
Avonmouth	2.06	2.05	2.04	2.03	0.02
Ilfracombe	0.83	0.83	0.83	0.83	0.00
Hinkley Point	1.30	1.29	1.29	1.29	0.01
Flat Holm	1.43	1.43	1.43	1.43	0.00
Station	Peak Timing (day)				
	C_f (1)	C_f (2)	C_f (3)	C_f (4)	Max. Difference
Avonmouth	8.61	8.61	8.61	8.61	0.00
Ilfracombe	8.60	8.60	8.58	8.57	-0.03
Hinkley Point	8.60	8.60	8.58	8.58	-0.01
Flat Holm	8.58	8.58	8.60	8.60	0.01

between different coefficients occurs at the Ilfracombe station with a phase lag of 0.03 day, which is less than 1 hour.

As discussed in Section 2.2.1, selection of the bed friction coefficient is essential for the model simulations since it affects the main tidal hydrodynamics, namely the amplitude and phase of tidal constituents, in the channel. While for the residual component of the total water level, it is driven mainly by the wind shear stresses and atmospheric pressure variation, which are conditions of the upper water layer and would not be significantly affected by bed friction. This result is also shown in Table 2.15. As the surge results are only slightly modified by different friction values, the value determined using the tidal analysis is used in this work.

2.4 Representation of the Barrage in Numerical Modelling

As introduced in the Literature Review in Section 1.4.3, the tidal barrage behaviour within the domain, which can be split into two sub-domains, can be represented by the discharge or velocity through the barrage. In order to include the effects of hydrodynamic structures of sluices and turbines in the tidal barrage, a barrage boundary incorporated in DG-SWEM is used. This section will mainly focus on a brief description of the implementation of the barrage boundary into the two-dimensional model and an introduction of the Severn Barrage and Swansea Lagoon proposals that will be considered in this project. Relevant modelling parameters that make a significant difference to the final results will be discussed. The detailed verification of the barrage implementation can be found in [147]. The approach of the barrage implementation in the numerical models is introduced in Section 2.4.1. Section 2.4.2 describes the details and the application of the barrage and lagoon proposals. Adjustments of relevant additional parameters considered in the numerical modelling of the barrage are introduced in Section 2.4.3.

2.4.1 Implementation of Sub-grid Model to Represent the Effect of Barrage

The sub-grid-scale barrage model is developed based on a culvert model already present in DG-SWEM [169, 46], which adds an internal barrier into the finite element mesh. The internal barrier acts as a reflective boundary throughout its length with zero perpendicular velocity, except at the node pairs where hydraulic structures are

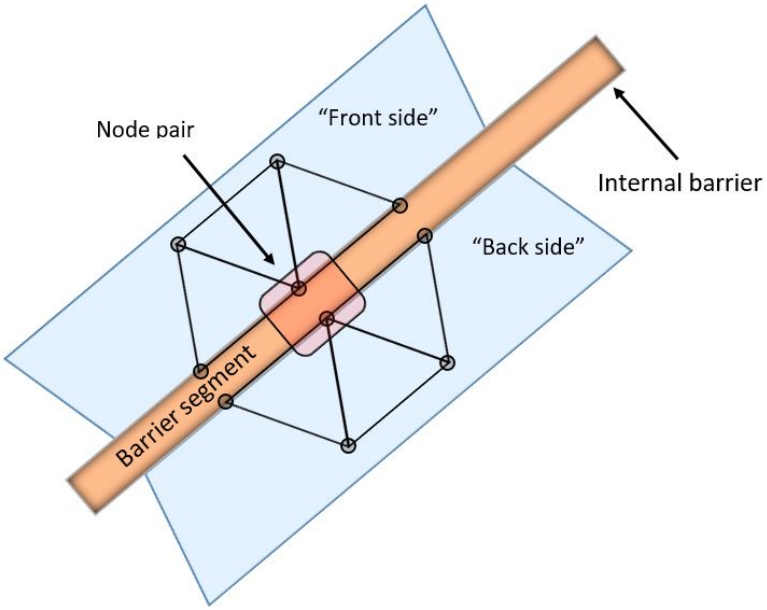

Figure 2.33: Top view of internal (barrage) barrier and triangular element representation taken from [46, 114, 147].

simulated (Figure 2.33). The flow through these node pairs is calculated as a function of the water head developed between 'front' and 'back' sides.

The flow during the sluicing phase is modelled using the orifice equation with $C_D = 1$ [16, 134], which relates head difference to the flow through the boundary as seen in Equation 2.5. The flow through the turbines is modelled using characteristics for a low head bulb turbine following [7, 130],

$$Q(H) = C_D A_t \sqrt{2gH}, \tag{2.5}$$

where Q is the flow rate, H the head difference, C_D the discharge coefficient, A_t the flow area though the barrage opening (sluice area) and g the gravity constant.

The turbine's flow and power characteristics are obtained from a low head bulb turbine chart made available by Andritz Hydro, seen in Figure 2.34 [7, 130, 147] and shows how turbine unit speed n_{11} and specific unit discharge Q_{11} (obtained experimentally) are related. The Figure also shows wicket gate and running blade openings (in degrees) and efficiency curves, E_f.

The values on the Hill chart can be used to simulate the turbine performance by manipulating the following equations for flow, head and efficiency on which the model is based [16]. By specifying the parameters of the turbine–diameter D_t, number of generating poles G_p and grid frequency f_g–the turbine rotation S_p (rpm) can be

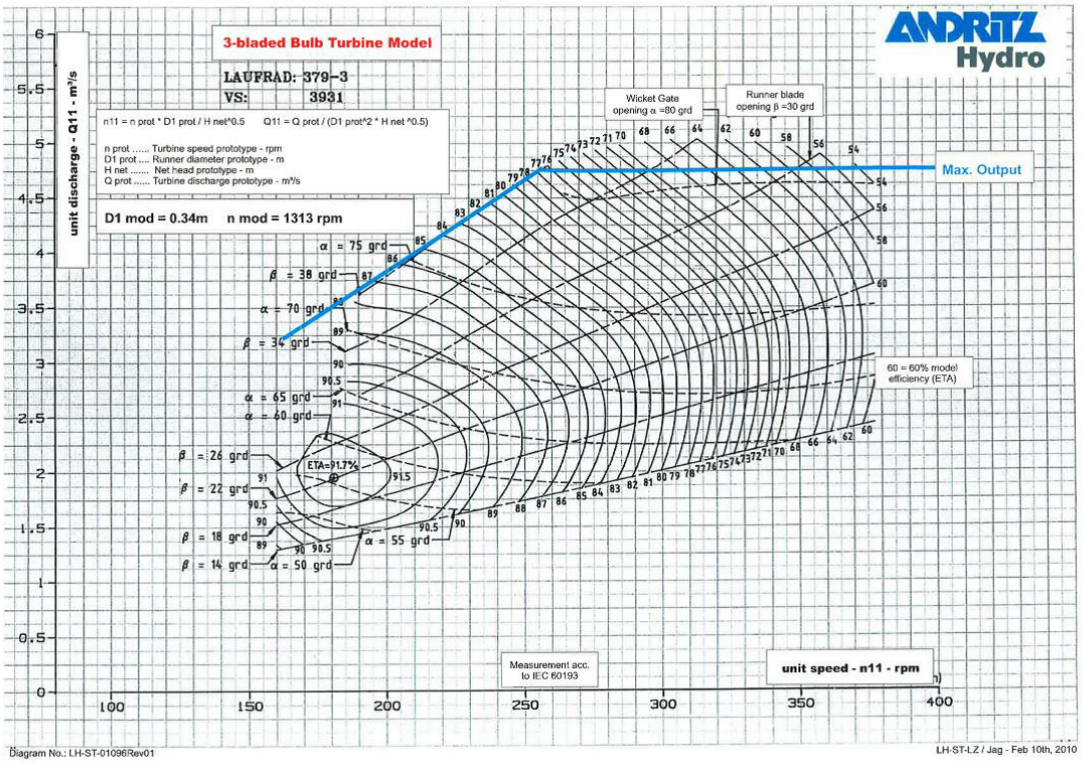

Figure 2.34: Andritz Chart for low-head bulb turbines taken from [130].

obtained from $S_p = 120 f_g / G_p$. From S_p, both unit speed n_{11} and specific discharge Q_{11} are calculated as:

$$n_{11} = \frac{S_p D_t}{\sqrt{H}}, \quad Q_{11} = \frac{Q_t}{D_t^2 \sqrt{H}}. \tag{2.6}$$

Manipulating the specific discharge equation in Equation 2.6, the dimensional turbine flow-rate Q can be described as:

$$Q = Q_{11} D_t^2 \sqrt{H}. \tag{2.7}$$

When a forcing head is present, n_{11} is calculated from Equation 2.6, while Q_{11} is obtained by adjusting the opening of the wicket gate, the pitching of the runner blades and crossing the values with the obtained n_{11}. A parametrized curve of maximum power output is obtained by digitising the chart [7], and following the path where the

product between E_f, Q and H is maximised:

$$\begin{aligned} Q_{11} &= 0.0166 n_{11} + 0.4861; \text{ (when } n_{11} =< 255), \\ Q_{11} &= 4.75; \text{ (when } n_{11} > 255), \\ \eta &= -0.0019 n_{11} + 1.2461, \end{aligned} \tag{2.8}$$

where η is the turbine efficiency. Since n_{11} is acquired from the head difference, flow rate through the turbines can be calculated using Equations 2.7-2.8. Power output P_t through the turbines can also be calculated using the above approach, Equation 2.8 and the following equation:

$$P_t = \left| \rho g Q H \eta \right|, \tag{2.9}$$

where ρ is the water density. These equations provide good approximations of the turbine performance represented by the Hill chart, as can be seen in Figure 2.34, over a variety of different heads.

2.4.2 Introduction of the Severn Barrage and the Swansea Lagoon

Tidal energy is a clean and predictable way of generating power. Wise utilisation of the large tidal ranges of the Bristol Channel would be beneficial, as introduced in the literature review in Chapter 1. As such, there have been many proposals for the installation of hydrodynamic devices in the channel. The largest proposal is that for a Severn Barrage which would be the largest tidal scheme in the world. The other considered in this thesis is the relatively small project of the Swansea Lagoon.

The first detailed proposals for the Severn Barrage began with the seminal technical study into the feasibility of the project led by Bondi [24] and developed further by the Severn Tidal Power Group (STPG) [153]. More recently, the Department of Energy and Climate Change study [49], which was based on the original Bondi and STPG proposals, and the Hendry Report [88] have provided an up-to-date summary of the proposed project. Estimates of the power that the scheme might generate are given in Table 2.16. Recent academic research includes analytical studies such as [139, 55] and numerical modelling including [8, 61, 179].

The focus of this project is the proposal based on the original STPG scheme for the Cardiff-Weston Barrage (B3) within the Severn Estuary as shown in Figure 2.35 (see the whole domain of the project in Figure 2.1). The barrage has 216 40-MW, 9-m diameter bulb turbine generators, 166 sluice gates with a total $35,000$ m^2 sluicing

Table 2.16: Estimates of the power generated by a Severn Barrage.

Source	Annual energy output (TWh)	Total capacity (MW)
Bondi Committee [24]	12.9	7,200
STPG [153]	17	8,640
DECC [49]	16.8	8,640
Xia [179]	17.7	8,640
Hafren Power [82]	16.5	6,500

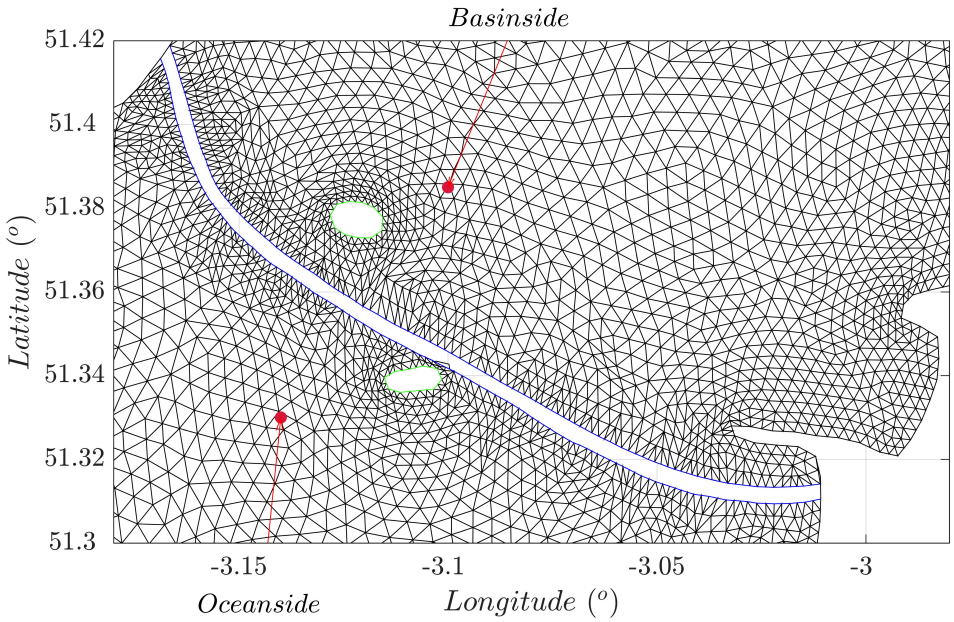

Figure 2.35: Model computational details of the barrage layout for Severn Barrage, the blue lines indicate the barrage boundary and as shown, the region at the left hand side is defined as Basinside and the right as Oceanside.

area, ship locks and other structures. The scheme is tested here under the two-way generation regime as suggested by [179] and follows the configuration of the barrage design shown in Table 2.17. The detailed layout of the turbines and sluices is based on [153] (Figure 2.36).

The second scheme considered is the Swansea Bay Lagoon based on the proposal in [17] with a 'U'-shaped breakwater as shown in Figure 2.37. The proposed lagoon has a surface area of 11.5 km^2 and its layout is given in Figure 2.38. The project would have an installed capacity of 320 MW and is predicted by the developer to generate an average power of 48 MW. This relatively localised project would generate electricity

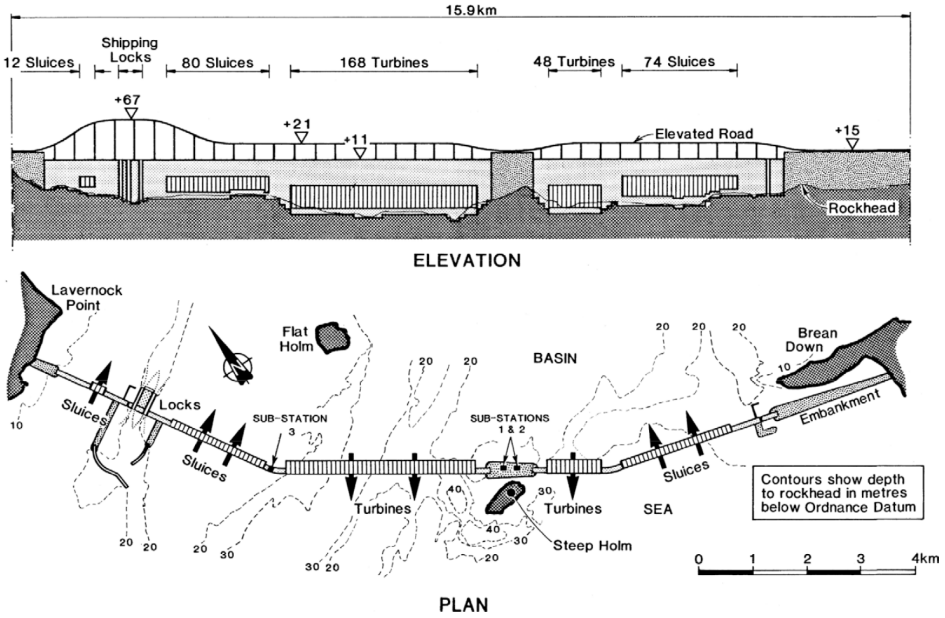

Figure 2.36: Schematic of the Severn Barrage layout (taken from [153]).

Table 2.17: Specifications of the Severn Barrage and Swansea Lagoon considered.

	Severn Barrage Design	Swansea Lagoon Design
Operation Scheme	Two-way	Two-way
Number of Turbines	216	16
Turbine Diameter (m)	9.0	7.35
Number of Sluice	166	8
Sluice Area (m^2)	35,000	800
Barrage Length (km)	16.1	9.5

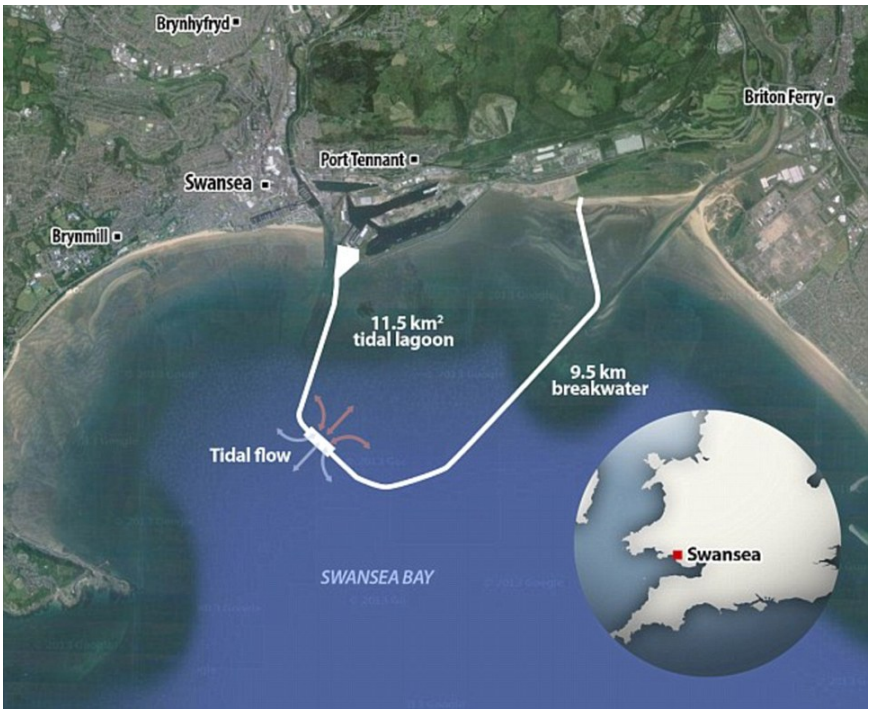

Figure 2.37: Schematic of the Swansea Bay Lagoon taken from [89].

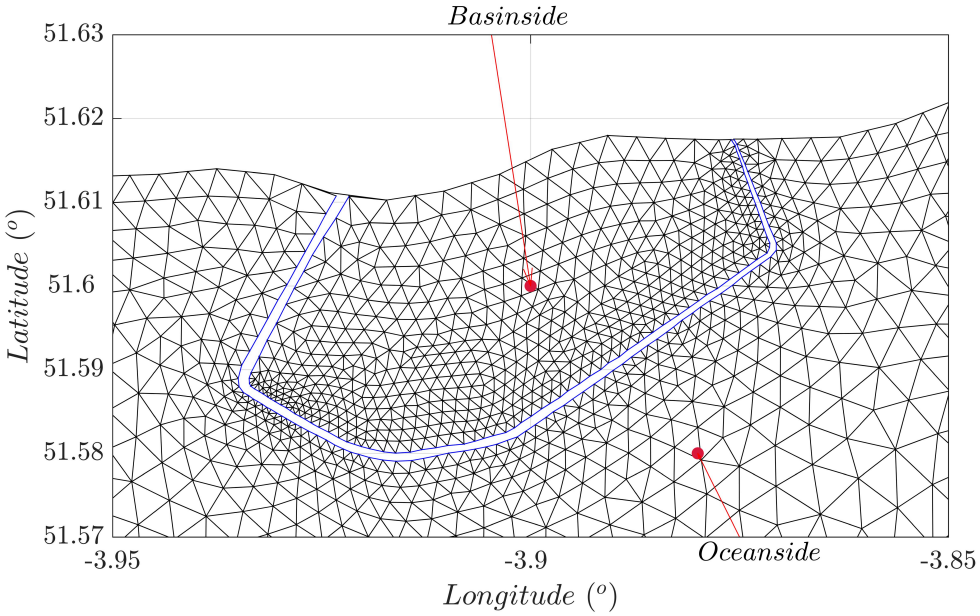

Figure 2.38: Model computational details of the lagoon layout for the Swansea Lagoon, the blue lines indicate the lagoon boundary and as shown, the region within the lagoon boundary is defined as Basinside and the rest as Oceanside.

to meet up to 11% of Welsh domestic annual electricity consumption. The detailed chosen parameters of the lagoon are shown in Table 2.17.

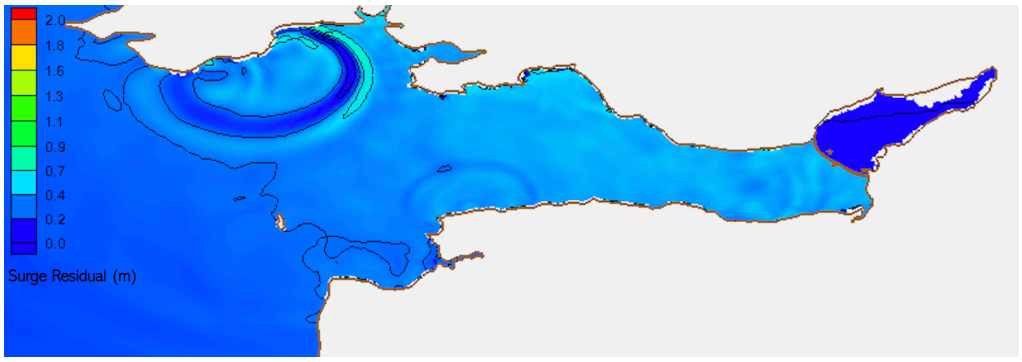

Figure 2.39: Residual results with the appearance of un-physical high-frequency oscillations in the Bristol Channel. The oscillations occur after a barrage addition and are shown by the DG-SWEM with ERA5 dataset. The colour bar indicates the residual levels.

2.4.3 Additional Parameters in the Numerical Model for Model Stability

Due to the appearance of un-physical high-frequency oscillations in the simulation outputs (observed in an animation of residual levels in the domain with barrage addition, a capture of which is shown in Figure 2.39), various attempts in changing parameters in the numerical model have been made to control this additional noise output, in order to improve model stability. The three additional parameters that have been adjusted are: the 'slopeflag' parameter that affects the elevation gradient in the model mesh, the resolution of the model, and the 'ESLM' parameter that represents the spatially constant horizontal eddy viscosity. The tuning process involves adjusting these parameters and verifying the results of each adjustment by visual confirmation of the decreased appearance of un-physical high-frequency oscillations in the residual levels.

In order to selectively limit the maximum elevation gradient across elements in the numerical model in an attempt to avoid oscillations in the solution domain, the 'slopeflag' parameter in the DG-SWEM is used as a slope limiter. When the limiter is active at a node, the water surface elevation will be reset to that of the average of the surrounding nodes, thus improving numerical stability. The slope limiter parameter in the code is an integer value greater or equal to zero, with zero being the default state of no application of slope limitation. This parameter is modified to find a balance between model stability and computation efficiency, which decreases as the the slope limiter increases. The best value, found following several trials, is determined to be a 'slopeflag' value of five. The reduced numerical efficiency in this case will not be a

problem with the utilisation of a supercomputer for these simulations.

Further model refinement is carried out by changing the resolution of the Bristol Channel region. The original mesh has $31,341$ nodes and $59,084$ elements, which has been refined to an overall amount of $51,458$ nodes. A time step of 0.5 s has been chosen according to the mesh resolution, as the finer the mesh, the smaller the time step required for satisfying model stability criteria (for example the Courant-Friedrichs-Lewy (CFL) condition).

The background of the last parameter considered for numerical model stability is rooted in the realistic problem of water turbulence and its inclusion in the momentum equations. Within the DG-SWEM, an 'ESLM' parameter exists that represents the spatially constant horizontal eddy viscosity (with a unit of m^2/s) in the momentum equations in order to account for the turbulence closure problem, which may be magnified during storm surge events. According to Garzon & Ferreira [75], the ADCIRC model for storm surge modelling is relatively sensitive to variations in 'ESLM' when forced by tides and winds. For this study, model simulations with an 'ESLM' value of 1.5, 2.5, 4, 20, 40 and a high value of 100 (with units of m^2/s) are carried out. The best model result is achieved with the application of ESLM = 2.5. However, unlike Garzon & Ferreiras finding, strong sensitivity to this parameter is not observed in the present work.

All the relevant parameters and solutions considered for removal of the high-frequency waves are illustrated in Table 2.18. In addition to the three parameters included above, extra small and anomalous waves (the exact cause of which is unknown despite discussions with the original code developer) are removed by the application of a low-pass filter that excludes signal frequencies above 0.00015 Hz. Application of the low-pass filter will further remove the high-frequency oscillations and its effect on the final result such as the event's peak is limited, with only 0.0078 m of difference.

The final effects of improvements with adjustment of additional parameters are shown in Figure 2.40, which applies the 2000 storm surge event and with residual results on the ocean side of the barrage. From the Figure, it can be seen that the oscillations in the final results have been removed without having an impact on the magnitude of the surge peak. The adjustments of the additional parameters and the use of the low-pass filter are applied in the later stages of the project.

Table 2.18: Parameter or solution considered to remove the high-frequency oscillation waves in the numerical modelling due to the barrage implementation.

Relevant Parameters or Solutions	Actions	Reasons
Slopeflag	Adjusted for the model	/
Artificial Diffusion	Inapplicable	Unknown numerical issue in ADCIRC
ELSM	Adjusted for the model	/
H0 (Minimum Water Depth)	Inapplicable	Un-physical and inaccurate simulation
Wave Setup	Not considered	Not significant in Bristol Channel
Higher Order Polynomial	Inapplicable	Issue with wetting and drying routines
Mesh Resolution Improvement	Mesh resolution improved	/
ARC System Application	Applied to the simulation	/
Rush Inland Boundary Outwards	Considered as the land-extension modified model; Inapplicable	Modified model results show no significant Improvement (Appendix A)

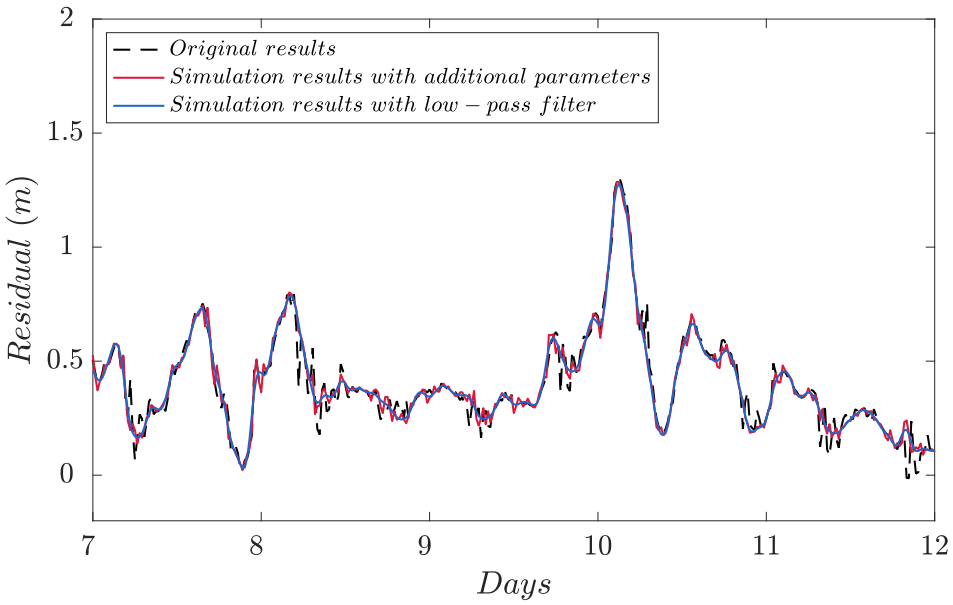

Figure 2.40: Residual results with adjustment of additional parameters in the numerical model for model stability for barrage case on the ocean side during 2000 storm surge event. Parameters considered are slope limiting, ELSM and increased model resolution in the Bristol Channel region.

2.5 Discussion

2.5.1 DG-SWEM

A calibrated and validated DG-SWEM for storm surge simulations of the M_2, S_2 and N_2 tides around the south-west coasts of the UK, particularly in the Bristol Channel regions, has been presented. The most suitable meteorological database for storm surge simulations has been selected as well. Comparisons of varying parameters with independent data sources, the BODC database and the TotalTide database demonstrate that the overall model achieves an acceptable level of agreement with the pattern of tidal hydrodynamics within the regions of interest. Discrepancies displayed with individual measurement stations are at a reasonable level of error consistent with that found by similar investigations (as can be seen for example in [45, 73]).

Acceptable agreements (within an error percentage of 6%) have been demonstrated between model predictions and field measurements during a harmonic analysis of the tides. However, the usage of a depth-averaged two-dimensional tidal model to predict wave currents is slightly more difficult due to the three-dimensional nature of the wave currents, and there are uncertainties attached to the available observed measurements. To validate the storm surge predicted by the model, two surge events are used and

the DG-SWEM results are mainly affected by two factors: the inaccuracy in the meteorological dataset applied and the age of the BODC field measurements for the Bristol Channel regions, which could be a factor of error due to the limitations of the measuring equipment used at the time. In terms of modelling accuracy, the model mesh is drawn with a resolution within the Bristol Channel that captures the details of channel geometry. The model boundaries, however, do not include the discharge from River Severn or any other rivers into the Bristol Channel. This may affect the level of accuracy of predictions in the channel. A final limitation to consider is the use of a single constant bed friction coefficient, which is a simplification of the real variation of this parameter in the channel.

2.5.2 Specimen Storm for Simulations in this Project

Several storm surges have occurred in the Bristol Channel since tidal gauge records have started to become available. However, there has been a lack of exceptionally severe storms that have coincided with very high astronomic tides. Chapters 3 and 4 are written with the goal to examine the impact of such a severe surge. In order to achieve this goal, a completely artificial simulation is used to perform a sensitivity check on the main results. However, to try and maintain realism, it has been decided that real meteorological inputs are to be used for a severe storm and this storm is shifted in time so that the surge corresponds to a high astronomical tide. This allows the difference a barrage would make to be examined more clearly.

Based on the current simulation results, the timing of the peak surge events (including their meteorological information such as atmosphere pressure and wind speed) is moved to a period of high astronomic tide in order to simulate the largest possible water level elevations. Due to tide-surge interaction [70], it is probable that in the historical data the highest total water elevation will not coincide with either the highest tide or the most severe surge. Therefore, Table 2.19 shows numerical predictions of peak water level and surge elevation changes for different shift intervals between the surge and astronomical tide. Even though the maximum surge elevation appears when timing of peak surge moves to the high tide at a simulation time of 11.83 days, the focus of this project is to evaluate the barrage effects on the level of flooding based on the total water elevation, which is maximum when peak surge moves to the spring tide (simulation time of 10.32 days). Thus, the surge inputs with meteorological characteristics applied to a spring tide are used to analyse the potential benefits of a barrage on the south-west UK coasts. Figure 2.41 and Figure 2.42 illustrate the simulation results of the final 'modified' storm surge event applied on a spring

Table 2.19: Simulation results of different timings of peak surge movements for the 2000 surge event at Avonmouth (the original storm surge event happens at a simulation time of 10.15 days).

2000 Event at Avonmouth		
Modified surge position	Elevation (m)	Surge (m)
High tide at 9.74 days	7.44	1.71
High tide at 10.32 days (spring tide)	8.50	1.61
High tide at 10.79 days	7.71	1.79
High tide at 11.29 days	7.38	1.72
High tide at 11.83 days	7.75	2.00

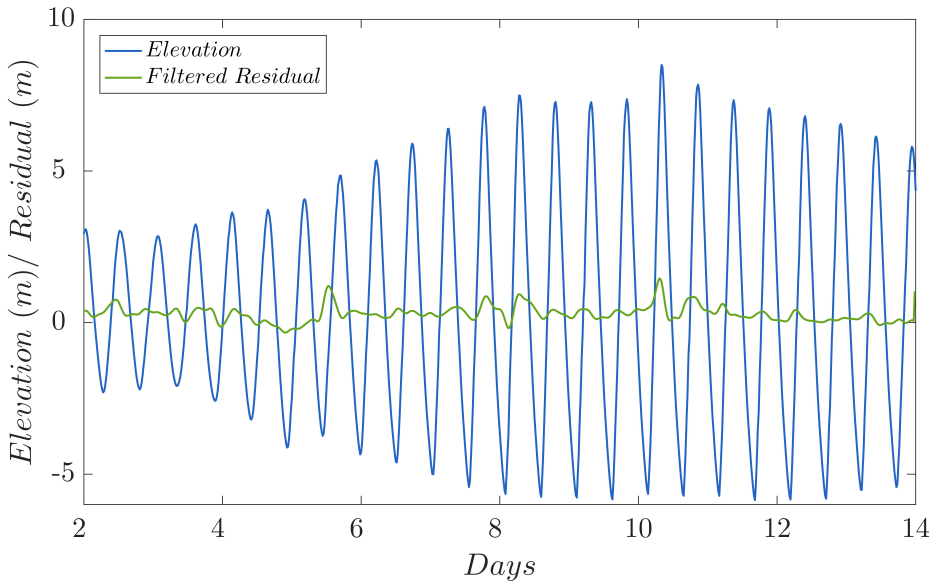

Figure 2.41: Simulation results of modified storm surge events of 2000 (spring tide) at Avonmouth predicted by DG-SWEM.

tide. One thing to be noted is that for the 2014 surge events, due to the original events occurring within a neap tide period, more simulation days (up to 18 days) are required to align the spring tide with the meteorological conditions which would give the most severe surge.

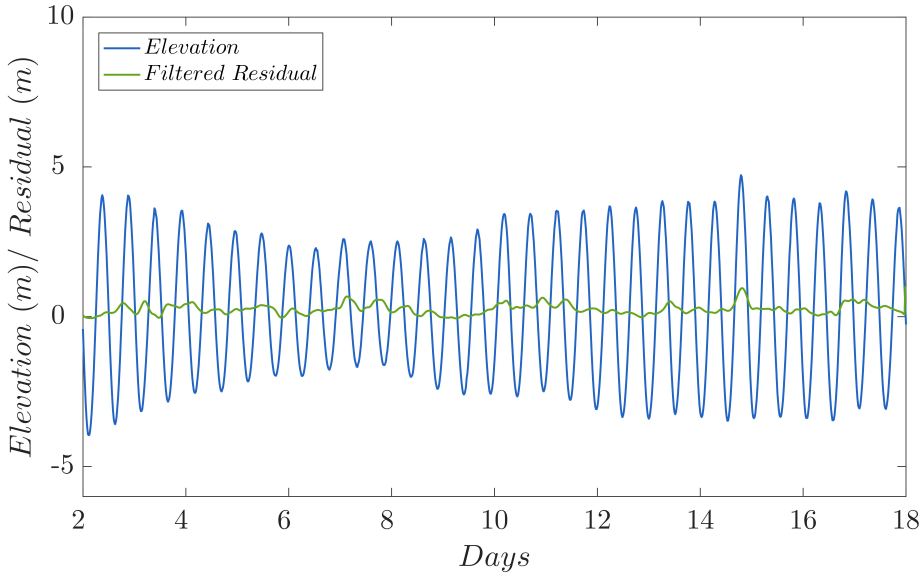

Figure 2.42: Simulation results of modified storm surge events of 2014 (spring tide) at Ilfracombe predicted by DG-SWEM.

2.6 Conclusion

The first part of this chapter presented the construction of a two-dimensional DG-SWEM of the south-west coasts of the UK. The objective was to develop the best possible model to simulate storm surge events. A set of bed friction coefficients, wind surface drag coefficients and meteorological datasets were used in the calibration tests and the best fit was achieved with the ERA5 dataset. The calibrated model was then validated against observations obtained from various sources (for example the Admiralty Tide Tables and field data from BODC). The validation tests involved tidal harmonic analysis, currents at several stations, storm surge events in the Bristol Channel and the effect of bed friction on the designed surge event. Comparisons with the available data demonstrated that the overall model achieves an acceptable (defined by this project) prediction of the pattern of natural tidal hydrodynamics throughout the Bristol Channel region. The parameters used to tune the tidal hydrodynamics did not have a significant impact on the predicted storm surge. However, the agreement for the validation of storm surge events when compared against field measurements was slightly more concerning. The exact reason for this is unclear but it is likely due to several shortcomings of the numerical model, the accuracy of the meteorological inputs and the age of the recorded field measurements. However, these inaccuracies are consistent with other depth-averaged storm surge models (see for example [73]). Further, whilst ideally the model would accurately reproduce historical events, for this

study it is the change caused by the barrage that is the main aspect of interest. Small inaccuracies in the model are not likely to make a significant difference to assessing the impact of a barrage. Thus the model is satisfactory for the purpose of this thesis. To use as a test case, the meteorology that causes the worst recorded storm in the region was shifted in time so that it coincides with a high tide.

A barrage boundary was introduced into the two-dimensional model to represent the effect of sluice gates and turbines for the barrage implementation. Meshes containing representations of the Severn Barrage and Swansea Lagoon were created and the parameters adjusted to improve the smoothness of the results.

Chapter 3

Impact of Barrage and Lagoon on Storm Surges by 2D Model

This chapter investigates interactions between a storm surge and tidal barrages in the Bristol Channel. Specifically, the chapter examines the Bristol Channel's extreme water levels and looks at both how they are changed by the presence of a barrage and at how barrage operation may impact flooding. This is done by applying the discontinuous Galerkin ADCIRC shallow water model described and validated in Chapter 2. In analysing a storm surge, meteorological data from hindcast models are combined with tidal conditions for a spring tide, which has also been described in Chapter 2. In terms of hydrodynamic device construction, this chapter takes into consideration projects of different scales, from the relatively large Severn Barrage project, to the relatively small Swansea Lagoon project.

Section 3.1 presents the results of the changes to the tidal hydrodynamics within the channel due to the addition of a barrage. Sections 3.2 and 3.3 interpret the interactions in terms of the surge residual and total water level, respectively, obtained for different barrage operation strategies. Additionally, the impact of a barrage is also investigated for a synthetic storm surge event in Section 3.4 to analyse the sensitivity of the conclusions to different storms. Section 3.5 presents a similar analysis for the Swansea Lagoon and Section 3.6 presents the comparison of the impacts of operating a barrage and a lagoon on the channel. Section 3.7 concludes the discussion and lists the major findings.

Table 3.1: Barrage operational scenarios with different starting heads and finishing heads.

Case	Starting head (m)	Finishing head (m)
A	1.5	0.7
B	3.0	1.0
C	4.0	2.0
D	-	-

3.1 Impact of the Severn Barrage on Tidal Hydrodynamics

It is important to understand the impact of the Severn Barrage on tidal hydrodynamics before considering its impact on storm surges. As the tide is the key contributor to water levels, it is therefore something that coastal flooding is dependent upon. The tidal hydrodynamics of the Bristol Channel is a resonant system [67, 72], and these can be sensitive to small changes (although in Chapter 7 it was found that resonance has a smaller impact than might be anticipated). The Severn Barrage is a relatively large project and thus might be expected to have some impact on the tidal hydrodynamics of the channel. However, previous studies such as those by [30] suggest that the impact on water levels outside the barrage is surprisingly small and localised.

Becker [19] found that using a low starting head has a significantly smaller impact on the tide, hence minimising the environmental impact. In this project, different barrage operational strategies are considered in assessing the change to the naturally occurring hydrodynamics. The operational scenarios are set out in Table 3.1. Standard works for the discussion of starting and finishing heads of normal barrage operations can be found in [134].

As illustrated in the Table, operation cases 'A', 'B' and 'C' are carried out with different barrage starting and minimum heads. The final case, 'D', is essentially a closed barrage that is included as a limiting case. A total of 28 simulation days are analysed following a spin-up of 4 days. Both the water levels on the basin side and the ocean side are analysed, the precise locations of which can be seen in Figure 2.35 in Chapter 2. These two representative points are taken based on the visualised simulation results of the whole model domain, and the limited variation between

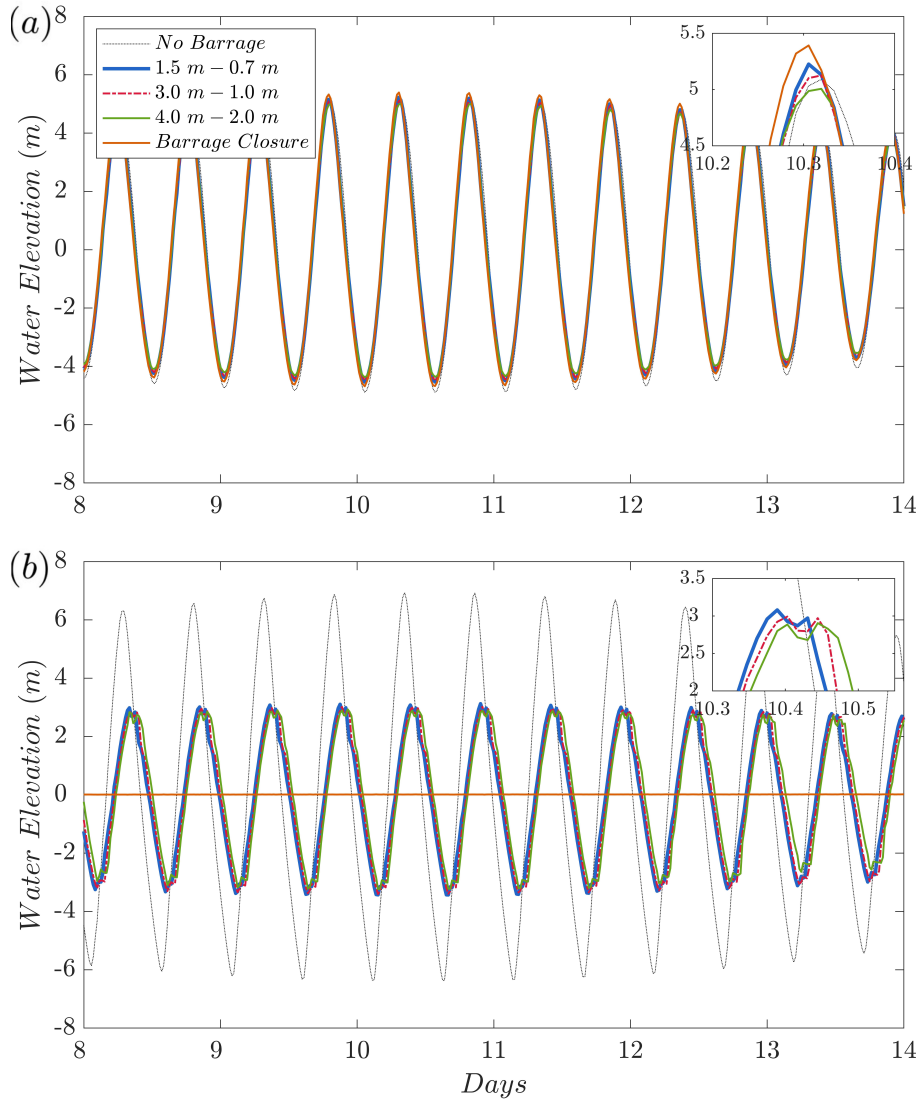

Figure 3.1: Impact of different operational heads on the water elevations without meteorological forcing: a) on the ocean side (51.36°N 3.67°W) (top); b) on the basin side (51.48°N 2.90°W) (bottom).

adjacent points within regions of interests are shown for the whole simulation period. The approach taken is to use water level in the channel as a proxy for flooding.

Figure 3.1 shows a comparison between the model-predicted water elevation for the natural case (no barrage) and for different barrage operation scenarios. The results generally show limited impact on the tides west of the Severn Barrage (ocean side) and a significant reduction of the tidal range east of the barrage (basin side) for all scenarios considered. Also, reducing the starting head leads to a reduced impact on the tidal range within the barrage.

With respect to the ocean region, maximum water elevations are predicted to rise by a limited amount for head operation cases 'A' and 'B' and are predicted to decrease if operation 'C' is adopted compared with the natural no barrage case. The effects of a barrage on the minimum water level are limited with little increments for all three operation cases.

Contrarily, the barrage implementation has a significant influence on the enclosed basin region. The maximum water elevation is predicted to decrease by approximately 4 m (the mean level for cases 'A', 'B' and 'C') for a spring tide. The shifted phase of the peak should be related to the barrage operation stages. The barrage effects on the minimum water levels are noticeable as well in the basin. The predicted level is -6.36 m without the barrage and approximately -3.18 m for all the head cases. These influences would lead to variations of the inter-tidal area and affect the process of wetting and drying within the basin; thus, negative environmental impacts would be expected. This analysis of the change in tidal levels is consistent with other works as concluded in Section 1.4.3.

For the extreme case of complete barrage closure, the Figure indicates limited amount of ocean side water level increase whereas, as expected, there is virtually no movement of water within the basin. In this case, the barrage would act as a barrier with no flow passing through, and there would be larger environmental impacts as a result.

The overall reduction in the water elevation and tidal range at the head of the channel suggests that the construction of a barrage would have an impact on the return levels of an extreme flooding event in the Severn Estuary. However, it should be noted that the barrage addition would lead to some water level increase to the west of the barrage, and might cause environmental damage from the risk of flooding, especially during the complete closure holding stages of the barrage operation in the basin.

The impacts of a barrage have also been considered by performing harmonic analysis. However, a standard harmonic analysis is not suitable within the basin as it is hard to identify whether the reduction in amplitude is associated with the introduction of increased damping into the resonant system or whether it is to do with the change in channel geometry–these are of course interconnected. Also, the water level is no longer well-approximated by a simple sinusoid. Water elevation oscillations are observed in the basin region as shown in Figure 3.1. This phenomenon could be explained as a seiche in the enclosed basin region with a frequency of approximately 1.2 hours.

Table 3.2 presents the amplitude and phase of the main tidal constituent M_2 on the seaward side of the barrage (including selected sites outside of the Bristol Channel). All cases lead to a reduction in the tidal amplitude outside the barrage, most likely due to the effective shortening (and damping) of the channel moving it further from resonance and generally with the biggest reduction occurring for the largest starting head. A small amount of phase change can also be observed.

3.2 Impact of Barrage on Storm Surge Hydrodynamics

As stated in Chapter 2, a synthetic event based on the year 2000 storm surge was included in order to achieve an extreme flooding event in this project. The modified peak surge occurs at the time of high tide during the spring tide with an extreme south-southwest wind speed of approximately 20 m/s and atmospheric pressure of 99.5 kPa within the channel region. The 14-day simulation begins on the 3 December of 2000 with a two-day ramping period, and the peak surge event happens within day 10. The peak values of water levels and residuals (i.e. the difference between the water level just from tides and the water level with tides and meteorological forcing, see Section 1.2) of the original case without barrage implementation during this storm surge event are summarised in Table 3.3. For the ocean region, high water level rises to approximately 5.76 m by 0.87 m from the no surge case without any meteorological input. The minimum water level increases as well. For the regions at the head of the channel, the water level increment (due to the surge) is larger with higher tidal levels, which can be explained by the funnelling shape and the resonance effect of the channel. The maximum water level during the surge event is up to 8.03 m and the extreme residual is approximately 1.37 m. Higher flooding levels, therefore, would be expected in the region near the head of the channel.

The presence of a barrage is examined to see how it modifies the synthetic storm surge event, particularly the residual. A number of scenarios are considered to see how these influence the storm surge. The first scenarios considered are the simple normal operation of a barrage (case 'A') and the case of having a completely closed barrage (case 'D'). Further scenarios considered include the operation, where at low tide and prior to the storm surge event, the barrage is closed off to create low water levels within the basin with acknowledgement of the timing of the surge event and the hydrodynamics of the channel tides. This void could, potentially, be filled with the excess water from the storm surge, hence mitigating flooding. Two such cases are

Table 3.2: M_2 tidal elevation amplitudes and phases at different stations for different barrage operation scenarios.

Station	M_2 Amplitude (m)					
	Obs.	No Barrage	Case A	Case B	Case C	Case D
Pwllheli	1.48	1.51	1.49	1.48	1.49	1.52
Barmouth	1.47	1.52	1.50	1.50	1.50	1.53
Fishguard	1.35	1.42	1.40	1.39	1.40	1.43
Stackpole Quay	2.51	2.54	2.47	2.45	2.46	2.53
Mumbles	3.18	3.09	2.92	2.88	2.88	3.00
Barry	3.82	3.91	3.44	3.37	3.32	3.50
Hinkey Point	3.80	3.97	3.47	3.39	3.33	3.53
Ilfracombe	3.04	3.01	2.86	2.83	2.82	2.88
Lundy	2.67	2.56	2.47	2.45	2.45	2.51
Station	M_2 Phase (°)					
	Obs.	No Barrage	Case A	Case B	Case C	Case D
Pwllheli	239	239	237	237	237	236
Barmouth	244	236	234	234	233	233
Fishguard	207	208	206	206	206	205
Stackpole Quay	168	174	172	171	171	170
Mumbles	171	176	172	172	170	169
Barry	185	183	177	176	174	169
Hinkey Point	185	184	178	177	175	170
Ilfracombe	162	167	165	165	164	162
Lundy	160	165	163	163	162	161

Table 3.3: Results of peak water and residual level in the ocean (51.36°N 3.67°W) and basin (51.48°N 2.90°W) region of the original case during the 2000 synthetic storm surge event.

Levels	Water level		Residual level	
Parameter	Ocean	Basin	Ocean	Basin
Timing (days)	10.31	10.33	10.25	10.29
Observation value (m)	5.76	8.03	0.87	1.37

Table 3.4: Barrage operational strategies during the storm surge event.

Case	Normal operation (days)	Closure period (days)	Opening period (days)	Details
E	0-8.1	8.1-10.2	10.2-14	Fully-area opening of turbine and sluice gates
F	0-8.1	8.1-10.2	10.2-14	Half-area opening of turbine and sluice gates

considered, which are set out in Table 3.4, where once the surge occurs the sluices are completely opened (case 'E') or just partially opened (case 'F'). Both strategies are operated under the starting head of 1.5 m and finishing head of 0.7 m (i.e. operation as case 'A').

Figures 3.2 and 3.3 present the residual on the ocean side and the basin side of the barrage for cases 'A', 'D', 'E' and 'F'. The different peak values are summarised in Table 3.5. Using the original case without a barrage as a reference, the relative variations in surge time and peak amount for the cases with different barrage strategies shown in the Table can be calculated.

The colour bars beside the Figures illustrate different phases of the barrage operation: generating, sluicing and holding, and manual barrage control. The normally operated barrage (case 'A') is considered first. With implementation of the Severn Barrage, the results indicate limited amounts of ocean side residual level increment at the surge peak compared with the results of the tide-only phenomenon. Meanwhile, the impacts of the barrage become larger for the regions within the basin. From the Figure, it can be seen that the barrage leads to a significant drop of the residual amount for the entire simulation period, especially at the peak surge (by 42%) when

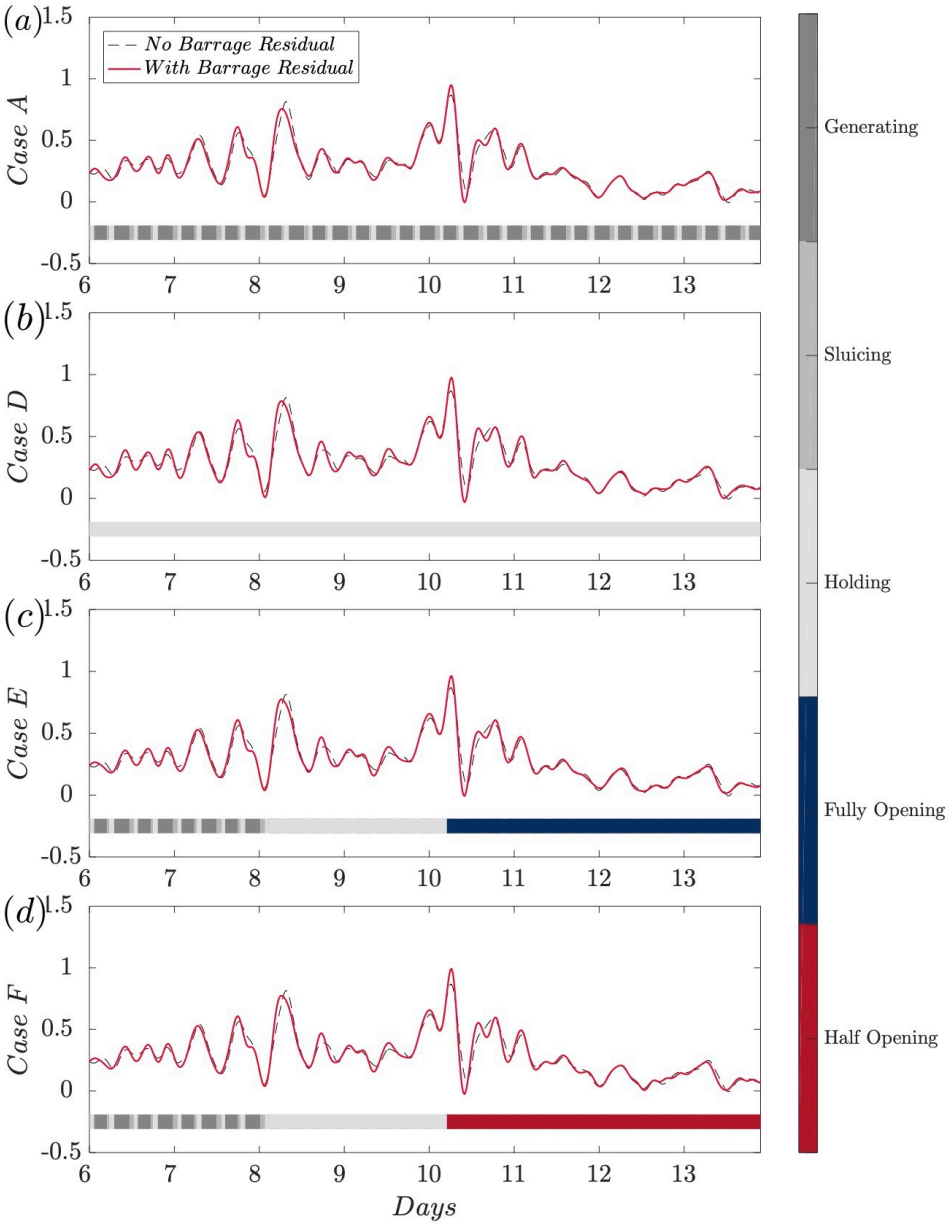

Figure 3.2: Residual level results (m) in the ocean-side region (51.36°N 3.67°W) of the four barrage operation strategies during storm surge: a) barrage normal operation (first); b) barrage complete closure (second); c) barrage operation Case 'E' (third); d) barrage operation Case 'F' (fourth).

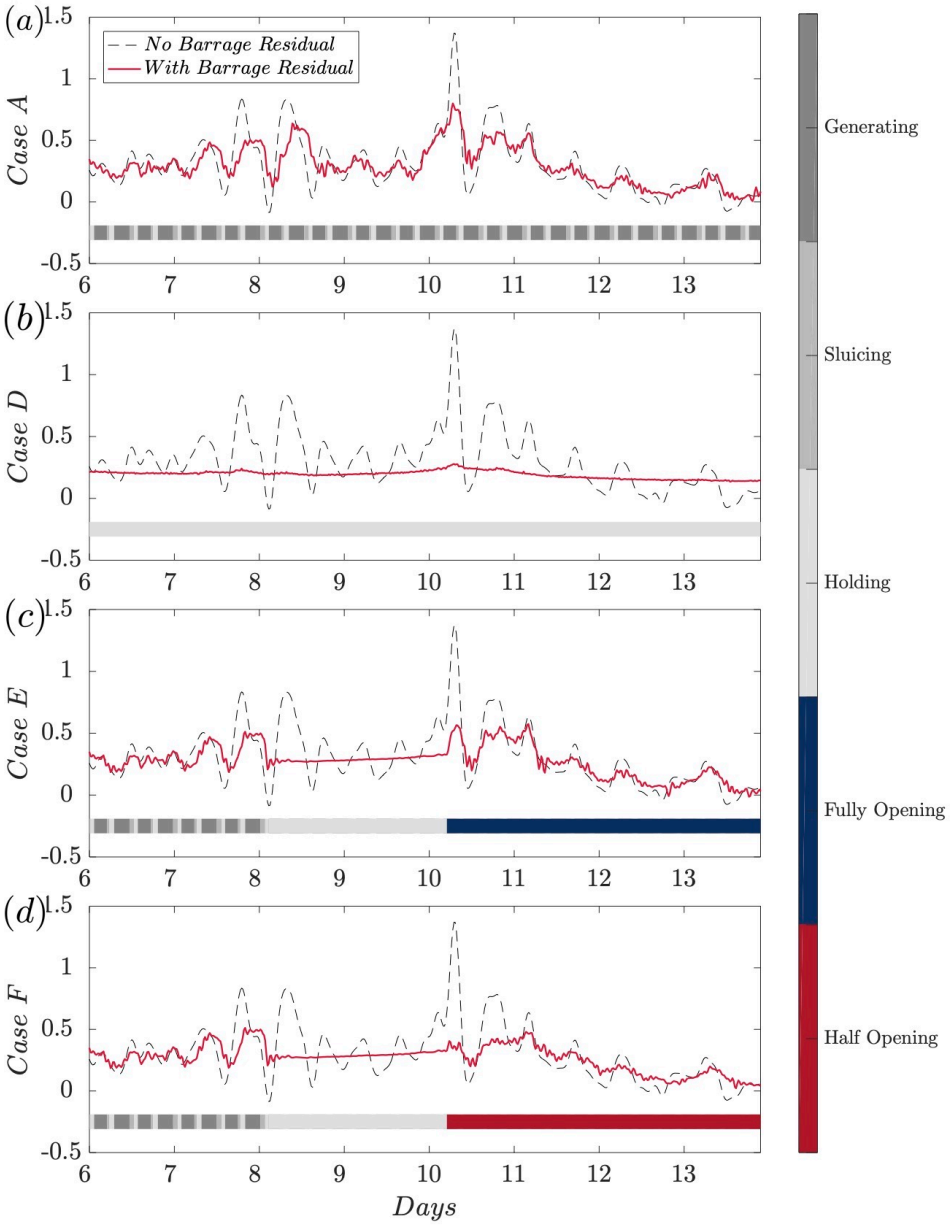

Figure 3.3: Residual level results (m) in the basin-side region (51.48°N 2.90°W) of the four barrage operation strategies during storm surge: a) barrage normal operation (first); b) barrage complete closure (second); c) barrage operation Case 'E' (third); d) barrage operation Case 'F' (fourth).

Table 3.5: Comparison of results of different strategies for residual level in the ocean (51.36°N 3.67°W) and basin (51.48°N 2.90°W) region relative to the original no barrage results.

Case	Case A		Case D		Case E		Case F	
Parameter	Ocean	Basin	Ocean	Basin	Ocean	Basin	Ocean	Basin
Observation value (m)	0.95	0.80	0.98	0.28	0.96	0.57	0.99	0.39
Peak time change (hrs)	0.24	-0.24	0.24	0.00	0.24	0.72	0.24	1.44
Magnitude change (m)	0.08	-0.57	0.11	-1.09	0.09	-0.81	0.12	-0.98

compared with the no barrage case.

For the other cases 'D', 'E' and 'F', the presence of the control strategies of the barrage increases the size of the residual on the ocean side as well. This increase is between 10-14% (approximately 0.1 m) compared with the original case. There is a small delay in the timing of the peak residual, but in all cases this is less than 15 minutes and so unlikely to make a practical difference. The peak in the residual is found to be only weakly dependent on the strategy used and in fact case 'F' presents the greatest residual on the ocean side. On the other hand, the more complex strategies show more advantage when concentrating on the results on the basin side. The peak residual is reduced considerably and is strongly dependent on the strategy used. The greatest reduction is found in case 'D' (simply closing the barrage) where the change in water level is simply due to local meteorological forcing of the water inside the barrage as no storm water enters the basin; therefore, the most basin protection can be achieved. This is of course expected. The reduction for case 'D' is predicted to be approximately 80%. However, the peak residual can be reduced nearly as much by operating the strategy in case 'F', where the residual level is decreased by 72% during the event. In case 'F', the time of the peak in the residual is also delayed by the largest amount compared with the other cases.

3.3 Impact of Barrage on Extreme Water Level

As with the analysis of results performed in Section 3.2, in this section, the impact of barrage implementation on the maximum water level during all simulations is now examined, which is clearly the variable of greatest interest in terms of coastal flooding during storm surge events in the channel. Generally, as stated in Section 3.1, barrage implementation would result in the reduction of the peak water level and thus

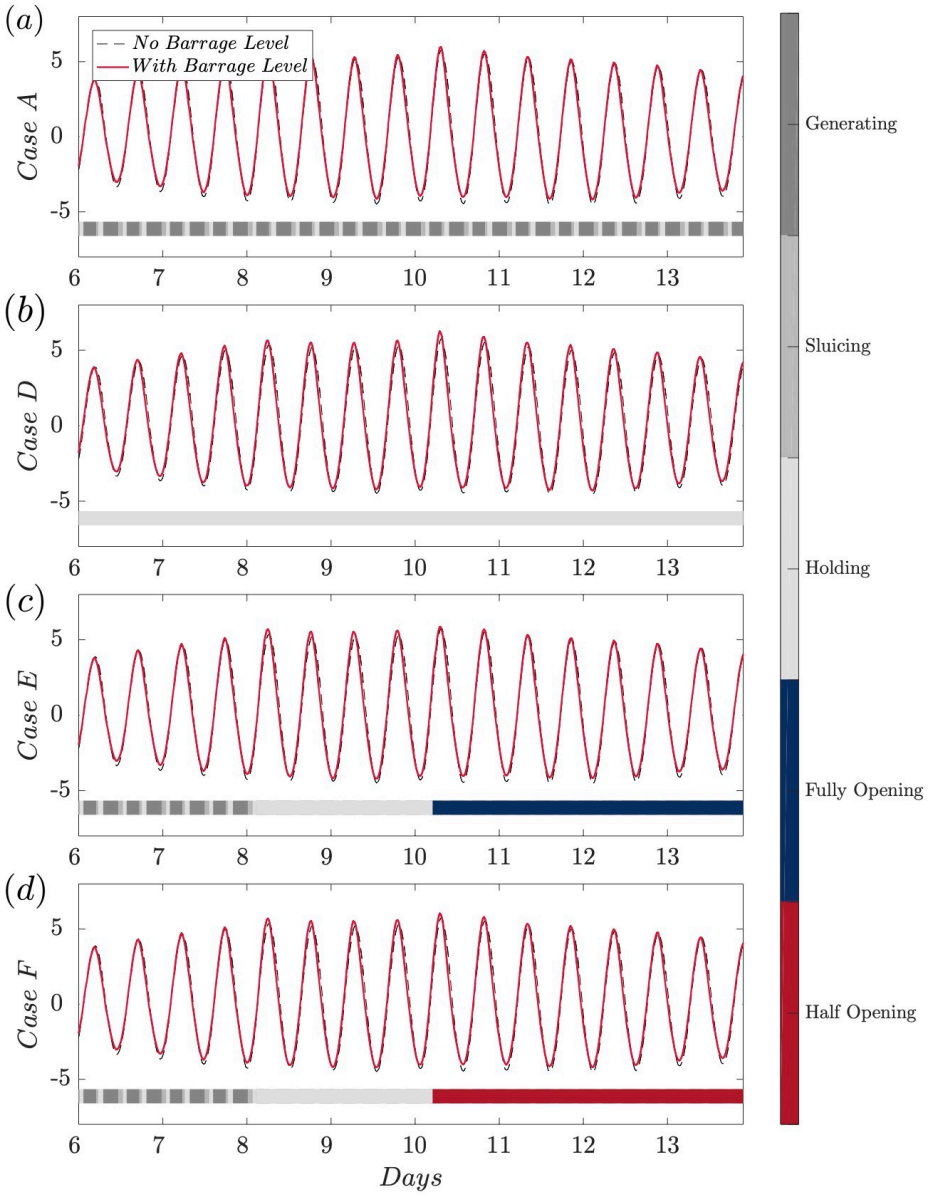

Figure 3.4: Water level results (m) in the ocean-side region (51.36°N 3.67°W) of the four barrage operation strategies during storm surge: a) barrage normal operation (first); b) barrage complete closure (second); c) barrage operation Case 'E' (third); d) barrage operation Case 'F' (fourth).

potential flooding would be eased. Again, two representative points on either side of the barrage are used for the analysis here. Figures 3.4 and 3.5 compare the time histories of the water levels on either side of the barrage for the different strategies considered, against the undisturbed water level. The peak levels are summarised in Table 3.6. The water level results can be compared with those in the no barrage case shown in Table 3.3.

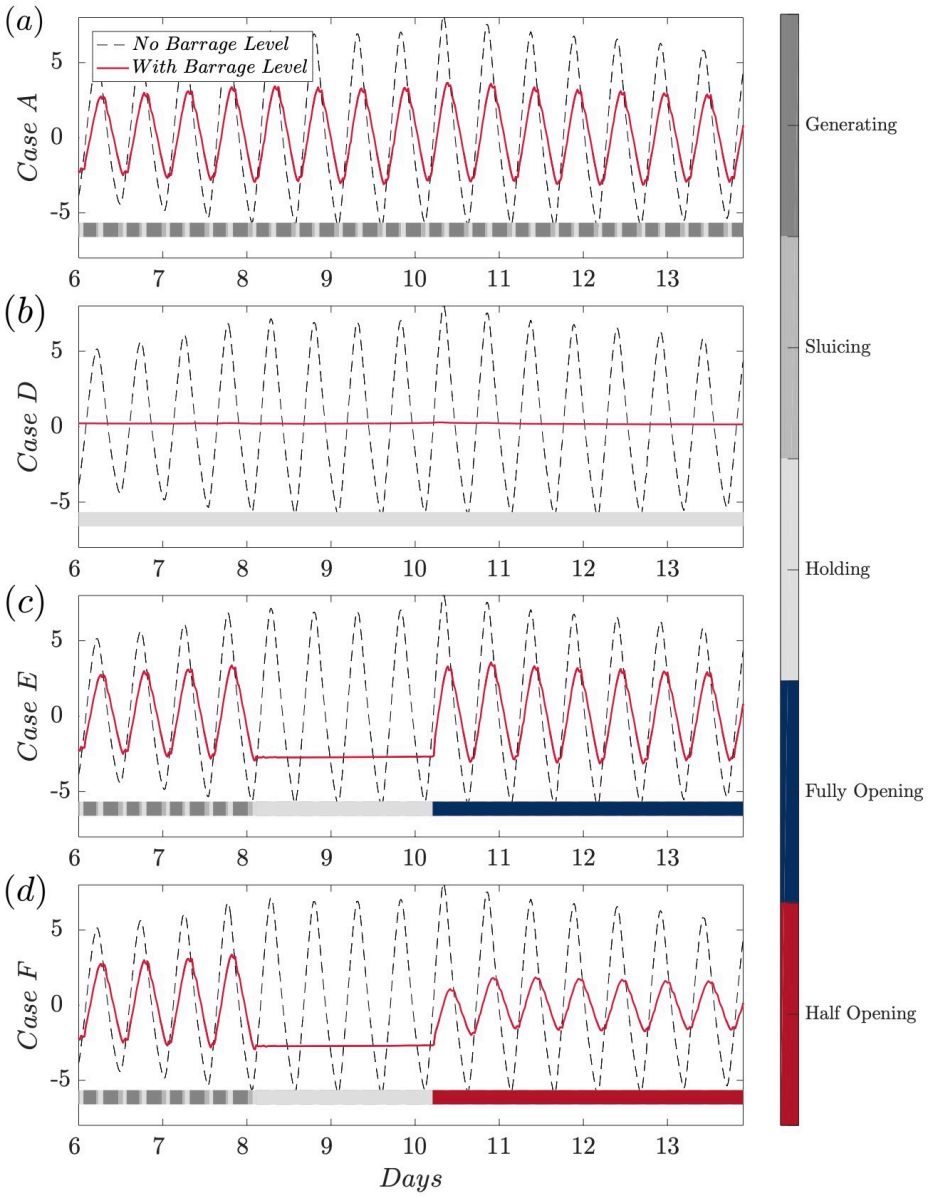

Figure 3.5: Water level results (m) in the basin-side region (51.48°N 2.90°W) of the four barrage operation strategies during storm surge: a) barrage normal operation (first); b) barrage complete closure (second); c) barrage operation Case 'E' (third); d) barrage operation Case 'F' (fourth).

Table 3.6: Comparison of results of different strategies for water level in the ocean (51.36°N 3.67°W) and basin (51.48°N 2.90°W) region relative to the original no barrage results.

Case	Case A		Case D		Case E		Case F	
Parameter	Ocean	Basin	Ocean	Basin	Ocean	Basin	Ocean	Basin
Observation value (m)	5.99	3.66	6.28	0.29	5.86	3.30	6.05	1.08
Peak time change (hrs)	0.00	1.44	-0.48	-0.24	-0.48	1.44	-0.48	2.16
Magnitude change (m)	0.23	-4.38	0.52	-7.75	0.10	-4.73	0.29	-6.95

With respect to the normally operated barrage (case 'A'), it can be seen from the Table that there is, again, a limited water level increment for the regions on the ocean side. The difference is relatively small as there are two competing effects – the reduction in the tidal amplitude and the increment in storm surge elevation, both due to the barrage. While for the regions within the basin, there is the expected reduction in peak water level given that both tidal amplitudes and storm surges are reduced by the presence of the barrage. This reduction is very significant as it shows that the barrage would provide considerable protection against flooding. From the results, there are significant water level decrements by up to 4.38 m, around 54% reduction at the surge peak during the storm surge event. Also a clear phase lag can be observed for the peak total water level on the basin side during the surge event, of approximately 1.44 hours. From the literature (see Chapter 1), a typical storm surge event occurring in the Bristol Channel has an approximate five-hour time period, hence this delayed peak would be significant and can be a benefit for flooding protection measures.

Considering the other operation cases, on the ocean side of the barrage, all the peak water levels are slightly higher than the no barrage case. The strategy chosen has an influence on these levels but all of the increments are within 0.60 m. The most favourable strategy is case 'E' with the smallest water increase when the barrage is closed at low water prior to the surge event and then opened to absorb the excess water during the storm surge. For the peak water level on the basin side, all cases observe a significant water level drop. The amount of the reduction is dependent on the operation strategy used – operating the barrage following case 'F' gives almost as much reduction in water level as completely isolating the water inside the barrage (case 'D'). However, over-protection of the landward region is experienced in case 'D', which leads to the highest water level rise on the ocean side. The timing of the peak

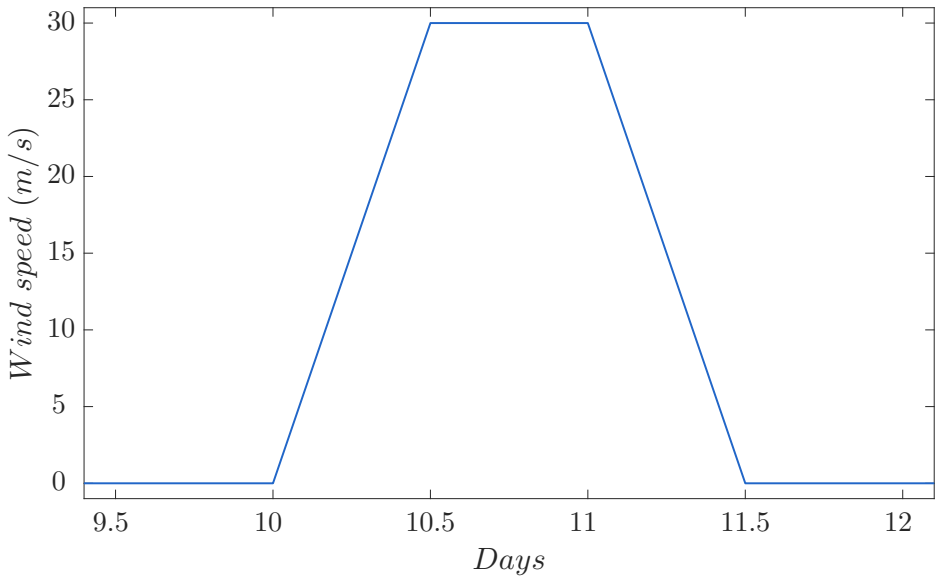

Figure 3.6: Variation of input wind forcing with simulation time for barrage case.

of the surge can also vary by over an hour depending on the strategy used and case 'F' has the best performance here.

3.4 Impact of Barrage for Synthetic Storm Surge

The leading order cause of uncertainty in the above conclusions is that only one storm was used. There are no other suitable storms over the recent 50 years for which data is available. In this section, the barrage impact on an entirely synthetic storm will be considered to examine whether the above conclusions alter. The model is run with a total 14-day period with south-westerly winds increasing from 0 to 30 m/s linearly in time beginning on day 10 (from 00:00 to 12:00), kept constant for 12 hours and then decreased to 0 from day 11 (from 00:00 to 12:00). Detailed wind conditions are shown in Figure 3.6. The wind speed is kept to 0 m/s for the rest of the simulation. The atmospheric pressure is held constant (at $101,325$ Pa) for the whole period. The designed surge is superimposed on the tidal condition in the 2000 event and is coincident with high tide. The resulting synthetic storm surge event has a peak water level of 7.99 m and a surge residual of 2.32 m during the event on the basin side of the channel (Table 3.7).

The same barrage control strategies introduced in Section 3.2 are then applied. The impact of different barrage strategies on the water level and residual are shown in Tables 3.8 and 3.9, respectively. Compared with the no barrage case, the surge resid-

Table 3.7: Results of water and residual level in the ocean (51.36°N 3.67°W) and basin (51.48°N 2.90°W) region of the original case during the entire synthetic storm surge event.

Levels	Water level		Residual level	
Parameter	Ocean	Basin	Ocean	Basin
Timing (days)	10.83	10.85	10.65	10.69
Observation value (m)	5.80	7.99	1.19	2.32

Table 3.8: Comparison of results of different strategies for residual level in the ocean (51.36°N 3.67°W) and basin (51.48°N 2.90°W) region relative to the original no barrage results during the synthetic storm surge event.

Case	Case A		Case D		Case E		Case F	
Parameter	Ocean	Basin	Ocean	Basin	Ocean	Basin	Ocean	Basin
Observation value (m)	1.21	1.71	1.25	\	1.21	1.63	1.21	1.34
Peak time change (hrs)	0.96	-0.48	0.96	\	0.96	0.00	0.00	0.72
Magnitude change (m)	0.01	-0.62	0.06	\	0.01	-0.69	0.02	-0.98

ual is reduced by 0.62 m, 0.69 m and 0.98 m on the basin side for barrage strategies of normal operation (case 'A'), fully- (case 'E') and partially-reopened (case 'F') operations, respectively. The barrage entirely closed (case 'D') scenario unsurprisingly gives the best basin-side performance with almost no residual level. For the timing of the surge peak, case 'F' provides the largest peak time delay by 0.72 hour. Considering the ocean side, except for case 'D', other strategies give insignificant water level rises. For the water level results, it can be seen from Table 3.9 that case 'F' provides a decrease of 5.59 m (70%) in the level of the basin and largest event delay time of 2.16 hours. For all strategies, the total water level rise in the ocean are also insignificant, with the largest rise up to 0.26 m in case 'D'.

Compared with the storm surge event in the year 2000, similar conclusions can be drawn for barrage strategy selections in this extreme synthetic event. One interesting thing to note in comparison with the year 2000 event considered earlier is that more limited ocean level rise is observed (i.e. less water level rise on the ocean side) yet similar significant basin reductions are seen in the controlled barrage operations. This provides the firm evidence that the conclusions drawn for the 2000 storm can be generalised to other events in the region.

Table 3.9: Comparison of results of different strategies for water level in the ocean (51.36°N 3.67°W) and basin (51.48°N 2.90°W) region relative to the original no barrage results during the synthetic storm surge event.

Case	Case A		Case D		Case E		Case F	
Parameter	Ocean	Basin	Ocean	Basin	Ocean	Basin	Ocean	Basin
Observation value (m)	5.86	4.32	6.06	\	5.82	4.08	5.92	2.40
Peak time change (hrs)	-0.24	1.20	-0.48	\	-0.24	1.92	-0.24	2.16
Magnitude change (m)	0.06	-3.67	0.26	\	0.02	-3.91	0.12	-5.59

3.5 Impact of the Swansea Lagoon Implementation

This section looks at the impact that a small tidal barrage has on storm surge. The Swansea Bay Lagoon (see Section 2.4.2) is applied to the model in addition to the modified storm surge event. Again, the entire simulations are carried out with a time period of 28 days, with a four-day spin-up period to avoid the initial transient response of the model. Observation sites on the basin side and ocean side are considered and the detailed locations can be seen in Figure 2.38 in Chapter 2. Both the hydrodynamic impact of the lagoon implementation and the impact due to different lagoon operations during a storm surge event are considered and applied with the same operation strategies as the Severn Barrage (see Table 3.4).

3.5.1 Hydrodynamic Impact

The lagoon is small in geographical size relative to the Severn Barrage and might be expected to have only a correspondingly small impact on the large-scale tidal hydrodynamics. However, the tidal hydrodynamics of the Bristol Channel is, as mentioned above in Section 3.1, a resonant system and such systems can change significantly with relatively small disturbances. For the lagoon hydrodynamic impact analysis, a slightly different combination of head values are applied for the operation strategies due to the difference in impoundment sizes compared to the barrage. A number of different operational scenarios can be found in Table 3.10.

Similar to the barrage, cases 'A', 'B' and 'C' have different head values and the final case, 'D', is essentially a closed lagoon. It is found that, despite the tidal resonance, there is very little impact on the tides outside of the Swansea Lagoon for any of the scenarios considered. The magnitude of the M_2 tidal constituent at measurement stations on the ocean side of the lagoon for the different scenarios is

Table 3.10: Lagoon operational scenarios with different starting heads and finishing heads.

Case	Starting head (m)	Finishing head (m)
A	2.5	1.0
B	3.0	1.0
C	3.5	1.5
D	-	-

shown in Table 3.11. From the Table, it can be seen that the tidal amplitude outside the lagoon is slightly reduced everywhere. Although this reduction in tidal range is very small in percentage terms, this might have an impact on the return levels of an extreme flooding event. There is no clear relationship that can be concluded between the starting head and the impact on amplitude with respect to the harmonic analysis.

Within the lagoon, no harmonic analysis was conducted due to the water holding phase as seen in Figure 3.7, which means the signal is no longer fundamentally sinusoidal in form. This Figure presents the comparison results of different lagoon operation cases on both ocean and basin sides. The Figure confirms that limited influence is exhibited on the main hydrodynamics in the ocean for all operation cases. However, for the basin region, overall reduction in the water level or tidal range can be observed compared with the regular condition (no lagoon case). Smaller operational head leads to a comparably higher water elevation and less flooding impact, which is consistent with the conclusion drawn for the much larger Severn Barrage in Section 3.1. Some minimal water level increments are still observed, which would lead to negative flooding impacts; contrarily, reduction of the maximum water level is also observed, which would be beneficial in terms of flooding protection within the lagoon. However, the enclosed regions are relatively small and both impacts are less than 1 m. The phase shift within the basin can be explained as being due to the operational holding stage of the lagoon. Under the extreme condition of lagoon closure, there is essentially no water elevation within the basin, and hence the largest deviation from the natural range is observed. Generally speaking, similar but lower influences on the surrounding land regions and flooding protection can be expected from lagoon implementation compared to that of the barrage. The overall reduction in the water elevations and tidal ranges due to the addition of a lagoon would fractionally ease the flooding level expected in the Severn Estuary.

Table 3.11: M_2 tidal elevation amplitudes and phases at different stations for different lagoon operation scenarios.

Station	M_2 Amplitude (m)					
	Obs.	No Lagoon	Case A	Case B	Case C	Case D
Pwllheli	1.48	1.51	1.51	1.51	1.51	1.51
Barmouth	1.47	1.52	1.52	1.52	1.52	1.52
Fishguard	1.35	1.42	1.41	1.41	1.41	1.41
Stackpole Quay	2.51	2.54	2.54	2.54	2.54	2.54
Mumbles	3.18	3.09	3.08	3.08	3.08	3.08
Barry	3.82	3.91	3.89	3.89	3.89	3.89
Hinkey Point	3.80	3.97	3.95	3.95	3.95	3.95
Ilfracombe	3.04	3.01	3.00	3.00	3.00	3.00
Lundy	2.67	2.56	2.55	2.55	2.55	2.55
Station	M_2 Phase (°)					
	Obs.	No Lagoon	Case A	Case B	Case C	Case D
Pwllheli	239	239	238	238	238	238
Barmouth	244	236	235	235	235	235
Fishguard	207	208	207	207	207	207
Stackpole Quay	168	174	174	174	174	174
Mumbles	171	176	176	176	176	176
Barry	185	183	184	184	184	183
Hinkey Point	185	184	185	185	185	185
Ilfracombe	162	167	167	167	167	167
Lundy	160	165	165	165	165	165

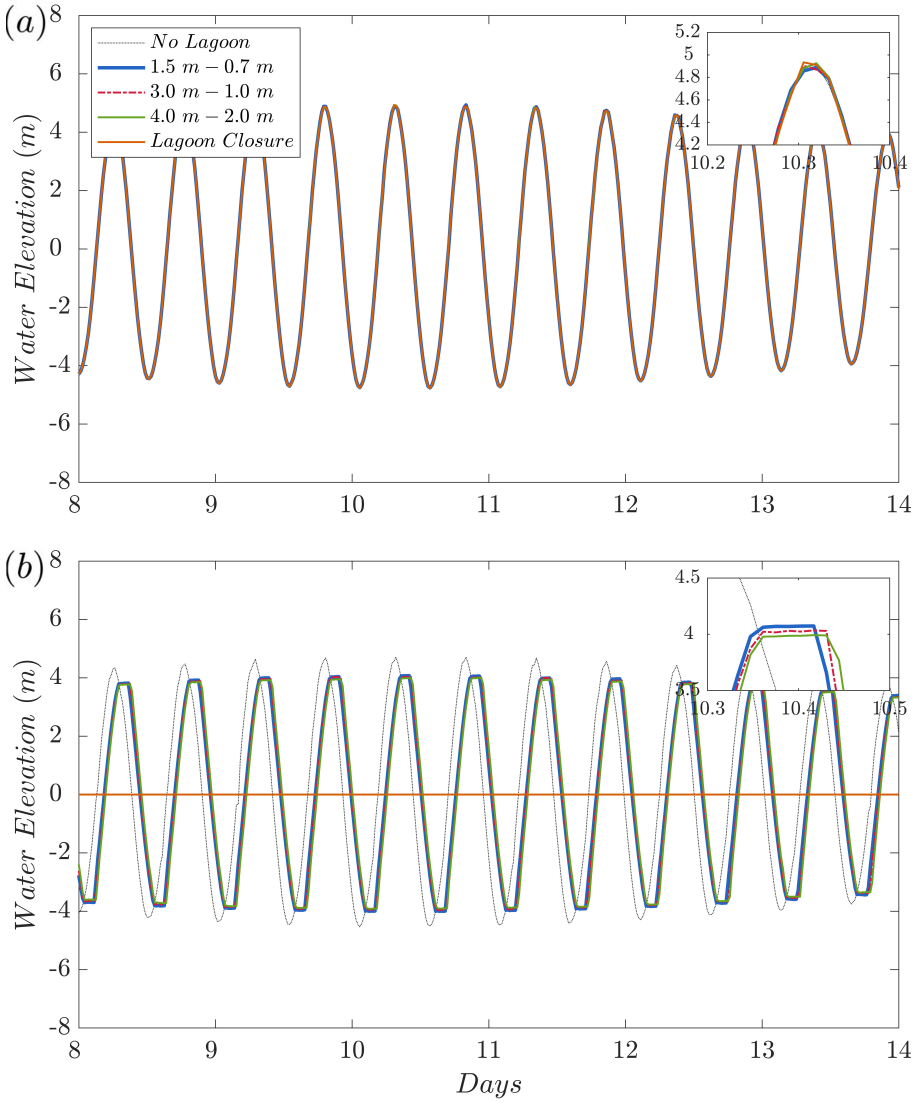

Figure 3.7: Impact of lagoon operational heads on the water elevations without meteorological forcing: a) on the ocean side (51.38°N 3.76°W) (top); b) on the basin side (51.60°N 3.90°W) (bottom).

3.5.2 Impact of Different Lagoon Operations

This section investigates the effects of the implementation of a lagoon with different operational strategies and examines its benefits on flooding protection, with the same modified storm surge event in the year 2000 as the barrage case described in the section above. The lagoon cases 'A' and 'D' seen in Table 3.10 are included, along with two of the same operational cases as the barrage during the storm surge event, which are cases 'E' and 'F' in Table 3.4. Figures 3.8, 3.9, 3.10 and 3.11 present the residual and water level results on the ocean side and the basin side of the lagoon for cases 'A', 'D', 'E' and 'F'.

For case 'A' with normal lagoon operation, from the Figures it can be seen that on the ocean side there is an small water elevation decrease of up to 1% at the peak of the surge. This is similar to the results of the tide-only phenomenon discussed previously and this may be due to some surge-tide interactions that result from lagoon implementation. No clear difference can be observed for the residuals of the case with the lagoon compared with the no lagoon case on the ocean side. Within the lagoon, from the Figures, water elevation has dropped in the case with lagoon operation (case 'A') by approximately 9% at the surge peak. Also there is a phase lag of approximately 2 hours. Regarding the residual, even though there is a lower reduction in the amplitude (7%), the residual peak time has been delayed again for about 2 hours. The same delay of peak residual is also found at some regions near the lagoon site. Another useful feature of the lagoon is that it appears to reduce the area susceptible to flooding in this test event. Here the surge residuals during the storm surge events is considered and comparison is made between the flood-affected regions (around the lagoon site) between the original no lagoon case and the case with lagoon implementation. Figure 3.12 shows the comparison of residual results around the lagoon site captured at the time of the peak surge of the storm surge event. The surge condition is considered severe when the residual exceeds 1 m. From the Figure it can be seen that regions within the lagoon are well protected in the case of its addition. The areas immediately surrounding the lagoon, especially the upper coastline where impacts of flooding are severe, also see a reduce in residual levels due to the lagoon implementation. However, the addition of a lagoon may increase the residual elevation at certain locations further away from its position, as seen in the upper right quadrant of the Figure. Despite these changes in the vicinity of the lagoon, its implementation has no significant benefits to flood protection at the head of the channel and other areas far from the lagoon.

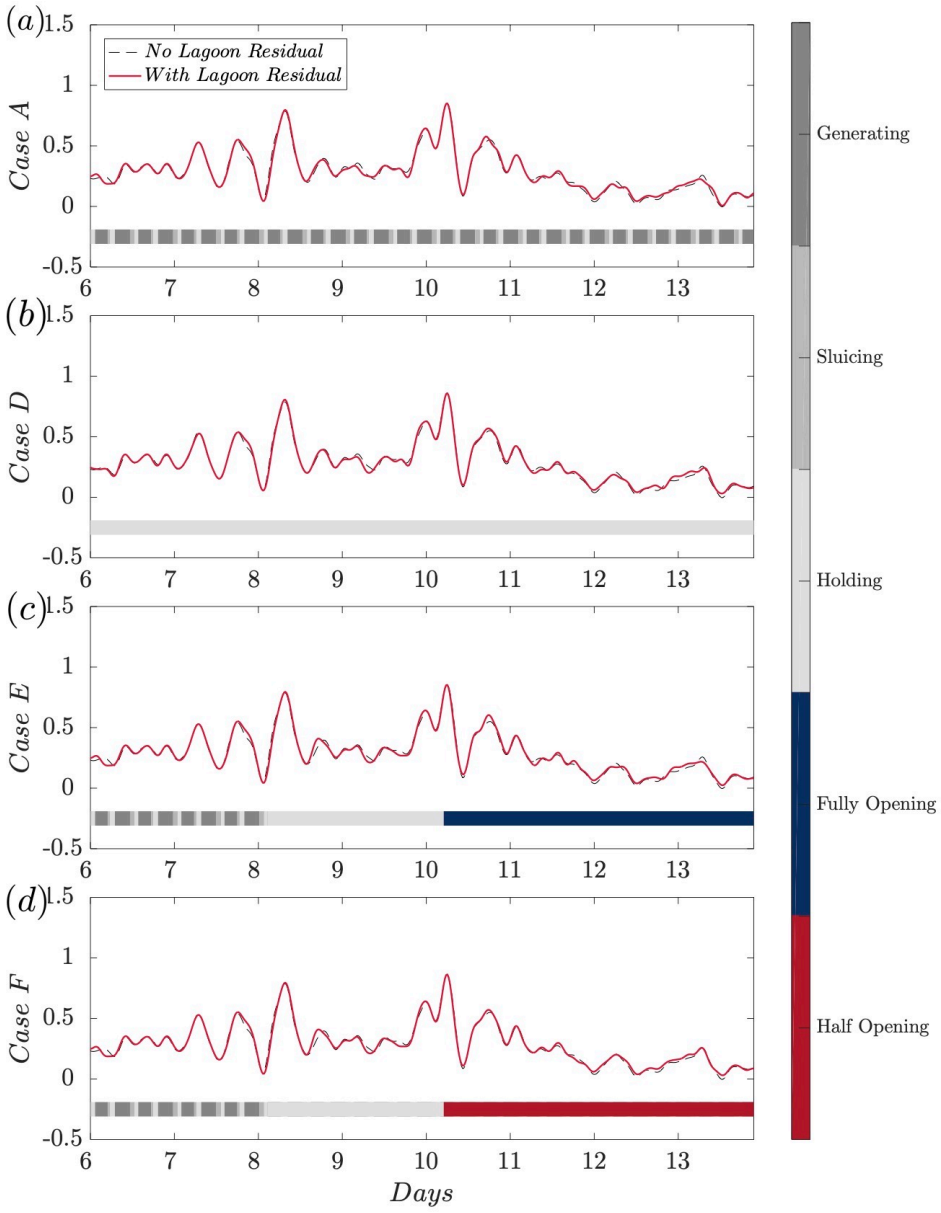

Figure 3.8: Residual level results (m) in the ocean-side region (51.38°N 3.76°W) of the four lagoon operation strategies during storm surge: a) lagoon normal operation (first); b) lagoon complete closure (second); c) lagoon operation Case 'E' (third); d) lagoon operation Case 'F' (fourth).

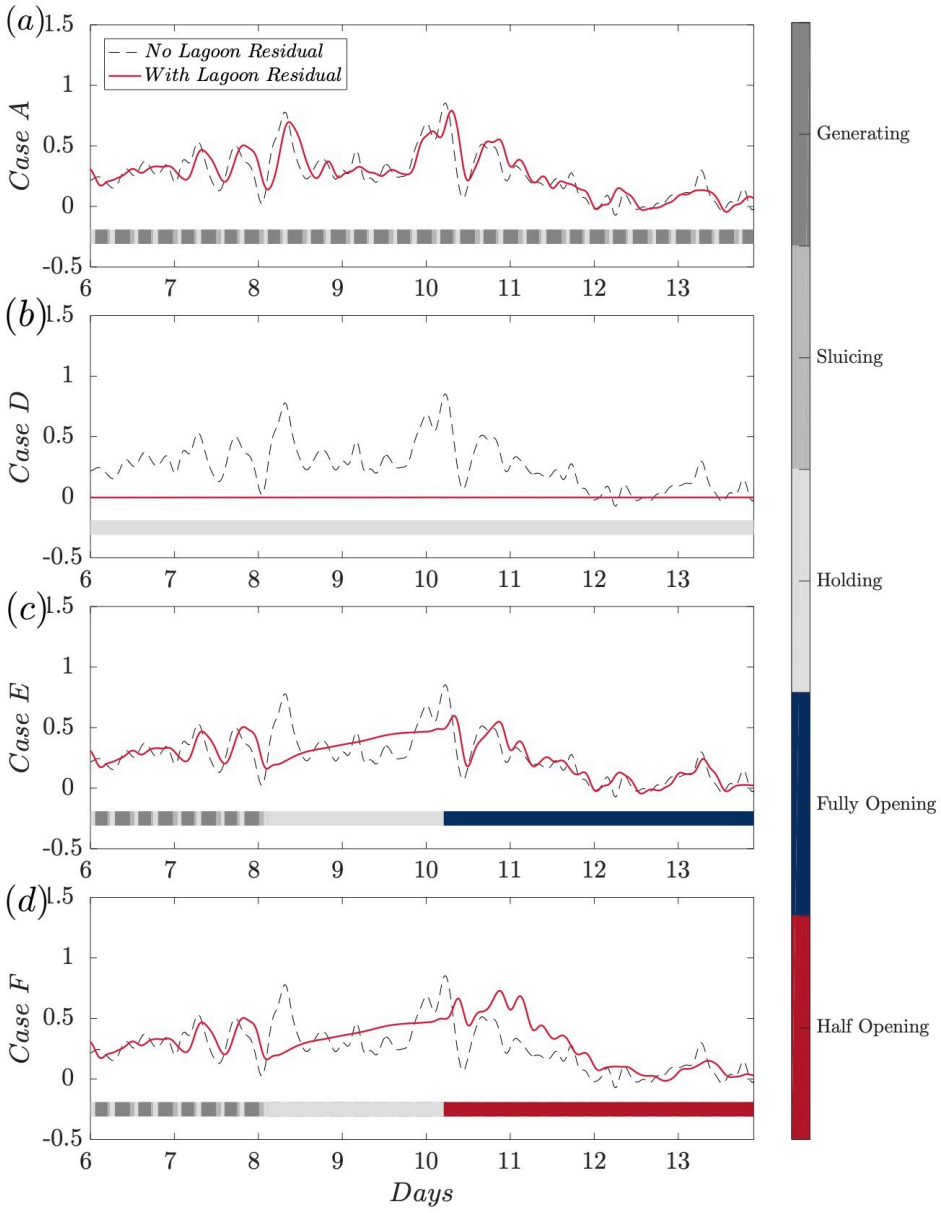

Figure 3.9: Residual level results (m) in the basin-side region (51.60°N 3.90°W) of the four lagoon operation strategies during storm surge: a) lagoon normal operation (first); b) lagoon complete closure (second); c) lagoon operation Case 'E' (third); d) lagoon operation Case 'F' (fourth).

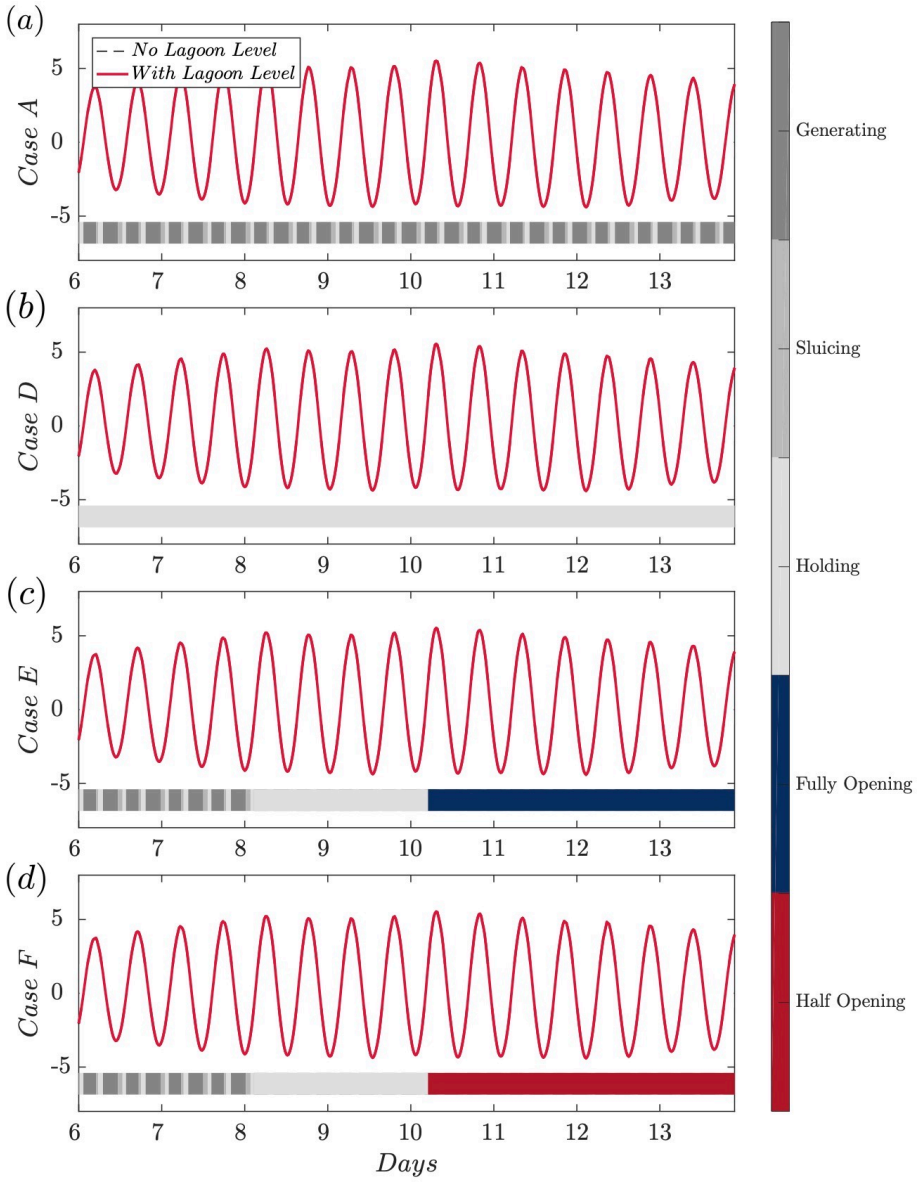

Figure 3.10: Water level results (m) in the ocean-side region (51.38°N 3.76°W) of the four lagoon operation strategies during storm surge: a) lagoon normal operation (first); b) lagoon complete closure (second); c) lagoon operation Case 'E' (third); d) lagoon operation Case 'F' (fourth).

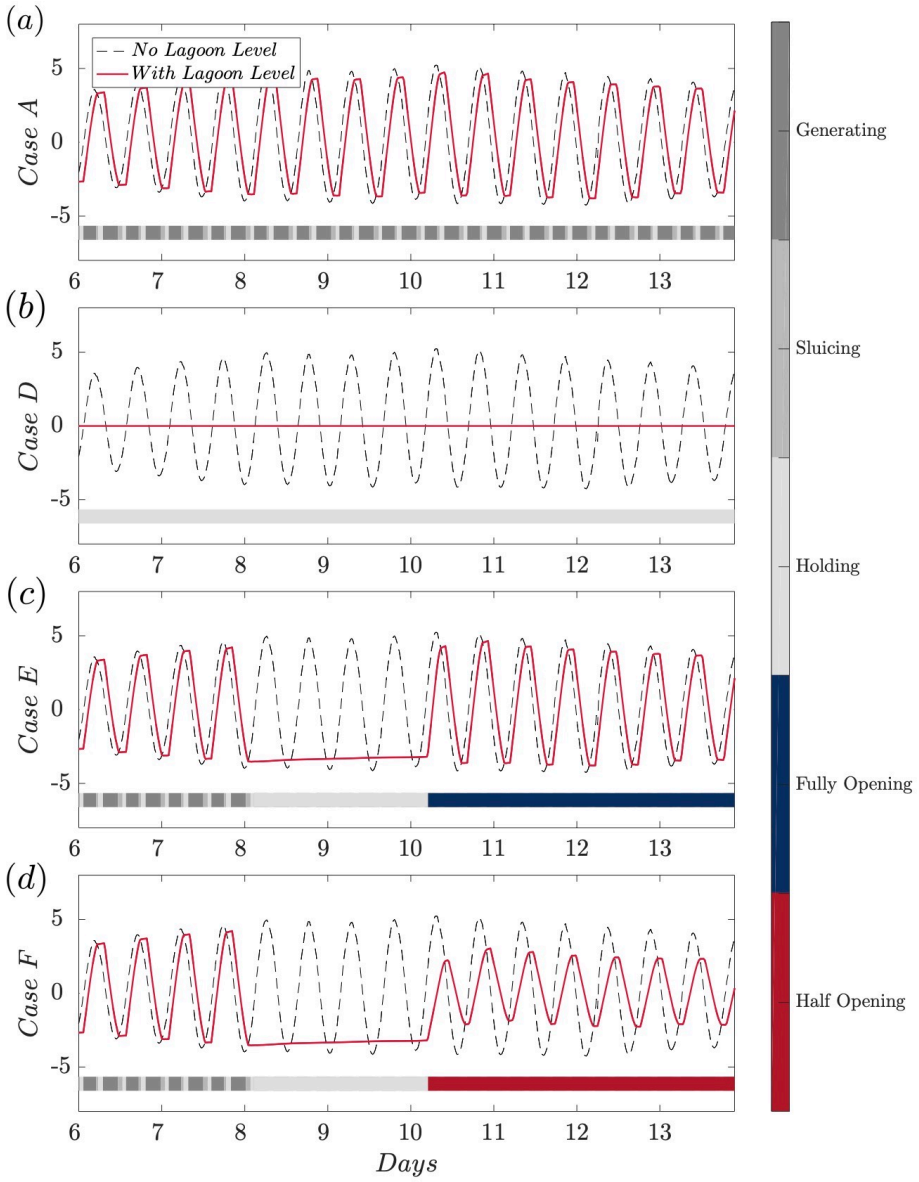

Figure 3.11: Water level results (m) in the basin-side region (51.60°N 3.90°W) of the four lagoon operation strategies during storm surge: a) lagoon normal operation (first); b) lagoon complete closure (second); c) lagoon operation Case 'E' (third); d) lagoon operation Case 'F' (fourth).

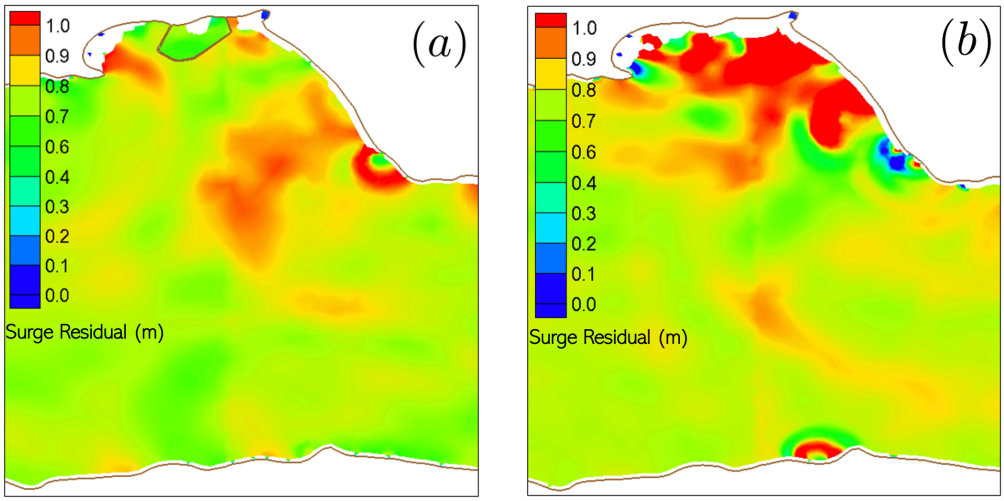

Figure 3.12: Comparison of surge residual level simulation results (m) around proposed lagoon site at the time of the peak surge of the storm surge event displayed by SMS: a) lagoon implementation (left); b) original case (right).

For the simulation of the extreme case 'D' where turbines and sluices are fully closed, a minor modification is made to the meteorological forcing. This is done as the application of wind shear stress to the small enclosed body of water inside the lagoon clearly gave non-physical results (probably due to insufficient energy dissipation in the lagoon which does not balance the energy input). The wind shear stress is therefore not applied within the lagoon area. Thus the results within the lagoon are not really meaningful. Outside the lagoon, shutting it off completely leads to a lower decrease of 0.01 m in the water level. Therefore, shutting the lagoon off completely is seen to have a small effect of decreasing the water level elsewhere. No clear difference can be observed in this case in terms of the residual.

For cases 'E' and 'F', as can be seen in Figures 3.8 and 3.10, there are no clear differences in the timing of the surge peak. There is only a small decrease of elevation or residual (within 1%) when compared with the original no lagoon case in the ocean regions (due to the small impact of lagoon implementation to the ocean region during surge events as discussed above). It is more important to compare the different cases for the basin region. Consequently, the basin results and the different peak values are presented in detail in Table 3.12.

As can be seen from the Table, both cases 'E' and 'F' show more benefits in terms of surge peak time delay than the case with normal lagoon implementation. For case 'F' especially, the time lag is approximately 3.84 hours with respect to the surge residual and the lag would be significant considering the five-hour period of the storm surge event in the Bristol Channel.

Table 3.12: Comparison of results of different strategies for residual and water level in the ocean (51.38°N 3.76°W) and basin (51.60°N 3.90°W) region relative to the original no lagoon results.

Case	Case A		Case E		Case F	
Parameter	Residual	Water Level	Residual	Water Level	Residual	Water Level
Observation value (m)	0.79	4.74	0.60	4.30	0.67	2.22
Peak time change (hrs)	2.16	2.16	2.64	2.64	3.84	2.88
Magnitude change (m)	-0.06	-0.49	-0.26	-0.93	-0.19	-3.02

For the residual, both cases indicate a peak level reduction of over 20% and case 'E' achieves optimum results with a 0.26 m reduction. From the residuals in Figure 3.9, some increment of the residual level for cases 'E' and 'F' have been observed after the surge event. The gradual rise of the residual level during the holding period between day 8 and day 10 can be explained as non-physical features due to the implementation of the relatively small enclosed area of the lagoon and wind shear (the same simulation issue as case 'D'). In terms of water level, again more benefits can be observed by controlling lagoon operation. The water elevation decreases approximately 18% and 58% for cases 'E' and 'F' respectively, and case 'F' provides the best flooding protection to the basin region with a reduction of 3.02 m of the storm water level.

3.6 Comparison of the Impact of Barrage and Lagoon Implementation

In this section, comparisons between implementation of the Severn Barrage and the Swansea Lagoon in the Severn Estuary are carried out. A combined project with both a barrage and a lagoon is also considered to examine the interactions between the two.

From the above sections, it can be concluded that both implementation of the barrage and lagoon can provide flooding protection to the estuary, especially to the impounded areas. The water level can be reduced by approximately 6.95 m and 3.02 m for the optimal barrage and lagoon operations, respectively, during the surge events. Also, the delay of the surge peak during the event for over 2 hours can be another beneficial feature for flooding control and more actions can be taken ahead of surge events. However, with respect to those regions, they may experience some

negative environmental impacts due to the rise of the minimum water level and some phase shifts. For the lagoon, which is a relatively small project compared with the barrage, only a small area of Swansea would be effected, so both the flooding control function and the negative environmental impact provided by the lagoon would be eased.

For the regions outside of the impoundment, the impacts are not significant. The lagoon implementation does not induce negative impacts on the ocean side in terms of water rising while, for a barrage, the extreme water level in the ocean would be increased by approximately 0.30 m for the optimal barrage operation. This may have a small impact on flooding in areas such as the Somerset Levels.

3.6.1 Project with both Severn Barrage and Swansea Lagoon Implemented

A combined project with both barrage and lagoon is carried out to investigate how these would interact. The model utilises both design proposals of the Severn Barrage and the Swansea Lagoon and the domain is shown in Figure 3.13. Both devices are normally operated throughout the simulations with a starting head of 1.5 m and a minimum operation head of 0.7 m without any additional operation strategies in the presence of the storm surge applied. Simulations are carried out with a time period of 14 days with a two-day spin-up period and applied with the artificial storm surge event in the year 2000, described in Section 2.5.2.

Figures 3.14, 3.15 and 3.16 show the simulation results of the different devices during the surge events. The ocean result is selected at the region between the lagoon and barrage so that their interactions can be captured. As expected, due to the relatively small impoundment, there are limited effects that can be observed within the barrage basin with an additional lagoon implemented, in terms of both residuals and water level features (shown in Figure 3.14). Significant flooding protection can be provided considering both residual and water level. However, an additional barrage implementation would have some effects on the basin regions with a lagoon. In Figure 3.15, it is observed that for the residual level during the surge event, instead of the former benefits provided by the lagoon, there are rises in the residual level even higher than the no lagoon case (by 0.03 m) because of the inclusion of both schemes. The water levels are increased as well even though the region is still under the flooding protection provided by both devices. The phase shifts also still exist.

Looking specifically at the ocean region in between the barrage and the lagoon (Figure 3.16), their interactive effects are seen to be complex. Considering both

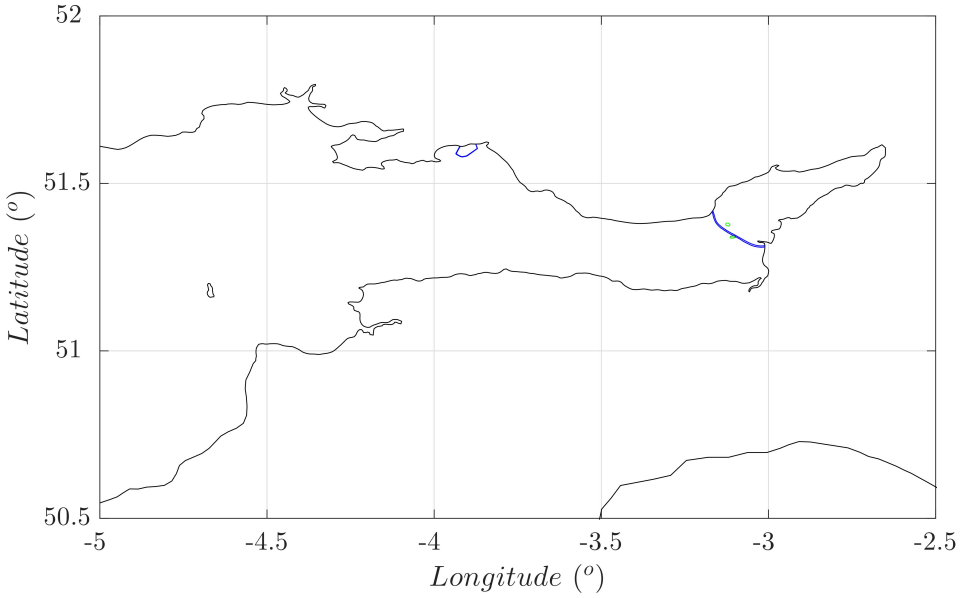

Figure 3.13: Model computational details of the model domain, blue lines show the ocean boundaries and the barrages boundaries of the Severn Barrage and the Swansea Lagoon.

residual and water level, with solely lagoon implementation, ocean water level is expected to decrease as seen in Section 3.5.1). However, with the implementation of solely the barrage as well as both the barrage and the lagoon, water level rise is introduced to the peak surge, negatively impacting the flooding of surrounding areas. Especially for the residual, the impact of including both devices becomes largest in terms of increment level. It can be seen that the effect from a coupled system is not a simple superposition of the effects from individual device implementations and there would be some specific interactions between devices.

3.7 Discussion and Conclusion

This chapter examined the impact of placing a tidal barrage or lagoon in the Bristol Channel on the water elevation during storm surges. Two projects were chosen: the Severn Barrage and the Swansea Lagoon. For the analysis, both residuals and extreme water levels were considered in order to examine the potential flooding protection benefits that can be provided by the structures. An evaluation was performed on whether it is possible to influence storm surge elevations by changing how a tidal barrage operates. The analysis within the chapter is based on the meteorological

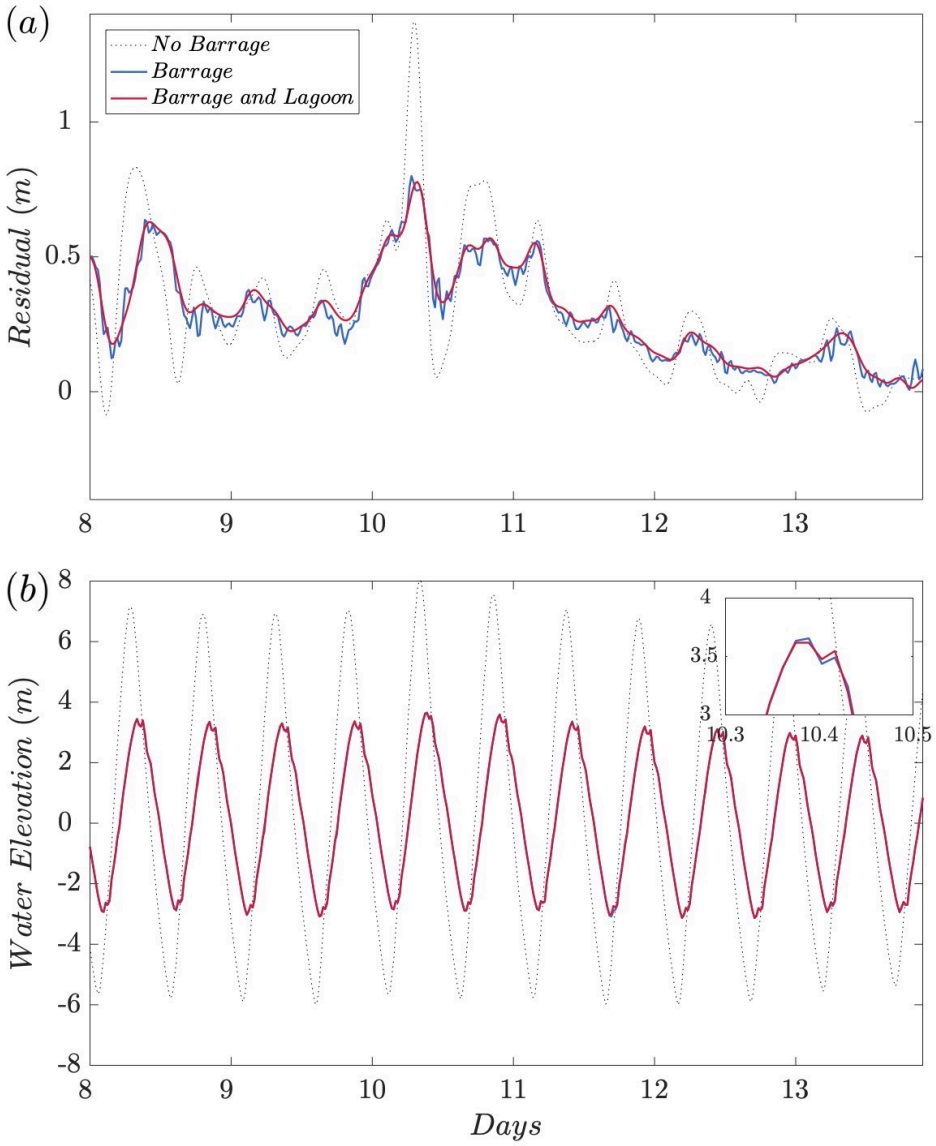

Figure 3.14: Simulation results of barrage and barrage&lagoon implementation on the barrage basin side (51.48°N 2.90°W): a) residual results (top); b) water level results (bottom).

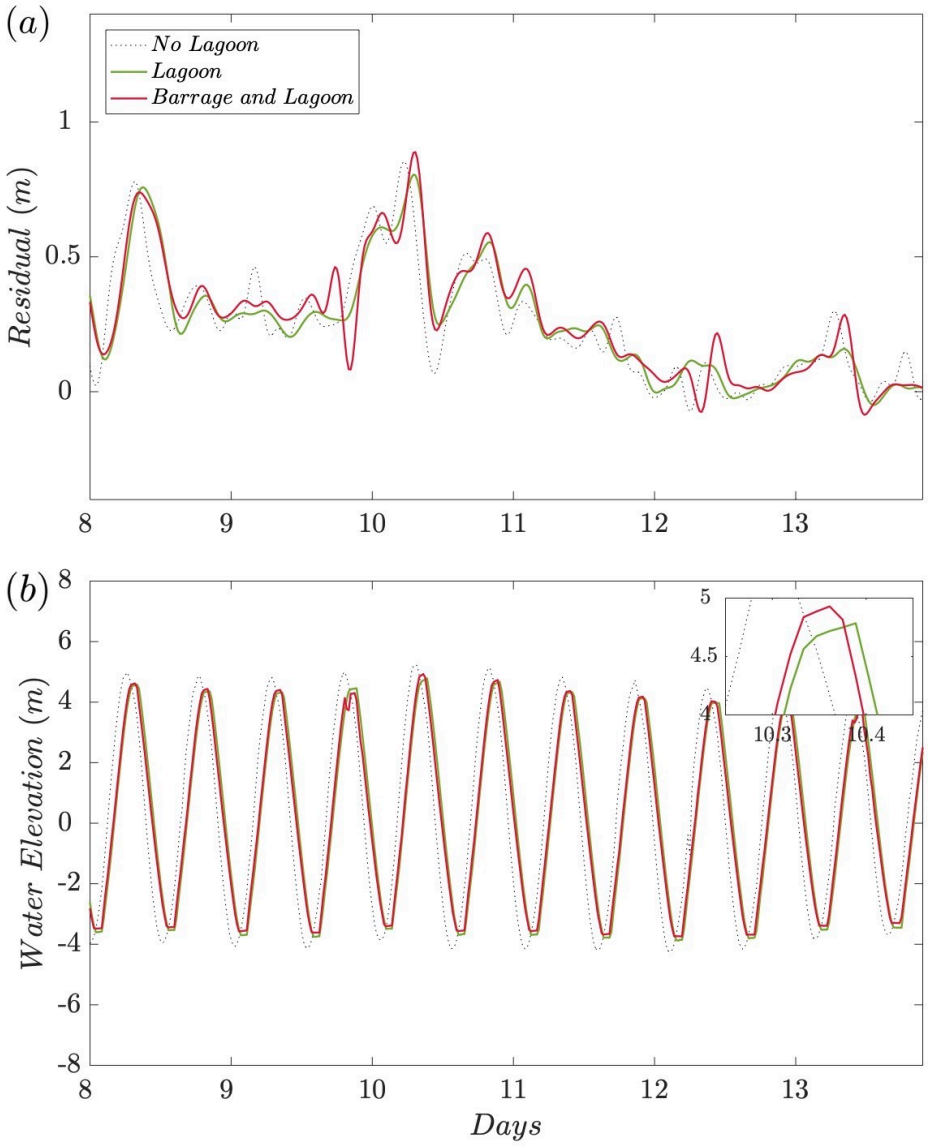

Figure 3.15: Simulation results of lagoon and barrage&lagoon implementation on the lagoon basin side (51.60°N 3.90°W): a) residual results (top); b) water level results (bottom).

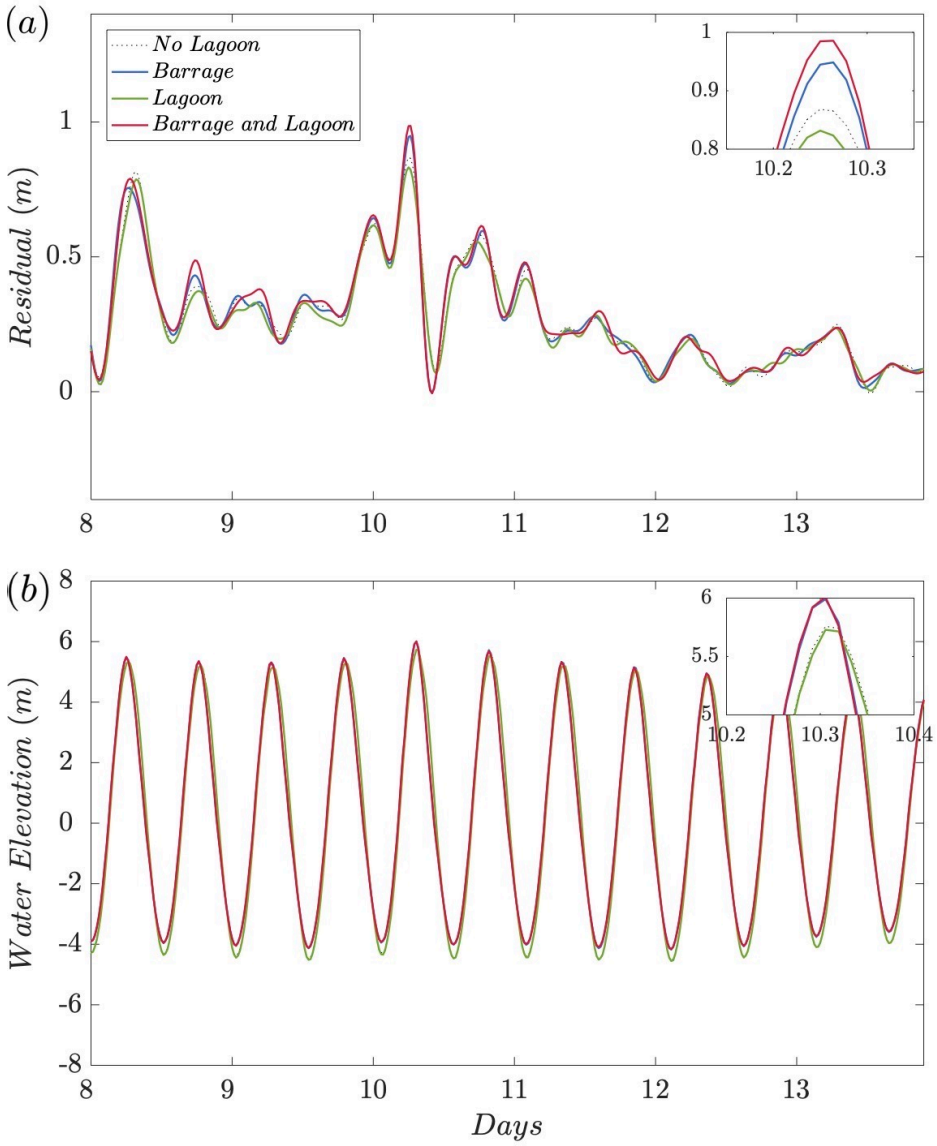

Figure 3.16: Simulation results of barrage and lagoon and barrage&lagoon implementation on the ocean side (51.36°N 3.67°W): a) residual results (top); b) water level results (bottom).

conditions for the most significant storm surge in recent times in the area. A second, synthetic, event was simulated to check that the results can be generalised.

It is clear that the Severn Barrage can provide significant protection from coastal flooding for the cities of Bristol and Cardiff and other locations to the east of the barrage. However, there would be an increase in the extreme water level to the west of the barrage, which might impact flooding in areas such as the Somerset Levels. An exact calculation of the different flooding levels is challenging, but qualitatively, the increase in water level expected is of the same order of magnitude as that from sea level rise (10s of cm). Careful operation of the barrage can make a small, but perhaps significant, difference to the extreme water level during a storm surge event. In the case of the Swansea Lagoon, some flooding protection can be provided for the regions within and outside the lagoon. However, the benefits are relatively small and localised compared with the barrage, and different lagoon operation strategies during the storm surge event can have some effects on the flooding around the lagoon site. Some negative flooding impacts due to the rise of the minimum water level and wetting and drying within the basin along with the device operation can occur due to the introduction of both devices.

Exactly which strategy is optimal would depend on the weight placed on the changes to the water level both upstream and downstream, as well as the impact of power generation interruption during a spring tide (analysed further in Chapter 4). Besides the projects considered in this chapter, as with other storm surge barrages (e.g. the Thames Barrier or Maeslant Barrier), the structures could also be used to reduce the impact on river flooding in the Severn River and other rivers flowing into the basin to the east of any barrage. This would require the barrage to be operated appropriately. This operation might be sub-optimal in terms of flooding from storm surge, if river and storm surge flooding were to coincide.

The primary aim of this project is to examine the impact of barrage implementation on storm surge events. Particularly in this chapter, the impacts of a barrage were examined by considering the resulting water levels during a storm surge event. However, the barrage impacts on flooding over the surrounding low-lying areas (especially in the Somersets Levels region) during a surge event can also be a factor of interest. As such, a modified model is considered which includes the low-lying area around the channel head with the land data captured from the GEBCO bathymetry dataset. Details of the model and its results on the susceptible flooding regions during a surge event is given in Appendix A.

Chapter 4

Impact of Barrage Operation Strategies on Power Output

In Chapter 3, specific barrage operation strategies have been considered to provide protection from flooding during storm surge events. In changing the operation of the barrage, this would, of course, have an impact on the power generated. To the author's knowledge the only literature on this topic is by Lewis *et al.* [108], who have suggested that the additional energy present in storm surges could increase the power output of barrage-type structures by around 10%.

This chapter investigates the power and energy generation by both the Severn Barrage and Swansea Bay Lagoon during a surge event under the various scenarios discussed in the previous chapter. As the main focus of this thesis is not on the power produced by the barrage, the objective of this chapter is to conduct a preliminary study of the topic. A more detailed analysis of the impact of meteorological disturbances on power would require significant code development and an abundance of computational resource. However, to the author's knowledge, this chapter is the first to look at power production from a barrage during a storm surge that goes beyond simplistic zero-dimensional modelling. Zero-dimensional modelling has poor accuracy when modelling the power output of large tidal barrage schemes [12]. As discussed earlier, storm surges in the Bristol Channel will only be a flooding risk around spring tide. However, spring tides are when the most power would be produced by a barrage when recalling that, in a simplified analysis, power is proportional to tidal amplitude squared.

Section 4.1 presents an introduction of power generation by the Severn Barrage and the Swansea Lagoon and also the simulation details of the project. Section 4.2 investigates the impact of a storm surge on the power output. Section 4.3 compares

the power output from the scenarios of different barrage operations and Section 4.4 does the same for the Swansea Lagoon. Section 4.5 concludes the chapter.

4.1 Introduction

Power generated from a tidal barrage can be evaluated as set out in Section 1.4.1.1. The detailed methodology of power calculation with the numerical model used in this thesis can be seen in Equations 2.8 and 2.9 in Section 2.4.1. Numerous studies such as [10, 180] have used two-dimensional hydrodynamic models to estimate power production from tidal barrages. As such, the methodology to do this calculation in this project is well established.

From the initial project proposals by [23, 17], the total installed capacity of the Severn Barrage with two-way generation is approximately 8.6 GW and for the Swansea Lagoon, the equivalent figure is around 0.32 GW. The same reports predicted the average power output for the schemes to be 1.94 GW and 0.06 GW, respectively (estimated from the average annual energy output of 17 TWh and 0.52 TWh).

Simulations are conducted over the period that covers both spring and neap tides within a 14-day period (with a two-day ramping period). The barrage is normally operated with a two-way generation strategy. Power results for the tide-only case are illustrated in Figure 4.1 and variation in power generation can be observed from spring to neap tides. Results suggest that the major contribution to total power production comes from spring tides and the total energy that would be generated is about 413 GWh during the simulation period. The peak power output is approximately 6.6 GW at the time of 247 hours after the start of the simulations. The average power generated over this spring/neap cycle is 1.2 GW, which is comparable to the predicted output in the literature above of 1.94 GW. The simulations here only use three tidal constituents, which may explain the discrepancy.

4.2 Interaction of Storm Surges and Tidal Barrage

The synthetic extreme storm surge event as described in Section 3.4 is used to evaluate storm surge impact on tidal power output. The surge is introduced with the maximum south-westerly winds of 30 m/s and a constant atmospheric pressure of $101,325$ Pa. The designed surge is coincident with high tide with a resulting surge residual of 2.32 m during the event at the region approaching the head of the channel.

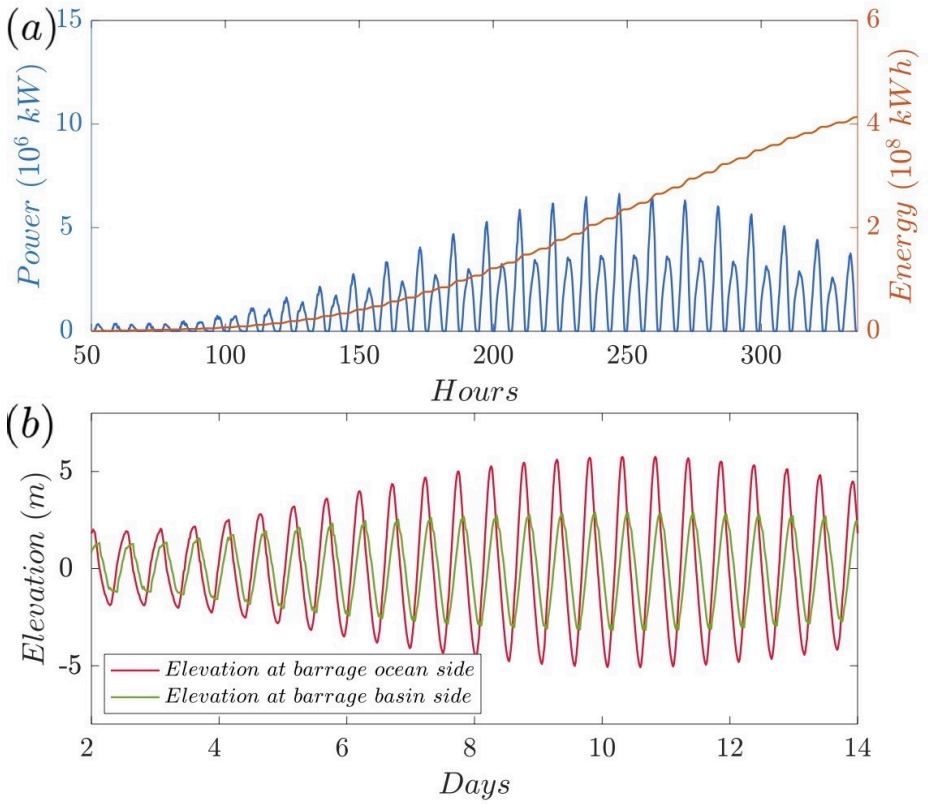

Figure 4.1: Simulation results of power output from the Severn Barrage under tides only phenomenon: a) power and energy generated (top); b) water elevation difference across the barrage (bottom).

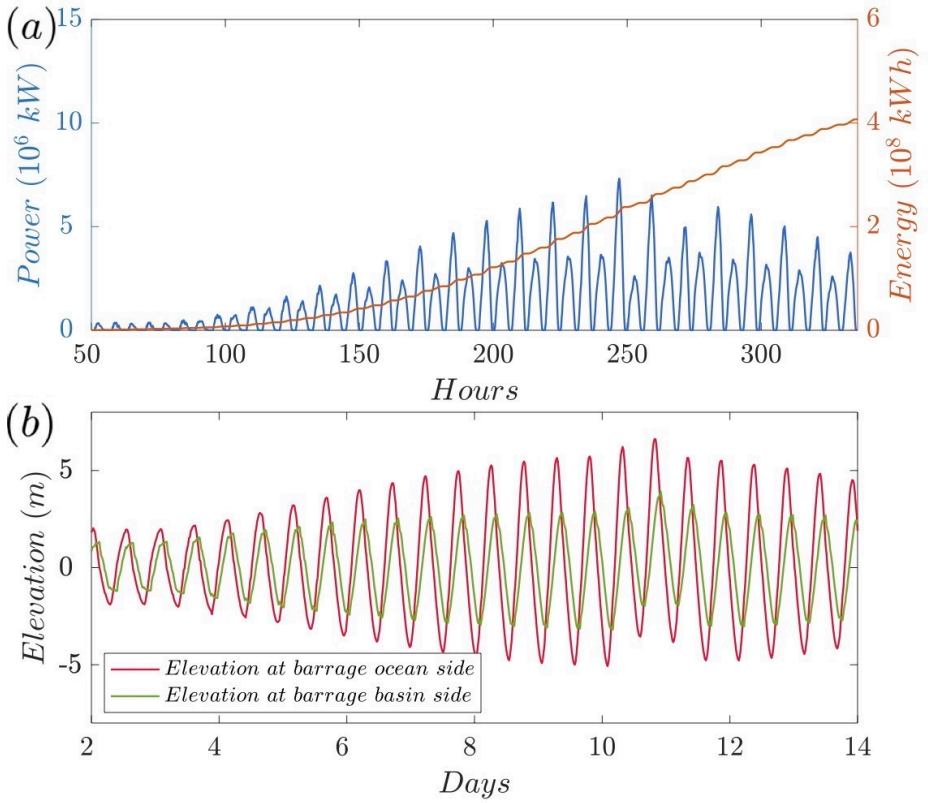

Figure 4.2: Simulation results of power output from the Severn Barrage for synthetic storm surge event: a) power and energy generated (top); b) water elevation difference across the barrage (bottom).

Figure 4.2 shows the power generation of the tidal barrage under the synthetic storm surge event and with the same operating strategy as above. The peak power output is approximately 7.3GW, which is about 11% more than the power estimated for the tide-only event. The net energy generated during the period is 407 GWh. Thus, for this particular scenario, there is a slightly higher peak in the power produced but a small decrease in the overall energy generated. This seems reasonable – a higher water level would lead to a greater peak in power, but maintaining the same strategy as the case without a surge is likely to lead to the incomplete emptying and filling of the basin, thus reducing the overall power. Also, since the surge event coincides with the spring tide and the spring tide is a major contributor to energy output, there may be complex tide-surge interactions during this time period that would negatively affect energy generation. However, these differences are small.

Table 4.1: Comparison of results of different barrage strategies for power generation during the synthetic storm surge event.

Barrage	No Surge	Normal Barrage	Case E	Case F
Energy Output (GWh)	413.29	407.17	298.17	397.0
Energy Difference (GWh)	\	-6.12	-115.12	-16.22
% of Energy Loss	\	1.48	27.85	3.92

4.3 Impact of Barrage Operation Strategies

Chapter 3 shows that the application of barrage operation strategies during the storm surge event can achieve benefits of flooding protection to the regions eastwards (i.e. basin-side) of the barrage in the Bristol Channel. In this section, both barrage control scenarios – case 'E' with completely opened sluices and case 'F' with partially opened sluices, as introduced in Table 3.4 – are considered for their impacts on power generation. It would be possible to consider an alternative operating scenario where power production was optimised. However, any small extra energy generated would not be as significant as the damage that flooding would cause. Thus this thesis will not consider additional barrage operation strategies that prioritise maximum power output.

Figures 4.3 and 4.4 illustrate the power output results with barrage control strategies 'E' and 'F', respectively under the synthetic storm surge event. Significant power generation can be observed at the time of sluice re-opening due to the large water head difference across the barrage. Higher power output (larger water head difference) is expected after the half re-opening of gates in case 'F'. As a result, more energy would be generated at the end of the period. Results for different cases are shown in Table 4.1. Both cases result in energy loss: 27.9% for case 'E' and 3.9% for case 'F'. The main loss comes from the barrage shutting down during the storm surge event. Barrage operation following case 'F' gives limited energy loss compared with the scenario of a normally operated barrage during the surge event. However, its benefit of flooding protection, especially to the regions approaching the head of the channel (approximately 5.6 m of water level reduction), is significant.

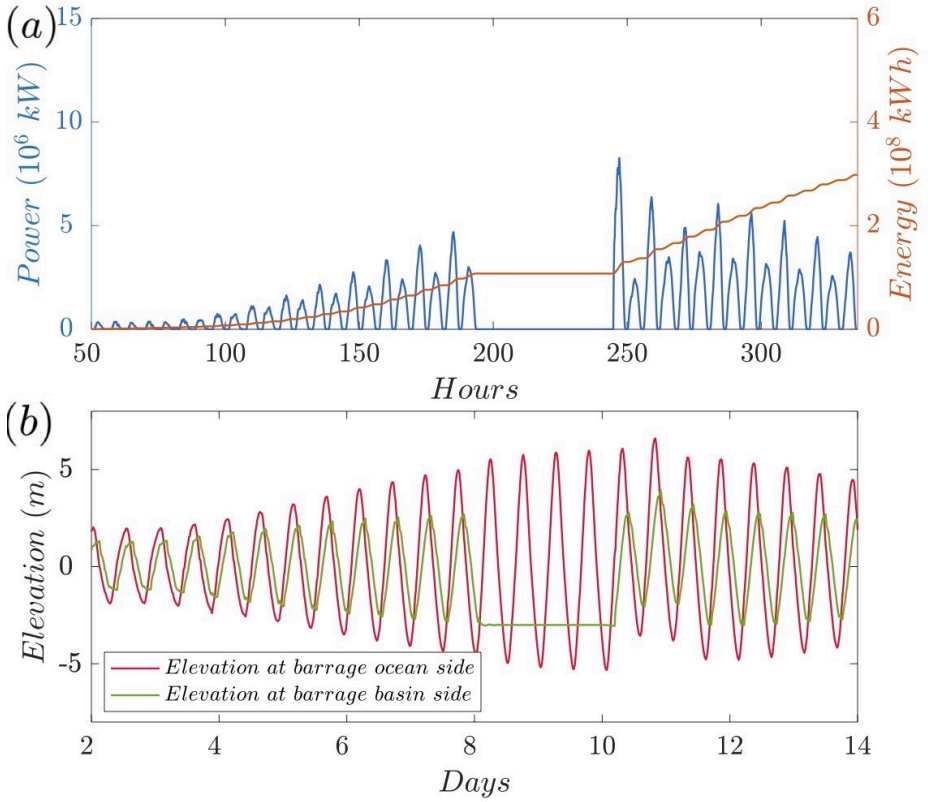

Figure 4.3: Simulation results of power output from the Severn Barrage with fully re-opening strategy (case 'E') during the surge: a) power and energy generated (top); b) water elevation difference across the barrage (bottom).

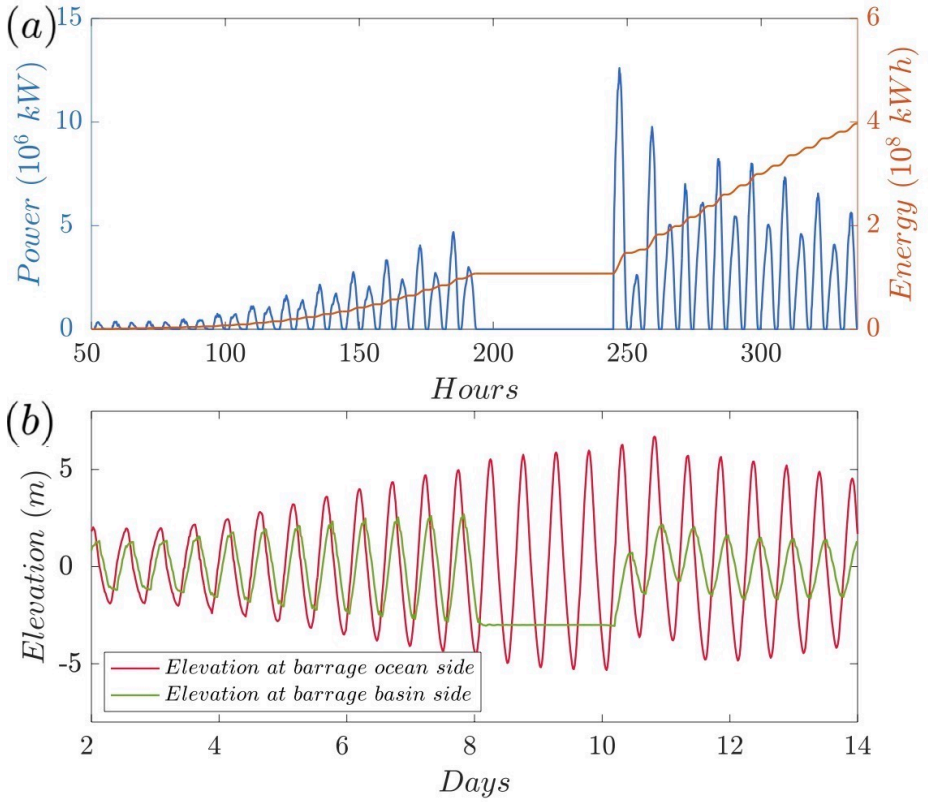

Figure 4.4: Simulation results of power output from the Severn Barrage with half re-opening strategy (case 'F') during the surge: a) power and energy generated (top); b) water elevation difference across the barrage (bottom).

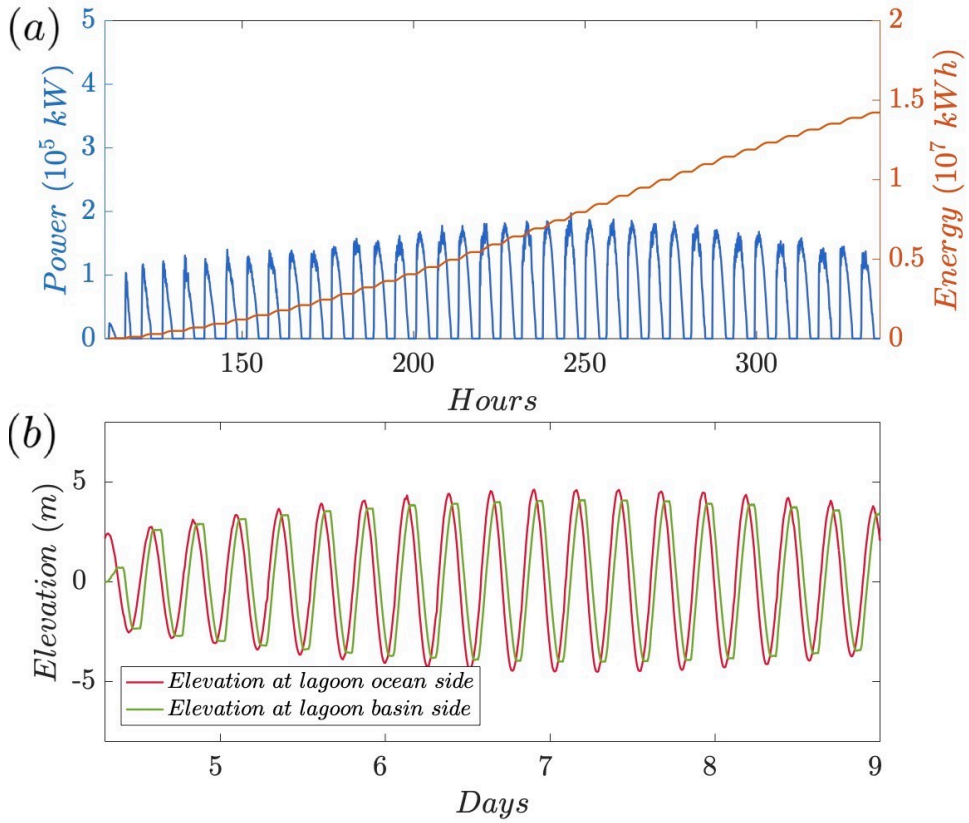

Figure 4.5: Simulation results of power output from the Swansea Bay Lagoon under tides only phenomenon: a) power and energy generated (top); b) water elevation difference across the barrage (bottom).

4.4 Swansea Lagoon

The same investigation is carried out for the Swansea Lagoon. Figures 4.5 and 4.6 show the power output by the lagoon considering tide-only and storm-tide scenarios, respectively. The peak power output estimated under the tide-only phenomenon is about 197 MW and the magnitude is similar in comparison with the power output with storm surge involved (193 MW [108]). However, when considering the net energy production during the whole simulation period, the addition of a storm surge phenomenon leads to approximately 0.7% energy reduction. The same explanation as made in the barrage case, assuming that there are complex tide-surge interactions for the duration of the spring tides, would account for this. Since it is a small-scale project, the impact of the storm surge component on the power estimation is rather limited.

Different lagoon operations (cases 'E' and 'F') during the event are simulated with results shown in Figures 4.7 and 4.8. Similar to the barrage case, for both operations,

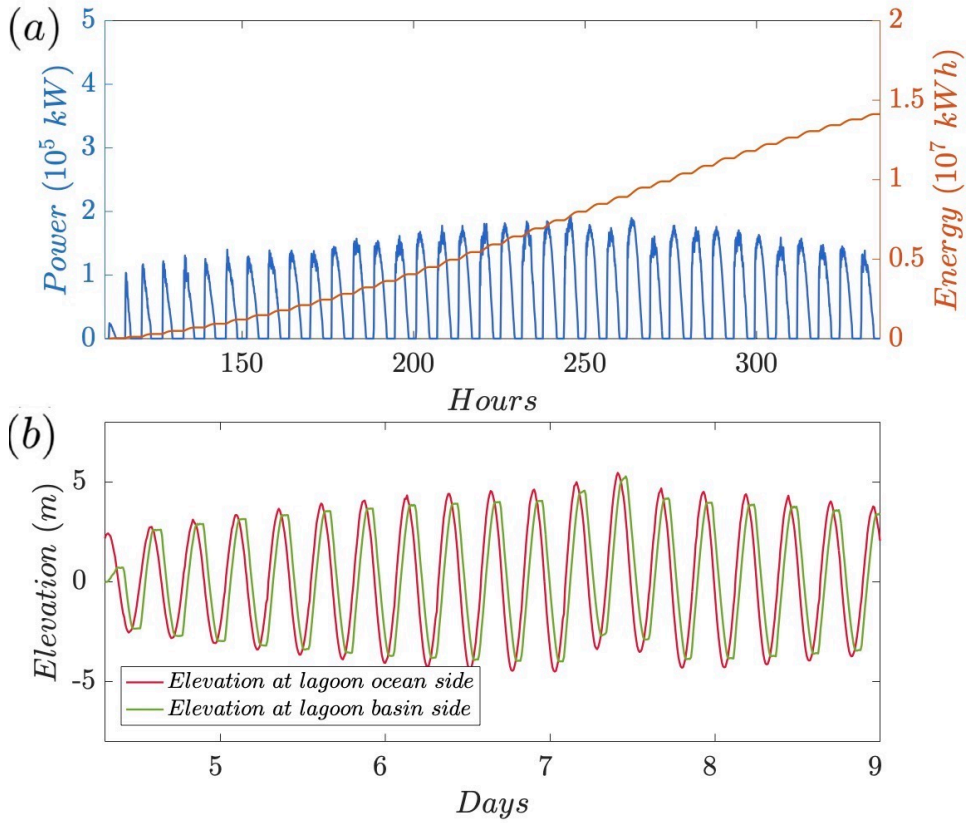

Figure 4.6: Simulation results of power output from the Swansea Bay Lagoon for synthetic storm surge event: a) power and energy generated (top); b) water elevation difference across the barrage (bottom).

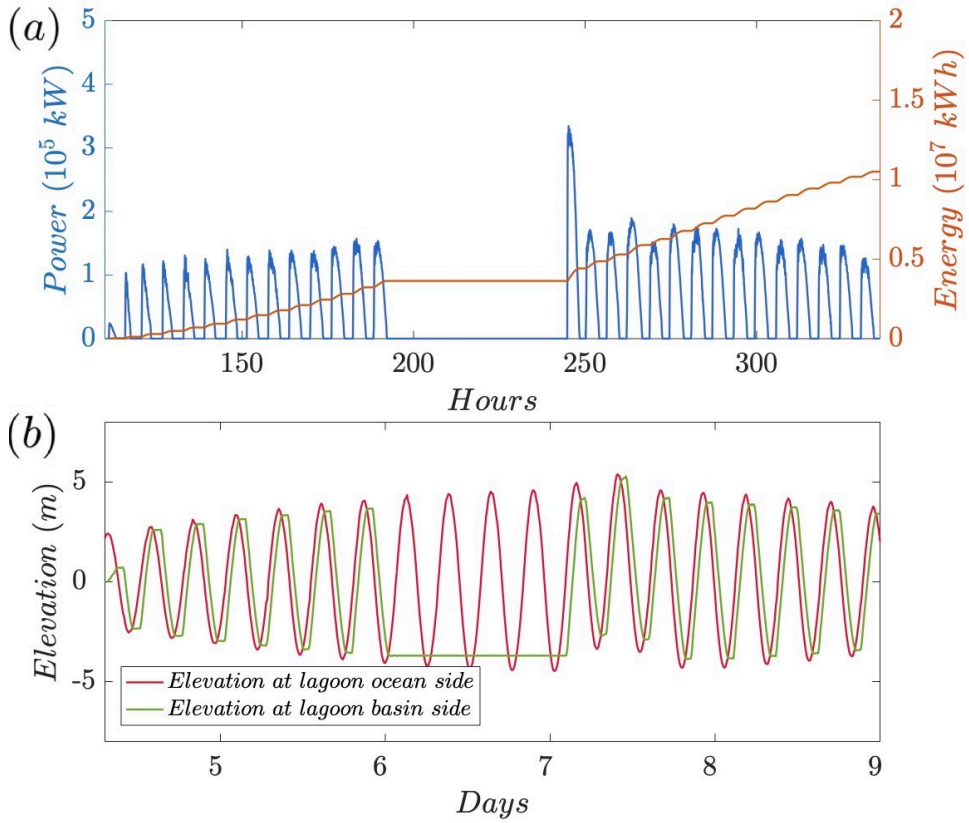

Figure 4.7: Simulation results of power output from the Swansea Bay Lagoon with fully re-opening strategy (case 'E') during the surge: a) power and energy generated (top); b) water elevation difference across the barrage (bottom).

increased power generation can be observed at the time of the lagoon re-opening. Due to the operation strategies, compared with normal lagoon operation, larger amounts of water head difference across the lagoon can be generated and hence more power can be output during the rest of the period. Table 4.2 shows the result comparisons between different scenarios. From the Table, it can be concluded that, especially for case 'F', even a larger amount of energy (up to 16%) can be produced during the storm surge event.

4.5 Conclusion

This short chapter presented a case study of what happens to the power produced by both the Severn Barrage and the Swansea Lagoon when an extreme storm surge occurs. Two key conclusions can be drawn. Firstly, if the barrage continues to be operated normally, even for a very severe storm surge there is a rather small impact on the power production. This result suggests that for minor atmospheric disturbances,

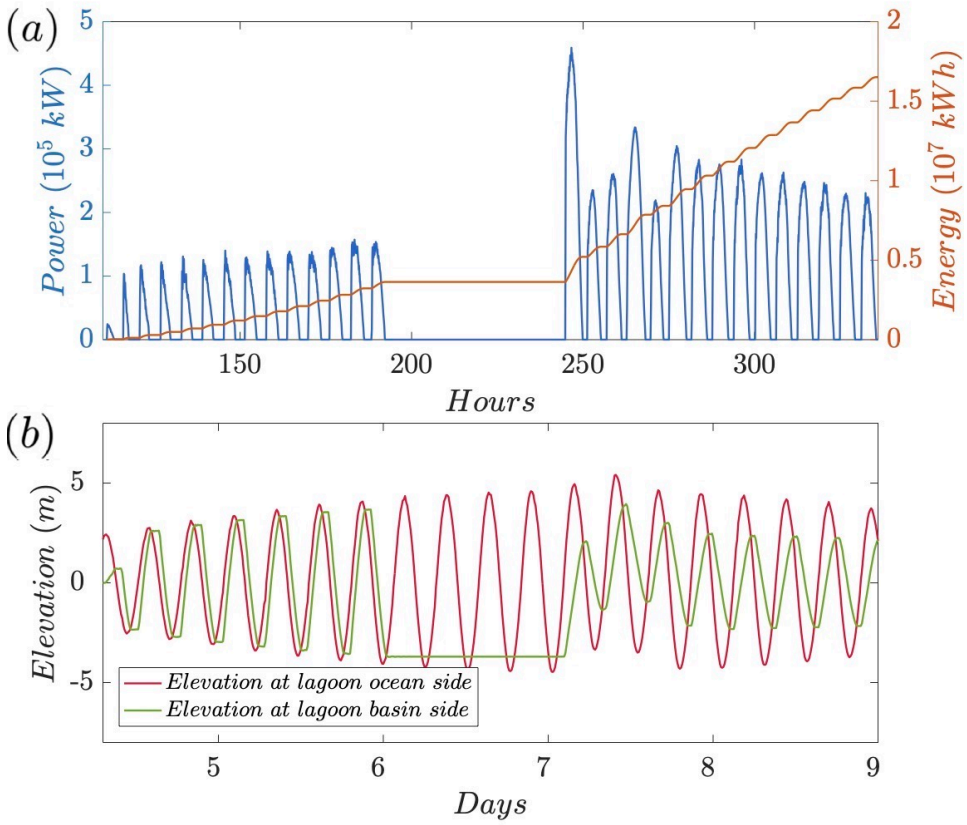

Figure 4.8: Simulation results of power output from the Swansea Bay Lagoon with half re-opening strategy (case 'F') during the surge: a) power and energy generated (top); b) water elevation difference across the barrage (bottom).

Table 4.2: Comparison of results of different lagoon strategies for power generation during the synthetic storm surge event.

Lagoon	No Surge	Normal Lagoon	Case E	Case F
Energy Output (GWh)	14.22	14.12	10.50	16.51
Energy Difference (GWh)	\	-0.10	-3.72	2.29
% of Energy Loss	\	0.69	26.14	-16.10

the impact on power production will be minor. Secondly, when the barrage is used for flooding defense (as set out in Chapter 3) when a severe surge corresponds to a high tide, there will be a significant interruption in power production. Although, this will not occur frequently and can be neglected in long-term estimates of power production.

An important aspect not examined here is the impact on the predictability of the tides. A central advantage of tidal power as a renewable resource is its predictability. Atmospheric forcing will reduce how predictable the power is. This is relatively minor compared with the other advantages and disadvantages of a barrage and would generally only make a small change to the timing and magnitude of power production. However, for a structure as large as the Severn Barrage, its peak power output is around 6 GW, which is 7.2% of the UK power production [79]. Suddenly removing this from the supply, as would happen if it had to be closed due to potential flooding, would be significant and something that would need to be decided as far as possible in advance, making forecasting these interruptions crucial. It also means that the closure of the barrage would have more severe consequences than a structure like the Thames Barrier, which has the sole purpose of flood defense and not power generation.

Chapter 5

1D Model and Comparison with 2D Model

In Chapters 2 and 3, a two-dimensional model was used to analyse a barrage in the Severn Estuary. This model is computationally demanding and is usually run on a supercomputer. In the present chapter, this expensive two-dimensional model is compared to a more computationally efficient one-dimensional model, which only simulates the hydrodynamics in the Bristol Channel itself. The model is verified using several channel scenarios and the tidal barrage is added within the model. The objective is to understand the accuracy of the one-dimensional model relative to its two-dimensional counterpart and see whether further insight into the problem can be gained from the computationally faster model. It is obviously possible to do a wider parametric study with the one-dimensional model compared to the two-dimensional one.

Section 5.1 provides information and features of the model including the model domain, boundary conditions, resolution analysis and a sensitivity test of the model. Section 5.2 includes model verification against the analytical solution of the one-dimensional shallow water equations, and with the two-dimensional model considering different domain shapes. A simplified barrage is applied in the model, as introduced in Section 5.3. Section 5.4 presents the one-dimensional model simulation results. These include the effects of barrage location on the water level and the barrage interactions in terms of peak water levels and flooding protection functions provided by different barrage operation strategies, as well as comparisons between the one- and two-dimensional models. Section 5.5 concludes this chapter.

5.1 1D Hydrodynamic Model

The real three-dimensional hydrodynamics can be integrated across the depth and width of the channel to produce a one-dimensional model [48]. This model assumes uniform velocity at any cross-section across the channel, meaning that velocity is only varying along the length of the channel. This allows for computationally quicker simulations compared to two- or three-dimensional models. As stated by [48], one-dimensional models have been widely applied to represent the hydrodynamic processes of both free surfaces and velocity under time-varying conditions in un-stratified estuarine and coastal waters. The lack of significant flow stratification displayed in the Bristol Channel, due to the large tidal range and relatively small river discharge, justifies the use of the one-dimensional shallow water model in the tidal analysis [109]. [12] presents a comparison between zero-, one- and two-dimensional models of the Severn Estuary. The region has also been modelled analytically using a one-dimensional model by [139]. In this project, the one-dimensional model is created by time-marching the one-dimensional shallow water equations (Saint-Venant equations), as seen in Equation 1.17 in Section 1.3.1, using a fourth-order Runge-Kutta scheme to solve the equations.

The one-dimensional model can of course only model the flow in the estuary and not in the Celtic Sea or beyond, as in these regions the flow cannot be approximated as uniform across a spatial transect. The domain of the one-dimensional model can be represented by a small two-dimensional ADCIRC model (the Bristol Channel section of the DG-SWEM as described in Chapter 2), and it will be used for the one-dimensional verification. The main features of the one-dimensional model are obtained from its two-dimensional counterpart. As much as possible, parameters have been kept consistent between the one- and two-dimensional models. As can be seen in Figure 5.1, the model domain covers the Severn Estuary and the Bristol Channel, in which the western seaward boundary is set from Bosherton to Polzeath and the eastern riverine boundary is at the Severn Bridge. The domain is approximately 160 km long, narrowing down from the channel entrance, which has a width of around 112 km, towards the head of the estuary, which is the landward boundary with a width of approximately 1.4 km. For the small two-dimensional model, the mesh has $14,606$ unstructured triangular cells.

In the cross-sectionally-averaged model, the channel can be considered as a series of slices [16], which are created along the centreline of the channel. The direction of the slices are determined to be perpendicular to the centreline at each individual

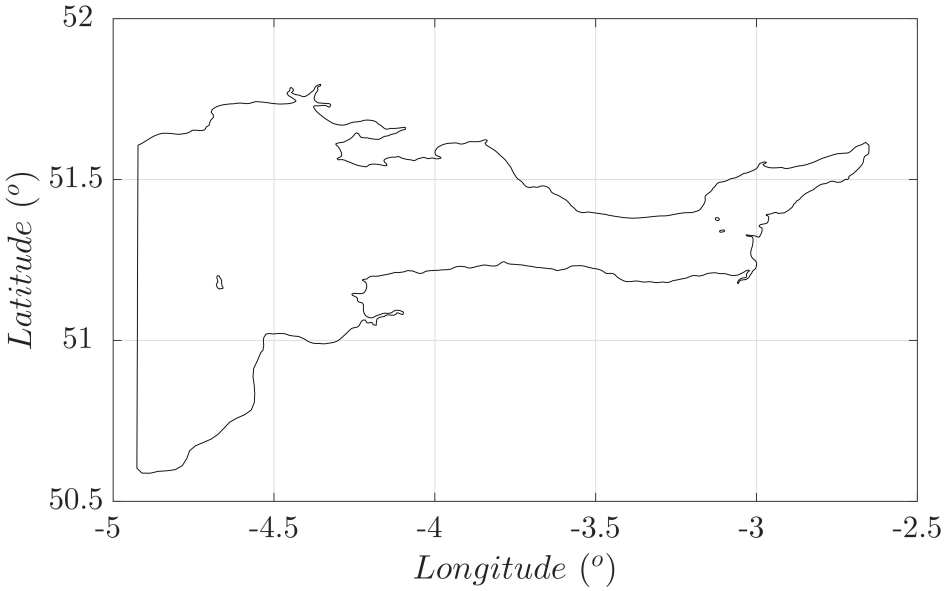

Figure 5.1: 1D model domain, represented by the small 2D ADCIRC model.

location, in order to better capture the features of the channel along its bathymetry. The detailed bathymetry data is extracted from the two-dimensional model, as seen in Figure 5.2. The one-dimensional model can be obtained by cross-sectional integration of the channel along the centre line of the model domain. The bathymetry data is then captured according to each cross-section: the width of the channel is determined by the cross-sectional lengths and the depth of the channel is determined in Section 5.1.3.

It should be noted that the large inter-tidal zone (the area that dries out at low tide) is not modelled. The cross-sections that are less than 20 m deep are modified to have a depth of 20 m to prevent them from drying out. This is the case at the head of the channel. The final modified bathymetric data of the Bristol Channel in the one-dimensional model can be seen in Figure 5.3 and the data is smoothed from the raw data to improve the condition of results.

5.1.1 Boundary Condition

In the two-dimensional hydrodynamic model as described in Chapter 2, the ocean boundary is driven by the predicted tides, which are produced by tidal harmonic analysis from a larger model (or measurements). Whilst for the simplified one-dimensional model, the open ocean boundary is forced with a single sinusoidal wave. This value is obtained from running the two-dimensional model at the one-dimensional boundary

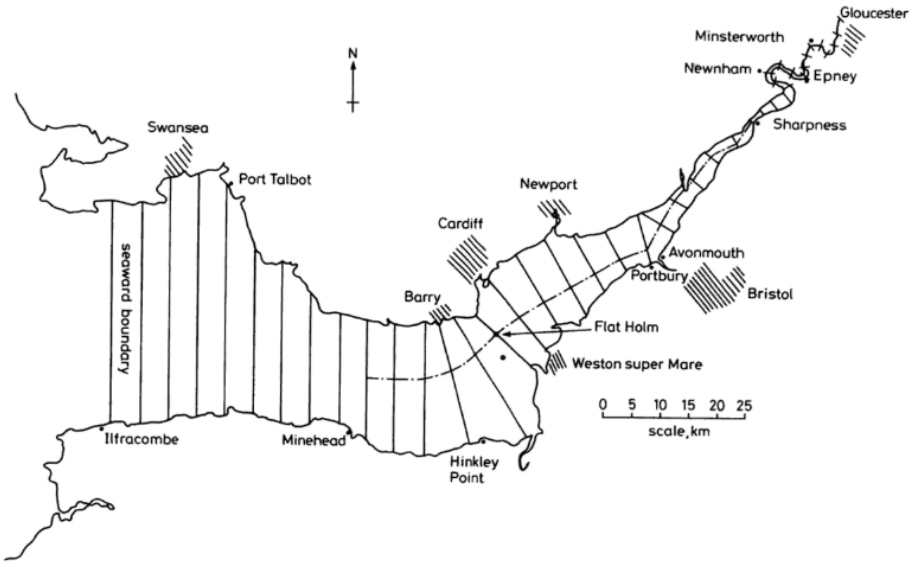

Figure 5.2: 1D model slice sections of the Bristol Channel, dash line indicate the estuary centreline taken from [16].

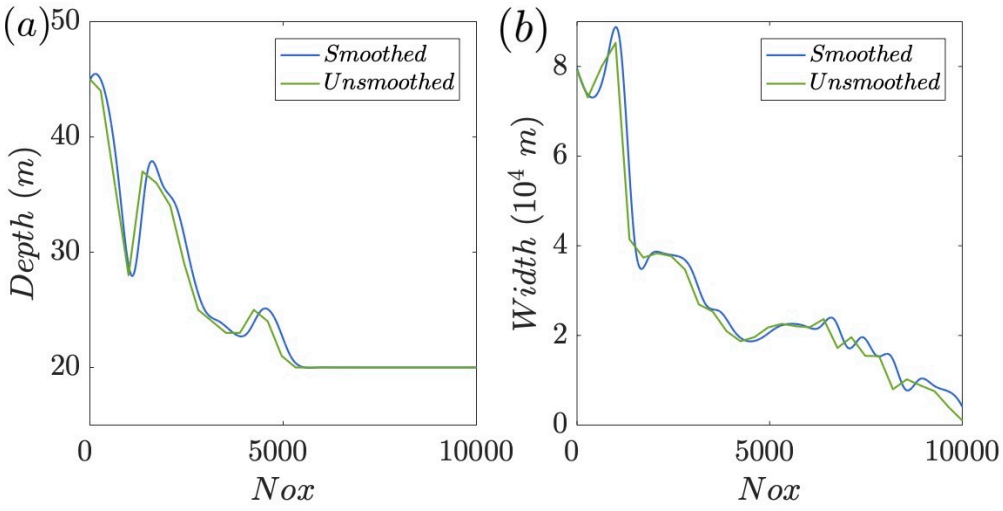

Figure 5.3: The bathymetry of the Bristol Channel applied in the 1D model, captured from the 2D ADCIRC (Nox is the number of nodes in the model): a) depth of the channel (left); b) width of the channel (right).

location, and is the averaged value over the results of the two-dimensional model simulations. Storm surge phenomenon will also be represented by the two-dimensional model simulation results, at the one-dimensional model boundary, where additional meteorological inputs are included.

5.1.2 Resolution Analysis

In numerical simulations, it is necessary that the model is grid independent. For an explicit scheme as used herein, the Courant-Friedrichs-Lewy condition (CFL) must be satisfied to ensure numerical stability. This dictates that the time step must be less than the time taken for the wave to travel between two adjacent space points [145]. The resolution check for the numerical model regarding the CFL condition can be represented by:

$$C = \frac{c\Delta t}{\Delta x} \leq C_{max}, \tag{5.1}$$

where C is the Courant number and C_{max} should be less than 1, and c is the wave celerity, which is the wave travelling speed in shallow water (equal to $\sqrt{gD}$) and can represent the speed for information to traverse a computational grid cell in a given time step. Under the CFL requirement, two cases with different node resolutions and computational time steps are then applied with this one-dimensional model: the first case with $10,000$ nodes and a time step of 0.5 s, and the second case with $5,000$ nodes and a time step of 1 s. The resolution analysis confirms that the above two cases provide almost the same result. In order to achieve better computational accuracy (since the computational time between the two cases would not differ by a great amount), the case with the time step of 0.5 s is then applied in the one-dimensional model for further simulations.

5.1.3 Sensitivity Test

Several sensitivity tests are performed to demonstrate the sensitivity of the model simulations. These involve varying the bottom friction coefficients (0.004 or 0.002), ramping time (one day or two days), and the channel depth estimation methods (taking mean, median or geometric mean of the whole depth values from each cross-section of the channel from the ADCIRC model, as can be seen in the Equations below). A ramping function is included at the beginning of the simulation period

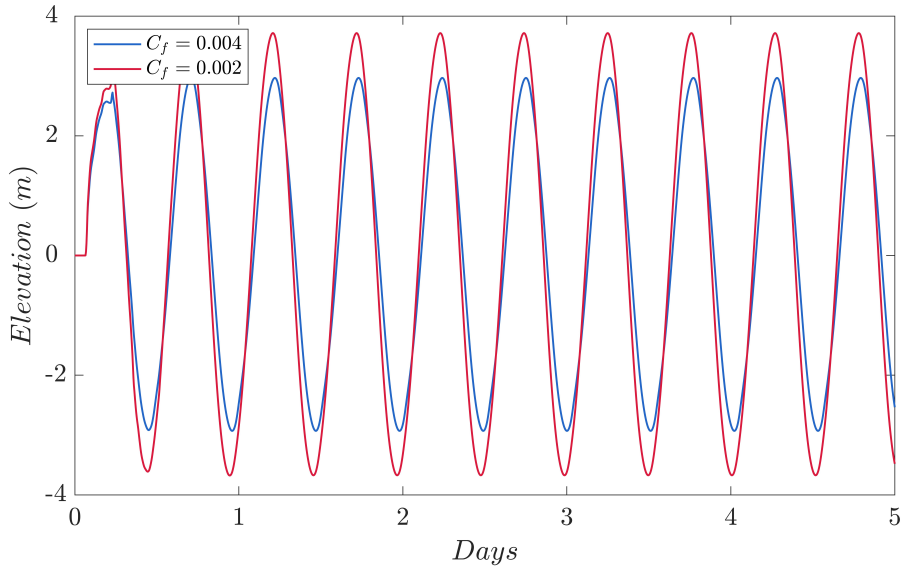

Figure 5.4: Sensitivity test results with varying bottom friction coefficients ($C_f = 0.004$ and $C_f = 0.002$) in the 1D model.

to avoid shocking in the model. The tests are run for a five-day simulation period without any storm surge phenomenon.

$$Mean = \frac{1}{N}\sum_{i=1}^{N} d_i, \tag{5.2}$$

$$Median = \left(\frac{(N+1)}{2}\right)^{th} d_i \ value, \tag{5.3}$$

$$Geometric\ Mean = \left(\prod_{i=1}^{N} d_i\right)^{\frac{1}{N}}, \tag{5.4}$$

where d is the channel depth value obtained for each cross-section of the channel and N represents the number of data points.

Model test results show clear changes in water elevation magnitude by varying the bed friction coefficient, which indicates its sensitivity to the bed friction. The same conclusion was drawn by the two-dimensional model as seen in Section 2.2.1. With a smaller bed friction coefficient, the water elevation in the middle region of the channel increases by approximately 23%, as seen in Figure 5.4. Even though the magnitude of the bed friction coefficient is mesh dependent, for simplification, the value of $C_f = 0.0025$ is applied, which was calibrated in the two-dimensional model.

The effects of varying ramping time and depth estimation methods on the water elevation are negligible, indicating that the model is not sensitive to these parameters.

A ramping time of two days is chosen and, following a parametric study, the median of all the depth values from each cross-section of the channel is used as the representative channel depth in the model for simplicity.

5.2 1D Model Verification

The parameters applied to the two-dimensional model are obtained from the highly calibrated two-dimensional DG-SWEM for the small simulation domain. Thus the one-dimensional model is not directly calibrated against field measurements but only against the two-dimensional model. Verification of the one-dimensional simulation is carried out by comparing the computed wave features with those calculated by analytical solutions and against the small two-dimensional model with different channel shapes. The simulations are run for five days with a two-day ramping period, and without any storm surge application in order to achieve the general flow of tides within the Bristol Channel regions.

5.2.1 Verified against Analytical Solution

The analytical solutions are derived from the one-dimensional shallow water equations as introduced in Section 1.3.1, with friction neglected. This solution is given in [48]. Simplifications are applied with the assumption of small values of elevations and velocity, as well as their products, and a single sine wave forcing the ocean boundary of the domain. The second-order terms of the shallow water equations are also ignored. The analytical solutions can be expressed as:

$$\begin{aligned} \xi &= \frac{a}{\cos(\frac{\omega l}{\sqrt{gD}})} \cos(\omega t) \cos\left(\frac{\omega(-x+l)}{\sqrt{gD}}\right), \\ U &= \frac{a}{\cos(\frac{\omega l}{\sqrt{gD}})} \sqrt{\frac{g}{D}} \sin(\omega t) \sin\left(\frac{\omega(-x+l)}{\sqrt{gD}}\right), \end{aligned} \tag{5.5}$$

where D is the total water depth, l is the length of the channel, a is the local tidal amplitude and ω is the local tidal frequency of the forcing tide at the ocean boundary ($x = 0$).

The analytical solution is compared with the one-dimensional model based on a rectangular channel with the same parameters, and the comparison results of the elevation at the middle of the channel are shown at the top of Figure 5.5(a). Small errors were observed with slight over-estimations in the numerical solution. It should be noted that some inaccuracy may be introduced due to the simplification necessary

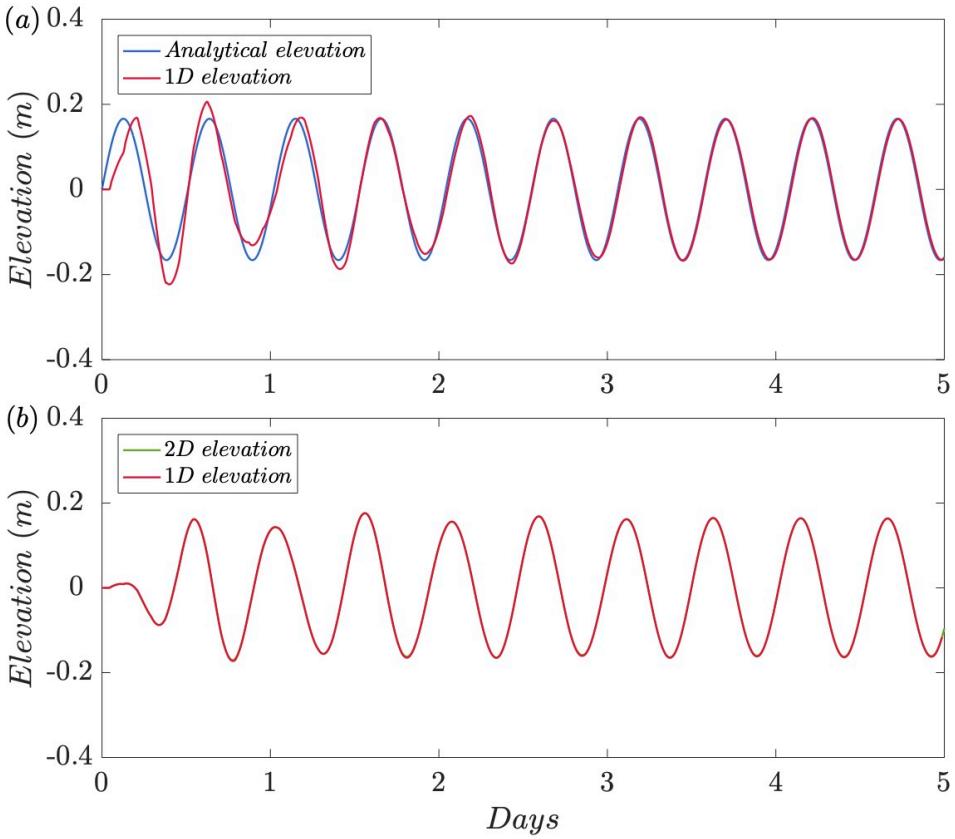

Figure 5.5: Comparisons between the 1D predictions and the analytical solution and 2D rectangular channel model predictions with the same scenario at the middle of the channel (at $Nox = 5,000$), respectively: a) with analytical solution (top); b) with 2D model (bottom).

to derive the analytical solution. The overall degree of agreement between the solution and one-dimensional simulation is very good, demonstrating that the equations are being solved accurately.

5.2.2 Verification of 1D Model against 2D Simulations

For more complex geometries, no analytical solutions exist. More general verification is made by considering different geometries and comparing the one-dimensional simulations against the results from the well-verified two-dimensional model. Three relevant cases are considered, varying from the most general assumptions to the more complex model. The process begins by applying a simple rectangular channel with straightforward geometry, and then a width- and depth- varying channel (a simplified wedge-shaped estuary to capture the funnelling effect [158]) is considered. The final case considered is with the real geometry of the Bristol Channel. The boundary

conditions of the one-dimensional model are taken from the two-dimensional model at the open boundary location.

5.2.2.1 Rectangular channel

A rectangular channel is considered with the total domain length of $1,000$ km, a constant water depth of 20m and channel width of 1 km. Tidal forcing at the ocean boundary of the domain uses the M_2 tide, the dominant harmonic tide in the Bristol Channel, allowing the current to vary freely at the ocean boundary. Figure 5.5(b) presents the comparison for the rectangular channel. Apart from some small finite amplitude effects, the two trend lines should be identical. Agreement is clearly excellent.

5.2.2.2 Shape-varying channel

For wider applications of the one-dimensional model, features of the channel with a varying depth or width are considered. To start with, only linear variation is considered in the channel shape. The width at the mouth of the channel is kept the same as the rectangular channel model (i.e. 1 km) and the depth remains unchanged at 20 m. Tidal parameters are kept the same. Figure 5.6(a) illustrates the comparison results between the one- and two-dimensional models. The one-dimensional model has excellent agreement with the two-dimensional one and is therefore shown to capture changing bathymetry effects.

5.2.2.3 Bristol Channel bathymetry

The one-dimensional model is then compared with a two-dimensional one considering a more complex geometry: that of the Bristol Channel. The small two-dimensional model with the domain seen in Figure 5.1 is applied for this verification. More discrepancies are expected between the simulation results of the one- and two-dimensional models than for the above cases as the integration across the channel is now a less accurate assumption.

The results from Figure 5.6(b) show that the one-dimensional model slightly underestimates the amplitude of the tide against its two-dimensional counterpart. This is presumably due to the failure to capture actual irregular cross-sections of the channel, and the physics resulting from these, in the one-dimensional model. There is an observable phase difference. This could be due to a difference in the speed at which the tidal wave travels in the two models. However, it should be noted that the tide in the channel is not a progressive wave but the sum of an in-going an out-going

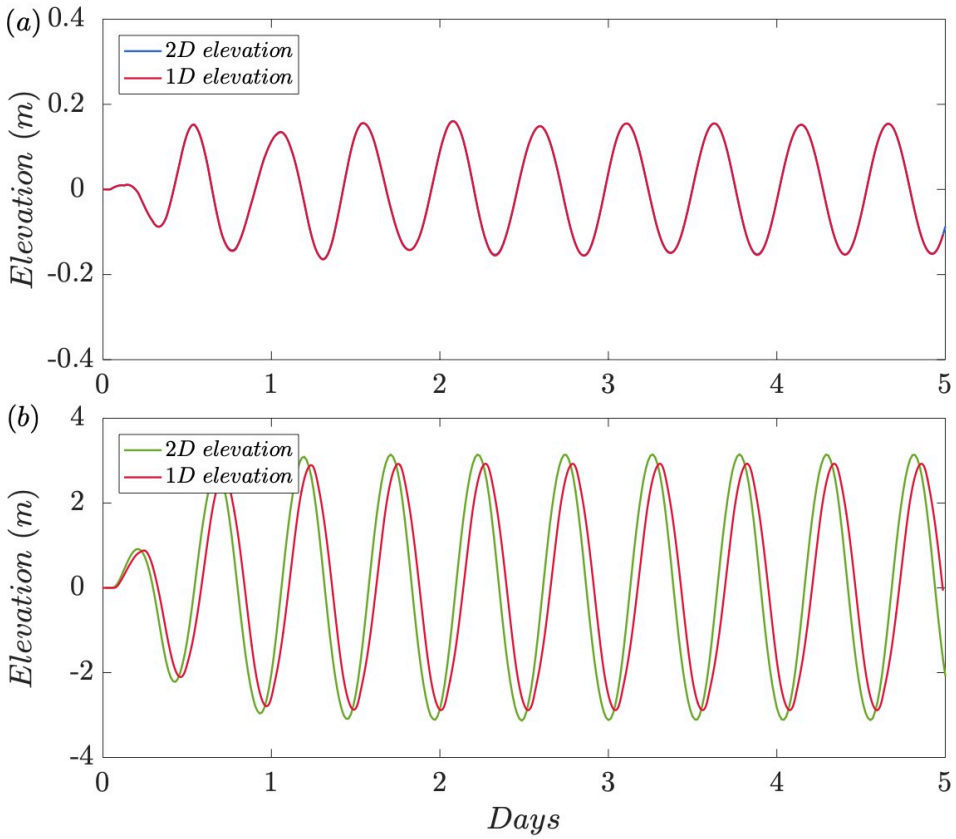

Figure 5.6: Comparisons between the 1D predictions and the 2D model predictions at the middle of the channel: a) shape-varying channel case (top); b) Bristol Channel case (bottom).

wave. Thus, the phase lag may also be due to the reflection being different in the two models.

The one-dimensional model has been verified by the analytical solution and the two-dimensional ADCIRC model based on several varying channel shapes with application of the M_2 tide at the ocean boundary. Comparisons with the two-dimensional model, particularly for the Bristol Channel case, demonstrate that this one-dimensional model achieves an acceptable agreement in terms of the tidal elevations. One thing to note is that this sectionally averaged model represents the key physical features and is a simplification of the two-dimensional or higher order simulations that model the flow conditions more accurately; therefore, perfect agreements are not expected. Further, since the two-dimensional model has been validated for the Bristol Channel in Chapter 2 (and also by [70]) this suggests that the one-dimensional model gives a good representation of the key hydrodynamics of this location and can be applied to study different barrage operation strategies.

5.3 Representation of the Barrage

The same basic approach is used to represent a barrage in the one-dimensional model as in the two-dimensional model (see Section 2.4). Two sub-domains are created which are linked by the $Q - H$ relationship, given by Equation 2.5. The locations as well as other details of the barrage are taken from the Severn Barrage proposal. In order to represent the turbine behaviour, a simplified approach relating the water head, discharge and maximum power generated using the Hill charts is adopted as proposed by Goldwag and Potts [78] for the Severn Barrage (see Figure 5.7). The $Q-H$ relations (for both sluice gates and turbines) can be incorporated into the one-dimensional model for the discharge calculation using the water head information from the previous time step.

5.4 Model Simulation Results

5.4.1 1D Model Barrage Locations

In the two-dimensional model it is impractical to do a wide parametric study of barrage location. This would require extensive re-meshing as well as computational costs. However, a simple investigation of barrage location is straightforward in the one-dimensional model.

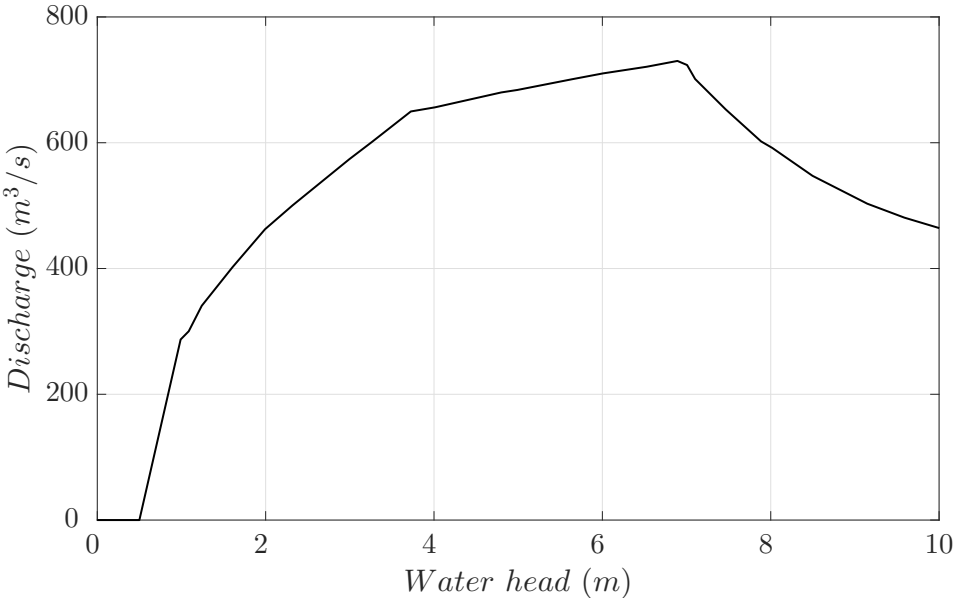

Figure 5.7: Relationship between water head, discharge and power for turbines for the Severn Barrage adapted from [78].

Several simplifying assumptions are made for this brief investigation. Only the M_2 tidal constituent is considered. The barrage is simplistically represented as an impermeable barrier. It is also noted that holding the water level at the ocean boundary constant is a questionable assumption. However, although not presented in this thesis, an alternative transmissive boundary condition is implemented, which allows waves to pass out of the domain. The conclusions drawn from this alternative boundary condition are similar to those drawn here.

The results of the elevation distributions of a barrage at various positions and the results, compared with those for the case of no barrage, are presented in Figure 5.8. The Figure shows that the model predicts that installation of a barrage would generally cause an increase in the tidal amplitude to the seaward side of the barrage. At the barrage position, a decrease in amplitude only occurs for the case that the barrage is constructed away from the head (barrage located with the shortest distance from the mouth) where the water elevation is decreased by 0.11 m. At the entrance of the channel, the water elevation can be affected by a barrage at the other end of the channel. For the case of barrage located the shortest distance from the boundary, the water elevation at the mouth would rise by a significant amount of 0.31 m. The Figure also demonstrates the features of tidal resonance in the Bristol Channel. If the effective length of the channel is shortened by the implementation of the barrage, then it would be expected that the overall resonant responses would be higher. This

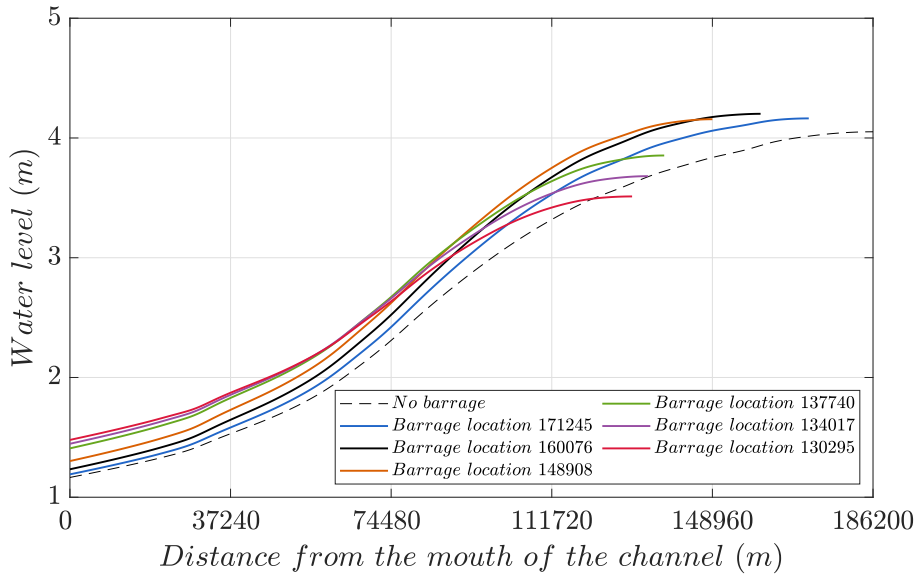

Figure 5.8: 1D model simulation results of the hydrodynamic impacts of the various applying barrage locations.

is explored in more detail in Chapter 7.

5.4.2 1D and 2D Model Comparisons with and without Barrage Implementation

In this section, comparison is made between the simulation results of the one- and two-dimensional models under the same scenario in order to understand the accuracy of the one-dimensional model's application. Two cases, with and without barrage implementation, are considered to examine the influence of the Severn Barrage to both the ocean-side and basin-side regions of the Bristol Channel. The hydrodynamic impacts of the barrage implementation have already been analysed using the two-dimensional model in Chapter 3. This section will concentrate on the barrage impacts on the maximum water levels during all simulations, which is clearly the variable of greatest interest in terms of coastal flooding during storm surge events in the channel. The synthetic storm surge event based on the year 2000, as applied in Chapter 3, is considered with the peak surge event happening on day 10. The one-dimensional model is forced at its boundary using the water level output of the two-dimensional model for the relevant simulation. No atmospheric forcing is applied to the one-dimensional model.

The baseline scenario of only tidal forcing without any meteorological inputs for both models are summarised in Table 5.1. Some underestimation can be observed

Table 5.1: Results of peak water levels in the ocean (51.36°N 3.67°W) and basin (51.48°N 2.90°W) region of the original case without any meteorological forcing.

Levels	2D Model		1D Model	
Parameter	Ocean	Basin	Ocean	Basin
Observation value (m)	5.09	6.94	4.63	5.74

in the one-dimensional results for both ocean and basin regions. The comparisons of the peak water levels by the one- and two-dimensional models for the case without barrage implementation during the storm surge event are shown in Figure 5.9. For the two-dimensional model results, Table 5.1 and Figure 5.9 show that the high water level for ocean region rises to approximately 5.76 m by 0.67 m from the no surge case and that the minimum water level also increases. For the basin-side regions, the basic tide levels are higher. As such, the water level increments due to the surge is larger by 1.09 m from no surge case and rises to 8.03 m. Higher flooding levels would be expected approaching the head of the channel. The same conclusion has been drawn in Section 3.2.

For the one-dimensional model, from the Table and Figure, it can be observed that the increment of high water level is 0.12 m (to 4.75 m) on the ocean side and by 0.18 m on the basin side during the storm surge event. By comparison, the one-dimensional model generally underestimates the predictions produced by the two-dimensional model and there are some changes in phase, which are as expected (similar issues are seen in the one-dimensional model verification in Section 5.2). However, greater discrepancy regarding the extreme water level can be observed here. This may be explained as the variations of the wind and pressure conditions captured during the storm surge events are localised features that can be demonstrated by the two-dimensional model. While, for the one-dimensional simulations, only introducing surge characteristics on the boundary cannot accurately represent the surge condition over the whole domain. Therefore, the one-dimensional model cannot accurately capture the flooding conditions during a storm surge event. However, this does not mean that no useful analysis can come from this. The one-dimensional model does predict an increase in water level and some insight can be obtained regarding how this phenomenon interacts with a barrage.

The presence of a barrage is examined to see how it modifies the synthetic storm surge event. Figure 5.10 presents the comparison results between the one- and two-dimensional models during the surge event with barrage implementation looking at both ocean and basin sides. As described in Chapter 3, the barrage is normally

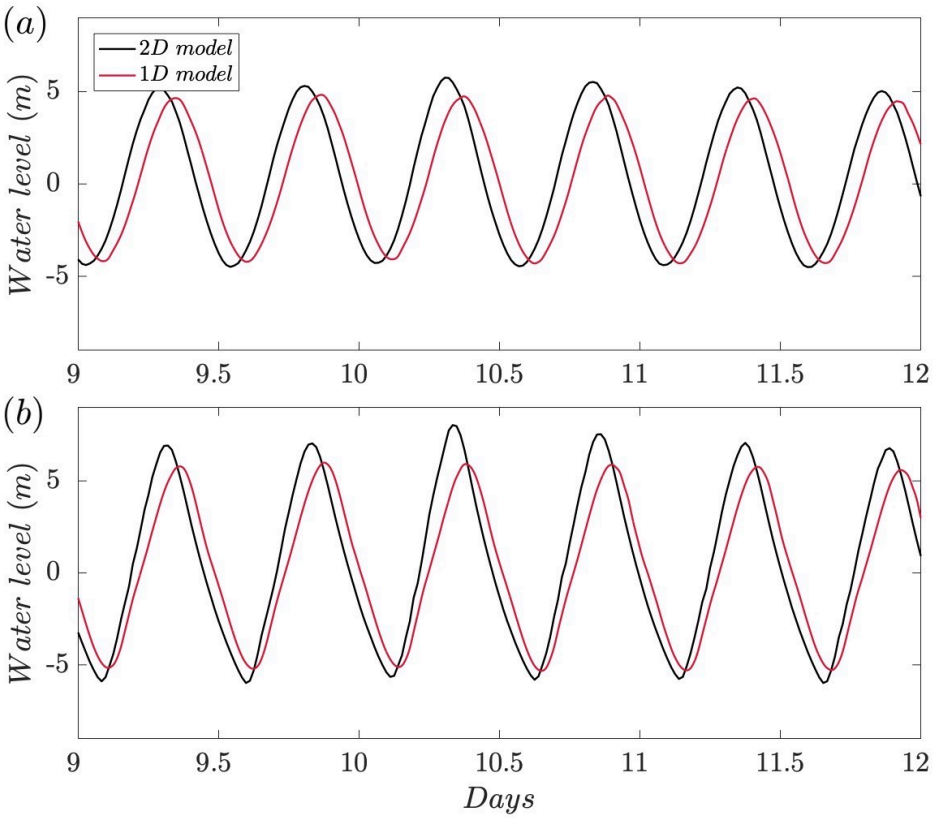

Figure 5.9: Simulation results of comparisons between the 1D and 2D model predictions of no barrage implemented case during the storm surge event: a) on the ocean side 51.36°N 3.67°W (top); b) on the basin side (51.48°N 2.90°W) (bottom).

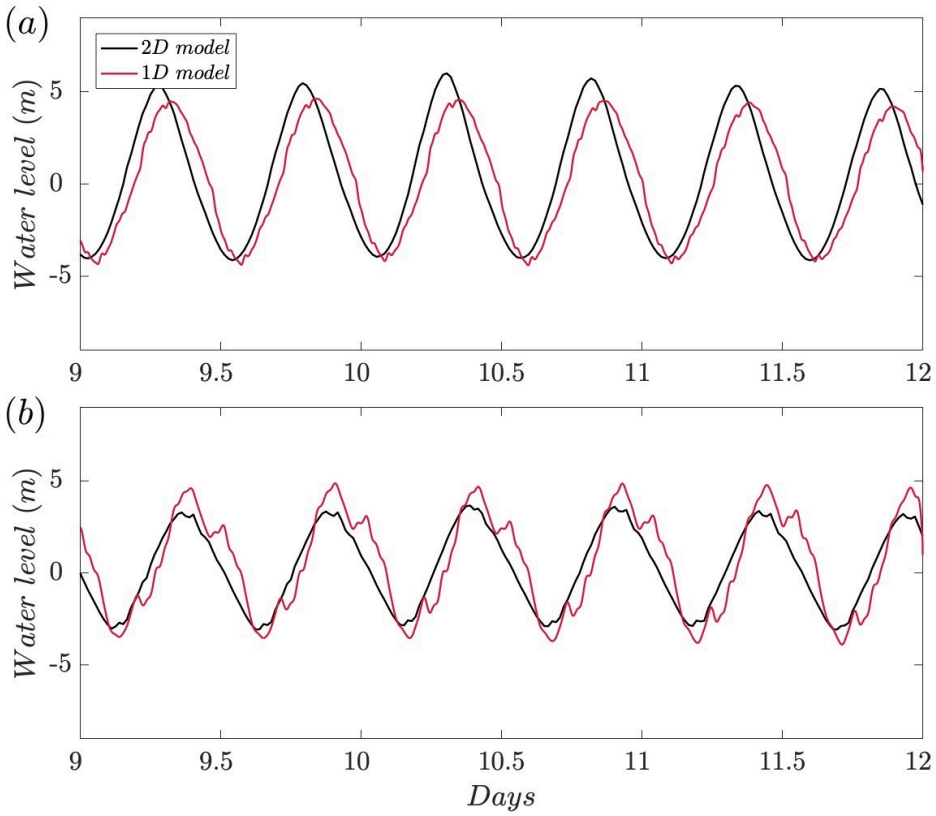

Figure 5.10: Simulation results of comparisons between the 1D and 2D model predictions of normal barrage operation case: a) on the ocean side 51.36°N 3.67°W (top); b) on the basin side (51.48°N 2.90°W) (bottom).

operated with a starting head of 1.5 m and a finishing head of 0.7 m. According to the analysis for the barrage impact with the two-dimensional model, there are limited amounts of water level increase for the regions on the ocean side and large reduction in peak water level in the basin region due to the presence of the barrage. The flooding protection provided by the barrage can be up to 4.37 m, around 54% reduction at the surge peak during the storm surge event within the basin. There is also some phase lag for the peak total water level on the basin side during the surge event, of approximately 1.44 hours, which can be a benefit. For the one-dimensional model results, compared with the no barrage case, again implementation of a barrage would lead to flooding protection in the basin region of 0.96 m, around 16% reduction at the surge peak. The phase lag shows a delay in the event about 1 hour for the one-dimensional case. However for the ocean side, it is observed that an opposite result, with some decrease in water level by a barrage addition, is obtained even though the difference is relatively small.

From the one- and two-dimensional model comparisons, it can be seen from the Figure that on the ocean side, there is again some phase lag and underestimated predictions for one-dimensional results. At the head of the channel, however, the water levels predicted by the one-dimensional model are higher. The flat feature in the one-dimensional results shown in the Figure indicates the holding phase of the barrage operation. The overestimation at the peak of the surge result is approximately 1.03 m, contributed to by two competing effects: the reduction in the amount of surge computed by the one-dimensional model and some increase in water level, which may be explained by inaccurate representation of the barrage in the one-dimensional simulation. The results indicate that there is more flow into the basin passing the barrage and correspondingly, higher water levels would be predicted in the basin region.

5.4.3 1D and 2D Model Simulations with Different Barrage Operation Cases

In this section the performance of the one-dimensional model for different barrage operations during a storm surge is conducted. This is to verify whether the conclusion drawn by the two-dimensional simulation, that different barrage operations can alter its performance for flooding protection, still stands utilising the one-dimensional model. The same set of scenarios as applied in the two-dimensional model in Section 3.2 are presented in Table 5.2 to see how these influence the storm surge. The first scenarios considered are normal barrage operation (case 'A') as investigated above,

Table 5.2: Barrage operational strategies during the storm surge event.

Case	Normal operation (days)	Closure period (days)	Opening period (days)	Details
C	0-8.1	8.1-10.2	10.2-14	Fully-area opening of turbine and sluice gates
D	0-8.1	8.1-10.2	10.2-14	Half-area opening of turbine and sluice gates

Table 5.3: Two-dimensional modelling results of the original no barrage and with barrage strategies results for water level in the ocean (51.36°N 3.67°W) and basin (51.48°N 2.90°W) region.

Model	2D Model								
Case	No Barrage		Case A		Case B	Case C		Case D	
Parameter	Ocean	Basin	Ocean	Basin	Ocean	Ocean	Basin	Ocean	Basin
Observation value (m)	5.76	8.03	5.99	3.66	6.28	5.86	3.30	6.05	1.08
Peak timing (hrs)	10.31	10.33	10.31	10.39	10.29	10.29	10.39	10.29	10.42

or a completely closed barrage (case 'B'). Further two operation strategies (cases 'C' and 'D') are considered with barrage closure at low tide level prior to the event and re-opened with different opening areas during the surge.

The different peak water level values for the two- and one-dimensional simulations considering barrage operation strategies as stated above are summarised in Tables 5.3 and 5.4, respectively. The basin side results for case 'B', barrage complete closure during the whole simulation period, are not included for analysis since no extra water will flow into the basin and the region is well protected. For the results of the two-dimensional model, it can be concluded from Table 5.3 that for all scenarios, there are limited water level increments (within 0.52 m) compared with the undisturbed no barrage case on the ocean side of the barrage. The most favourable strategy is case 'C' with the smallest water increase. For the basin, there is significant water level drops for all cases and the amount is dependent on the operational strategy applied. Operation following case 'D' gives the largest water level drop and the optimum delay of the timing of the peak.

The one-dimensional model gives similar predictions for the selection of the applicable barrage operation during the surge event. As can be seen from Table 5.4, completely isolating the water inside the barrage (case 'B') gives the highest water level rise on the ocean side. Cases 'C' and 'D' are sensitive to the strategies' re-opening times in the one-dimensional simulations. Both cases give a water level rise of 0.25 m compared with the no barrage case for the ocean side and considering the

Table 5.4: One-dimensional modelling results of the original no barrage and with barrage strategies results for water level in the ocean (51.36°N 3.67°W) and basin (51.48°N 2.90°W) region.

Model	1D Model								
Case	No Barrage		Case A		Case B	Case C		Case D	
Parameter	Ocean	Basin	Ocean	Basin	Ocean	Ocean	Basin	Ocean	Basin
Observation value (m)	4.75	5.92	4.54	4.69	5.44	5.00	3.43	5.00	1.35
Peak timing (hrs)	10.37	10.38	10.35	10.42	10.34	10.31	10.41	10.31	10.45

basin regions, operating the barrage following case 'D' can provide the greatest flooding protection. Regarding the timing of the peak within the basin, again, case 'D' gives the best result of over an hour in postponing the event. For model results comparison, the one-dimensional model underestimates water levels on the ocean sides and over-predicts on the basin side.

5.5 Conclusion

This chapter introduced the implementation of a one-dimensional hydrodynamic model for the Bristol Channel region. The model was verified with an analytical solution, and with the two-dimensional model considering varying domain shapes. Comparison results show that overall good agreements were achieved by this model and demonstrated its accuracy and efficiency for the tides simulations in the Bristol Channel. The model was then applied to simulate the Bristol Channel with deployment of the Severn Barrage. The results were compared with the results of the two-dimensional model as applied in Chapter 3. These are expected to capture more real physics and were taken as a baseline for comparison for this chapter.

The one-dimensional results showed qualitatively similar behaviour to the two-dimensional model. The exact propagation of a surge event up the channel is different for the two simulations. However, if it is just a case of determining the general behaviour of a barrage in the presence of a surge, and testing the response of the barrage, this is perhaps not a major issue. There will still be an increase in water level and a volume of water which needs to be moved. Given this, similar behaviour was found between the two models in terms of how a barrage influences water levels on either side of the barrage. There was also qualitative agreement in how this changes depending on the control strategy selected for the barrage. Thus, a one-dimensional model might be used to make a preliminary investigation of barrage behaviour (as

indeed it was for this thesis). However, detailed results require greater accuracy and the one-dimensional model is too simplistic for a thorough engineering analysis.

Chapter 6

Reconstruction of the Bristol Channel Floods in 1607 and the Impact of a Barrage

The worst coastal flooding events on record in UK history happened at approximately 09:00 in the morning on 30 January 1607 [91]. As introduced in Section 1.2.3.1, the flood water caused extensive damage to the Bristol regions and many surrounding lowlands on the Somerset Levels. In this chapter, an attempt is made to reconstruct the meteorological and tidal conditions according to the historical writings and reproduce the storm surge event in 1607 with the well-validated two-dimensional storm surge model in Chapter 2. Also considered is the application of the barrage that is operated with the strategy suggested in Chapter 3.

There has been some speculation that this flooding event was due to a tsunami [33]. It seems implausible given this would surely have impacted a much larger region and there is no obvious fault at which it could have been generated. Somewhat harder to discount is the recent suggestion that the flooding could have been due to a meteo-tsunami [170]. Meteo-tsunamis are caused by fast moving low pressure systems that travel at close to the shallow-water wave speed, causing a resonance that leads to a large wave. However, there appears to be no supporting evidence for this, or other instances of meteo-tsunamis in the region. In this chapter it is assumed that the flooding was the result of a conventional storm surge.

Section 6.1 describes the methodology of reconstruction of the 1607 event including the date conversion and the recorded tides and weather conditions. The simulated tides during January 1607 are validated with the tides prediction in [91] by astronomical forces. According to the event weather condition, the surge from a similar storm event in 2002 is introduced to reproduce the 1607 event. Sections 6.2 and 6.3 present

the flood simulation results during the event at several sites and the results with barrage implemented. Section 6.4 concludes this chapter.

6.1 Reconstruction of the 1607 Storm Surge Event

6.1.1 New Style and Old Style Dates

According to [91], by the 17th century, the Julian Calendar was acknowledged as 10 days out of step along with the passage of the seasons. To replace this incorrect calendar, the Gregorian Calendar was introduced in 1582. Until 1752, due to an Act of Parliament, England started to utilise this calendar and 1 January was determined to be the official start of the year. Previously, utilising the 'old style' calendar in England, the year began on 25 March and this extreme storm surge event would have been recorded as 20 January 1606. In this study, the 'new style' calendar is applied and the date of 30 January 1607 is used to represent the event.

6.1.2 Tide and Weather on 30 January 1607

The flooding in January 1607 is well documented and detailed sources can be checked in [91]. Figure 6.1 shows the affected regions and villages during the event.

6.1.2.1 Tide validation for January 1607

For the January 1607 event, tidal prediction in the Bristol Channel is possible as tides are driven by astronomical movements and therefore can be predicted backwards in time. This does assume that other factors remain as they are at present. In particular bathymetry could have changed significantly over the period in question. The tidal elevation at Avonmouth for the period is estimated by [91], as the dashed line shown in Figure 6.2. The greatest tidal amplitude (i.e. in the absence of meteorological forcing) occurred at 09:00 on the 30 January 1607, recorded as 7.86 m, and the event happened with a spring tide, which coincides with the written record [152]. As introduced in Chapter 2, in this study, the validated two-dimensional DG-SWEM is used to calculate the tidal hydrodynamics and storm surge phenomenon in the Bristol Channel. The simulation begins on 20 January 1607 with a 14-day run time without any meteorological input to model only the astronomic tide. Different numbers of tidal constituents are introduced. As introduced in Section 2.1.3, the results are accurate to within 95% significance level when M_2, S_2 and N_2 are included during

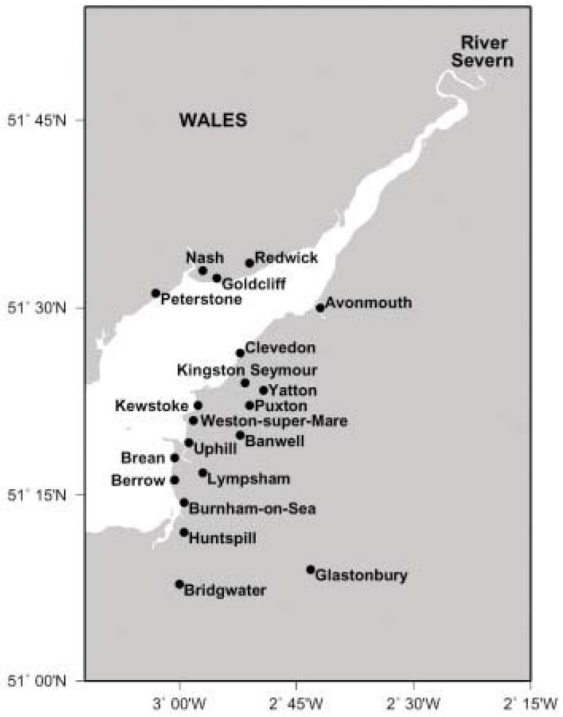

Figure 6.1: Locations affected by the 30 January 1607 flooding taken from [91].

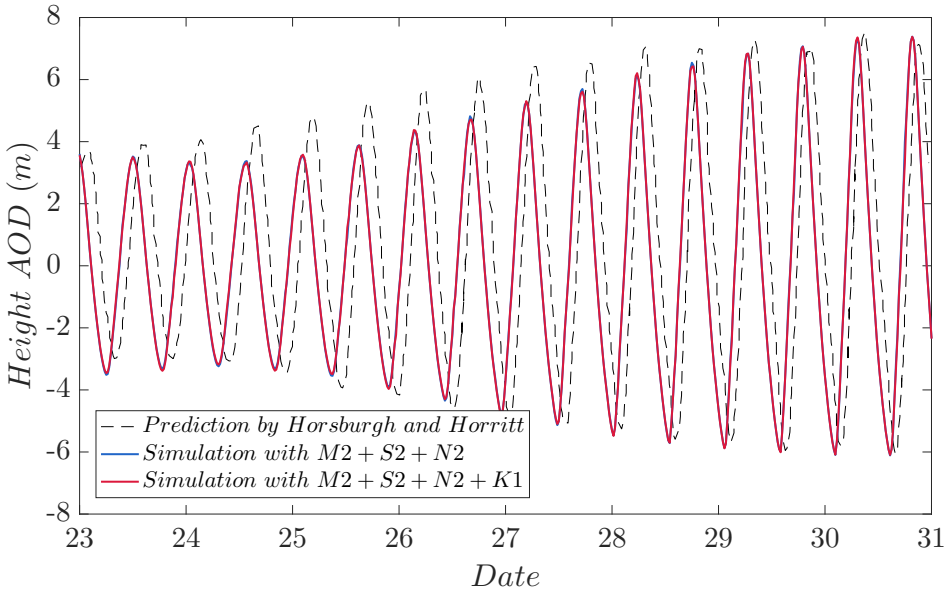

Figure 6.2: Validation with the tidal curve for Avonmouth for 23-31 January 1607 adapted from [91].

the simulation. A further fourth major K_1 constituent is considered to improve the simulation accuracy for the event.

Tide validation results are presented in Figure 6.2 with comparisons between tide

prediction and simulation results for the 1607 event period. There are no significant differences between the two simulation cases, which gives confidence that adding more constituents will not significantly improve the accuracy of the model. For the case with four constituents (M_2, S_2, N_2 and K_1) applied, a phase shift exists of about 2 hours and the tides are underestimated compared with Horsburgh and Horritt's prediction. This shift is not due to model inaccuracy since the phase predicted by the model is generally excellent (see for instance Table 2.11 and below). However, at the surge peak around 30 January, the model provides better simulation results with only 0.15 m, or 2%, of discrepancy in the maximum water level, which is deemed satisfactory.

For tidal harmonic analysis during this event, the simulations are run with a 45-day period with additional tidal constituents applied. Table 6.1 presents the harmonic analysis results for M_2 tidal elevation amplitudes and phases simulated with different numbers of major tidal constituents during the 1607 event and the observations from Admiralty Tide Tables data [81]. There is limited variance for different number of major tidal constituents applied (dependency with observations can be checked in Section 2.3.1), which provides evidence that no more constituents are required to improve the model accuracy.

6.1.2.2 Meteorological inputs from October 2002

The weather preceding and during the surge event would be the key evidence to reproduce the event. This was obviously not measured scientifically. One of the reliable sources is Stow and Howes [152], who stated there was a westerly wind over the region for 16 hours during the event. Camden [35] recorded that a strong wind was blowing from the south-west for 3 days without intermission. A storm from 03:00 until noon was noted by the Barnstaple Parish Register [91]. Considering all the material, the most probable weather condition was a storm with westerly or south-westerly winds over the Bristol Channel region, which was required to generate a severe storm surge event in the Bristol Channel.

In this study, a realistic storm surge event is superimposed on the tide of 30 January 1607 in the Bristol Channel. As suggested by Horsburgh and Horritt [91], the surge is introduced on 27 October 2002, which has a similar weather condition as in 1607. Detailed wind and pressure conditions during the 2002 event can be checked in Figure 6.3. As can be seen from the Figure, at the surge peak period, there was a south-westerly wind with a maximum magnitude of around 22 m/s at the head of the channel region, and atmospheric pressure was around 98 kPa with the low pressure

Table 6.1: M_2 tidal elevation amplitudes and phases at different stations simulating with different numbers of major tidal constituents (see T-Tide analysis in Bristol Channel in Figure 2.6) during 1607 storm surge event.

Station	M_2 Amplitude (m)			
	Location	Obs.	M_2+S_2+N_2	M_2+S_2+N_2+K_1
Pwllheli	4.35W 52.90N	1.48	1.51	1.51
Fishguard	4.99W 52.02N	1.35	1.42	1.42
Stackpole Quay	4.85W 51.63N	2.51	2.52	2.52
Mumbles	4.00W 51.57N	3.18	3.04	3.04
Barry	3.28W 51.40N	3.82	3.84	3.84
Flat Holm	3.12W 51.37N	3.90	3.95	3.95
Station	M_2 Phase (°)			
	Location	Obs.	M_2+S_2+N_2	M_2+S_2+N_2+K_1
Pwllheli	4.35W 52.90N	239	239	239
Fishguard	4.99W 52.02N	207	208	208
Stackpole Quay	4.85W 51.63N	168	174	174
Mumbles	4.00W 51.57N	171	176	176
Barry	3.28W 51.40N	185	184	184
Flat Holm	3.12W 51.37N	190	188	188

approaching to the channel head. These weather conditions are the key characteristics of a storm surge, which are similar to the event in 1607.

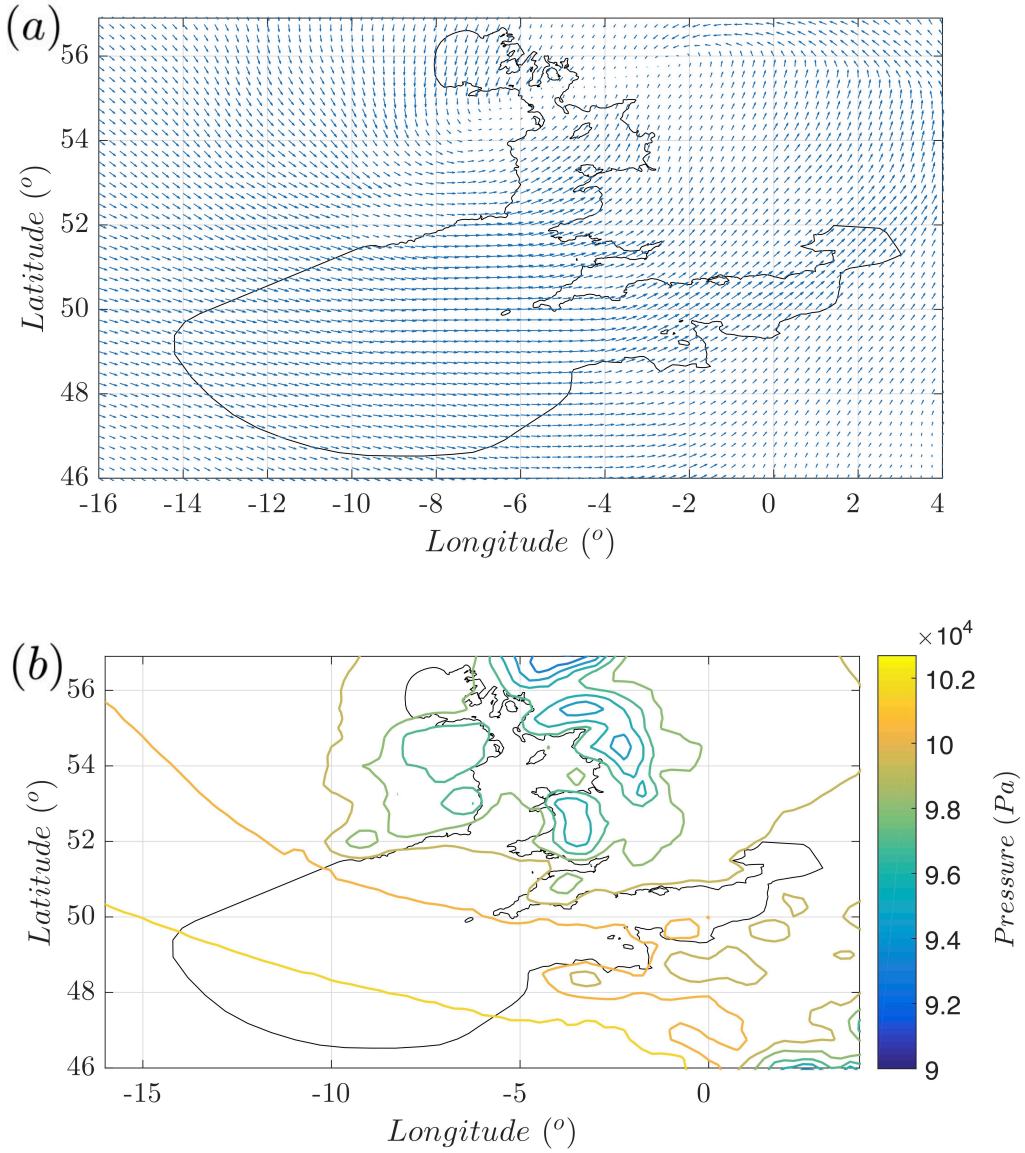

Figure 6.3: Meteorological input for the whole domain for 27 October 2002: a) wind velocity vector, speed obtained with U- and V- velocity components of the dataset (top); b) atmospheric pressure contour (bottom).

According to field measurements, the imposed surge residual in 2002 had a maximum level of 2.3 m. With application of corresponding meteorological condition from the ERA5 dataset, the maximum height of the simulated surge is 1.9 m (see Figure 6.4). This is added to the tide (with the discrepancy attributed to the inaccuracy

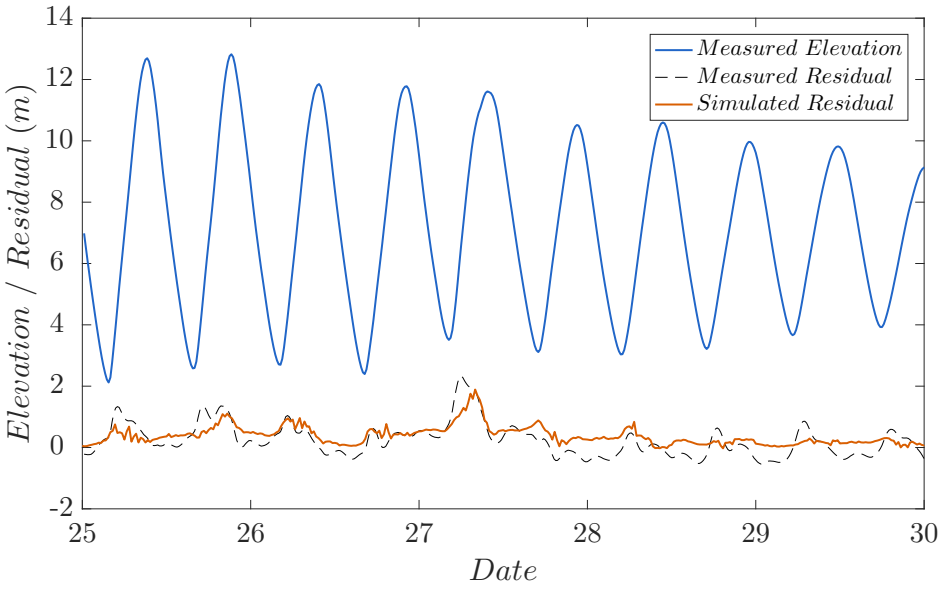

Figure 6.4: Measurement results from the BODC and simulated result for 25-30 October 2002.

of the ERA5 dataset, as discussed in Section 2.5.2). The worst case is assumed here with the peak of the surge residual coinciding with the high tide.

6.2 Simulation of the 1607 Storm Surge

Apart from Avonmouth, measurements at Goldcliff, near the Welsh Levels, and Kingston Seymour are also considered in this study. According to the historical event document, the height of the water elevation at Goldcliff was 7.14 m [25] and the water level at Kingston Seymour was reported as 7.74 m [174]. Detailed locations of the measurement sites are shown in Figure 6.5. All of these stations are located on the basin side of the hypothetical (Severn) barrage and Kingston Seymour is a measurement station that is near the Somerset Levels, characterised with low-lying lands. The ocean side (51.38°N 3.76°W) measurement is also calculated.

The simulation results of the 1607 storm surge event at different measurement sites are presented in Figure 6.6. The water elevation is 8.83 m at Avonmouth and 8.17 m at Goldcliff (compared with 7.14 m surveyed) whereas at Kingston Seymour the simulated elevation is 8.19 m (compared with 7.74 m surveyed). For those stations that are located at the head of the channel, along with the nature of low-lying land around Somerset Levels, the event provides sufficient water level to flood the surrounding towns and villages. For the ocean side of the hypothetical barrage, as

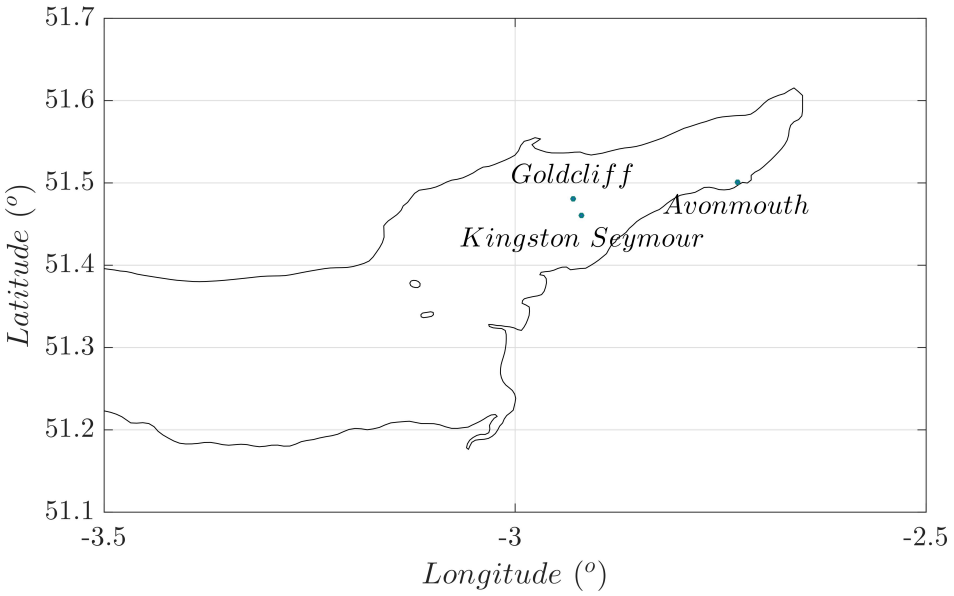

Figure 6.5: Measurement stations for 1607 storm surge event.

the maximum water height is 5.96 m with a residual height of 0.87 m, no severe flooding occurs.

There are 40 years of recorded water level measurements from the year 1961 to 2012 in the measured dataset. At the Avonmouth station, ignoring any measurement error, the maximum water level recorded was in 26 February 1990 with the height of 8.50 m. The maximum height at Avonmouth is 8.83 m in this simulation for the 1607 event, which is slightly more extreme than that in the 40-year record.

It appears that significant flooding could have resulted even from a less severe meteorological event than the one considered here. This could either be less severe in terms of winds and pressures or in terms of timing. What is clear is that it is plausible severe flooding, such as that recorded in 1607, could occur from a storm surge event consistent with the historical record.

6.3 Protection of the 1607 Flood for a Barrage Implementation

Two barrage cases are considered: normal barrage operation under the starting head of 1.5 m and finishing head of 0.7 m, and the selected barrage control operation strategy that had the best performance tested in Chapter 3, which had the barrage held at the lowest water level from the previous tidal cycle and partially re-opened

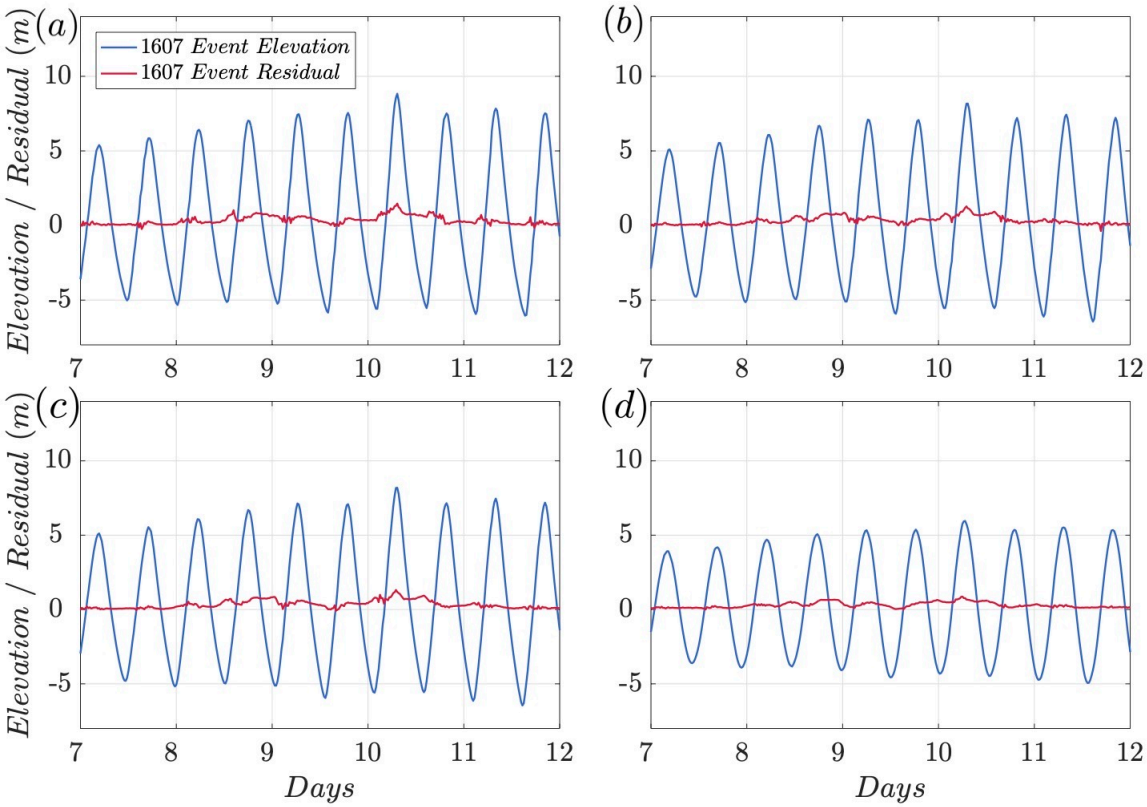

Figure 6.6: Reconstruction of the 1607 storm surge event at different measurement stations: a) water elevation and residual results at Avonmouth (top-left); b) water elevation and residual results at Goldcliff (top-right); c) water elevation and residual results at Kingston Seymour (bottom-left); d) water elevation and residual results at ocean side (bottom-right).

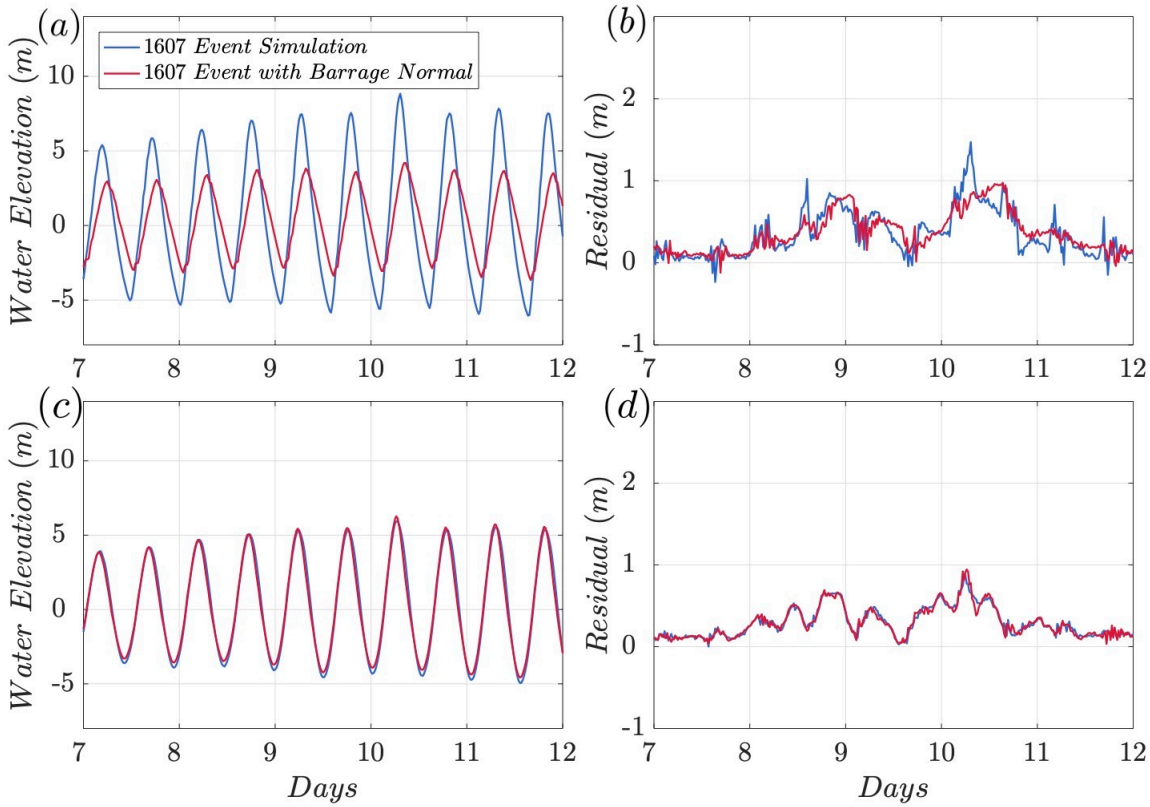

Figure 6.7: Reconstruction of the 1607 storm surge event with application of barrage normally operated during the event: a) water elevation results at Avonmouth (top-left); b) residual results at Avonmouth (top-right); c) water elevation results at ocean side (bottom-left); d) residual results at ocean side (bottom-right).

during the surge event. Detailed operation status can be seen in Table 3.4. Simulation results for the two cases compared with the no barrage case for the 1607 event at Avonmouth and ocean site can be seen in Figures 6.7 and 6.8, respectively. For the results with normal barrage operation, significant water level reduction can be observed at Avonmouth preceding and during the storm surge event. Residual level during the event is lower compared with the no barrage case and the timing of the peak has been delayed. On the ocean side, there are negative effects with limited water and residual level increments. Considering the protection function provided by the wisely controlled barrage operation, even more level reduction can be observed here for both water and residual levels within the basin and there are limited negative level rises in the ocean. Detailed statistics analysis including other measurement stations is presented in Table 6.2.

With respect to the water elevation, the level reduction observed by normally operating the barrage at Avonmouth, Goldcliff and Kingston Seymour can be 4.64 m,

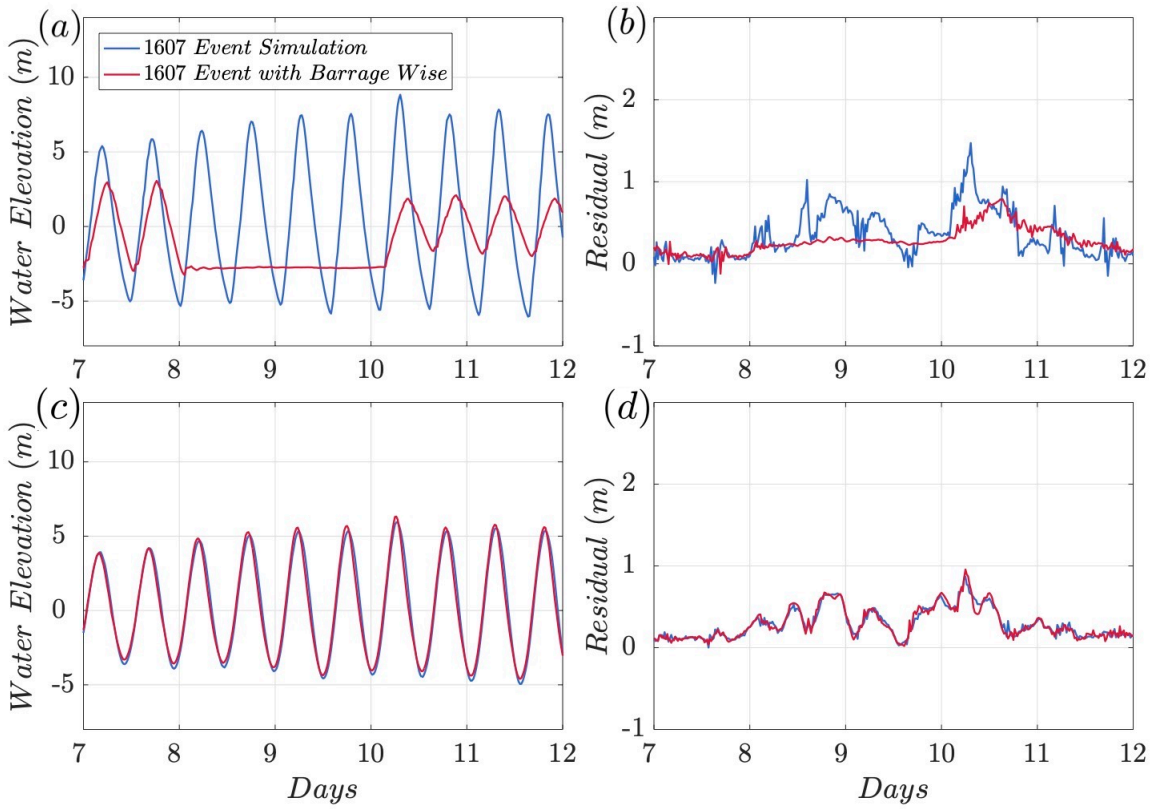

Figure 6.8: Reconstruction of the 1607 storm surge event with application of barrage wisely operated during the event: a) water elevation results at Avonmouth (top-left); b) residual results at Avonmouth (top-right); c) water elevation results at ocean side (bottom-left); d) residual results at ocean side (bottom-right).

Table 6.2: Comparison of results of different strategies for water elevation and residual at different sites for 1607 storm surge events.

	Elevation (m)			
	Avonmouth	Goldcliff	Kingston Seymour	Ocean side
1607 Event	8.83	8.17	8.19	5.96
Barrage Normally Operated	4.19	3.81	3.83	6.27
Barrage Wisely Operated	1.87	1.55	1.55	6.32
	Residual (m)			
	Avonmouth	Goldcliff	Kingston Seymour	Ocean side
1607 Event	1.47	1.28	1.32	0.87
Barrage Normally Operated	0.98	0.93	0.92	0.94
Barrage Wisely Operated	0.79	0.68	0.68	0.96

4.36 m and 4.36 m, respectively. The protection is particularly significant for Kingston Seymour. If the closed/partial reopening barrage strategy is considered, more water reduction would be expected with 6.96 m, 6.62 m and 6.64 m for Avonmouth, Goldcliff and Kingston Seymour, and greater flood protection at Kingston Seymour is observed. The negative aspect is that there is a limited water level rise of up to 6% on the ocean side. Considering surge residuals, the level reduction can be 48% at Kingston Seymour while there is a level increment of 12% in the ocean region. For both water and residual levels, compared with the significant benefits that can be provided in the regions susceptible to flooding, the barrage with the operational strategy is acceptable as a measure of flooding prevention for the extreme 1607 event.

6.4 Conclusion

In this chapter a scenario based on the 1607 flood was considered. The first part of the chapter detailed the recreation of this event. The tidal component of the water level is known although there is a 2 hours phase difference between the simulations presented here and the record from [91]. To these astronomic tides, the meteorological data corresponding to the most severe storm in the last 40 years is applied. This gives a high water level which appears to be consistent with the historical record, but one which is inconsistent with measured water levels (slight overestimation), suggesting that the historical flooding could be due to a combination of large-scale meteorology and high tides.

The second part of the chapter looks at how a tidal barrage would have altered the water level. The results are consistent with Chapter 3. A barrage would provide considerable protection from the storm surge to the east of the barrage with slightly higher water levels recorded to the west. Operating the barrage in different ways can make a small but significant difference to the water levels.

Chapter 7

Impact of Severn Barrage on Tidal Resonance

The Bristol Channel/Severn Estuary has one of the largest tidal ranges in the UK with a mean spring tidal range of 12.2 m, and numerous proposals have been made to exploit this for energy extraction as introduced in Chapter 1. The 'hyper-tidal' system is caused partly by the funnel-like shape of the estuary and partly by the resonance of the semi-diurnal tidal constituents [67]. The construction of a barrage would modify the tide and, in particular, change the resonant length or the damping of the tidal channel [120]. Systems which are at resonance can be sensitive to small changes (see [15, 14] for discussion of this in the context of tidal systems). In this chapter, the resonant response of the Bristol Channel system is examined, with and without a barrage structure deployed, using the validated two-dimensional DG-SWEM (see Chapter 2). The impact of a barrage on the resonance of the system can therefore be evaluated, which in turn leads to an understanding of the environmental impact of building a barrage and how a barrage might be designed to affect a particular change. The Swansea Lagoon scheme is also briefly considered.

Section 7.1 introduces the tidal resonance phenomenon in the Bristol Channel. Sections 7.2 and 7.3 provide an investigation of resonance in the unmodified channel system and resonance condition affected by the potential hydrodynamic devices. Section 7.4 gives a discussion regarding the findings and Section 7.5 concludes the chapter and gives recommendations.

7.1 Tidal Resonance

7.1.1 Forced Oscillation Tests

Tidal constituents are amplified or suppressed depending on how close they are to the natural period of oscillation of the ocean or region of ocean [77]. Large tides will tend to occur where the natural period is close to that of the semi-diurnal constituents [138]. The resonant nature of a tidal system can be examined by field measurements of different tidal constituents and careful comparison of these with theory (e.g. [74, 155]).

Various estimates, using different techniques, have been used to examine the resonant nature of the Bristol Channel system. These are summarised in Table 1.1 in the Chapter 1. There is clearly some variation in the estimate of the resonant period of the system. However, most estimates suggest that the system has a slightly lower natural period than the semi-diurnal tidal constituents.

To examine the resonance of the system, the approach of [72, 149] is followed. The model is run by forcing it simply with the M_2 tide. The period of the tidal forcing is then varied to examine how the amplitude of the response varies depending upon the input frequency. This is done for the unmodified system as well as for the cases with the Severn Barrage present. The Swansea Lagoon scheme is also briefly considered. To examine the unmodified response, an alternative approach is also tried. The model is run without tidal forcing but it is perturbed by applying a 'wind shear force' to part or all of the domain before removing the disturbance and the subsequent unforced response is observed.

7.2 Unmodified Resonance Response

To start with, the response of the Bristol Channel in its natural state without artificial tidal energy extraction is considered. The validated two-dimensional DG-SWEM is utilised in this study. A uniform bed friction of 0.0025 is applied, which has been tuned previously by comparison with field data in Chapter 2. However, [72] found the frequency of the resonant peaks in the channel varied slightly with different bed friction values (see also [41]). For the unmodified case, the model is driven by a single M_2 tidal component with a range of frequencies during the whole 30-day simulation period. In total, 19 frequencies are applied to force the model. The ratios between the driving frequencies and the M_2 frequency vary between 0 and 5. Harmonic analysis is then applied to obtain the amplitude at several measurement

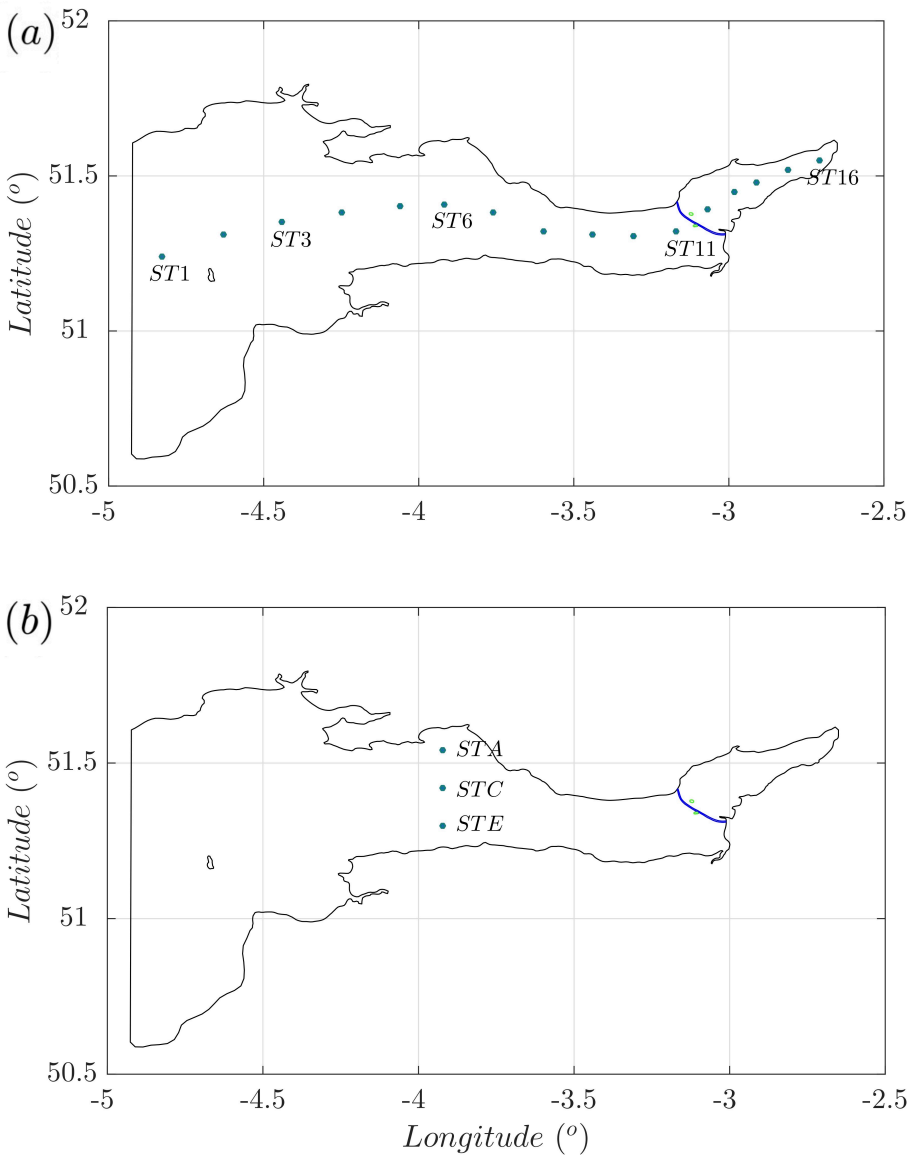

Figure 7.1: Resonance response measurement stations: a) stations along the channel (top); b) stations across the channel (bottom). Blue line indicates the purposed barrage location.

sites. The different stations along and across the channel used are shown in Figure 7.1.

Figure 7.2 presents the amplitude of the tide at different stations along the channel and across the channel, as well as the amplification of the response, which is the ratio of the amplitudes at stations located at the entrance, middle and head of the channel for different frequencies. For the stations considered, the response curves have a similar pattern, but with different magnitudes due to the station location. Figure 7.3

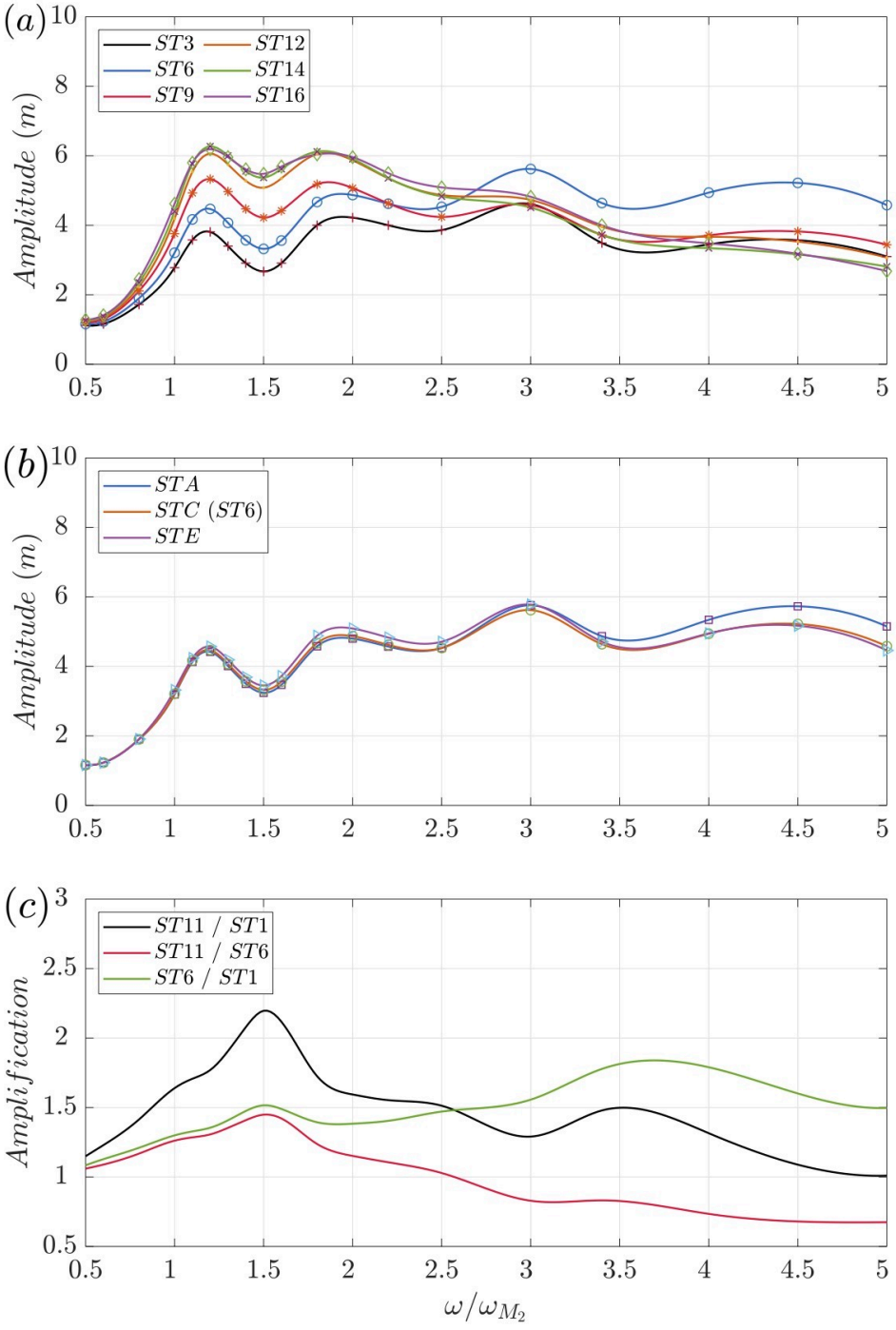

Figure 7.2: Resonance responses for the case without a barrage: a) responses results along the channel (top); b) responses results across the channel (middle); c) amplification of the response (the ratio of the amplitudes) (bottom).

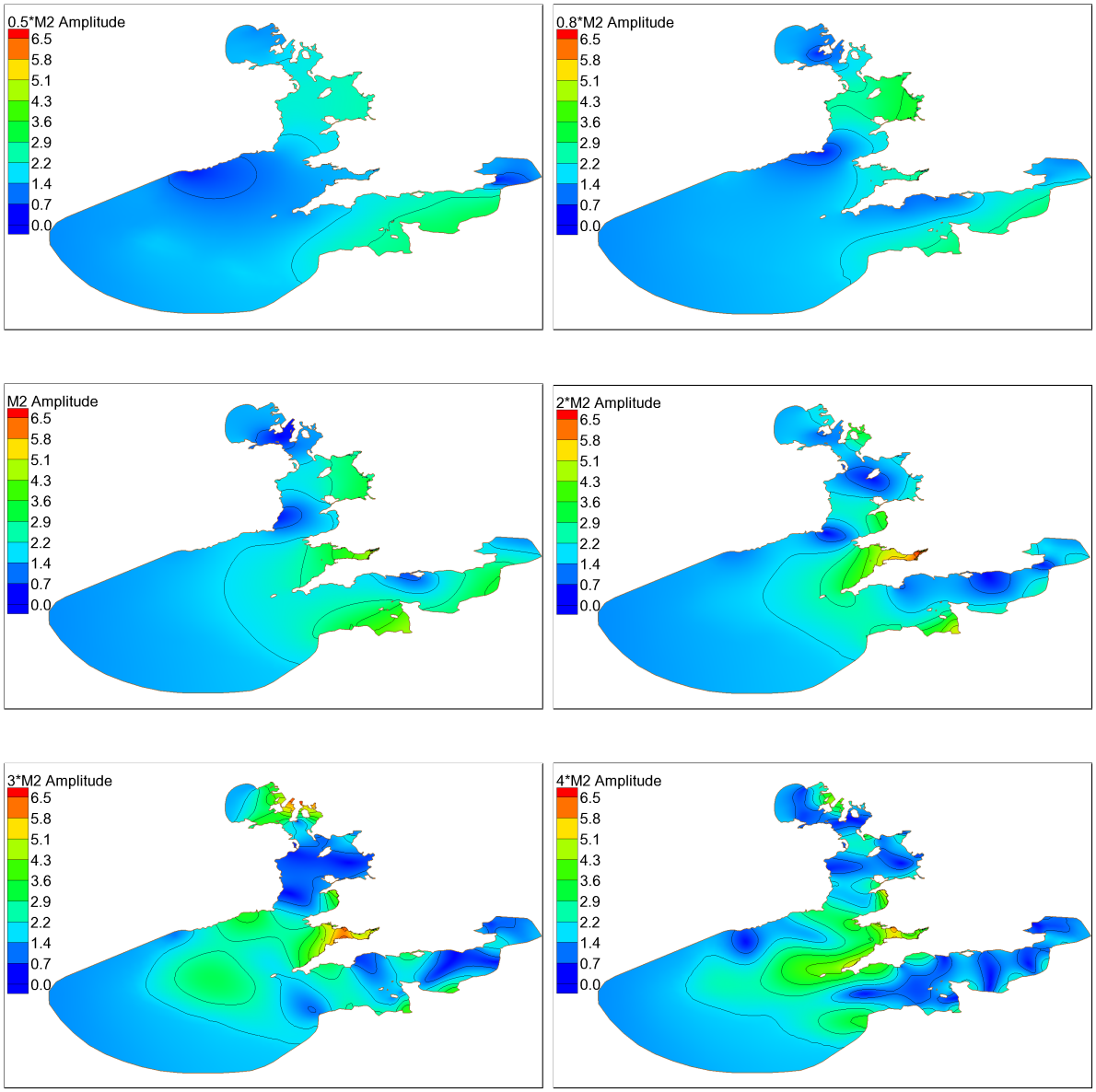

Figure 7.3: Co-tidal amplitude contours (m): $0.5M_2$ (top-left); $0.8M_2$ (top-right); M_2 (middle-left); $2M_2$ (middle-right); $3M_2$ (bottom-left); $4M_2$ (bottom-right) over the model domain.

presents the co-tidal charts for $0.5M_2$, $0.8M_2$, M_2, $2M_2$, $3M_2$ and $4M_2$ over the whole model domain. These show different areas resonate with different frequencies. The response of areas far from the Bristol Channel is primarily driven by local resonances rather than the change in the dynamics of the Bristol Channel itself.

7.2.1 Free oscillation tests

To analyse the natural case further, the free response of the unforced system is considered. Essentially this is equivalent to a 'hammer test' commonly performed on mechanical systems. Thus the system is perturbed from equilibrium and then allowed to oscillate freely. This is simply an alternative approach for examining the naturally occurring resonances in the system. This is done by applying a force equivalent to a wind shear from the west for two days to disturb the system. This produces an increase in the water level in the estuary (with a hydrostatic pressure gradient to balance this steady force). The model is then left to oscillate. A 15-day simulation period is used. Winds are linearly increased from $0 - 20$ m/s on day 5 from 00:00 to 12:00, keep unchanged for 24 hours and then decrease to 0 m/s at the end of day 6. Five measurement stations in the upper channel are being considered and the response to disturbances is shown in Figure 7.4.

From Figure 7.4, it can be seen that from day 10, the surge residual levels show the appearance of free resonating oscillations with a similar period and with heights within 0.1 m for all stations. It takes around four days for the oscillation to decay. The frequency content of the time series after day 10 of the simulation is analysed using a standard Fourier approach.

Both analysis methods show reasonably consistent results. The first peak is at $\sim 1.2\omega/\omega_{M_2}$. The second peak is at a slightly different frequency in the two approaches, being $\sim 1.8\omega/\omega_{M_2}$ using the forced approach and $\sim 1.6\omega/\omega_{M_2}$ in the free oscillation approach. It is assumed these are the same underlying phenomenon but cannot account for the apparent difference in frequency. There are some small resonances at much higher frequencies but these are well away from the semi-diurnal or diurnal forcing and they are not considered further.

7.2.2 Forcing over Different Regions of the Domain

Some extra simulations for the free oscillation approach are considered where the forcing is just applied to the Bristol Channel part of the domain and also where a much lower bed friction is used (the minimum friction necessary for model stability). Comparison of results can be seen in Figure 7.5. Note that friction will be much more significant in the shallower Bristol Channel than the deeper Celtic Sea. In both these cases the second peak ($\sim 1.6\omega/\omega_{M_2}$) is amplified relative to the first peak ($\sim 1.2\omega/\omega_{M_2}$). From this and other evidence, including the results below when a barrage is added to the model, the following can be concluded. The first peak

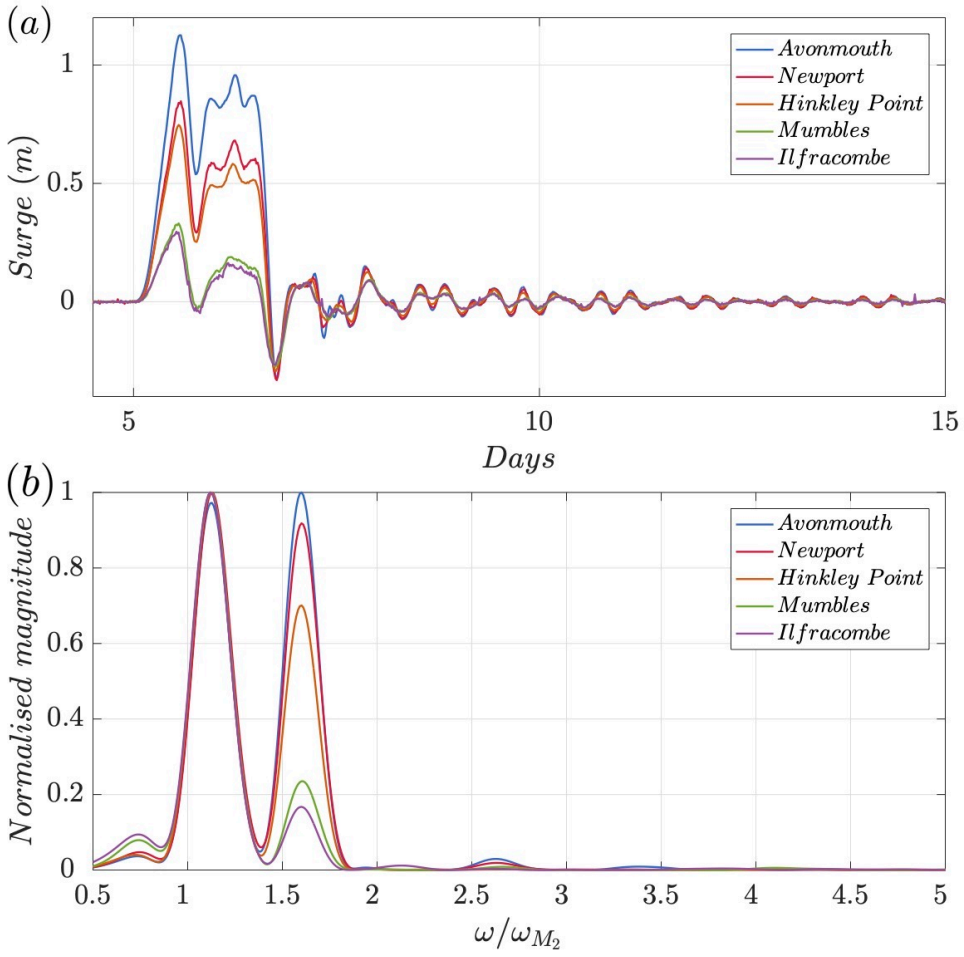

Figure 7.4: Disturbance analysis for a west wind within the Bristol Channel for the case without a barrage at five measurements stations: a) wind-driven surge (top); b) normalised magnitude spectrum (bottom).

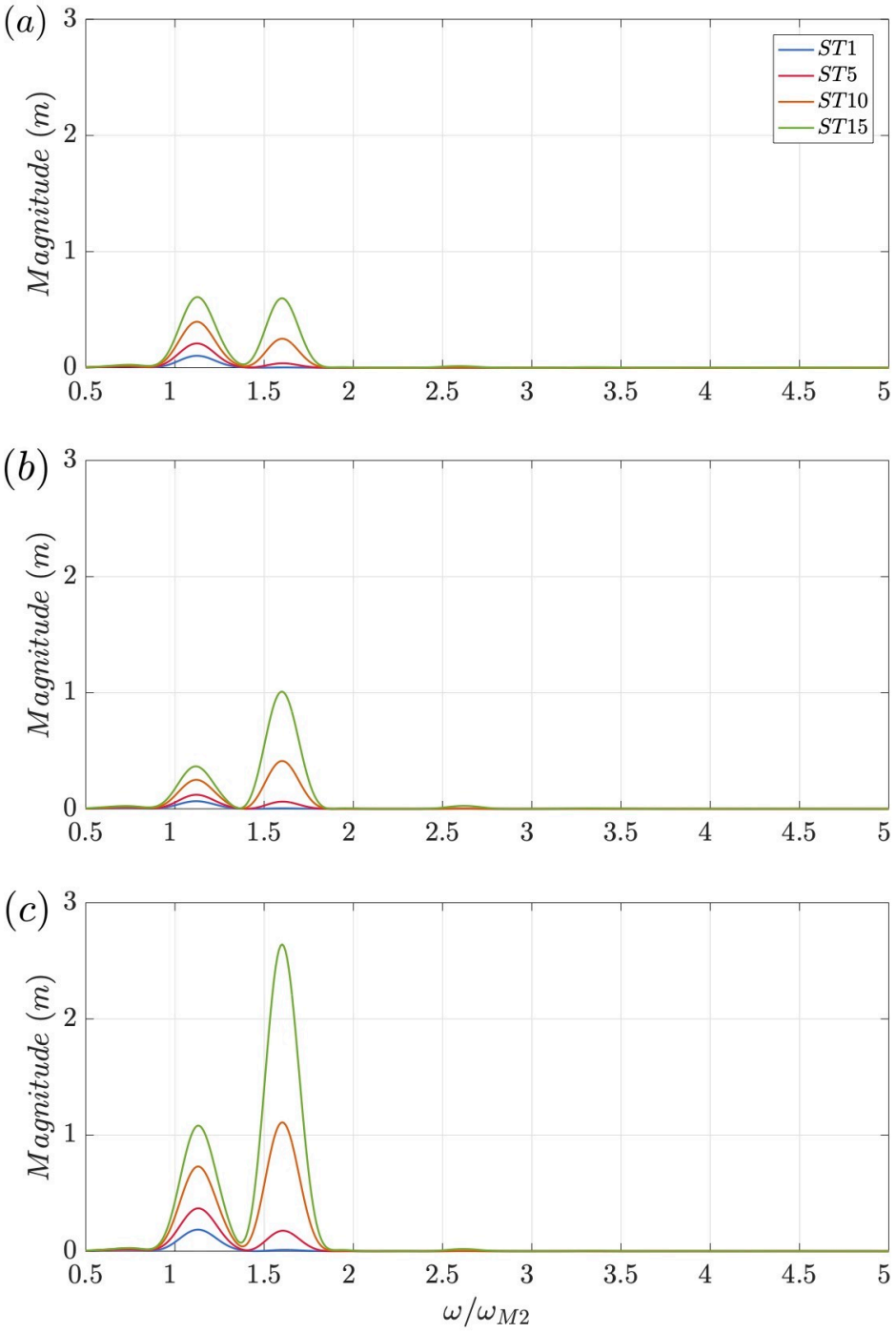

Figure 7.5: Magnitude spectrum distribution within the Bristol Channel for different cases at four measurements stations: a) original case with forcing over the whole domain (top); b) case with forcing only over the channel (middle); c) case with forcing over the whole domain with lower bed friction (bottom).

($\sim 1.2\omega/\omega_{M_2}$) appears to be due to the combined Celtic Sea and Bristol Channel system with a period of 10.35 hours. The higher frequency resonance appears to be a resonance within the channel itself, which indicates the quarter wavelength resonance of the system with a period of approximately 7.76 hours. This result is in good agreement with the previous research conducted on estimating the Bristol Channel resonance period of [87] and [109], and confirms that the channel is shorter than the quarter wavelength in the natural case. The results are also comparable with the investigation of [166] for resonance study of the English Channel and Irish Sea, which suggests the resonance periods of $10.8-11.6$ hours and $5.0-8.0$ hours for the coupled resonance system in the Bristol Channel.

From the response curves across the mid-channel, it is seen that when approaching the coasts, the response increases which may be explained by the decrement of water depth. Along the channel, the amplification of the response is shown in the bottom panel in Figure 7.1. It is developed by normalising the channel response by the amplitude at the channel entrance (shown as the black line). The amplification of the response in the outer channel (green line) and the inner channel (red line) are also presented. The results suggest that the observed responses of the channel to the tidal forcing may be the result of coupled resonances, as analysed above – some of the response are due to the forcing at the mouth within the channel itself, and some are related to both channel and the response of the Celtic Sea with forcing from the edge of the continental shelf. The inner region of the channel shows an obvious resonance response at $\sim 1.5\omega/\omega_{M_2}$, whilst the outer part exhibits the response at around $\sim 3.7\omega/\omega_{M_2}$. The coupled resonance system of the Bristol Channel is also suggested by [109].

7.3 Resonance Response of Modified System

The resonant response of the Bristol Channel to different frequencies when a tidal barrage is present is now presented. For the response to the Severn Barrage, three operating strategies are considered. Two different operational modes are considered where different starting heads (see [16, 134]) are used. Case 'A' has a starting head of 1.5 m and Case 'B' has one of 4 m. The extreme case where the barrage is completely closed is also considered as a limiting case (although such a scenario might happen if the barrage was used for flooding protection, as stated in Chapter 3, and possibly during construction). Chapter 3 showed that the hydrodynamic impact of

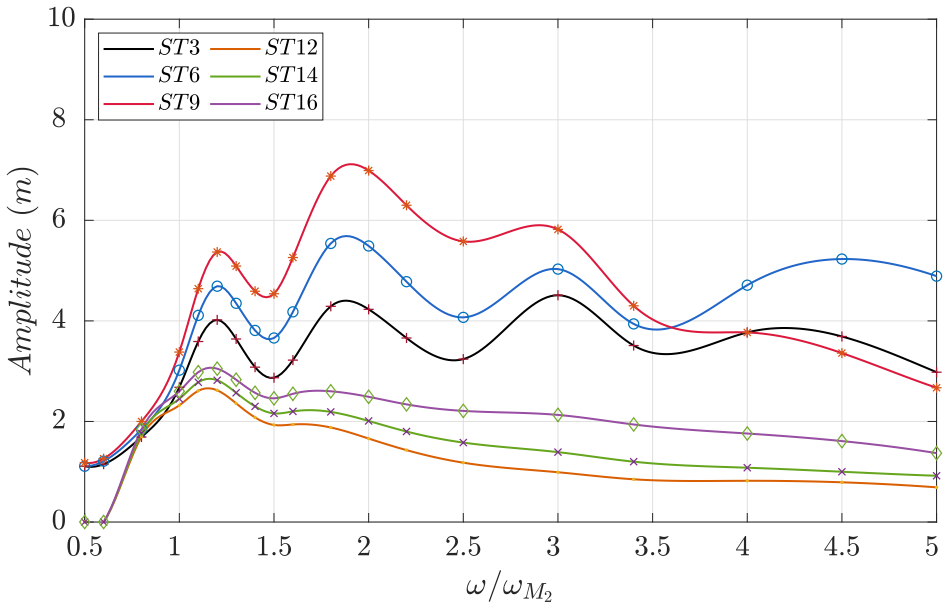

Figure 7.6: Resonance responses for the barrage formal operation case along the channel.

the Swansea Lagoon was localised and so only the most extreme case is considered: that of the closed lagoon. In all cases two-way generation is assumed.

7.3.1 Response to Severn Barrage

The response of the channel to the barrage under normal operation is shown in Figure 7.6. Figure 7.7 shows the co-tidal charts for the normal barrage operation case with varying driving frequencies. If the barrage is shortening the effective length of the channel then it would be expected that the resonances, especially those within the channel itself, would be shifted. It is slightly surprising that the resonant peaks in the channel do not appear to shift significantly with the barrage present (the second resonance peak is only shifted by approximately 13 minutes). On the ocean side of the barrage there is almost no change to the resonant frequencies. For the higher frequencies, there appears to be a reduction in the damping. This could be considered surprising since it would be expected that a barrage would extract energy although the barrage would also reduce the energy lost in friction in the shallower areas of the channel. From co-tidal charts and when compared with Figure 7.3, the limited impact of the barrage on the response of areas far from the Bristol Channel can be observed.

Different barrage operating strategies are now considered. Figure 7.8 presents the amplitude of the tide at three stations along the Bristol Channel for different tidal

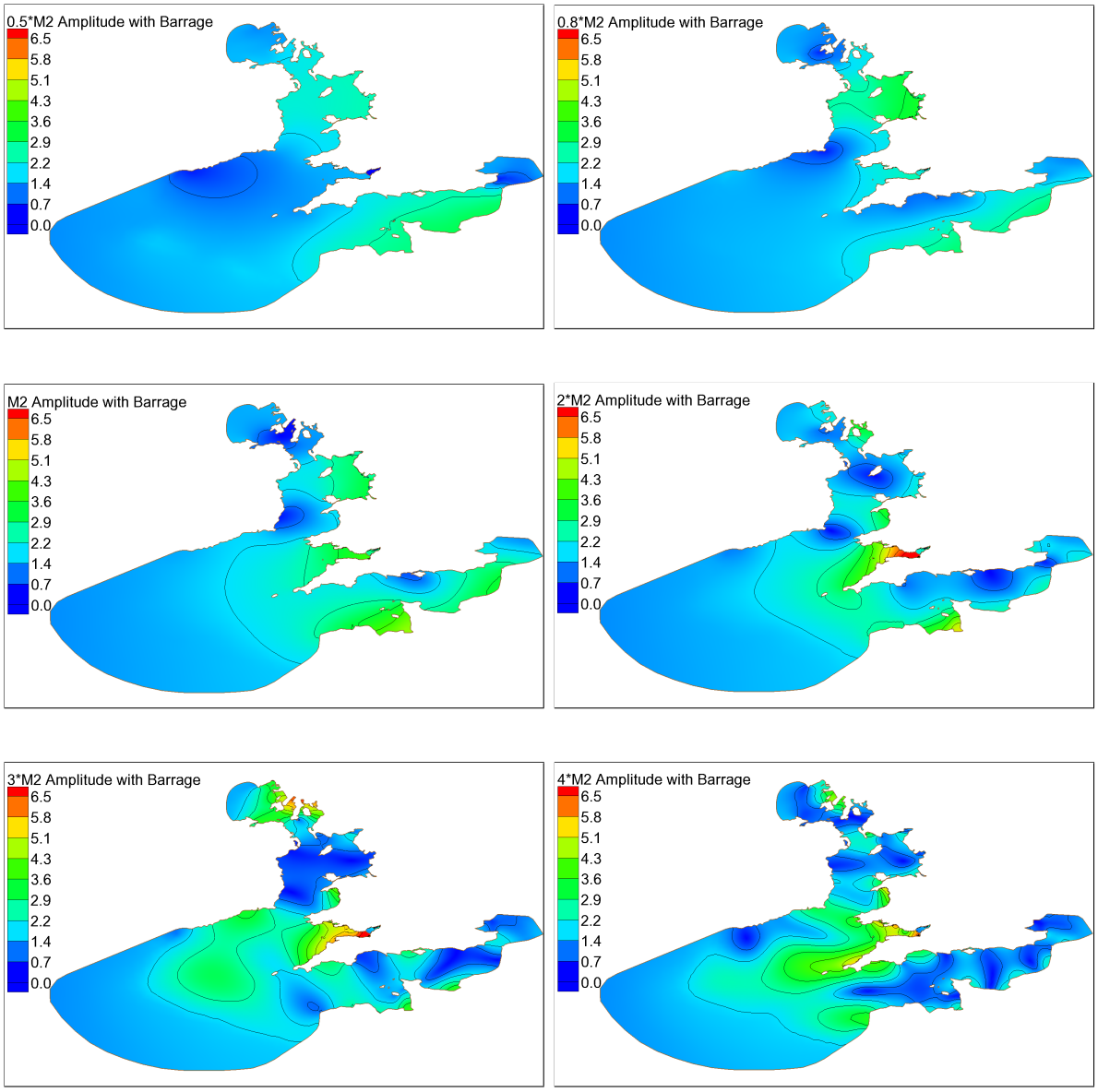

Figure 7.7: Co-tidal amplitude contours (m) with barrage normally operated case: $0.5M_2$ (top-left); $0.8M_2$ (top-right); M_2 (middle-left); $2M_2$ (middle-right); $3M_2$ (bottom-left); $4M_2$ (bottom-right) over the model domain.

frequencies. Approaching the mouth of the channel, the barrage causes negligible change when operated normally and very small changes across the whole spectrum for the case in which there is no flow through the barrage.

Within the channel, and particularly near the barrage, the barrage leads to very little change at the natural M_2 tidal frequency. This is in keeping with other studies which suggest the Severn Barrage would lead to a surprisingly small change in the tidal range on the ocean side of the barrage [178]. The reason for this is presumably that the resonant mode close to the semi-diurnal period is associated with the whole Celtic Sea/Bristol Channel system (see Section 7.2) and so modifying the dynamics in the Bristol Channel itself has a rather small impact. However, for higher excitation frequencies there is considerable change – particularly for the case where the barrage is completely shut. At the barrage itself, the amplitude of the tide increases considerably when excited by a higher frequency.

From the Figure, some resonances near the barrage close to the $\omega/\omega_{M_2} = 2$ frequency are suggested. This is close to the frequency of the M_4 tide. This constituent usually arises from the M_2 tide interacting with the varying cross-section of the channel. It is seen as important for sediment transport [132] and therefore has impacts on the environment. Given that this constituent is locally generated rather than driven by external forcing, it is hard to directly assess the implications of this peak and it is not further investigated in this project.

7.3.2 Impact of Lagoon Implementation

The impact of the Swansea Lagoon on resonance is now briefly considered. This is a small deployment compared to a barrage and thus the expected change to the large-scale tidal dynamics is small. This thesis only considers the extreme case where the lagoon is closed as this will be a limiting case.

Figure 7.9 presents the response curves for the lagoon and barrage implementation respectively. The response of the estuary with the lagoon present is nearly identical to the natural case. This result is in keeping with expectations that the Swansea Lagoon is too small to make major changes to the large-scale hydrodynamics of the region. There will, of course, be significant local changes (see Section 3.5).

7.4 Discussion

Around the semi-diurnal frequencies (i.e. those of the dominant M_2 and S_2 constituents) surprisingly little change is seen in the resonance system of the Bristol

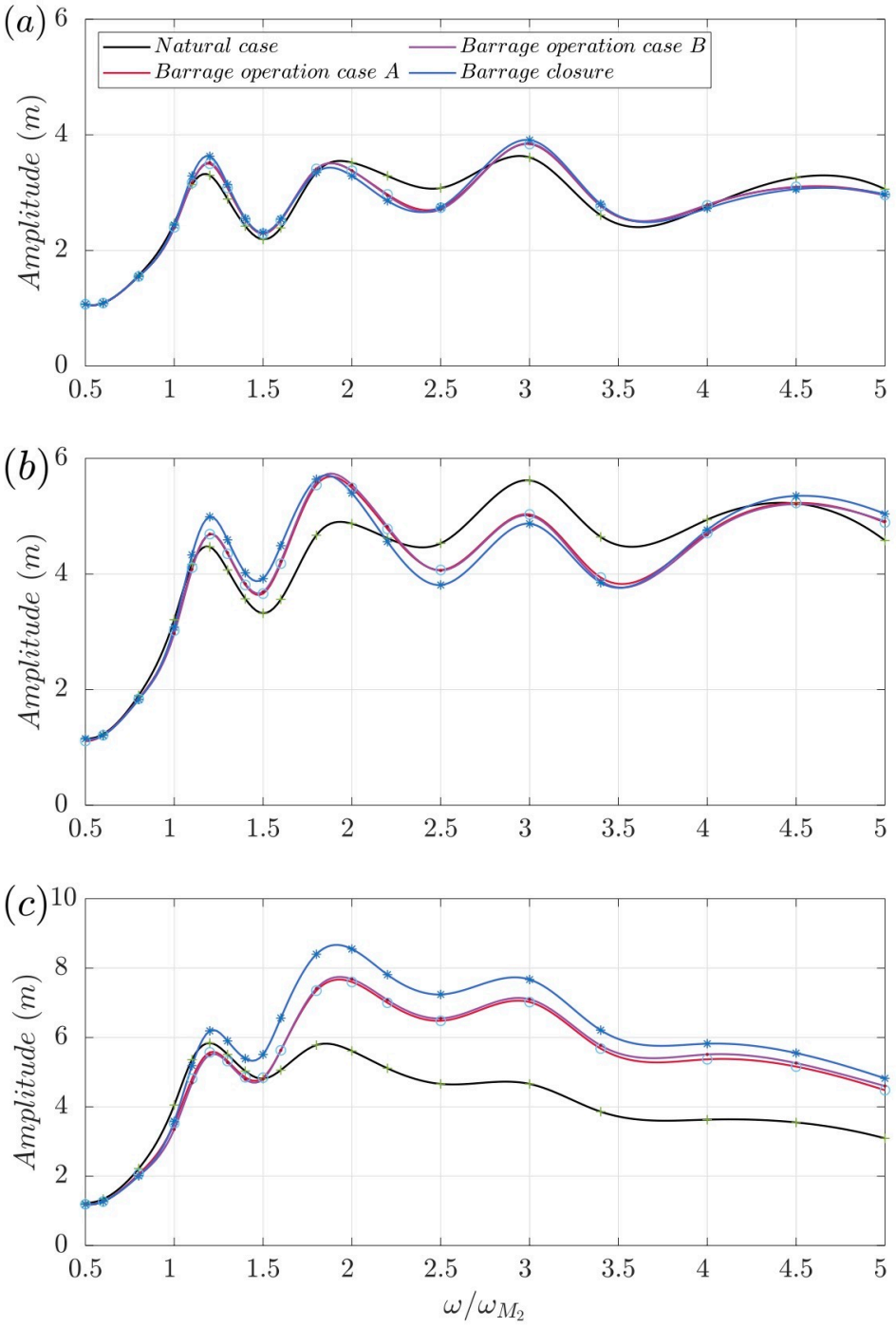

Figure 7.8: Resonance responses of the barrage operation cases comparisons: a) responses at the entrance, 51.24°N 4.83°W, of the channel (top); b) responses at the middle, 51.41°N 3.92°W, of the channel (middle); c) responses at the inner (barrage site), 51.32°N 3.17°W, of the channel (bottom).

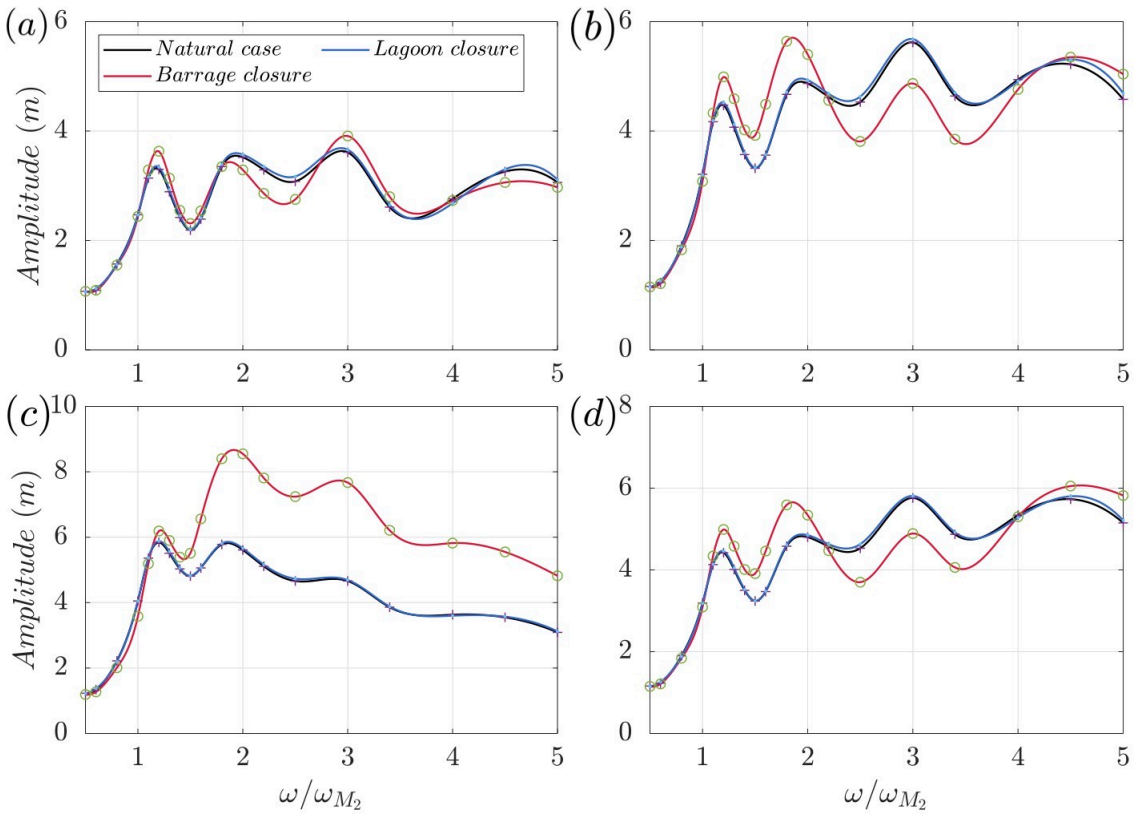

Figure 7.9: Resonance responses of the lagoon cases comparisons: a) responses at the entrance, 51.24°N 4.83°W, of the channel (top-left); b) responses at the middle, 51.41°N 3.92°W, of the channel (top-left); c) responses at the Severn Barrage site, 51.32°N 3.17°W, (bottom-left); d) responses at the Swansea Lagoon site, 51.54°N 3.92°W, (bottom-right).

Channel due to barrage implementation. This perhaps explains why changes to the tidal hydrodynamics outside the Bristol Channel are predicted to be relatively small (except where very simplistic models of energy extraction are used). Interestingly, resonance around twice the semi-diurnal frequency is observed. This is close to the M_4 frequency which is significant environmentally for its role in sediment transport. The M_4 constituent is (primarily) locally generated within the estuary rather than being an incoming tidal wave from outside. The methodology used in this chapter looks primarily at the amplification of incoming waves and so caution should be used in applying its conclusions to the M_4 constituent directly. Nevertheless, the method does suggest that resonant amplification of this constituent is possible when a barrage is present.

7.5 Conclusions

In this chapter, the tidal resonance characteristics of the Bristol Channel suggested a coupled resonance system which was, perhaps surprisingly, complex. Adding a barrage structure to this system increased this complexity further. However, the Severn Barrage appeared to make little difference to the resonant response for frequencies close to the dominant semi-diurnal frequencies, which dominate the tides in the region, even though the barrage was found to alter the response of the channel to excitation with higher frequencies than 12 hours. Given that changes to the resonant response are a potential cause of significant changes to the large-scale hydrodynamics, this is reassuring. These findings partially explain why changes to the tidal hydrodynamics are predicted to be relatively localised to a Severn Barrage, despite the magnitude of such a structure. If a barrage were to be installed in the Bay of Fundy, which has a resonance period slightly larger than that of the semi-diurnal tide, it is probable that there would be far more significant changes than have been found in this study. For the Swansea Lagoon scheme, it was found that such a device is too small to have a significant impact on the resonant response of the channel.

Chapter 8

Conclusions and Recommendations

Flooding induced by storm surge events has the potential to cause significant damage to the environment and human life. The high tidal range of the Bristol Channel means that coastal flooding from storm surges is relatively rare. However, if a storm surge event coincides with a spring tide, the potential for very major consequences will be high given the large amount of low-lying lands surrounding the estuary and the high population [67]. An example of this scenario occurred in 1607. The high tidal range also makes the Bristol Channel a promising candidate site for tidal energy extraction [23, 88]. Tidal power can offer significant promise as a renewable energy, with increasing concerns over carbon emissions and worldwide energy demand. The Severn Barrage and the Swansea Bay Lagoon are two options that have been proposed to generate energy from the Severn Estuary/Bristol Channel region. Aspects of these were evaluated in this thesis.

This thesis considered the interactions between storm surges and barrages and their impacts on water level, which was taken as a metric for flooding. A two-dimensional depth-averaged numerical model of the region with the Severn Barrage included was developed and the response to a storm surge event examined. Different barrage operational strategies during the event were considered for optimising flooding prevention. A one-dimensional numerical model was utilised to determine whether this simplified model could be used as an alternative to two-dimensional modelling. The effect on barrage power output and the resonance phenomenon were investigated with the two-dimensional model. This approach was also applied to examine the impact of a Swansea Lagoon in the Bristol Channel. The following sections summarise the main conclusions derived from the numerical model and results. Section 8.3 proposes the topics for future research.

8.1 Conclusion from the 2D Numerical Model

To the author's knowledge, this work is the first to simulate the Severn Barrage with a storm surge event within a two-dimensional model. The calibrated and validated numerical model was used to simulate tides and storm surges with the application of the discontinuous Galerkin method version of the ADCIRC (DG-SWEM) [168, 46], using unstructured triangular mesh [149] to solve the two-dimensional shallow water equations and with the meteorological input from the ERA5 dataset. The numerical model considered the south-west coasts of the UK including the Celtic and Irish Seas and the English Channel. According to the storm surge simulation results from the Chapter 2, taking the surge event on the 13 December 2000 as an example, the highest water level at Avonmouth approached 8 m with the surge residual level of over 1 m during the event. Clear flooding potential within the channel could be expected. As shown in Appendix A, the flooding condition of the event could also be observed considering the low-lying lands around the channel.

The impact of a Severn Barrage implementation was examined by modifying the DG-SWEM with an internal barrier to connect the ocean and basin sides of the barrage. With the addition of a normally operated barrage, as shown in Chapter 3, there would be an increase in the extreme water level that would be expected to the west of the barrage, which might impact flooding in areas such as the Somerset Levels during a storm surge event, although the impacts are of the same order of magnitude as that expected from sea level rise (10s of cm) and thus can perhaps be ignored. For the regions within the basin, the barrage would lead to significant reduction, around 54%, in peak water level due to its effect on both tidal amplitudes and surge residuals. The presence of the barrage would also delay the surge peak over 1 hour, which is an additional benefit. It is clear that a Severn Barrage would provide considerable protection against flooding for the cities to the east of the barrage such as Bristol and Cardiff.

Different barrage operation strategies during a storm surge event were considered and would make a small, but perhaps significant, difference to the extreme water level. By careful operation, the barrage would provide even more flooding protection to the east without huge negative impacts to the west side of the barrage. Exactly which strategy is optimal would depend on the weight placed on the changes to the water level both upstream and downstream, as well as the impact of power generation interruption during a spring tide, which was examined in Chapter 4. The interaction of storm surge and power output was also investigated and the impact of atmospheric

disturbances was found to make only a minor difference in power estimation. Different barrage operations would lead to significant interruptions in power production during a severe surge event although this would have a negligible effect on the long-term average power.

For the case of the Swansea Lagoon, some flooding protection was predicted for both within and outside the lagoon. This varied slightly depending on lagoon operation strategy. However, the benefits were rather small and local since it is a relatively small project. A wisely designed lagoon operation during a storm surge event would make limited difference to the extreme water and residual levels. The impact of different operations on the lagoon power generation is also limited. These small impacts suggest that for something the size of the Swansea Lagoon, storm surges are relatively unimportant to the design. For larger structures, storm surges do need to be considered.

In regards to the general impact of a Severn Barrage on tidal hydrodynamics, this study showed limited impact on the tides west of the barrage and a significant reduction of the tidal range for the head of the channel. Reduction of the barrage operation starting head led to a reduced tidal range impact within the basin, which, as a result, has a relatively smaller negative environmental impact. The analysis in this thesis is consistent with the literature on the change in tidal levels (e.g. [30]). To the best of the author's knowledge, this thesis is the first work to investigate the tidal hydrodynamic impact with a Swansea Lagoon implementation. It was found that the changes to the large-scale tidal dynamics from the Swansea Lagoon would be negligible.

The reason the impact of a barrage or a lagoon could be large is that there could be changes to the nature of the tidal resonance. The tidal resonance characteristics of the Bristol Channel as analysed in Chapter 7 suggested a coupled and complex resonance system, where the complexity would be further increased by a barrage implementation. The Severn Barrage was found to make limited difference to the resonant response for frequencies close to the dominant semi-diurnal frequencies, helping to explain why predicted changes would be localised to the structure. It was speculated that more significant resonance changes would be expected if a barrage was installed in sites with larger resonance periods, such as the Bay of Fundy.

The decision as to whether to build the barrage or lagoon is a complex one and will depend on many factors – political, economic and environmental. This thesis examined a part of this, and showed that there would be an economically valuable

flooding protection benefit from building a barrage. The thesis also contributed to the understanding of the environmental impact of barrage installation.

8.2 Comparison between 1D and 2D Numerical Model

The one-dimensional hydrodynamic model has been considered as a computationally cost-effective option that can capture key tidal hydrodynamic features in its simulations. This thesis also examined a one-dimensional model with simplified barrage addition for the Bristol Channel regions. Good agreement was achieved between the one- and two-dimensional models in the verification tests, in which the accuracy and efficiency of the one-dimensional model for tides and barrage simulations were demonstrated. However, less accuracy was achieved in the storm surge computations. Similar behaviour of barrage impacts was found between the two models and agreement in results on barrage control strategies were obtained. A one-dimensional model might be applied to make a preliminary investigation and qualitative analysis to capture main features of the tides and barrage behaviour with less computational time. However, for detailed investigations with greater accuracy and more features, a one-dimensional model was found to be too simplistic and multidimensional numerical models are required.

8.3 Future Research

8.3.1 Environmental Impact of Barrage Implementation

There is significant variation in the tidal dynamics which can result in measurable environmental impacts by a barrage construction. It is significant to consider the environmental impact along with social and economic assessments when making decisions for a tidal barrage construction. Draper *et al.* [56] have stated that basin geometry is significant to the tidal hydrodynamics, which would have an effect on the local environment. The overall water quality may be influenced by the effects of transportation of suspended sediment raised by the barrage implementation [125].

This thesis only examined the direct hydrodynamic impact of a barrage. Further studies are required to consider other environmental effects of the tidal barrage itself and different operation strategies. It is feasible to examine the sediment transportation with the model in-built in DG-ADCIRC and a water quality model can be further coupled with this solver to investigate the impact on the water quality due to a barrage or a lagoon.

8.3.2 River Flooding

Besides the coastal flooding considered in this thesis, as with other storm surge barrages (e.g. Thames Barrier and Maeslant Barrier), the analysis can also be used to reduce the impact of flooding in the River Severn and other rivers flowing into the basin to the east of any barrage. This would require the barrage to be operated appropriately. This operation might be sub-optimal in terms of flooding from storm surges, if river and storm surge flooding were to coincide. Further research can look at River Severn floods (and other tributaries) with respect to the Severn Barrage construction. The River Severn is the longest river in Britain and drains directly into the Severn Estuary and has several flood-risk areas. The discharge from this river can be modified by the water level out the outfall and hence will be modified by the Severn Barrage. A simplified one-dimensional model considering river discharge can be added into the current two-dimensional model to examine the effects of a barrage on both coastal and river flooding during storm surge events. A similar barrage strategy can be applied to other locations.

8.3.3 Future Changes to Climate

The probability of storm surge-induced flooding would be affected by changes to the meteorological systems caused by climate change. There is concern that more extreme weather could lead to a reduction in the return periods of extreme storm surge events [111]. Further, sea level rise would increase water levels and potentially make areas more vulnerable to climate change. The impact of climate change on storm surge has been considered by [131]. This study suggests that the 1-in-50-year storm surge event would have its surge residual increased by 0.8 mm annually, and a sea level rise of 2.4 mm could be expected per year in the Bristol Channel under the medium greenhouse gas emission scenario. Over the timescale of a century, the change to storm surge residual levels has been reported to be of the order of 50 cm and the largest changes were found in the Bristol Channel and Severn Estuary [5]. It is not known accurately what effect possible climate change could have on the meteorological changes and corresponding storm surge-induced flooding. The changes of storm surge with climate variations and possible future extreme surge conditions can be investigated in future projects.

Lyddon *et al.* [112] have stated that in certain locations, the implementation of tidal devices can act as a flooding defense under both present-day and future rising sea level conditions. The possible effects of flooding level reduction with a tidal barrage

have been investigated in this thesis. Further work can be done to draw together the impact of future sea level rises, changes in storm intensity, and the deployment of a barrage.

Appendix A

Barrage Impact of Low-lying Land with Modified Model

This appendix uses a modified model to explore the effect of barrage implementation on flooding, especially over the surrounding low-lying lands approaching the channel head. The model used in this thesis does not explicitly model inundation of low-lying land. Instead, water level is used as a proxy for flooding and a simpler model is adopted which does not directly simulate the low-lying areas. This is standard practice in the field and is the approach taken by [91] and the recent study at Imperial College, UK by [164]. Inundation of low-lying lands may be better studied using dedicated models such as LISFLOOD [161]. However, in this appendix, the ADCIRC DG-SWEM is used and modified to explicitly include regions which may flood.

A.1 Modified Model including Low-lying Regions

In order to visualise the barrage impact on the channel region, especially on the surrounding low-lying lands (e.g. the Somerset Levels), a modified model from the DG-SWEM presented in Chapter 2 is considered. This includes the low-lying area around the head of the channel (see Figure A.1), which may be inundated during a flooding event. The shape of the new mainland boundary approaching the channel head includes consideration of the barrage implementation.

The land elevation data is taken from the global GEBCO gridded bathymetry dataset and the data nodes with elevation less than 100 m are selected, which has been merged with the bathymetry in the channel. Extension of the original model requires a finer mesh resolution due to consideration of the resolution of the land elevation dataset and the wetting and drying features approaching the channel head.

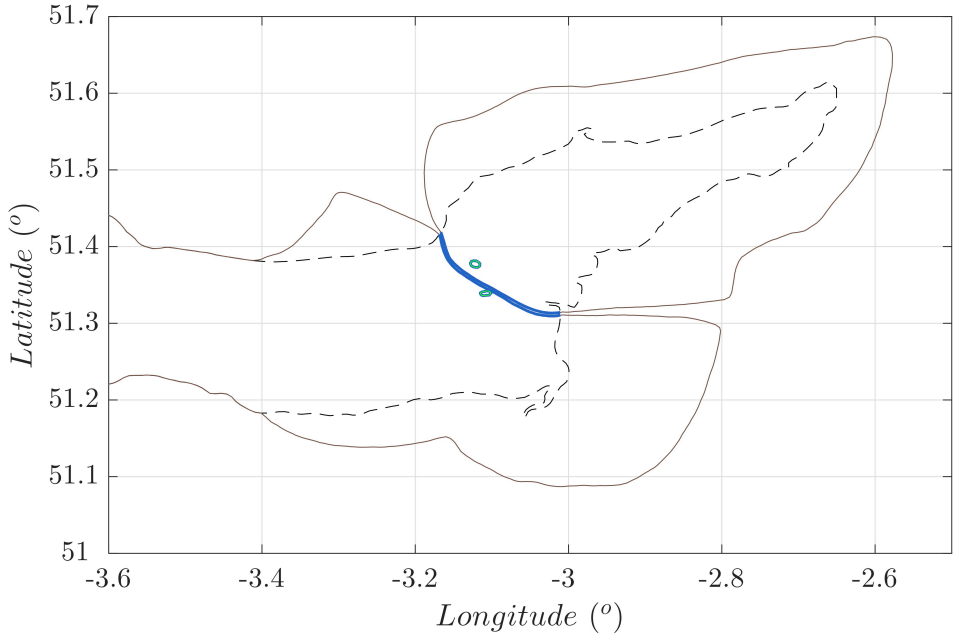

Figure A.1: Modified 2D model domain including low-lying areas (with barrage included). Brown line indicates the new land boundary considering the low-lying area and black dash line indicates the original model boundary.

The resulting modified model mesh consists a total of $55,011$ nodes and $103,558$ elements. The simulations are set up using the same model parameters as used in the model described in Chapter 2. The barrage boundary is implemented as stated in Chapter 2.

A.1.1 Modified Model Comparison

In order to determine whether the modified model is accurate to the original model, a comparison is conducted between the two, with and without normally operated barrage implementation. The test considers a simulation period of 14 days with a ramping period of two days. Tables A.1 and A.2 show these tests result without and with barrage implementation respectively.

For the case without the barrage included, compared with the original model, the modified model results do not have a significant difference in the peak water levels of the representative locations throughout the channel region. The largest discrepancy happens on the basin side of the barrage at a location with the coordinates of (51.48°N 2.90°W), with 4.86% of change. For the timing of the peak, negligible changes are also observed. Considering the case with barrage implementation, from the Table it can be seen that for both regions on the ocean side and barrage site, the difference of

Table A.1: Comparison test of modified model with original model for the case without barrage implemented in the ocean (51.36°N 3.67°W), barrage site (51.32°N 3.13°W) and basin (51.48°N 2.90°W).

	Original Model Case			Modified Model Case		
	Ocean	Barrage Site	Basin	Ocean	Barrage Site	Basin
Peak Water Level (m)	5.76	7.09	8.03	5.81	7.12	7.64
Timing of the Peak (days)	10.31	10.33	10.33	10.31	10.32	10.35

Table A.2: Comparison test of modified model with original model for the case with barrage implemented in the ocean (51.36°N 3.67°W), barrage site (51.32°N 3.13°W) and basin (51.48°N 2.90°W).

	Original Model Case			Modified Model Case		
	Ocean	Barrage Site	Basin	Ocean	Barrage Site	Basin
Peak Water Level (m)	5.99	6.76	3.66	5.96	6.71	3.56
Timing of the Peak (days)	10.31	10.31	10.39	10.31	10.31	10.39

the peak water levels between the two models is under 1.00%. While for the regions within the basin, the difference becomes larger, up to 2.73%. Again, the variance in the timing of the peak is negligible.

Both comparisons of the modified model, with and without barrage implementation, show satisfactory agreement for the timing of the surge event and the peak water levels on both the ocean side of the barrage and the barrage site itself. The peak water levels on the basin side show higher discrepancy between the two models. The water level approaching the head of the channel has high dependency on the model mesh resolution. As such, the discrepancy could be due to the application of finer mesh approaching the channel head, which in theory should have a better wetting and drying performance in the modified model. Generally, the comparisons show acceptable agreement and the explicit inclusion of the low-lying areas in the model is expected to make little difference to the results and hence does not change the conclusions reached using the original model in the main thesis.

A.2 Low-lying Regions Results

The storm surge event in the year 2000 and the same barrage operation strategies as stated in Chapter 3 are applied in this modified model. Figure A.2 shows the

modified model domain and the simulation results shown with the contours of total water elevation under different scenarios at the time of the event. As with the main model, there is no discharge from the River Severn or other rivers as this is small relative to the other movements of water.

For the no barrage case, it is clear that there would be some flooding over the low-lying lands around the Somerset Levels if no action is taken during the surge event. There would also be some flooding at the Welsh Levels on the north bank of the channel head at 07:40 of the surge day. For other cases with barrage implemented, the regions on the east side of the barrage are well-protected with almost no flooding water observed at the surge peak (except for the river discharge). Water levels in the barrage following the cases of complete closure and partial barrage re-opening are lower and therefore, the risk of river flooding would be reduced. However, all the barrage implementation cases lead to larger flood extent around the locations of Burnham-on-Sea and Huntspill (51.2°N 3.05°W) and would exacerbate river flooding in the River Parrett. The worst condition occurs for the barrage closure scenario. This is less severe for the fully and partially barrage re-opening cases. For the timing of the surge, both fully and partially re-open scenarios delay the worst flooding condition by 20 minutes, which can be another benefit for flooding protection.

It appears from these results that the inundation of the storm surge event can be prevented by the application of a barrage. It does not appear that the inclusion of additional areas of inundation lead to significantly different results to those found in Chapter 3. Thus, as it is more difficult to have additional large inter-tidal areas in the model, a simpler, more stable model is used for the majority of this thesis.

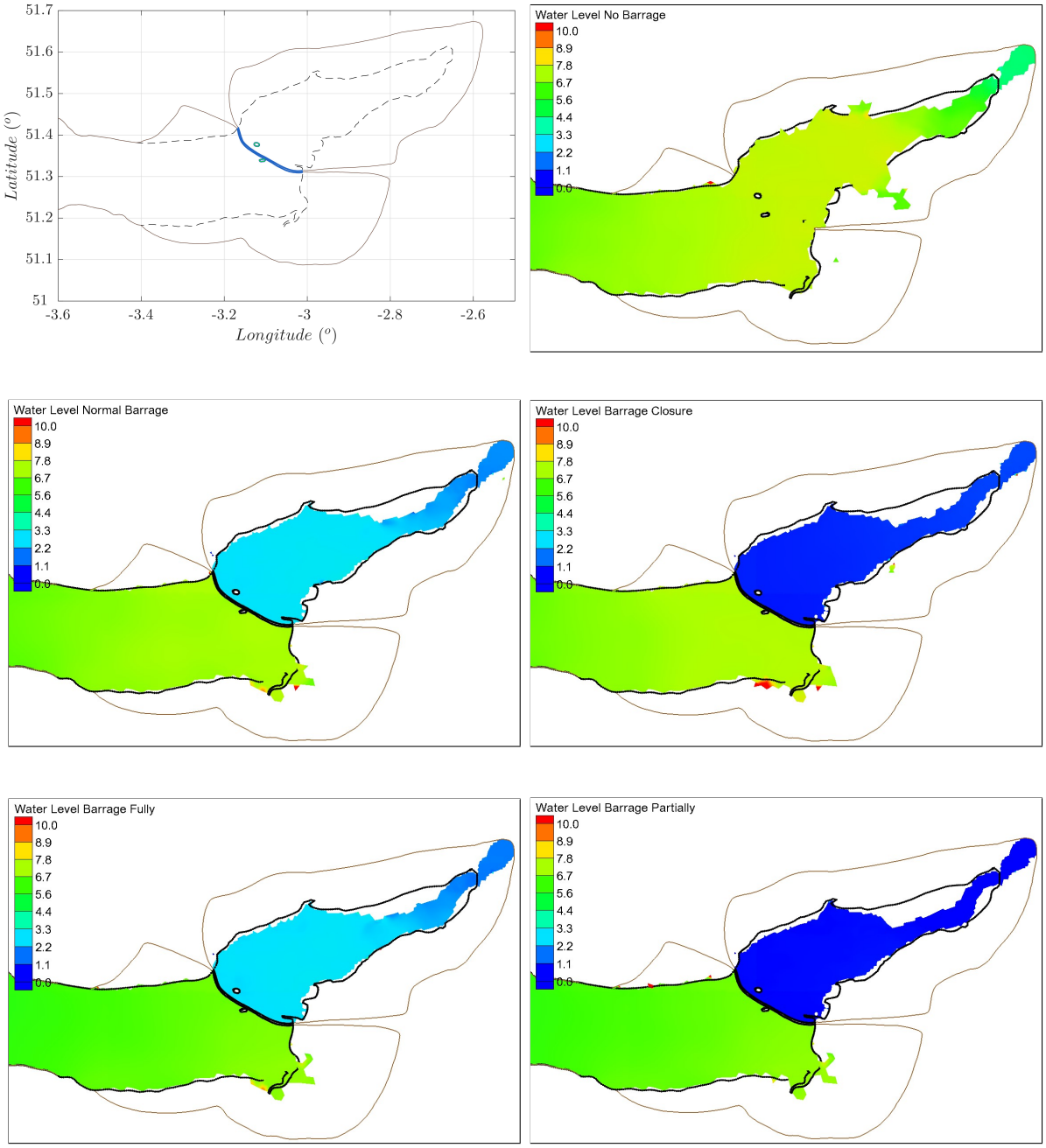

Figure A.2: Simulation result of barrage impact on the low-lying land by the modified model at the surge day (the black dash line indicate the original model domain and the brown line indicate the extended land model domain): Model domain of the modified model with surrounding low-lying land (top-left); Contours of total water elevation (m) during the storm surge event for no barrage case (top-right); Contours of total water elevation (m) during the storm surge event for normal barrage case (middle-left); Contours of total water elevation (m) during the storm surge event for barrage closure case (middle-right); Contours of total water elevation (m) during the storm surge event for barrage fully-reopen case (bottom-left); Contours of total water elevation (m) during the storm surge event for barrage fully-reopen case (bottom-right).

Appendix B

Wind Pattern for Severe Storm Surge Event in Years 1990, 1995 and 2014

This appendix provides the wind patterns of the several additional storm surge events that occurred in the Bristol Channel as shown in Table 1.2 in Chapter 1. Figures B.1, B.2 and B.3 show the wind condition during the storm surge events in the years 1990, 1995 and 2014, respectively.

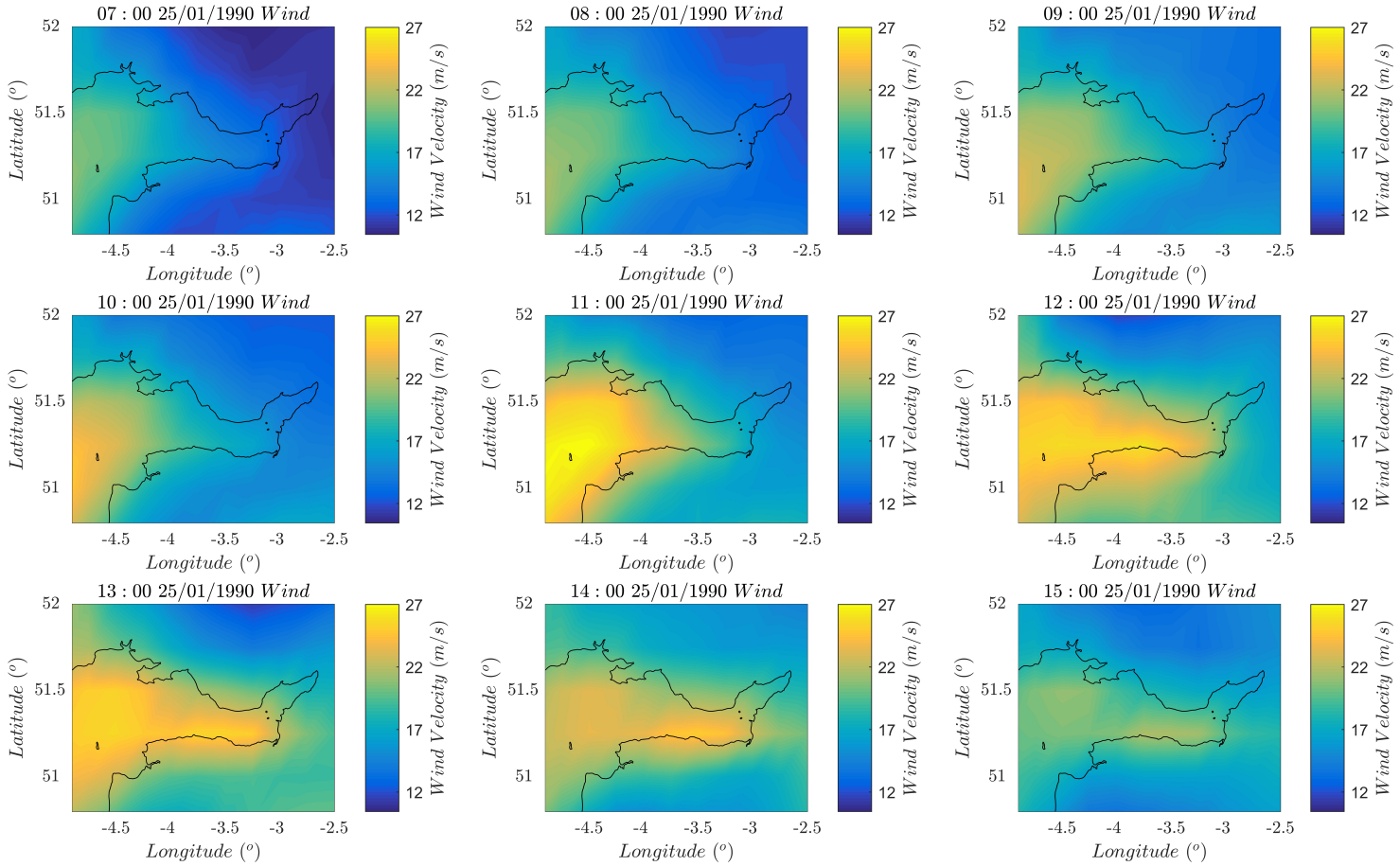

Figure B.1: Wind conditions (wind velocity in m/s) in Bristol Channel for the storm surge event on 25 January 1990 from ERA5 dataset.

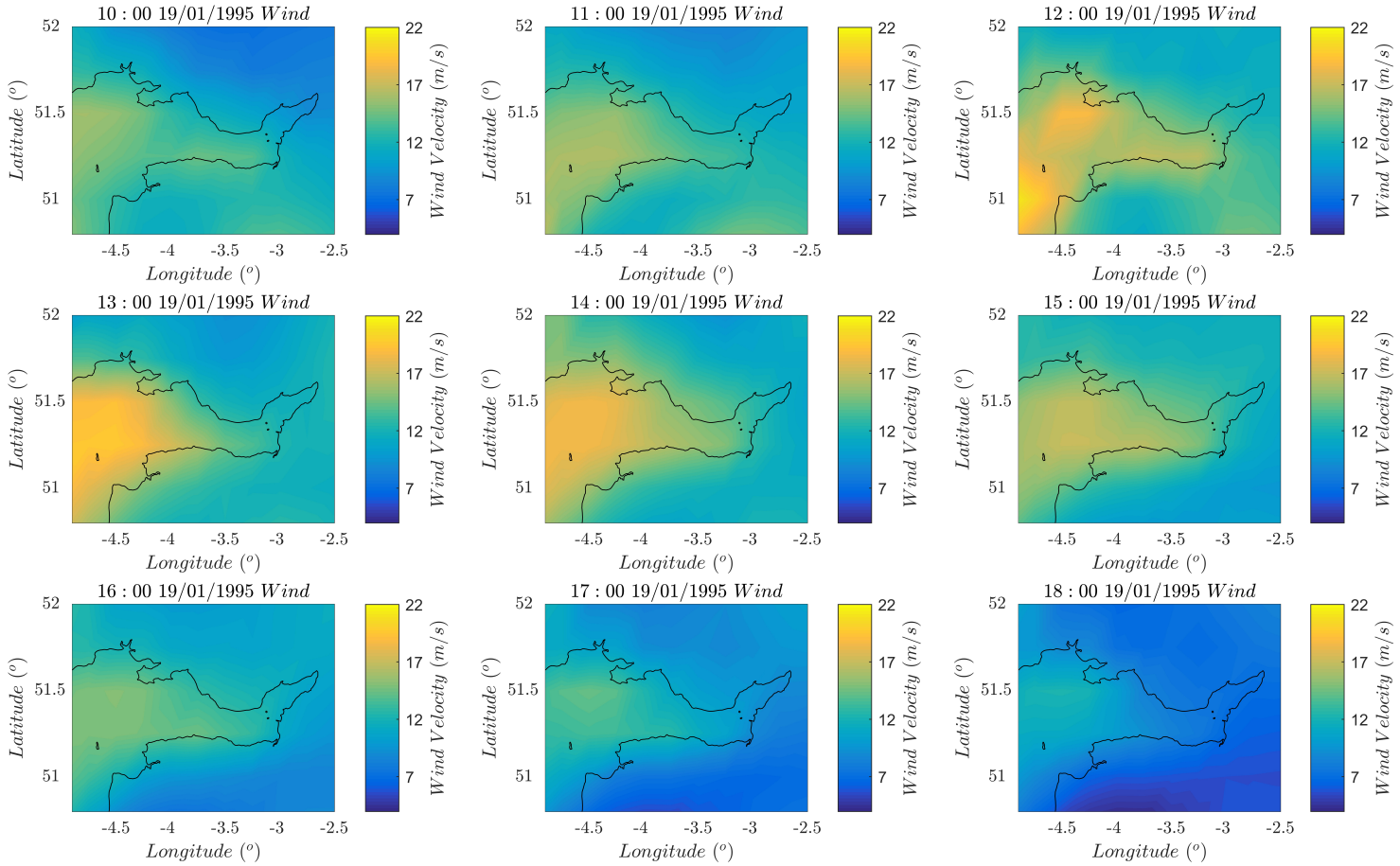

Figure B.2: Wind conditions (wind velocity in m/s) in Bristol Channel for the storm surge event on 19 January 1995 from ERA5 dataset.

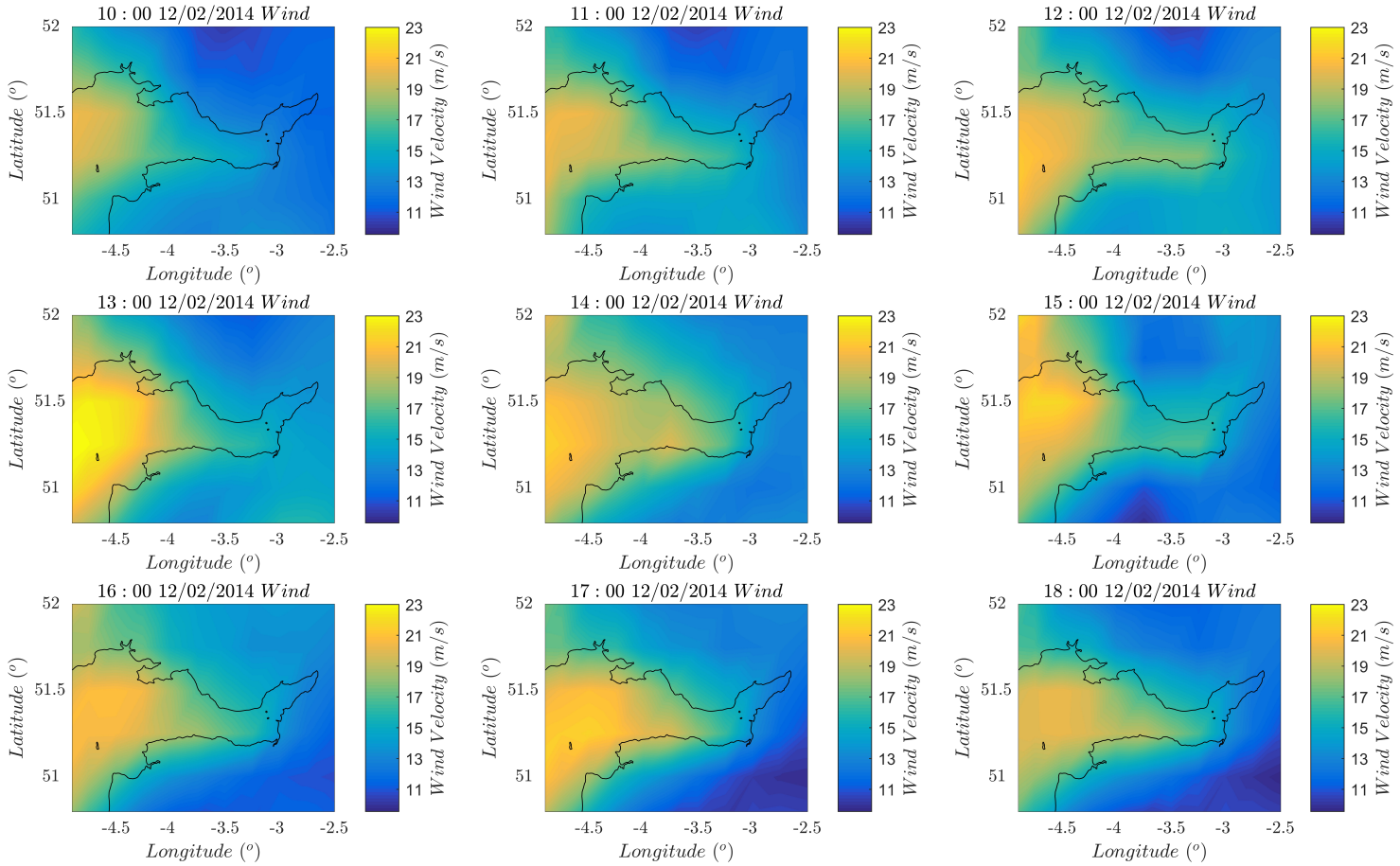

Figure B.3: Wind conditions (wind velocity in m/s) in Bristol Channel for the storm surge event on 12 February 2014 from ERA5 dataset.

References

[1] T. A. A. Adcock, A. G. L. Borthwick, and G. T. Houlsby. The open boundary problem in tidal basin modelling with energy extraction. In *Proceedings of the 9th European Wave and Tidal Energy Conference Series, Southampton, September 2011*, 2011.

[2] T. A. A. Adcock and S. Draper. On the tidal stream resource of two headland sites in the English Channel: Portland Bill and Isle of Wight. In *Proceedings of the International Conference on Offshore Mechanics and Arctic Engineering - OMAE*, volume 9A, pages 1–10, 2014.

[3] T. A. A. Adcock, S. Draper, and T. Nishino. Tidal power generation - A review of hydrodynamic modelling. *Journal of Power and Energy*, 229(7):755–771, 2015.

[4] Environment Agency. Severn at Bewdley Us, 2006.

[5] Environment Agency. Adapting to climate change: Guidance for risk management authorities. 2016.

[6] G. A. Aggidis and D. S. Benzon. Operational optimisation of a tidal barrage across the Mersey estuary using 0-D modelling. *Ocean Engineering*, 66:69–81, 2013.

[7] G. A. Aggidis and O. Feather. Tidal range turbines and generation on the Solway Firth. *Renewable Energy*, 43:9–17, 2012.

[8] R. Ahmadian, R. Falconer, and B. Lin. Hydro environmental modelling of proposed Severn Barrage, UK. In *Proceedings of the Institution of Civil Engineers-Energy*, volume 163, pages 107–117, 2010.

[9] A. Angeloudis, R Ahmadian, R. Falconer, and B. Bockelmann-Evans. Numerical model simulations for optimisation of tidal lagoon schemes. *Applied Energy*, 165:522–536, 2016.

[10] A. Angeloudis, R. A. Falconer, S. Bray, and R. Ahmadian. Representation and operation of tidal energy impoundments in a coastal hydrodynamic model. *Renewable Energy*, 99:1103–1115, 2016.

[11] A. Angeloudis, S. C. Kramer, A. Avdis, and M. D. Piggott. Optimising tidal range power plant operation. *Applied Energy*, 212:680–690, 2018.

[12] A. Angeloudis, M. Piggott, S. C. Kramer, A. Avdis, D. Coles, and M. Christou. Comparison of 0-D, 1-D and 2-D model capabilities for tidal range energy resource assessments. In *Proceedings of EWTEC 2017*, 08 2017.

[13] R. A. Anthes. Tropical cyclones, their evolution structure and effects. *American Meteorological Society*, 1982.

[14] B. K. Arbic and C. Garrett. A coupled oscillator model of shelf and ocean tides. *Continental Shelf Research*, 30(6):564–574, 2010.

[15] B. K. Arbic, R. H. Karsten, and C. Garrett. On tidal resonance in the global ocean and the back-effect of coastal tides upon open-ocean tides. *Atmosphere-Ocean*, 47(4):239–266, 2009.

[16] A. C. Baker. *Tidal power*. Energy Engineering Series. Institution of Engineering and Technology, 1991.

[17] C. Baker and P. Leach. *Tidal lagoon power generation scheme in Swansea Bay: A report on behalf of the Department of Trade and Industry and the Welsh Development Agency*. DTI London, 2006.

[18] P. D. Bates, R. J. Dawson, J. W. Hall, M. S. Horritt, R. J. Nicholls, J. Wicks, and M. Hassan. Simplified two-dimensional numerical modelling of coastal flooding and example applications. *Coastal Engineering*, 52(9):793 – 810, 2005.

[19] A. Becker, A. Plater, and J. Wolf. The energy river: Realising energy potential from the River Mersey. Technical report, Liverpool City Council, Liverpool, UK, 2017.

[20] M. Benjamin. A mathematical study of meteo and landslide tsunamis: The Proudman resonance. *Nonlinearity*, 28(11):4037–4080, 2015.

[21] P. K. Bhaskaran, R. Gayathri, P. L. N. Murty, S. Bonthu, and D. Sen. A numerical study of coastal inundation and its validation for Thane cyclone in the Bay of Benga. *Coastal Engineering*, 83:108 – 118, 2014.

[22] C. A. Blain, R. S. Linzell, P. Chu, and C. Massey. Validation test report for the ADvanced CIRCulation. *Security*, 2010.

[23] H. Bondi. Tidal power from the Severn Estuary. Technical report, Severn Barrage Committee Report to the Secretary of State for Energy, 1981.

[24] H. Bondi. Tidal power from the Severn Estuary: Report to the Secretary of State for Energy. Technical report, Department of Energy, Severn Barrage Committee, London, UK, 1981.

[25] G. C. Boon. Caerleon and the Gwent Levels in early historic times. *Archaeology and coastal change. Papers from meetings 1977*, pages 24–36, 01 1980.

[26] A. G. L. Borthwick. New perspectives on risk analysis and crisis. In *Proceedings of the 2nd international conference*, 2009.

[27] S. E. Bourban, S. J. Couch, A. Baldock, and S. Cheeseman. Coastal shelf model of northern European water to inform tidal power industry decisions: SMARTtide. *Underwater Technology*, 1(32):15–26, 2014.

[28] S. E. Bourban, N. Durand, M. Liddiard, S. Cheeseman, and A. Baldock. High resolution modelling of tidal resources, extraction and interactions around the UK. *In: EGU General Assembly 2015*, 2015.

[29] M. Bowman, R. Flood, D. Hill, and R. Wilson. Hydrologic feasibility of storm surge barriers to protect the metropolitan New York - New Jersey region. Technical report, Marine Sciences Research Center, 2002.

[30] S. Bray, R. Ahmadian, and R. Falconer. Impact of representation of hydraulic structures in modelling a Severn Barrage. *Computers Geosciences*, 89:96–106, 2016.

[31] A. J. Brewer. *Model investigation of storm surges in a shallow sea.* DPhil, University of Oxford, 1962.

[32] J. D. Brown, T. Spencer, and I. Moeller. Modeling storm surge flooding of an urban area with particular referenceto modeling uncertainties: A case study of Canvey Island, United Kingdom. *Water Resources*, 43, 2007.

[33] E. A. Bryant and S. K. Haslett. Catastrophic wave erosion, Bristol Channel, United Kingdom: Impact of tsunami. *The Journal of Geology*, 115(3):253–269, 2007.

[34] K. Bryant and M. Akbar. An exploration of wind stress calculation techniques in hurricane storm surge modeling. *Journal of Marine Science and Engineering*, 4(3):58, 2016.

[35] W. Camden. *Britannia (translated by Philemon Holland)*. London, 1610.

[36] D. E. Cartwright. Theory of ocean tides with application to altimetry. *Satellite Altimetry in Geodesy and Oceanography*, (50):100–141, 1993.

[37] L. Chen, P. Bonar, and T. A. A. Adcock. Design of a tidal turbine array for the Bohai Strait, China. In *Proceedings of the 37th International Conference on Ocean, Offshore and Arctic Engineering*, 2018.

[38] S. T. Chen and P. Yu. Real-time probabilistic forecasting of flood stages. *Journal of Hydrology*, 40:63 – 77, 2007.

[39] S. Chippada, C. Dawson, M. Martinez, and M. Wheeler. A Godunov-type finite volume method for the system of shallow water equations. *Computer Methods in Applied Mechanics and Engineering*, 151(1-2):105–129, 1998.

[40] World Energy Council. World energy resources 2016, 2016.

[41] X. Cui, G. Fang, and D. Wu. Tidal resonance in the Gulf of Thailand. *Ocean Science*, 15(2):321–331, 2019.

[42] S. Cutter, J. Mitchell, and M. Scott. Revealing the vulnerability of people and places: a case study of Georgetown County, South Carolina. *Annals of the Association of American Geographers*, 90:713 – 737, 2000.

[43] R. T. Damian. *An analysis of sea level change in the Severn Estuary*. PhD, University of Bristol, 1995.

[44] R. Davies. UK - Storm surge causes flooding along England's east coast., 2017.

[45] Davies A. M. and Jones J. E. A three dimensional model of the M2, S2, N2, K1 and O1 tides in the Celtic and Irish Seas. *Progress in Oceanography*, 29:197–234, 1992.

[46] C. Dawson, E. J. Kubatko, J. J. Westerink, C. Trahan, C. Mirabito, C. Michoski, and N. Panda. Discontinuous Galerkin methods for modeling hurricane storm surge. *Advances Water Resources*, 34(9):1165–1176, 2011.

[47] R. Dawson, P. Sayers, J. Hall, M. Hassan, and P. Bates. Efficient broad scale coastal flood risk assessment. In *Proceedings of the 29th International Conference*, 2005.

[48] R. G. Dean and R. A. Dalrymple. *Water wave mechanics for engineers and scientists*. Advanced series on ocean engineering. World Scientific, 1991.

[49] DECC. Analysis of options for tidal power development in the Severn Estuary. Interim options analysis report. Technical report, Department of Energy and Climate Change, 2008.

[50] D. P. Dee, S. M. Uppala, A. J. Simmons, P. Berrisford, P. Poli, S. Kobayashi, U. Andrae, M. A. Balmaseda, G. Balsamo, P. Bauer, P. Bechtold, A. C.M. Beljaars, L. van de Berg, J. Bidlot, N. Bormann, C. Delsol, R. Dragani, M. Fuentes, A. J. Geer, L. Haimberger, S. B. Healy, H. Hersbach, E. V. Hólm, L. Isaksen, P. Kållberg, M. Köhler, M. Matricardi, A. P. Mcnally, B. M. Monge-Sanz, J. J. Morcrette, B. K. Park, C. Peubey, P. de Rosnay, C. Tavolato, J. N. Thépaut, and F. Vitart. The ERA-Interim reanalysis: Configuration and performance of the data assimilation system. *Quarterly Journal of the Royal Meteorological Society*, 137(656):553–597, 2011.

[51] G. Di Baldassarre, G. Schumann, P. D. Bates, J. E. Freer, and K. J. Beven. Flood-plain mapping: a critical discussion of deterministic and probabilistic approaches. *Hydrological Sciences Journal*, 55:364 – 376, 2010.

[52] D. Didier, P. Bernatchez, G. Boucher-Brossard, A. Lambert, C. Fraser, R.L. Barnett, and S Van-Wierts. Coastal flood assessment based on field debris measurements and wave runup empirical model. *Journal of Marine Science and Engineering*, 3:560 – 590, 2015.

[53] D. Didier, P. Bernatchez, G. Marie, and G. Boucher-Brossard. Wave runup estimations on platform-beaches for coastal flood hazard assessment. *Natural Hazards*, 83, 2016.

[54] A. T. Doodson. The harmonic development of the tide-generating potential. In *Proceedings of the Royal Society of London. Series A*, volume 100, pages 305–329, 1921.

[55] S. Draper. On the optimum place to locate a tidal fence in the Severn Estuary. In *Proceedings of the 2nd Oxford Tidal Energy Workshop*, 2013.

[56] S. Draper, A. G. L. Borthwick, and G. T. Houlsby. Energy potential of a tidal fence deployed near a coastal headland. *Philosophical Transactions of the Royal Society A: Mathematical, Physical and Engineering Sciences*, 317:1985, 2013.

[57] S. Dube, P. Sinha, A. Rao, and G. Rao. Numerical modelling of storm surges in the Arabian Sea. *Applied Mathematical Modelling*, 9(4):289–294, 1985.

[58] ECMWF. What are the changes from ERA-Interim to ERA5?

[59] Met Éireann. Met Éireann re-analysis - climate re-analysis.

[60] G. P. Evans, B. M. Mollowney, and N. C. Spoel. Two-dimensional modelling of the Bristol Channel, UK. In *Proceedings of Estuarine and Coastal Modeling*, pages 331–340, 1990.

[61] R. A. Falconer, J. Xia, B. Lin, and R. Ahmadian. The Severn Barrage and other tidal energy options: Hydrodynamic and power output modeling. *Science in China Series E: Technological Sciences*, 52(11):3413–3424, 2009.

[62] R. A. Flather. Results from a storm surge prediction model of the north-west European continental shelf for April, November and December 1973. Technical report, Institute of Oceanographic Sciences, 1976.

[63] R. A. Flather. Recent results from a storm surge prediction scheme for the North Sea. *Elsevier Oceanography Series*, 25:385–409, 1979.

[64] R. A. Flather. Practical surge prediction using numerical models. *Floods due to high Winds and tides*, pages 21–43, 1981.

[65] R. A. Flather, L. Draper, and R. Proctor. Coastal flooding in the Bristol Channel and Severn Estuary on 13th December 1981. Technical report, 1982.

[66] R. A. Flather, J. A. Smith, J. D. Richards, C. Bell, and D. L. Blackman. Direct estimates of extreme storm surge elevations from a 40-year numerical model simulation and from observations. *Global Atmosphere Ocean System*, 6:165–176, 1998.

[67] S. W. Fong and N. S. Heaps. Note on quarter wave tidal resonance in the Bristol Channel. Technical report, Institute of Oceanographic Sciences, 1978.

[68] T. G. Frazier, N. Wood, B. Yarnal, and D. H. Bauer. Influence of potential sea level rise on societal vulnerability to hurricane storm-surge hazards, Sarasota County, Florida. *Applied Geography*, 30:490 – 505, 2010.

[69] T. Gallien, N. Kalligeris, M. Delisle, B. Tang, J. Lucey, and M. Winters. Coastal flood modeling challenges in defended urban backshores. *Geosciences*, 8:450, 12 2018.

[70] C. Gao. *Analysis of storm surge and tidal resonance in the Bristol Channel*. Mphil, University of Oxford, 2017.

[71] C. Gao and T. A. A. Adcock. The characteristics of storm surges in the Bristol Channel. In *The 26th International Ocean and Polar Engineering Conference*, pages 1–8, 2016.

[72] C. Gao and T. A. A. Adcock. On the tidal resonance of the Bristol Channel. *International Journal of Offshore and Polar Engineering*, 27(2), 2017.

[73] J. Gao. *A numerical modeling study of storm surge and inundation in the Chesapeake Bay during the November 2009 Mid-Atlantic Nor'easter*. Msc, The College of William and Mary in Virginia, 2011.

[74] C. Garrett. Tidal resonance in the Bay of Fundy and Gulf of Maine. *Nature*, 238(5365):441, 1972.

[75] J. Garzon and C. Ferreira. Storm surge modeling in large estuaries: Sensitivity analyses to parameters and physical processes in the Chesapeake Bay. *Journal of Hydraulic Engineering*, 4(3):45, 2016.

[76] B. Glahn, A. Taylor, N. Kurkowski, and W. A. Shaffer. The role of the SLOSH model in national weather service storm surge forecasting. *National Weather Digest*, 33:3 – 14, 2009.

[77] G. Godin. On tidal resonance. *Continental Shelf Research*, 13(1):89–107, 1993.

[78] E. Goldwag and R. Potts. Development in tidal energy. In *Proceedings of the Third Conference on Tidal Power*, pages 75–92, 1989.

[79] GOV.UK. Digest of UK energy statistics (DUKES): Electricity.

[80] GOV.UK. Flood warnings for England, 2018.

[81] Great Britain Hydrographic Department. *Admiralty tide tables. Volume 1, United Kingdom and Ireland, including European Channel ports*, volume 1. The Hydrographer of the Navy, 1997.

[82] Hafren Power. Severn Barrage business case. Technical report, Hafren Power, London, UK, 2013.

[83] I. D. Haigh, M. P. Wadey, S. L. Gallop, H. Loehr, R. J. Nicholls, K. Horsburgh, J. M. Brown, and E. Bradshaw. A user-friendly database of coastal flooding in the United Kingdom from 1915-2014. *Scientific Data*, 2, 2015.

[84] W. C. Haneberg. Deterministic and probabilistic approaches to geologic hazard assessment. *Environmental and Engineering Geoscience*, 6:209 – 226, 2000.

[85] M. R. Hashemi, M. J. Abedini, S. P. Neill, and P. Malekzadeh. Tidal and surge modelling using differential quadrature: A case study in the Bristol Channel. *Coastal Engineering*, 55(10):811–819, 2008.

[86] A. Hatzikyriakou and N. Lin. Simulating storm surge waves for structural vulnerability estimation and flood hazard mapping. *Natural Hazards*, 89:939 – 962, 2017.

[87] R. A. Heath. Resonant period and Q of the Celtic Sea and Bristol Channel. *Estuarine, Coastal and Shelf Science*, 12(3):291–301, 1981.

[88] C. Hendry. The role of tidal lagoons. Technical report, UK Government, 2016.

[89] P. Homewood. Booker on the Swansea Bay Lagoon, 2015.

[90] D. Horn. Storm surge warning, mitigation, and adaptation. *Coastal and Marine Hazards, Risks, and Disasters*, pages 153–180, 2015.

[91] K. Horsburgh and M. Horritt. The Bristol Channel floods of 1607 reconstruction and analysis. *Weather*, 61(10):272–277, 2006.

[92] A. S. Iyer, S. J. Couch, G. P. Harrison, and A. R. Wallace. Analysis and comparison of tidal datasets. In *Proceedings of the 8th European Wave and Tidal Energy Conference*, 2009.

[93] A. S. Iyer, S. J. Couch, G. P. Harrison, and A. R. Wallace. Variability and phasing of tidal current energy around the United Kingdom. *Renewable Energy*, 51:343 – 357, 2013.

[94] J. H. Jang, S. H. Yeh, J. C. Fu, C. J. Huang, and P. S. Yu. A probabilistic model for real-time flood warning based on deterministic flood inundation mapping. *Hydrological Processes*, 26:1079 – 1089, 2012.

[95] P. Jeffcoate, P. Stansby, and D. Apsley. Flow and bed-shear magnification downstream of a barrage with swirl generated in ducts by stators and rotors. *Journal of Hydraulic Engineering*, 143(2), 2017.

[96] C. P. Jelesnianski. SPLASH (Special Program to List Amplitudes of Surges from Hurricanes) I: Landfall storms. Technical report, U.S. Department of Commerce, 1972.

[97] B. Johns and M. Ali. The numerical modelling of storm surges in the Bay of Bengal. *Quarterly Journal of the Royal Meteorological Society*, 106(447):1–8, 1980.

[98] S. N. Jonkman and I. Kelman. Deaths during the 1953 North Sea storm surge. In *Solutions to Coastal Disasters 2005*, pages 749–758. 2005.

[99] V. Khare, C. Khare, S. Nema, and P. Baredar. *Tidal energy systems*. Elsevier, 2019.

[100] S. Kim, T. Yasuda, and H. Mase. Wave set-up in the storm surge along open coasts during Typhoon Anita. *Coastal Engineering*, 57(7):631–642, 2010.

[101] R. Kirby and C. Retière. Comparing environmental effects of Rance and Severn barrages. In *Proceedings of The Institution of Civil Engineers-maritime Engineering*, volume 1, pages 11–26, 2009.

[102] R Krzysztofowicz. The case for probabilistic forecasting in hydrology. *Journal of Hydrology Amsterdam*, 249:2 – 9, 2001.

[103] E. Kubatko, J. Westerink, and C. Dawson. Hp Discontinuous Galerkin methods for advection dominated problems in shallow water flow. *Computer Methods in Applied Mechanics and Engineering*, 196(1-3):437–451, 2006.

[104] E. J. Kubatko, S. Bunya, C. Dawson, J. J. Westerink, and C. Mirabito. A performance comparison of continuous and discontinuous finite element shallow water models. *Journal of Scientific Computing*, 40(1-3):315–339, 2009.

[105] P. Kumar and R. Saini. Study of cavitation in hydro turbines - A review. *Renewable Sustainable Energy Reviews*, 14(1):374–383, 2010.

[106] C. Le Provost, M. Genco, and F. Lyard. Modeling and predicting tides over the World Ocean. *Coastal and Estuarine Studies*, page 175, 1995.

[107] R. J. LeVeque. *Finite volume methods for hyperbolic problems*. Cambridge University press, NY, USA, 2002.

[108] M. Lewis, A. Angeloudis, P. Robins, P. Evans, and S. Neill. Influence of storm surge on tidal range energy. *Energy*, 122:25–36, 2017.

[109] D. Liang, J. Xia, R. A. Falconer, and J. Zhang. Study on tidal resonance in Severn Estuary and Bristol Channel. *Coastal Engineering*, 56(01), 2014.

[110] M. Longuet-Higgins and R. Stewart. Radiation stresses in water waves; A physical discussion, with applications. *Deep Sea Research and Oceanographic Abstracts*, 11(4):529–562, 1964.

[111] J. A. Lowe, J. M. Gregory, and R. A. Flather. Changes in the occurrence of storm surges around the United Kingdom under a future climate scenario using a dynamic storm surge model driven by the Hadley Centre climate models. *Climate Dynamics*, 18:179–188, 2001.

[112] C. Lyddon, A. Plater, J. Brown, T. Prime, and J. Wolf. The impact of tidal lagoons on future flood risk on the North Wirral and Conwy coastline. Technical report, National Oceanography Centre, Liverpool, UK, 2015.

[113] Q. Ma and T. A. A. Adcock. Modification of tidal resonance in the Severn Estuary by a barrage and lagoon. *Journal of Ocean Engineering and Marine Energy*, 6:171–181, 2020.

[114] Q. Ma, T. M. Moreira, and T. A. A. Adcock. Impact of the Swansea Bay lagoon on storm surges in the Bristol Channel. In *Proceedings of the 38th International Conference on Ocean, Offshore and Arctic Engineering, Glasgow, UK*, 2019.

[115] Q. Ma, T. M. Moreira, and T. A. A. Adcock. The impact of a tidal barrage on coastal flooding due to storm surge in the Severn Estuary. *Journal of Ocean Engineering and Marine Energy*, 5:217–226, 2019.

[116] D. MacKay. Enhancing electrical supply by pumped storage in tidal lagoons. 2007.

[117] R. Mawdsley and I. Haigh. Spatial and temporal variability and long-term trends in skew surges globally. *Frontiers Marine Science*, 3, 2016.

[118] R. Maxey, M. Cranston, A. Tavendale, and P. Buchanan. The use of deterministic and probabilistic forecasting in countrywide flood guidance in Scotland. *British Hydrological Society*, 2012.

[119] J. Meixner, J. C. Dietrich, C. Dawson, M. Zijlema, and L. H. Holthuijsen. A Discontinuous Galerkin coupled wave propagation/circulation model. *Journal of Scientific Computing*, 59:334–370, 2014.

[120] S. P. Neill, A. Angeloudis, P. E. Robins, I. Walkington, S. L. Ward, I. Masters, M. J. Lewis, M. Piano, A. Avdis, M. D. Piggott, G. Aggidis, P. Evans, T. A. A. Adcock, A. Židonis, R. Ahmadian, and R. Falconer. Tidal range energy resource and optimization–Past perspectives and future challenges. *Renewable Energy*, 127:763–778, 2018.

[121] S. P. Neill, E. J. Litt, S. J. Couch, and A. G. Davies. The impact of tidal stream turbines on large-scale sediment dynamics. *Renewable Energy*, 34(12):2803–2812, 2009.

[122] R. J. Nicholls, R. S. Tol, and A. T. Vafeidis. Global estimates of the impact of a collapse of the West Antarctic ice sheet: An application of FUND. *Climate Change*, 91(1-2):171–191, 2008.

[123] Met Office. Floods and flooding, 2016.

[124] C. O'Neill, A. Saulter, J. Williams, and K. Horsburgh. NEMO-surge: Application of atmospheric forcing and surge evaluation. Technical report, 2016.

[125] F. O'Rourke, F. Boyle, and A. Reynolds. Tidal energy update 2009. *Applied Energy*, 87(2):398–409, 2010.

[126] J. Osment, P. Halstead, and N. I. Pontee. Reassessing the Severn Barrage: Operational modes and their impacts. *In press: Coastal Management 2011. Innovative Coastal Zone Management: Sustainable Engineering for a Dynamic Coast*, 2011.

[127] A. Owen. A three-dimensional model of the Bristol Channel. *Journal of Physical Oceanography*, 10(8):1290–1302, 1980.

[128] European Parliament. Directive 2009/28/EC of the European Parliament and of the Council of 23 April 2009 on the promotion of the use of energy from renewable sources and amending and subsequently repealing directive. *Official Journal of EU*, pages 16–62, 2009.

[129] R. Pawlowicz, B. Beardsley, and S. Lentz. Classical tidal harmonic analysis including error estimates in MATLAB using T_TIDE. *Computers & Geosciences*, 28(8):929–937, 2002.

[130] S. Petley and G. Aggidis. Swansea Bay tidal lagoon annual energy estimation. *Ocean Engineering*, 111:348–357, 2016.

[131] M. R. Phillips and S. Crisp. Sea level trends and NAO influences: The Bristol Channel\Severn Estuary. *Global and Planetary Change*, 3(73):211–218, 2010.

[132] R. D. Pingree and D. K. Griffiths. Sand transport paths around the British Isles resulting from M2 and M4 tidal interactions. *Journal of the Marine Biological Association of the United Kingdom*, 59(2):497–513, 1979.

[133] D. Prandle. Storm surges in the Southern North Sea and River Thames. In *Proceedings of the Royal Society of London. Series A, Mathematical and Physical Sciences*, volume 344, pages 509–539, 1975.

[134] D. Prandle. Simple theory for designing tidal power schemes. *Advances Water Resources*, 7(1):21–27, 1984.

[135] D. Prandle. Design of tidal barrage power schemes. In *Proceedings of The Institution of Civil Engineers-maritime Engineering*, volume 162, pages 147–153, 2009.

[136] R. Proctor and R. A. Flather. Storm surge prediction in the Bristol Channel - the floods of 13 December 1981. *Continental Shelf Research*, 9(10):889–918, 1989.

[137] D. Pugh and P. Woodworth. *Sea-level science: Understanding tides, surges, tsunamis and mean sea-level changes*. Cambridge University Press, Cambridge, U.K., 2014.

[138] D. T. Pugh. *Tides, surges and mean sea-level*. 1996.

[139] R. C. Rainey. The optimum position for a tidal power barrage in the Severn Estuary. *Journal of Fluid Mechanics*, 636:497–507, 2009.

[140] J. A. Ramirez, M. Lichter, T.J. Coulthard, and S. Chris. Hyper-resolution mapping of regional storm surge and tide flooding: comparison of static and dynamic models. *Nat Hazards*, 82:571 – 590, 2016.

[141] A. D. Rao, P. L. N. Murty, I. Jain, R. S. Kankara, S. K. Dube, and T. S. Murty. Simulation of water levels and extent of coastal inundation due to a cyclonic storm along the east coast of India. *Natural Hazards*, 2012.

[142] RMS. 1607 Bristol Channel floods: 400-year retrospective. Technical report, Risk Management Solutions Report, 2007.

[143] I. S. Robinson. Tides in the Bristol Channel - An analytical wedge model with friction. *Geophysical Journal of the Royal Astronomical Society*, 62(1):77–95, 1980.

[144] F. L. Santiago-Collazo, M. V. Bilskie, and S. C. Hagen. A comprehensive review of compound inundation models in low-gradient coastal watersheds. *Environmental Modelling & Software*, 119:166 – 181, 2019.

[145] J. Sanz-Serna and M. Spijker. Regions of stability, equivalence theorems and the Courant-Friedrichs-Lewy condition. *Numerische Mathematik*, 49:319–329, 03 1986.

[146] N. Schaller, A. Kay, R. Lamb, N. Massey, G. Van Oldenborgh, F. Otto, S. Sparrow, R. Vautard, P. Yiou, I. Ashpole, A. Bowery, S. Crooks, K. Haustein, C. Huntingford, W. Ingram, R. Jones, T. Legg, J. Miller, J. Skeggs, D. Wallom, A. Weisheimer, S. Wilson, P. Stott, and M Allen. Human influence on climate in the 2014 southern England winter floods and their impacts. *Nature Climate Change*, 6(6):627–634, 2016.

[147] A. M. Schnabl, T. M. Moreira, D. Wood, E. J. Kubatko, G. T. Houlsby, R. A. McAdam, and T. A. A. Adcock. Implementation of tidal stream turbines and tidal barrage structures in DG-SWEM. In *Proceedings of the 38th International Conference on Ocean, Offshore and Arctic Engineering, Glasgow, UK*, 2019.

[148] D. Schwanenberg and M. Harms. Discontinuous Galerkin finite-element method for transcritical two-dimensional shallow water flows. *Journal of Hydraulic Engineering*, 130(5):412–421, 2004.

[149] S. Serhadlioglu. *Tidal stream resource assessment of the Anglesey Skerries and the Bristol Channel*. DPhil, University of Oxford, 2014.

[150] J. Shankleman. The world's 10 biggest tidal power projects., 2014.

[151] G. D. Smith. *Numerical solution of partial differential equations: Finite difference methods*. Oxford University press., UK, 1978.

[152] J. Stow and E. Howes. *Annales, or a general chronicle of England*. 1631.

[153] STPG. The Severn Barrage project: General report. Technical report, Severn Tidal Power Group, Department of Energy (DE), London, UK, 1989.

[154] R. Sutcliffe and G. Lennon. The identification of weather conditions associated with the generation of major storm surges along the west coast of the British Isles. *Quarterly Journal of the Royal Meteorological Society*, 89(381):381–394, 1963.

[155] G. Sutherland, C. Garrett, and M. Foreman. Tidal resonance in Juan de Fuca Strait and the Strait of Georgia. *Journal of Physical Oceanography*, 35(7):1279–1286, 2005.

[156] Y. Tang, B. Sanderson, G. Holland, and R. Grimshaw. A numerical study of storm surges and tides, with application to the North Queensland coast. *Journal Physical Oceanography*, 26(12):2700–2711, 1996.

[157] A. A. Taylor and B Glahn. Probabilistic guidance for hurricane storm surge. In *Proceedings of the 19th conference on probability and statistics*, 2008.

[158] G. I. Taylor. Tides in the Bristol Channel. In *Proceedings of the Cambridge Philosophical Society*, volume 20, pages 320–325, 1921.

[159] C. M. Thompson and T. G. Frazier. Deterministic and probabilistic flood modeling for contemporary and future coastal and inland precipitation inundation. *Applied Geography*, 50:1–14, 2014.

[160] ADCIRC user's manual V51. Single file meteorological input file (fort.22), 2015.

[161] J. M. Van Der Knijff, Younis J., and A. P. J. De Roo. LISFLOOD: A GISbased distributed model for river basin scale water balance and flood simulation. *International Journal of Geographical Information Science*, 24(2):189–212, 2010.

[162] Lennon G. W. The identification of weather conditions associated with the generation of major storm surges on the west coast of the British Isles. *Quarterly Journal of the Royal Meteorological Society*, 89:381–394, 1963.

[163] G. Walton. Life threatening' floods and a NINE FOOT storm surge as the entire East-Coast of Britain is on flood alert., 2017.

[164] C. S. Warder. *Sensitivity analysis, uncertainty quantification and parameter estimation for a numerical tide and storm surge model.* PhD, Imperial College London, 2020.

[165] R. Weaver and D. Slinn. Effect of wave forces on storm surge. *Coastal Engineering*, 2004.

[166] D. J. Webb. On the shelf resonances of the English Channel and Irish Sea. *Ocean Science*, 9(4):731–744, 2013.

[167] J. Westerink, R. Luettich, C. Blain, and N. Scheffner. ADCIRC: An advanced three-dimensional circulation model for shelves, coasts, and estuaries. Technical report, Army Engineer Waterways Experiment Station Vicksburg MS, 1994.

[168] J. J. Westerink, R. A. Luettich, J. C. Feyen, J. H. Atkinson, C. Dawson, H. J. Roberts, M. D. Powell, J. P. Dunion, E. J. Kubatko, and H. Pourtaheri. A basin- to channel-scale unstructured grid hurricane storm surge model applied to Southern Louisiana. *Monthly Weather Review*, 136(3):833–864, 2008.

[169] J. J. Westerink, R. A. Luettich, and A. Militello. Leaky internal-barrier normal-flow boundaries in the ADCIRC coastal hydrodynamics code. Technical report, US Army Corps of Engineers, 2001.

[170] J. A. Westlake. Meteotsunami: The AD 1607 Bristol Channel flood. *Emporium*, 1(2), 2019.

[171] J. Williams and K. Horsburgh. Evaluation and comparison of the operational Bristol Channel model storm surge suite. Technical report, National Oceanography Centre, Southampton, UK, 2013.

[172] J. Williams, K. J. Horsburgh, J. A. Williams, and R. Proctor. Tide and skew surge independence: New insights for flood risk. *Geophysical Research Letters*, 43(12):6410–6417, 2016.

[173] J. Williams, C. Wilson, and K. Horsburgh. Re-analysis of the December 1981 storm surge event in the Bristol Channel using the current operational tide-surge model suite. *Ocean Science*, 5(3):369–378, 2012.

[174] M. Williams. The draining and reclamation of the Somerset Levels, 1770-1833. *Transactions and Papers (Institute of British Geographers)*, (33):163–179, 1963.

[175] J. Wolf. Coastal flooding: Impacts of coupled wave-surge-tide models. *Natural Hazards*, 49(2):241–260, 2008.

[176] J. Wolf and R. A. Flather. Modelling waves and surges during the 1953 storm. *Philosophical Transactions of The Royal Society A Mathematical Physical and Engineering Sciences*, 363:1359–1375, 2005.

[177] N. Wood and Geological Survey (U.S.) Hawaii Pacific Disaster Center. Variations in community exposure and sensitivity to tsunami hazards in the state of Hawai'i. *U.S. Department of the Interior, U.S. Geological Survey, Reston, VA*, 2007.

[178] J. Xia, R. A. Falconer, and B. Lin. Hydrodynamic impact of a tidal barrage in the Severn Estuary, UK. *Renewable Energy*, 35(7):1455–1468, 2010.

[179] J. Xia, R. A. Falconer, and B. Lin. Impact of different operating modes for a Severn Barrage on the tidal power and flood inundation in the Severn Estuary, UK. *Applied Energy*, 87(7):2374–2391, 2010.

[180] N. Yates, I. Walkington, R. Burrows, and J. Wolf. Appraising the extractable tidal energy resource of the UK's western coastal waters. *Philosophical Transactions of The Royal Society A Mathematical Physical and Engineering Sciences*, 371, 2013.

[181] N. Yates, I. Walkington, R. Burrows, and J. Wolf. The energy gains realisable through pumping for tidal range energy schemes. *Renewable Energy*, 58:79–84, 2013.